

**Formulation of cerium oxide nanoparticles
towards the prevention and treatment of cataract**

Belal I. Hanafy

A thesis submitted in partial fulfilment of the requirements of Nottingham
Trent University for the degree of Doctor of Philosophy

March 2020

This work is the intellectual copyright of the author. You may copy up to 5% of this work for private study, or personal, non-commercial research. Any re-use of the information contained within this document should be fully referenced, quoting the author, title, university, degree level and pagination. Queries or requests for any other use, or if a more substantial copy is required, should be directed in the first instance to the owner of the Intellectual Property Rights.

Dedication

I dedicate this thesis to my parents: Professor Ibrahim Hanafy and Dr. Zozo Al-Gendy, for their unconditional support and love they provided me with throughout my PhD. Without them, none of this work would have been possible and I am forever grateful for their help.

Acknowledgments

Praise be to Allah the Merciful who blessed me to successfully complete this work.

First, I would like to thank my supervisor and director of studies professor Barbara Pierscionek who has supported me in every possible way to successfully complete this project. Her advice, insights, kindness, patience and encouragement throughout my studies have had a great and positive impact on my work and professional life for which I will be forever grateful. She has this unmatched motivational power that can push anyone forward. She was always available when I needed her help and has fully supported me in critical decisions that made my PhD life a lot easier. Simply, I have been tremendously fortunate and blessed to have had her as my supervisor.

Secondly, my great appreciations go to my supervisors: Dr Gareth Cave and professor Yvonne Barnett without whom I would not have achieved so much. Dr Gareth Cave has been incredibly supportive and has generously provided me with my own space in his laboratory. His insights and ideas have brought so much to the work in this thesis. He guided and encouraged me to learn new techniques, skills and software which have made me a better researcher. Professor Yvonne Barnett has been so supportive to me and has reviewed my publications extensively improving them dramatically. She was my first point of contact to get this PhD position for which I am very thankful.

Special thanks to Dr Biola Egbowon whose impact on my work was beyond imaginable. She gave me all the resources and consumables she had to help me start this project without any delays. She taught me cell culturing and acquainted me with the university system the moment I started. Her selfless spirit is just worthy of admiring. God bless you Biola!

I would also like to send my sincere appreciations to many people who have made my PhD experience much more rewarding. The wonderful technical team in ISTeC, Jayne Spence, Diego Lo Destro and Adam Coburn, who have welcomed me in their labs and provided me with everything I needed. Many thanks to all my friends and colleagues Grace, Kehao, Laura, Eden, Jack, Subba and Anita who always had faith in me and encouraged me to keep going.

No words can express my gratitude for my brothers Ahmed, Mohamed and Abdelrahman, and my caring sisters Zahraa and Samaa for their continuous support and encouragement during this journey. They were always there for me in my ups and downs. God bless you all!

Finally, I would like to sincerely thank my lovely fiancée Hadeer for her tremendous support and encouragement during this work.

Resulting publications and awards

Journal articles

Hanafy, B.I.; Cave, G.W. V.; Barnett, Y.; Pierscionek, B. Ethylene glycol coated nanoceria protects against oxidative stress in human lens epithelium. **RSC Adv.** **2019**, 9, 16596–16605.
<https://rsc.li/2QvjVXi>

Hanafy, B.I.; Cave, G.W. V.; Barnett, Y.; Pierscionek, B. Treatment of Human Lens Epithelium with High Levels of Nanoceria Leads to Reactive Oxygen Species Mediated Apoptosis. **Mol.** **2020**, Vol. 25, Page 441 2020, 25, 441.
<https://www.mdpi.com/1420-3049/25/3/441>

Conference proceedings

Hanafy, B.I.; Cave, G.W. V.; Barnett, Y.; Pierscionek, B. A novel nanoceria formulation as a promising non-surgical cataract treatment. **47th IUPAC World Chemistry Congress and 50th General Assembly**, 5-12 July 2019, Paris, France.

https://hopsotch.key4events.com/ftp/IUPAC/Abstract_book_IUPAC2019.pdf

Awards

- Best Poster Presentation award (1st) | STAR Conference | Nottingham Trent University | May 2019.
- Best Poster Presentation award (2nd) | Royal Society of Biology Symposium, Leicester | May 2019.

Resulting presentations

- 47th IUPAC World Chemistry Congress and 50th General Assembly, 5-12 July 2019, Paris, France (**oral presentation**)
- RSC Dalton Division Northern Regional Meeting, 13 June 2019, University of York, UK (**oral presentation**)
- School of Science and Technology Annual Research Conference, 16-17 May 2019, Nottingham, UK (**oral and poster presentations**)
- Royal Society of Biology Postgraduate Symposium, 2 May 2019, Leicester, UK (**poster presentation**)

Contents

1	Introduction	1
1.1	The human lens: Structure and physiology	1
1.1.1	Lens capsule	2
1.1.2	Lens epithelium	3
1.1.3	Lens cortex and nucleus	3
1.2	Lens development and homeostasis	4
1.3	Aetiology of cataract: a human lens disorder	5
1.4	Who is affected? Statistics on cataract	8
1.5	Cataract Surgery	8
1.6	The current treatments and the prospects of future medications	9
1.6.1	Carnosine	10
1.6.2	Multivitamins	11
1.6.3	Aspirin, paracetamol and ibuprofen	11
1.6.4	Lanosterol	12
1.7	Nanotechnology for cataract	14
1.8	Cerium oxide nanoparticles (nanoceria) as a potential cataract therapeutic	14
1.8.1	Synthesis of cerium oxide nanoparticles	15
1.8.2	Cerium oxide structure and redox properties	15
1.8.3	Cerium oxide multi-enzyme mimetic properties	17
1.8.4	Cerium oxide for oxidative stress-related diseases	19
1.9	Project aims	21

2	Development of cerium oxide nanoparticles for biomedical applications.....	23
2.1	Introduction	23
2.2	Materials and methods.....	25
2.2.1	Synthesis of cerium oxide nanoparticles.....	25
2.2.2	Transmission electron microscopy (TEM)	25
2.2.3	Powder X-ray diffraction (XRD)	26
2.2.4	Ultraviolet-visible spectrophotometry (UV-vis) and fluorescence studies....	26
2.2.5	Fourier-transform infrared spectroscopy (FTIR)	27
2.2.6	Scanning electron microscopy-energy dispersive x-ray spectroscopy (SEM-EDX)	27
2.2.7	Thermogravimetric analysis - gas chromatography – mass spectrometry (TGA-GC-MS).....	27
2.2.8	Dynamic light Scattering (DLS) and zeta potential	28
2.2.9	Colloidal stability and sterilisation	28
2.3	Results and discussion.....	29
2.3.1	EGCNPs morphology and crystallinity (TEM and XRD)	29
2.3.2	FTIR characterisation.....	34
2.3.3	UV-vis characterisation.....	36
2.3.4	SEM-EDX characterisation.....	37
2.3.5	EGCNPs coating characterisation by TGA-GC-MS.....	38
2.3.6	EGCNPs photoluminescence and optical properties.....	43
2.3.7	EGCNPs colloidal stability and sterilisation.....	46

2.3.8	Europium doping to enhance the photoluminescent properties of EGCNPs	52
2.4	Conclusion	55
3	Toxicity evaluation of EGCNPs in human lens epithelial cells	56
3.1	Introduction	56
3.2	Materials and methods	59
3.2.1	Cell culture and maintenance	59
3.2.2	Cell viability of HLECs after EGCNPs exposure (MTT assay)	59
3.2.3	Proliferation of HLECs after EGCNPs exposure (live cell imaging)	60
3.2.4	Cell membrane integrity of HLECs after EGCNPs exposure (live cell imaging)	60
3.2.5	Basal ROS level measurement (H ₂ DCFDA assay)	61
3.2.6	EGCNPs mitochondrial uptake and localisation (SEM-EDX)	62
3.2.7	Mitochondrial morphology (confocal microscopy)	62
3.2.8	Mitochondrial membrane potential (JC-1 staining)	63
3.2.9	ATP quantification (Luciferase assay)	63
3.2.10	Genotoxicity (immunocytochemistry)	64
3.2.11	Caspase-3,7 assay (live cell imaging)	65
3.2.12	Annexin V/Cytotox Red assay (live cell imaging)	65
3.2.13	Statistical analysis	65
3.3	Results and discussion	66
3.3.1	Effect of EGCNPs on cell viability, membrane integrity, proliferation and morphology of HLECs	66

3.3.2	Acute exposure to high EGCNPs concentrations increases basal ROS	71
3.3.3	EGCNPs localise in the mitochondria.....	73
3.3.4	Effect of EGCNPs on the mitochondrial network	75
3.3.5	Effect of EGCNPs on the mitochondrial membrane potential ($\Delta\Psi_m$).....	77
3.3.6	Effect of EGCNPs on ATP level (luciferase assay).....	80
3.3.7	Genotoxicity (pH2AX immunocytochemistry).....	81
3.3.8	Effect of EGCNPs on caspase-3,7 activity	83
3.3.9	Annexin V/Cytotox Red assay	85
3.4	Conclusion.....	89
4	Uptake, localisation and anti-cataract properties of EGCNPs in human lens epithelium	90
4.1	Introduction	90
4.2	Materials and methods.....	92
4.2.1	Time-dependent uptake of EGCNPs in HLECs (ICP-MS studies).....	92
4.2.2	Mechanism of EGCNPs uptake in HLECs	93
4.2.3	Localisation of EGCNPs and EuCNPs in HLECs (SEM-EDX studies).....	93
4.2.4	Localisation of EGCNPs and EuCNPs in HLECs (confocal studies).....	94
4.2.5	Protective effect of EGCNPs against oxidative stress in HLECs	94
4.2.6	The effect of EGCNPs pre-treatment and co-treatment on HLECs viability and proliferation when exposed to oxidative stress (live cell imaging).....	95
4.2.7	Catalase mimetic activity of EGCNPs in HLECs	95
4.2.8	Effect of EGCNPs on GSH/GSSG ratio	96

4.2.9	Measuring Antiglycation properties of EGCNPs.....	97
4.3	Results and discussion.....	99
4.3.1	Time dependent uptake of EGCNPs in HLECs and its mechanism	99
4.3.2	Localisation of EGCNPs and EuCNPs in HLECs	103
4.3.3	EGCNPs protect the normal proliferation of HLECs when exposed to oxidative stress	112
4.3.4	EGCNPs protect against oxidative stress (H ₂ DCFDA staining).....	116
4.3.5	Catalase-like activity of EGCNPs in HLECs.....	118
4.3.6	Effect of EGCNPs on GSH/GSSG ratio	120
4.3.7	Effect of EGCNPs on protein glycation.....	124
4.4	Conclusion.....	129
5	General discussion, conclusions and recommendations for future work.....	130
5.1	Discussion and conclusions.....	130
5.2	Recommendations for future work.....	136
6	References	138
	Publication 1	161
	Publication 2	171

List of Figures

Figure 1-1 Cross section of the human eye.	1
Figure 1-2 Cross section of the human lens.	2
Figure 1-3 Cerium oxide crystal structure.	16
Figure 1-4 Proposed mechanism of superoxide dismutation by cerium oxide.	18
Figure 2-1 Transmission electron microscopic (TEM) images of nanoceria.	31
Figure 2-2 High resolution TEM micrographs showing the lattice fringes.	32
Figure 2-3 X-ray diffractogram displaying characteristic planes (annotated) typical of face-centered cubic fluorite structure of EGCNPs.	33
Figure 2-4 FTIR analysis of nanoceria.	35
Figure 2-5 UV-visible spectrum of EGCNPs showing absorption at 255 nm and 300 nm confirming the presence of surface Ce^{3+}	36
Figure 2-6 SEM-EDX analysis of EGCNPs.	37
Figure 2-7 Thermogravimetric analysis (TGA) of EGCNPs showing two main weight loss regions.	39
Figure 2-8 Gas chromatography - mass spectrometry analysis (GC-MS) of EGCNPs coating after decomposition in TGA.	40
Figure 2-9 Acetylated ethylene glycol coating does not interfere with the antioxidant and regenerative properties of EGCNPs.	42
Figure 2-10 Photoluminescent properties of EGCNPs.	44
Figure 2-11 EGCNPs maximum emission is blue shifted to 350 nm upon excitation with a wavelength of 270 nm.	45
Figure 2-12 Confocal images of a cluster of EGCNPs powder upon 405 nm excitation with emissions detected at (a) 450 nm, (b) 550 nm and (c) 630 nm.	45
Figure 2-13 Distribution of the intensity-weighted hydrodynamic diameters (Z-average) of EGCNPs in different aqueous media.	49
Figure 2-14 The hydrodynamic diameter (Z-average) of non-coated cerium oxide nanoparticles in water showing polydispersity and aggregation.	49
Figure 2-15 Colloidal stability of ethylene glycol-coated nanoceria (EGCNPs) and non-coated nanoceria kept in water at room temperature for a week.	52

Figure 2-16 Characterisation of europium-doped nanoceria (EuCNPs).....	54
Figure 3-1 MTT cell viability assay in HLECs with different EGCNPs concentrations.....	66
Figure 3-2 Effect of different EGCNPs concentrations on HLECs proliferation.....	68
Figure 3-3 Live cell analysis showing cytotoxicity, morphology and proliferation in HLECs upon EGCNPs exposure up to 72 h.....	70
Figure 3-4 Effect of EGCNPs (24 h exposure) on basal ROS level in HLECs employing H ₂ DCFDA fluorescent probe.....	72
Figure 3-5 SEM-EDX analysis of isolated mitochondria.....	74
Figure 3-6 Confocal examination of mitochondria in HLECs.....	76
Figure 3-7 Effect of EGCNPs concentrations on mitochondrial membrane potential ($\Delta\Psi_m$) measured using JC-1 staining.....	78
Figure 3-8 Representative Incucyte [®] S3 images used for the quantification of JC-1 red/green ratio in HLECs after treatment with different EGCNPs concentrations.....	79
Figure 3-9 Effect of EGCNPs on ATP production in HLECs measured by luciferin-luciferase bioluminescent assay at 24 h and 48 h.....	81
Figure 3-10 Schematic representation of the steps employed for the quantification of DNA damage (genotoxicity) by the detection of phosphorylated histone variant H2AX.....	82
Figure 3-11 Effect of EGCNPs on DNA damage in HLECs (24 h) measured by immunocytochemistry through detection and quantification of pH2AX mean intensity.....	83
Figure 3-12 (a) Effect of different EGCNPs concentrations on caspase-3,7 activity in HLECs.....	85
Figure 3-13 Annexin V/Cytotox Red assay comparing non-treated (0 $\mu\text{g/ml}$) and EGCNPs-treated (400 $\mu\text{g/ml}$) HLECs over 24 h.....	87
Figure 4-1 Time dependent uptake of EGCNPs in HLECs.....	100
Figure 4-2 EGCNPs uptake in HLECs is endocytosis-dependent.....	103
Figure 4-3 SEM images showing uptake and localisation of EGCNPs in HLECs at different time points.....	105
Figure 4-4 EDX analysis HLECs compartments.....	106
Figure 4-5 Confocal images showing autofluorescence of human lens epithelial cells.....	107
Figure 4-6 Uptake and perinuclear localisation of unlabelled EGCNPs in HLECs.....	108
Figure 4-7 Uptake and perinuclear localisation of EuCNPs in HLECs.....	110
Figure 4-8 Mitochondrial localisation of EuCNPs observed by confocal microscopy.....	111

Figure 4-9 Live cell analysis of HLECs proliferation showing protective effect of EGCNPs against oxidative stress induced by H ₂ O ₂	113
Figure 4-10 Live cell analysis of HLECs pre-treated with EGCNPs for 24 h then treated with H ₂ O ₂ for 72 h.	115
Figure 4-11 EGCNPs protect against H ₂ O ₂ -induced oxidative stress in human lens epithelial cells (H ₂ DCFDA staining).....	117
Figure 4-12 Chemical structure of the catalase inhibitor 3-Amino-1,2,4-triazole (3-AT).	118
Figure 4-13 Dose and time dependent effect of the catalase inhibitor 3-AT on HLECs viability measured by the MTT assay.....	119
Figure 4-14 Catalase-mimetic activity of EGCNPs in HLECs. EGCNPs protect against damage induced by the catalase inhibitor 3-AT (100 mM).....	120
Figure 4-15 Effect of EGCNPs on GSH/GSSG ratio in HLECs.	122
Figure 4-16 Effect of EGCNPs (50 µg/ml) on GSH and GSSG concentrations in HLECs after 48 h exposure.	123
Figure 4-17 Effect of EGCNPs on the inhibition of the formation of advanced glycation end products (AGEs) for bovine serum albumin (BSA) when incubated with glucose (glu) for 72 h.....	125
Figure 4-18 Effect of EGCNPs on the inhibition of the formation of advanced glycation end products (AGEs) for bovine α-crystallin when incubated with glucose (glu) for 72 h.....	127

List of abbreviations

- ACF: Autocorrelation function
- AMP: Adenosine monophosphate
- ATCC: American Type Culture Collection
- ATP: Adenosine triphosphate
- ATR: Attenuated total reflectance
- DLS: Dynamic light scattering
- DMSO: Dimethyl sulfoxide
- DNA: Deoxyribonucleic acid
- EDX: Energy-dispersive X-ray spectroscopy
- EGCNPs: Ethylene glycol coated cerium oxide nanoparticles
- EMEM: Eagle's minimum essential medium
- EuCNPs: Europium-doped cerium oxide nanoparticles
- Ex/em: Excitation/emission
- FBS: Foetal bovine serum
- FTIR: Fourier transform infrared spectroscopy
- GC: Gas chromatography
- GSH: Reduced glutathione
- GSSG: Oxidised glutathione
- H₂DCFDA: 2',7'-dichlorodihydrofluorescein diacetate
- HLECs: Human lens epithelial cells
- ICP: Inductively coupled plasma
- KeV: Kilo electronvolt
- kV: Kilovolt
- MS: Mass spectroscopy
- MTT: 3-(4,5-Dimethylthiazol-2-yl)-2,5-diphenyltetrazolium bromide
- mV: millivolt
- PBS: Phosphate-buffered saline
- PPi: Inorganic pyrophosphate
- PTM: Post-translational modifications
- ROS: Reactive oxygen species
- RPMI: Roswell Park Memorial Institute
- SD: Standard deviation
- SEM: Scanning electron microscopy

- SOD: Superoxide dismutase
- TEM: Transmission electron microscopy
- TGA: Thermogravimetric analysis
- UV-Vis: Ultraviolet-visible spectroscopy
- XRD: Powder X-ray diffraction

Abstract

Chronic diseases are rising in incidence and prevalence because of the increase in life expectancy in many parts of the world and the advances in medicine that manage disease progression, rather than curing and alleviating the causes. Cataract is one such chronic condition. Identifying a therapeutic intervention that is successful in reversing or preventing cataracts may have applications for other chronic diseases of protein misfolding, such as diabetes and Alzheimer's disease as these have similar causation factors, notably oxidative stress and/or glycation. To date, surgery remains the only effective treatment for cataract and the search for alternatives is still ongoing. Cerium oxide nanoparticles (nanoceria) which have antioxidant, radioprotective and enzyme-mimetic properties have the potential to lead to an effective non-surgical treatment. However, nanoceria stability in physiological media is poor thus hindering their effective use in biomedical applications. In the work described in this thesis, a highly efficient one-pot synthesis of nanoceria (2–5 nm) has been achieved. The nanoparticles were coated with a novel hybrid coating (ethylene glycol, ethylene glycol mono- and di- acetates) providing the formulation with superior colloidal stability in physiological media. The ethylene glycol coated nanoceria formulation (EGCNPs), up to concentrations of 200 µg/ml, is not toxic to human lens epithelial cells and has no adverse effect on the cellular morphology, proliferation rate, mitochondrial morphology, mitochondrial membrane potential, ATP level, DNA integrity and basal reactive oxygen species (ROS) level. Exceeding the safe concentration of nanoceria leads to genotoxicity and apoptotic cell death mediated by ROS elevation and mitochondrial damage, a mechanism which is comprehensively investigated for the first time in human lens epithelial cells (HLECs). EGCNPs uptake in HLECs was found to be endocytosis-dependent and the nanoparticles localised extensively in the mitochondria. This localisation has enabled the nanoparticles to protect HLECs against oxidative stress, act as a catalase mimetic and increase reduced glutathione/oxidised glutathione ratio (GSH/GSSG). Furthermore, it is shown for the first time that these nanoparticles can protect lens proteins against glucose-induced glycation that is a major cause of cataract particularly in diabetics. Together, these results demonstrate great potential for nanoceria in protecting against cataract and should be taken to *in-vivo* studies.

1 Introduction

1.1 The human lens: structure and physiology

The human lens is positioned in the anterior segment of the eye behind the cornea and the iris (Figure 1-1). It is a biconvex structure within a semi-elastic basement membrane, the capsule to which are attached suspensory ligaments, collectively called the zonule that hold the lens in place and mediate the forces of shape change.¹ The main function of the eye lens is to refract image-forming light to the retina which transmits this information to the higher visual processes.² The ability of the lens to carry out its function requires transparency which can be ascribed to the organisation of its proteins, the crystallins.^{3,4} The crystallins are contained within long fibre cells arranged in layers. When these cells differentiate their nuclei and endoplasmic reticulum become pyknotic (*i.e.* irreversible condensation of chromatin in the nucleus) and move to the equatorial region away from the optics axis to prevent light scattering.^{3,4}

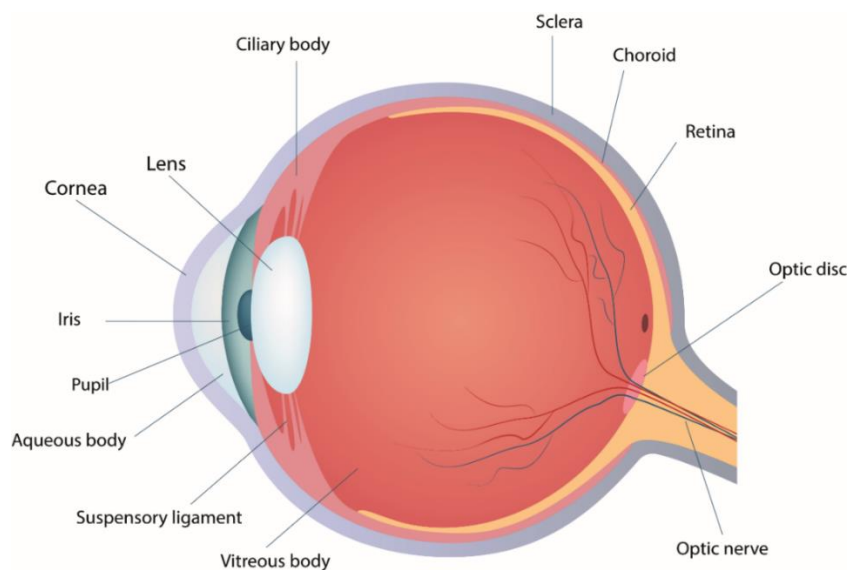


Figure 1-1 Cross section of the human eye.⁵

The human lens is a unique organ that continually grows over the lifetime of the individual by laying down new layers of fibres over existing cells without shedding any tissue.⁶ It weighs approximately 65 mg at birth, 160 mg at the age of 10 and continues to grow to about 250 mg by the age of 90.^{2,7} Its composition can be dissected into three main parts: the epithelium, the cortex and the nucleus all of which are enveloped in a capsular membrane (Figure 1-2).^{1,2} The function of each part is summarised in the following section:

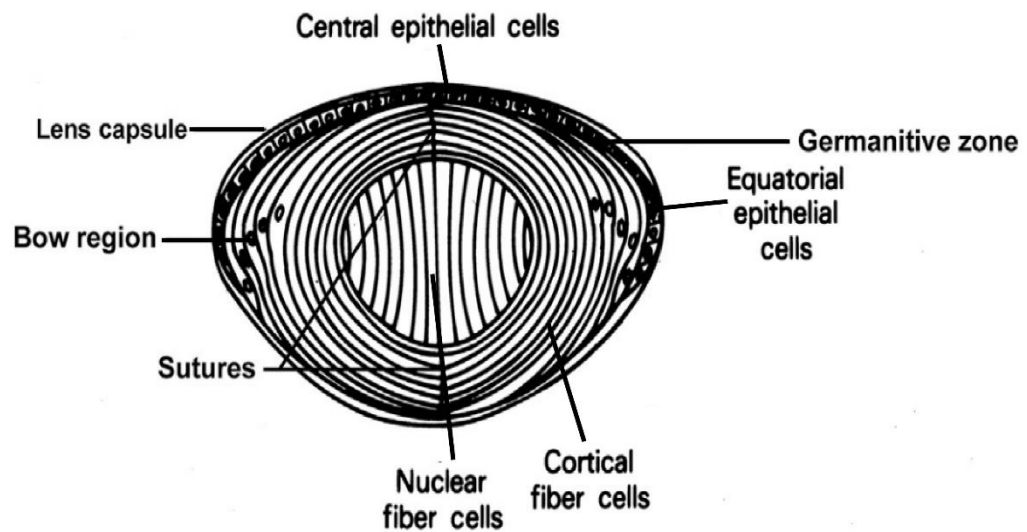


Figure 1-2 Cross section of the human lens.²

1.1.1 Lens capsule

The capsule is a collagenous base membrane that encases the lens structure and mediates forces from the ciliary muscle allowing the lens to alter its shape in the first four to five decades of life before it hardens and the lens loses accommodation for near and far vision.⁸ In humans, it is first detected at 5-6 weeks from pregnancy.² The elasticity of the capsular membrane plays an important role in the ability of the lens to change its shape, a process called accommodation to allow clear focus for near and far vision.⁹ Furthermore, the capsule acts as a diffusion barrier blocking the passage of infectious materials while maintaining healthy supply of essential nutrients such as glucose, amino acids and vitamin C.^{1,10}

1.1.2 Lens epithelium

The human lens epithelium is a monolayer of cuboidal cells located at the anterior part of the lens just below the lens capsule.¹¹ These cells are responsible for the majority of the metabolic activity of the lens including differentiation into the lens fibre cells that form the bulk of the lens.¹¹ The lens epithelium plays an important role in regulating the flow of nutrients, ions and antioxidants by virtue of having water channels (aquaporins) and sodium/potassium ATPase pumps within its structure.¹ Three different aquaporins AQP0, AQP1 and AQP5 are expressed in different regions of the ocular lens maintaining a microcirculation inside the lens.¹ Additionally, the lens epithelium actively synthesises important defence systems such as glutathione and ultraviolet filters (*e.g.* tryptophan derivatives protecting the lens from UV induced damage) which are transported into the lens cortex and nucleus protecting the lens against oxidative and radiative damage.¹² As such, The lens allows efficient light transmittance with wavelengths up to 1200 nm with very little transmittances for wavelengths below 390 nm.² The lens epithelial cells, contrary to their differentiated fibrous form in the cortex and nucleus, are rich with organelles and cytoskeletal proteins such as actin, α -actinin, myosin, microtubules, spectrin and vimentin which play their roles by maintaining the lens homeostasis and stabilising cell structure during vision accommodation respectively.¹³ The presence of tight junctions in the lens epithelium allows exchange of low molecular weight metabolites and ions.²

1.1.3 Lens cortex and nucleus

The lens epithelial cells differentiate into elongated fibre cells that are arranged in concentric layers to form the cortex and nucleus of the lens. There is no clear distinction between the cortex and nucleus as they have similar structure. These fibrous cells are predominantly made of crystallins proteins with increasing distribution towards the innermost part of the cortex creating a refractive index gradient. Therefore, the refractive index of the human lens

increases from 1.38 (73-80% water) in the cortex to 1.42 (68% water) in the nucleus.² These proteins are mainly made of the crystallins protein family α -, β - and λ - crystallins.¹⁴⁻¹⁸ The lens nucleus refer to the innermost part of the lens and its structure is similar to that of the cortex besides the fact that the cells are more tightly packed due to the accrual of cells overtime.¹⁹ The very limited extracellular space between the fibre cells is critical for maintaining the lens transparency.² Due to the lack of protein turnover or recycling in the lens, the its continuous growth and the formation of new cellular layers pushing the old layers inwards, the lens nucleus contains the oldest proteins in the body that exist at birth.²⁰

1.2 Lens development and homeostasis

The human lens epithelial cells are the metabolically active cells in the lens.¹¹ Some of these cells differentiate into elongated fibre cells and move towards the lens equator.^{1,2,11} The elongation into fibre cells can be quite significant reaching up to 1000 times in length compared to the lens epithelial cells.²¹ In the lens epithelium, the majority of the lens crystallins are synthesised. The differentiated fibre cells are formed on top of each other in concentric layers with a rate of one cellular layer per day where older layers are pushed towards the cortex and nucleus.²¹ This growth pattern of the layers creates a protein gradient where the oldest proteins are found in the nucleus and the newly synthesised ones are present in the epithelium.²¹

The absence of blood supply in the lens is compensated for by the presence of the aqueous humour in which the lens is bathed.²² The aqueous humour acts as a source of nutrients and antioxidants needed for the lens, in addition to a means of disposal of metabolites such as lactic acid.^{1,22} The in and out movement of nutrients and metabolites is regulated by water and ion channels which are positioned in both the lens epithelium and the cortex.²³ The aqueous humour is rich with antioxidants (*e.g.* ascorbic acid) which are trafficked into the

lens through molecular transporters. In the lens epithelium, glutathione (GSH), a major lenticular antioxidant, is synthesised and subsequently transported into the nucleus through gap junctions.²⁴ Contrary to GSH, ascorbic acid cannot be biosynthesised and has to be supplied exogenously.²⁵ These antioxidants are essential in providing the lens with protection against oxidative damage throughout life by deactivating reactive oxygen species (ROS).²⁶ This in turn provides the lens proteins with the necessary protection against post-translational modifications (PTMs) such as glycation and oxidation maintaining the lens transparency.²⁶

1.3 Aetiology of cataract: a human lens disorder

Cataract can be defined as the loss of the eye lens transparency causing opacification and resulting in the inability of the lens to properly focus light on the retina leading to blurred vision or complete blindness.^{21,22,26,27} Cataracts represent approximately half of the blindness cases worldwide with populations over 60 mainly affected.^{28,29} Although many factors have been associated with cataract, it is predominantly an age-related disorder where aging represents the major risk factor for its development.²⁶ This is commonly referred to as senile cataract. Cataract can also be less commonly caused by other factors such as trauma, infections, or as a congenital disorder.²⁹⁻³¹ Cataract can be subcategorised into three main types based on where the opacity develops. These are cortical, nuclear and posterior subcapsular cataracts.³² Subcapsular cataract presents the first signs of opacity under the lens capsule and have been associated with certain medications such as corticosteroids.²⁹ Cortical cataract develops in the lens cortex and is linked to diabetes.²⁹ Finally, nuclear cataract is the most common type of cataracts which develops in the lens nucleus and is strongly associated with age, hence its commonly referred to as age-related nuclear cataract (ARNC).²⁶

The loss of the lens transparency is thought to be caused by the aggregation of crystallins as the lens ages and this may be linked to a progressive loss of solubility of lens proteins.^{22,26,33–35} The formed aggregates in turn are thought to absorb and/or scatter light preventing it from being focused on the retina.³³ Aggregation of the lens proteins can be induced by a number of post-translational modifications such as glycation, oxidation, deamination, truncation, phosphorylation, racemisation and crosslinking.^{1,22,26,33} These changes occur very slowly over decades and affect different layers of the lens. Additionally, with ageing, the chaperone activity of α -crystallin decreases making the other structural proteins more susceptible to aggregation.^{35,36} α -crystallin is a known molecular chaperone with structural similarity to small heat shock proteins (sHsps) which inhibits protein aggregation by binding to intermediates that are generated during cellular stress or protein translational *in-vivo*.³⁷ Several studies have demonstrated that α -crystallin can prevent thermal aggregation of the lens proteins and enzymes.³⁵ Therefore, chaperones are deemed important for the control of the growth of human lens epithelial cells by preventing aggregation of key proteins during cell differentiation.³⁷

Oxidative stress is believed to be one of the major causes for protein modifications and inactivation in the human lens.³⁸ For example, crystallins can undergo truncation at C- and N- terminal which leads to pronounced effect on solubility and stability.²⁰ Many amino acids are also more prone to oxidation particularly tryptophan, cysteine and methionine. Oxidation of cysteine residues is particularly common in early stage cataract with more than 90% residues oxidised in late stages of progression.²⁰ Oxidation of proteins can also lead to the formation of disulphide insoluble species.²⁰ In the mitochondria, four electron reduction of oxygen (O_2) into water (H_2O) takes place to generate the necessary cellular energy in the form of ATP molecules, a process known as the electron transport chain.²¹ When oxygen is partially reduced, various reactive oxygen intermediates are generated which are commonly

known as reactive oxygen species (ROS).³⁸ These include superoxide (O_2^-), hydroxyl radicals ($\bullet OH$) and hydrogen peroxides (H_2O_2).³⁸ ROS can also be introduced from exogenous sources such as smoking, ionising radiation, diet and air pollutants.²¹ In particular, UV exposure is commonly thought to be one of cataract inducers especially after middle age because of its ability to induce oxidative stress.³⁹ The lens possesses natural UV filters such as the tryptophan derivatives, that with age, can be altered, lose their function, and potentially act as photosensitisers (*i.e.* an intrinsic source of ROS).¹³ Another common source of oxidative stress is diabetes, which accounts for 10-12% of extracted cataracts, where there is strong association between hyperglycaemia and ROS generation.⁴⁰ Therefore, sugars are frequently used experimentally to induce cataracts *in-vivo* and *ex-vivo*.^{41,42}

Under normal physiological conditions, the generated ROS are deactivated by the antioxidant defence systems present in the lens. The defence systems in the lens can be enzymatic or non-enzymatic.²⁹ Enzymatic antioxidants in the lens involve superoxide dismutase (SOD) that deactivates superoxide radicals, and catalases and peroxidases that break down hydrogen peroxide.³⁸ On the other hand, non-enzymatic antioxidants mechanisms include the presence of GSH and ascorbic acid.⁴³ The presence of these mechanisms ultimately protects the proteins from oxidative stress-induced protein damage.⁴³ In ARNC, however, these defence mechanisms weaken, and ROS generation exceeds the lens ability to neutralise them.^{21,22,26} ROS can then slowly damage the protein structure in the lens, and because of the lack of protein turnover, the damaged crystallins proteins will accumulate and aggregate over time causing the lens to lose its transparency.^{21,22,26} One prominent example of the weakened antioxidant system and its association with cataract development is the loss of GSH. The loss of GSH in the nucleus is evident in the majority of experimentally induced cataract.²⁶ The loss is mainly attributed to the oxidation of the active reduced form of glutathione (GSH) into the inactive oxidized form GSSG. It is also

notable that the lens normally functions in an environment where oxygen is tightly controlled.⁴⁴ This is reported to be necessary in preserving the lens transparency as experiments run in hyperbaric oxygen were shown to reduce GSH content and induce cataract formation.⁴⁵

1.4 Who is affected? Statistics on cataract

Cataract is the leading cause of blindness worldwide and it is primarily a disease of the elderly given that 95% of cataracts are senile.⁴⁶ The recent advances in medicine and healthcare services have led to an increase in the average lifespan worldwide. This unsurprisingly has led to higher number of people who develop cataract during their lifetime. In 2010, global figures estimated that approximately 11 million people were blind due to cataract while 35.1 million were visually impaired.^{47,48} In the UK, visual impairment is prevalent with cataract accounting for one third of the cases.⁴⁷ It is estimated that 30% of people aged 60 and above are visually impaired in one or both eyes because of cataract.⁴⁷ In England, approximately 400,000 cataract surgeries were performed annually by the NHS in 2015.⁴⁷ This number is projected to increase by 50% by 2035.⁴⁷ In the US, 24 million people aged over 40 are affected by cataract and half of Americans aged 80 develop cataract.⁴⁶ The annual spending on cataract treatment in the US amounts to \$10.7 billion which include the cost of diagnosis, surgery, vision aids and other associated medical interventions.⁴⁶

1.5 Cataract Surgery

To date, surgery remains the only effective treatment for cataract once it develops.²⁷ Cataract surgery involves the removal of the cataractous lens and replacing it with an intraocular lens implant that is positioned inside the capsular membrane.⁴⁹ Phacoemulsification is currently the standard surgical technique for cataract worldwide and represent 99.7% of cataract

operations performed in the NHS.⁴⁶ The process involves the emulsification of the affected lens by ultrasonic waves and subsequently aspirating the lens as a fluid.⁴⁹ Other forms of surgeries are intracapsular, extracapsular and manual small incision cataract extraction.⁴⁹ Although cataract surgeries are highly successful, the procedure still comes with complications such as posterior capsular opacification (PCO), capsular tear, endophthalmitis and retinal detachment.⁴² PCO is an abnormal growth of the remaining epithelial cells on the posterior capsular membrane after surgery; often referred to as secondary cataract which, in many cases, requires further surgical intervention.⁵⁰ Additionally, to date there is no single implant model that can replicate the image quality and the capacity to alter focus of the biological lens.⁵¹ A significant drawback to surgery is its limited accessibility in the developing countries and the long waiting times in the developed world as the demand on surgery increases which adversely impacts the quality of life for the waiting patients.⁵² For these reasons, there is a growing interest in developing a therapeutic means of reversing, or at least halting, the progression of cataracts. It has been predicted that delaying the onset of cataract by 10 years would result in decrease in surgery need by 50%.^{29,53}

1.6 The current treatments and the prospects of future medications

To date, there is no pharmacological treatment to reverse cataract, but efforts have been made to search for new therapeutics that can delay its onset. Delaying cataract progression can have positive impact on both the patients' quality of life and the cost of healthcare spent on cataract treatment. The availability of surgery alternative will alleviate the burden on healthcare services and increase the affordability of cataract treatment worldwide. Over the past few decades, many drugs were proposed as potential cataract treatments with a great

emphasis on the relief of oxidative stress as a means of halting the progression of the disease. In the following sections a summary of the most common proposed drugs will be discussed.

1.6.1 Carnosine

L-Carnosine is a naturally occurring dipeptide (β -alanyl-L-histidine) that has been recently marketed for cataract prevention in the form of a prodrug N-acetylcarnosine (NAC) as 1% eye drops.⁵⁴ The drug is commercially available under the name Can-C™ that is intended for eye lubrication with the marketed off-label benefit of cataract prevention.⁵⁵ NAC is more soluble than the parent compound and can pass through the cornea before being metabolised in the aqueous humour by carnosinase into active L-carnosine.⁵⁴ *In-vitro* and *in-vivo* studies have shown that L-carnosine is a powerful water-soluble antioxidant and prevent against cell membrane lipid peroxidation.²⁷ Babizhayev *et al.* carried out an experiment in which NAC was used as eye drops in 50 canine eyes and compared the results to 40 control eyes after 6 months of treatment.⁵⁶ The results obtained from slit image and retro-illumination photographs showed improvement in the lens clarity in 96% of the treated eyes.⁵⁴ A randomised double-blind clinical trial of NAC was performed on 49 patients with an average age of 65 where they received NAC eye drops twice a day or a placebo.⁵⁷ The eyes were assessed on several criteria such as best corrected visual acuity (BCVA), glare sensitivity, and lens clarity based on slit image and retro-illumination photographs. After 6 months of treatment, 90% of the NAC treated group showed BCVA improvement, 89% showed glare sensitivity improvement and the clarity of the treated lens improved in 42% of treated eyes. Similar results were also obtained after 2 years of NAC treatment.⁵⁷ Although the results were promising, many limitations were noted for the study including the limited number of patients, low statistical power, and being carried at two-different time points where many patients dropped out of the trial at the latest point (45%). However, in another *in-vitro* study carried out on cultured porcine lenses, L-carnosine was shown to have no or limited

antioxidant activity.⁴² The study also showed that it does not protect human lens epithelial cells against hydrogen peroxide induced oxidative stress.⁴² The study finally concluded that L-carnosine is more of an anti-glycating agent than an antioxidant one and warned of L-carnosine's potentially damaging effects to the glutathione system if used in normal glucose levels.⁴²

1.6.2 Multivitamins

Some vitamins such as ascorbic acid and vitamin E are known for their protective roles in preventing protein aggregation in the lens by the inhibition of formation of protein disulphide bonds.²⁷ *In-vitro* studies showed that ascorbic acid was able to protect rat lenses against oxidative stress. Similarly, *in-vivo* experiments on diabetic rats, which notably have a different complement of crystallins to humans, showed significant delay in cataract progression when their diet was supplemented with 1% ascorbate.⁵⁸ Robertson *et al.* showed that decreased self-reported consumption of ascorbic acid or vitamin E correlated with high incidence of lens opacity in 175 patients aged over 55.⁵⁹ Another non controlled prospective study found that patients who took multivitamins experience less cataract risk after a five years period.⁶⁰ However, blood levels of vit E and ascorbate linked poorly with cataract progression. A clinical trial concluded that long term use of antioxidant supplements is of limited benefit in populations with balanced diet.⁶¹ Vitamin E, Cataract, and Age-Related Maculopathy Trial (VECAT) carried out on 1193 patients that daily consumption of vitamin E (500 IU) did not inhibit the progression of any of the three main cataract types.⁶²

1.6.3 Aspirin, paracetamol and ibuprofen

Aspirin was first noted to delay cataract progression from a study intended to treat rheumatoid arthritis in diabetics.⁶³ Subsequent experiments showed some evidence of aspirin and other analgesics in protecting against cataract. Aspirin was shown to provide *in-vitro* protection of rat lenses against lens opacity induced by cyanates.⁶⁴ An *in-vivo* study showed

that aspirin, paracetamol and ibuprofen counter the progression of cataract in diabetic rats.⁶⁵ It is not currently known how these analgesics delay cataract development and several mechanisms have been suggested. Aspirin like drugs are known for their blood thinning actions which may improve the blood flow providing the lens with more nutrients and antioxidants.¹ Aspirin (acetyl salicylic acid) is an acetylating agent which could in turn acetyl proteins protecting them from being modified by cyanates, steroids or glucose.⁶⁶ Aspirin was suggested to have an indirect effect of increasing GSH concentrations in the lens.⁶⁶ A study carried out on 909 patients in England reported that the risk in cataract progression is halved in the group treated with aspirin and aspirin like drugs.⁶⁷ That being said, other studies failed to find a relationship between aspirin and protective effects against cataract.⁶⁸ One significant disadvantage of aspirin therapy is that it requires the use of large oral doses (1.5 g/day) to achieve significant cataract protection.¹ This undoubtedly poses great risk for developing the common non-steroidal anti-inflammatory drugs (NSAIDs) associated side effects such as gastritis, peptic ulcers, renal failure and cardiovascular diseases. Even the topical application of such drugs is associated with adverse effects of burning sensation, corneal defects, conjunctival hyperaemia and corneal melt.^{69,70} This renders the use of such drugs for long term, that is needed for cataract prevention, highly problematic. Another discouraging factor is the lack of incentive for pharmaceutical companies to carry out long term studies on the efficacy and safety of such drugs as most of these are out of patent.⁷¹

1.6.4 Lanosterol

Perhaps one of the most interesting and potentially paradigm shifting results was the studies carried out by Zhao *et al.* and Makley *et al.* on lanosterol and similar sterols.^{72,73} In these studies, lanosterol was reported to have the ability to reverse cataract by dissolving protein aggregates and amyloid-like fibril proteins in *in-vivo* and *ex-vivo* animal models with congenital cataracts. This was attributed to the ability of lanosterol to bind to α -crystallin

and enhance its chaperone like activity. Subsequent studies were carried out expanding the results on different mouse models developing congenital cataracts.^{74,75} Lanosterol was subsequently marketed in the form of eye drops for cataract treatments. However, recent studies on these compounds reported the inability of lanosterol to reverse cataract in various experimental models. In one study, 40 human lenses developing senile cataract were incubated for six days in 25 mM lanosterol solution and the results showed no effect of the compound on reversing cataract.⁷⁶ A study carried out on a single patient with juvenile nuclear cataract failed to show any improvement after administering lanosterol eye drops (5 mM) for 8 weeks.⁷⁷ Furthermore, a very recent study showed that lanosterol liposomes (15 mM) failed to reverse or delay the progression of cataract in *in-vitro* rat lenses against induced cataracts.⁷⁸ Together these results show that it is still early to conclude whether lanosterol and related compounds provide any benefit in the realm of cataract treatment.

1.7 Nanotechnology for cataract

Nanotechnology is rapidly developing for the diagnosis and treatment of a plethora of diseases including ocular diseases.⁷⁹ This is attributed to the extraordinary ability of nano systems to control the delivery and release of various drug entities hence significantly enhance the pharmacokinetics and pharmacodynamics of therapeutics.⁷⁹ Nano systems can harbour multiple drugs in the same time and their surface can be modified with ligands that have various functionalities.⁷⁹ Research on the use of nanotechnology for cataract treatment has been mainly focused on enhancing lens penetration, retention and release profiles of antioxidants and other drugs known for their potential to delay cataract. In that sense, nano systems in the field of cataract prevention and treatment were more of vehicles or vectors to deliver other entities. Cetinel and Montemagno have reviewed the use of several polymeric (*e.g.* PLGA nanoparticles) and lipidic (*e.g.* liposomes) nano systems in enhancing the bioavailability or efficacy of antioxidants and molecular chaperones in various cataract models.⁸⁰ In the following sections, the potential of one type of nanoparticles to act as a therapeutic on its own rather than just a vehicle for other drug entities is discussed.

1.8 Cerium oxide nanoparticles (nanoceria) as a potential cataract therapeutic

Cerium (Ce) is one of the lanthanides or rare earth metals positioned in the f-block of the periodic table.⁸¹ The chemistry of lanthanides is unique because of the presence of 4f electrons that are sandwiched between 4d and 5p electrons isolating them from the atom's environment.^{81,82} This configuration provides lanthanides with exclusive electronic, catalytic and magnetic properties that are not found in other metals. Such properties are currently heavily explored and used in various industrial applications such as magnets production,

electric motors, LCDs, surface polishing, catalysis, diagnostics, radiation therapy, biosensing, and bioimaging.⁸²

Cerium, which is the first element of rare earths with 4f electrons, has garnered great attention for its versatility of use in various biological, chemical and material science applications. The oxidation of cerium creates cerium oxide (CeO₂) crystals with a face centred cubic fluorite structure which possesses remarkable redox and catalytic properties.⁸¹ These properties have already been utilised in various applications in diverse products such as solar cells,⁸³ oxygen sensors,⁸⁴ catalysis,⁸⁵ UV filters,⁸⁶ and polishing.⁸⁷ Cerium oxide (CeO₂) nanoparticles or “nanoceria”, have also shown potential for the treatment and prevention of various disorders including cancers,⁸⁸ inflammatory diseases,⁸⁹ neurodegenerative disorders,⁹⁰ retinopathy,⁹¹ and cardiovascular dysfunctions⁹² owing to the nanoparticles’ powerful antioxidant activity.

1.8.1 Synthesis of cerium oxide nanoparticles

Cerium oxide nanoparticles can be synthesised using various techniques such as aqueous co-precipitation, hydrothermal decomposition, solvothermal decomposition, electrochemical deposition, flame spray, sol-gel, and micellar or microemulsion synthesis.^{93–96} In these methods, various parameters can be systematically altered to control the size, shape, surface charge, and the coating material of the produced nanoparticles which significantly alters their behaviour. Therefore, the choice of the synthesis method is critical for fitting the intended application. For example, aqueous synthetic methods are more suitable for producing nanoparticles for use in aqueous media.

1.8.2 Cerium oxide structure and redox properties

The potential cerium oxide nanoparticles have shown in treating various medical conditions can be attributed to their remarkable redox and antioxidant properties. In CeO₂ crystals,

cerium atoms can exist in two different oxidation states; reduced (Ce^{3+}) and oxidised (Ce^{4+}).⁹⁷ The oxidised state is the preferred stable form in the crystal structure of cerium where each cerium atom is coordinated with eight neighbouring oxygen atoms, and each oxygen atom is coordinated with four neighbouring cerium atoms.⁹⁸ However, surface defects are normally present on the surface of the crystals and these are associated with Ce^{3+} existence (Figure 1-3). The decrease in the positive charge is compensated by the arising of oxygen vacancies on the crystal surface. It is now known that the smaller the particle size of CeO_2 nanoparticles, the higher the number of defects and the higher $\text{Ce}^{3+}/\text{Ce}^{4+}$ ratio.⁸¹ Such ratio can be studied by means of X-ray photoelectron spectroscopy and UV–visible absorption spectroscopy.⁸¹

The co-existence of Ce^{3+} , Ce^{4+} and O_2 vacancies in the same crystal lattice enables the nanoparticles to act in a versatile way in redox reaction as either an oxidiser or a reducer depending on the environment. In another words, the electronic configuration of cerium can alternate between Ce^{3+} and Ce^{4+} to best fit the environment.⁸¹ When CeO_2 loses oxygen in the process of forming surface Ce^{3+} , the formed crystal retains its original fluorite structure and is often referred to as CeO_{2-x} where x is the number of oxygen vacancies.⁹⁸

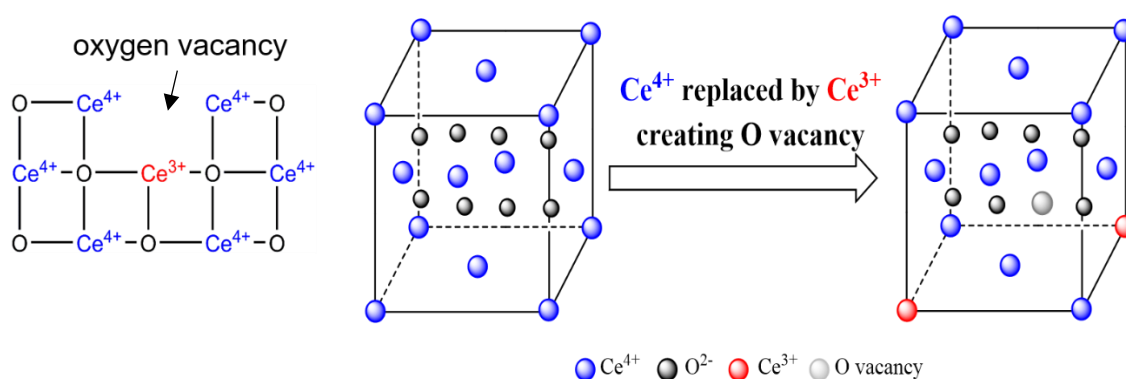
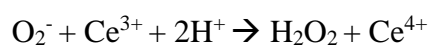
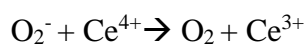


Figure 1-3 Cerium oxide crystal structure.⁹⁹

1.8.3 Cerium oxide multi-enzyme mimetic properties

Cerium oxide nanoparticles redox properties have been found to mimic key natural antioxidant enzymes such as superoxide dismutase (SOD) and catalase.^{100,101} SOD converts superoxide into H₂O₂ and water. A study has shown that this activity could be achieved *in-vitro* by CeO₂ nanoparticles owing the ease of transition between Ce⁴⁺ and Ce³⁺ valence states and a mechanism was proposed as shown in the following equations:¹⁰¹



A more elaborative mechanism for superoxide dismutation by CeO₂ has been subsequently proposed by Celardo *et al* (Figure 1-4).¹⁰² The catalytic rate of this reaction exceeds that known for SOD itself.¹⁰¹

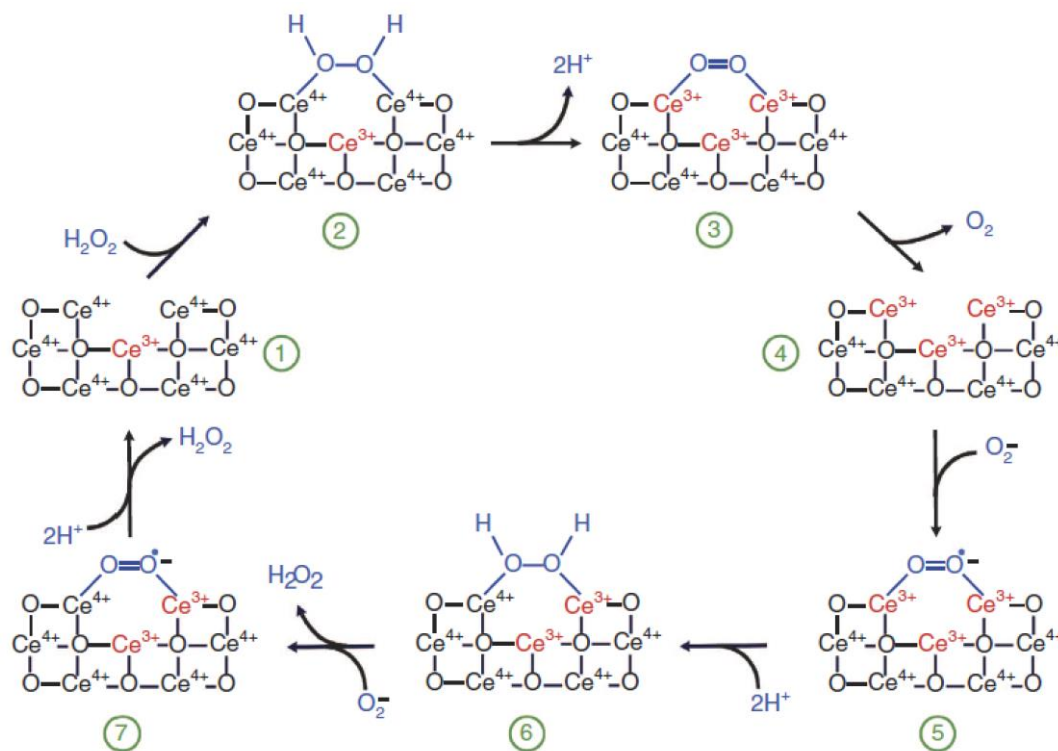
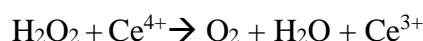
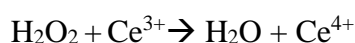


Figure 1-4 Proposed mechanism of superoxide dismutation by cerium oxide.¹⁰²

Similarly, CeO₂ nanoparticles were shown *in-vitro* to mimic catalase activity that is known for breaking H₂O₂ into oxygen and water. A mechanism has been proposed as follows:¹⁰³



In-vitro testing has shown that SOD activity is associated with higher Ce³⁺/Ce⁴⁺, while catalase-mimetic activity is more pronounced with higher Ce⁴⁺/Ce³⁺ ratio.^{81,100,101} It is noteworthy that the SOD activity of CeO₂ nanoparticles generate H₂O₂ which is more lethal for the cells compared to superoxide.¹⁰⁴ However, the generated H₂O₂ can enter the catalase cycle of CeO₂ and this damage is often negated. This makes the nanoparticles powerful antioxidants with the ability to nullify multiple kinds of ROS simultaneously. Various studies have shown the effect of many factors such as particle size, buffer species and pH on

the enzymatic activity of CeO₂ nanoparticles.⁸¹ One of the most biologically relevant factors is the presence of phosphate buffer that is reported to increase the catalase activity and decrease SOD activity.¹⁰⁵ This has to be considered given that the use of such buffers is ubiquitous in *in-vitro* and *in-vivo* studies. In addition to these enzyme mimetic activities, CeO₂ has shown that it is able to scavenge for multiple ROS and reactive nitrogen species (RNS) such as hydroxyl radical and nitric oxide radical (as reviewed).⁸¹

1.8.4 Cerium oxide for oxidative stress-related diseases

The versatility of cerium oxide nanoparticles in scavenging for multiple ROS makes them superior to traditional antioxidants or enzymes whereas the latter often scavenge for a single kind of free radicals. This, in addition to the nanoparticles being able to recycle themselves, has encouraged researchers to investigate the use of the nanoparticles for the treatment of oxidative stress related conditions.⁸¹ The nanoparticles have shown promising results *in-vivo* and *in-vitro* in many of these diseases such as Parkinson's disease, Alzheimer's disease, cardiovascular diseases and diabetes where oxidative stress is reported to play a major role in their progression.^{92,106,107}

Additionally, cerium oxide nanoparticles have also shown promise in retinal diseases where photoreceptor cells have the highest oxygen consumption rate of any cells in the body and are constantly exposed to hazardous effects of oxidative stress and incident photons. The retinal diseases associated with oxidative stress include retinal detachment, diabetic retinopathy, and macular degeneration which can lead to partial or complete blindness.⁸¹ Chen *et al.* have shown in *in-vitro* and *in-vivo* experiments that cerium oxide nanoparticles protect against retinal degeneration induced by peroxides and hence protect the retinal morphology and function.¹⁰⁸ The protection mechanism was attributed to the ability of cerium oxide nanoparticles to decrease ROS levels and upregulate the expression of neuroprotective genes.¹⁰⁸

Despite the promising results of cerium oxide nanoparticle in the treatment of oxidative-stress related conditions, their use in cataract treatment remains largely unexplored. Pierscionek *et al.* have shown that negatively charged cerium oxide nanoparticles (5.5 nm) are not genotoxic in human lens epithelium when used with very low concentrations: 5 and 10 $\mu\text{g/ml}$.¹⁰⁹ However, their potential to provide anti-cataractogenic properties was not further investigated and hence requires further study.

1.9 Project aims

Finding an alternative for surgery will create a new dawn for cataract: the main cause of blindness worldwide. So far, surgery remains the only effective treatment which suffers from perioperative and postoperative complications, limited accessibility to patients in the developing world and the increased economic burden on health services as the aging population is increasing.

The aim of this project is to thoroughly investigate the potential of cerium oxide nanoparticles (nanoceria) to provide anti-cataractogenic effects *in-vitro*. To achieve this the following objectives were set:

- 1- To synthesise CeO₂ nanoparticles and optimise their properties for biomedical applications. For this, various considerations have to be taken into account. The size, the coating and the aqueous stability in biological media have to be optimised to ensure consistency of the results in subsequent biological testing. A strategy to fluorescently label the nanoparticles for biological imaging studies is needed with minimal alterations to the nanoparticles' properties.
- 2- To thoroughly investigate the safety and toxicity of the optimised nanoparticles in the metabolically active cells of the lens: the human lens epithelium. Various cellular parameters in response to different concentrations of the nanoparticles will be assessed for the first time. These include cellular proliferation, cell morphology, cell membrane integrity, mitochondrial morphology, mitochondrial membrane potential, cellular ATP level, basal ROS level, caspases activation, and cell membrane asymmetry.
- 3- To study the uptake, its mechanism and subcellular localisation of the nanoparticles in the lens epithelial cells.

- 4- To study if these nanoparticles provide anti-catarctogenic effects in the human lens epithelial cells. Protection against induced oxidative stress will be studied in addition to the ability of the nanoparticles to mimic the catalase enzyme in the cells. The effect of the nanoparticles on glutathione will be investigated. Finally, the ability to block one of the major post-translational modifications in cataracts, glycation, will be studied *in-vitro*.

2 Development of cerium oxide nanoparticles for biomedical applications

2.1 Introduction

Cerium oxide (CeO₂) nanoparticles “nanoceria” are rare earth metal oxides with multiple applications across diverse applications such as solar cells,⁸³ oxygen sensors⁸⁴, catalysis,⁸⁵ UV filters,¹¹⁰ and surface polishing.⁸⁷ Biomedically, nanoceria have been investigated over the last decade, and have shown potential for the treatment and prevention of various disorders including cancers,⁸⁸ inflammatory diseases,⁸⁹ neurodegenerative disorders,⁹⁰ retinopathy,⁹¹ and cardiovascular dysfunctions.⁹² The therapeutic effects of CeO₂ nanoparticles are attributed to their antioxidant properties and their capability to eliminate reactive oxygen species (ROS).⁸¹ These antioxidant attributes originate from the presence of surface crystal defects and their associated oxygen vacancies allowing cerium ions to co-exist in and transition between trivalent and tetravalent states (Ce³⁺ and Ce⁴⁺), a transition that is dependent on the ambient environment.^{81,111} This enables nanoceria to mimic key antioxidant enzymes such as catalase and superoxide dismutase. Hence, in order to maximise the antioxidant activity of nanoceria the number of surface defects has to be increased leading to concomitant increase in the surface Ce³⁺ and oxygen vacancies.¹¹² This can be achieved by reducing the particle size of the nanoparticles which gives rise to a fundamental problem namely aggregation. Aggregation is caused by the increase in the surface energy of the nanoparticles leading to excessive inter-particle interactions such as van der Waals forces.^{88,113} In addition to the loss of activity induced by the reduced surface area, aggregation results in a formulation with poor colloidal stability causing sedimentation of the nanoparticles in physiological media. Consequently, this leads to exposure of cellular

monolayers to a higher concentration than the stated bulk concentration, and so compromising the reliability of *in vitro* experiments.¹¹⁴ Efficient dispersibility of nanoparticles in media is therefore of paramount importance in order to draw accurate conclusions about the biological effects of the employed nanoparticle concentrations. Unfortunately, many of nanoceria formulations employed in biomedical studies reported in the literature are conducted on poorly characterised formulations where proper colloidal stability evaluation is lacking. This in turn leads to conflicting data when therapeutic and toxicological evaluations of nanoceria are concerned. Hence, in this study the aim was to aqueously produce thoroughly characterised nanoceria with a well-defined small particle size and proper colloidal stability before studying them *in-vitro*. Coating nanoceria with different materials has been shown to improve colloidal stability through minimising surface attractive interactions.¹¹³ However, this is often accompanied by drastic changes in particle size, surface charge, the use of biologically incompatible coatings, complex multistep synthesis, organic synthetic routes, in addition to the lack of sufficient colloidal stability data of the functionalised nanoceria.^{112,113,115}

In this chapter, the successful formulation and characterisation of aqueously monodisperse and ultrasmall (< 5 nm) nanoceria coated with ethylene glycol and ethylene glycol acetates (EGCNPs) is described using a simple, aqueous and scalable one pot co-precipitation reaction. Ethylene glycol was chosen as a coating material because of its safety, hydrophilicity, biocompatibility, and low cost making it a suitable coating material for biological use.¹¹³ The formulation demonstrated superior colloidal stability in aqueous solution and the nanoparticles were readily dispersible from dried powder with mild agitation. Finally, unique multi-coloured photoluminescence properties of the nanoparticles across the visible light spectrum are reported, and the photoluminescent properties were enhanced by europium doping to facilitate biomedical imaging studies.

2.2 Materials and methods

2.2.1 Synthesis of cerium oxide nanoparticles

Ethylene glycol coated cerium oxide nanoparticles (EGCNPs) were formulated using a modified alkaline precipitation method.¹¹³ Briefly, cerium(III) acetate hydrate (20 mmol, 6.3 g, Sigma Aldrich, UK), ethylene glycol (10 ml, 99.99 % purity, Fisher Scientific, UK), and HCl (0.2 ml, 1 M, Fisher Scientific, UK) were added to distilled water (100 ml), and left to homogenize (15 min at 40°C). Ammonia solution (35%, Fisher Scientific, UK) was then added dropwise until the pH reached 9.6 and a pale-yellow precipitate was immediately formed. This initial precipitate turned dark purple after stirring (*ca.* 10 min). The reaction was left stirring for 2 h and a colour change to pale yellow was observed. The reaction mixture was diluted with ethanol (50 ml, Fisher Scientific, UK), and the precipitate was then collected by centrifugation (1500 rcf, 5 min), washed with distilled water (50 ml x 2) and ethanol (50 ml x 1) and left to dry in an oven at 60°C for 12 h. After drying, the precipitate was ground into fine powder in an agate mortar and stored in an airtight container. For comparison, non-coated cerium oxide nanoparticles were prepared as before without the addition of ethylene glycol to the reaction mixture. Europium-doped nanocerium (EuCNPs) were synthesized as above by adding europium nitrate (99.99 %, Sigma Aldrich, UK) to the initial reaction mixture with a Ce : Eu molar ratio of 1:0.2.¹¹⁶

2.2.2 Transmission electron microscopy (TEM)

TEM was used to determine the morphology and particle size of the nanoparticles (EGCNPs and EuCNPs). The nanoparticles were suspended in distilled water (1 mg/ml) and sonicated for 5 min. 50 µL of the suspensions were placed on holey carbon coated 300 mesh copper grids (Agar Scientific, UK), left to dry and visualised using TEM operating at 200 kV (Jeol-2010, Japan). The average particle size was determined by measuring the diameter of 100

particles from different spots on the grid using ImageJ software (National Institutes of Health, USA).

2.2.3 Powder X-ray diffraction (XRD)

The crystalline structure of the powder EGCNPs nanoparticles was determined from the diffraction spectra obtained using a powder X-ray diffractometer (X'Pert PRO, PANalytical, UK) which operated with Cu $K\alpha_1$ radiation source ($\lambda=1.5406$) at 30 mA and 40 kV at continuous scanning mode. The scan range operated from 20 - 70 (2θ) with a step size of 0.017° and scan step time of 50.16 seconds. EGCNPs crystallite size (d_{XRD}) was calculated from the characteristic diffraction peak (1 1 1) using the Scherrer equation⁶:

$$d_{\text{XRD}} = \frac{0.94\lambda}{\text{FWHM} \cos \theta}$$

where λ is the x-ray radiation wavelength, θ is the Bragg diffraction angle for (1 1 1) plane, and FWHM is full width half maximum of the diffraction peak at (1 1 1).

2.2.4 Ultraviolet-visible spectrophotometry (UV-vis) and fluorescence studies

UV-vis absorption spectra of diluted nanoparticles water dispersions were obtained using a spectrophotometer (Cary 8454 UV-Vis, Agilent, USA) operating at wavelengths between 200 - 800 nm with 1 nm resolution. The suspensions were measured in quartz cuvettes (1 cm, Agilent, USA) and distilled water was used as a blank. Emission and excitation spectra of EGCNPs and EuCNPs in water were measured in a flat-bottom black 96-well plate using a spectrofluorometer (Clariostar, BMG Labtech, Germany). Fluorescence images of EGCNPs dry powder placed on glass slide was acquired using confocal laser scanning microscopy (Leica, Germany) using 20x dry objective and appropriate excitation laser lines and emission filters. Fluorescence microscope images of EuCNPs using RFP-compatible settings (excitation at 531 nm/40 nm, emission at 593 nm/40 nm) using EVOS FL epifluorescence microscope (Thermo Fisher, UK).

2.2.5 Fourier-transform infrared spectroscopy (FTIR)

Fourier transform infrared-attenuated total reflectance (FTIR-ATR) spectra were acquired using Cary 630 FTIR spectrometer (Agilent, USA). The dry nanoparticles were placed on the diamond ATR and measurements were taken between 650 and 4000 cm^{-1} with a resolution of 4 cm^{-1} . Eight sample scans were performed for each sample.

2.2.6 Scanning electron microscopy-energy dispersive x-ray spectroscopy (SEM-EDX)

SEM-EDX (Jeol JSM-7100f, Japan) was used to identify the elemental composition of the prepared nanoparticles. A thin layer of dry nanoparticles was spread on a carbon tape placed on an aluminium stub (13 mm in diameter) and examined using the secondary electron detector with an accelerating voltage of 10-15 kV and working distance of 10 mm. The spot size was adjusted so that the dead time was between 30 – 60%. No sample coating was required. EDX spectra were acquired and processed using Aztec software (version 2011, Oxford Instruments, UK).

2.2.7 Thermogravimetric analysis - gas chromatography – mass spectrometry (TGA-GC-MS)

The amount and composition of the surface coating of the nanoparticles were confirmed by thermogravimetric analysis (TGA 4000, PerkinElmer, USA) connected to a gas chromatography-mass spectroscopy system (GC Clarus 580 – MS Clarus SQ 8S, PerkinElmer, USA). Briefly, 16 mg of the nanoparticles were weighed in a TGA crucible and heated from 30 °C to 700 °C with a heating rate of 20 °C/min and gas flow of 30 ml/min. GC-MS sampling was set to be triggered after 9.5 min from the start of the run (at 200 °C).

2.2.8 Dynamic light scattering (DLS) and zeta potential

A stock water dispersion of the nanoparticles was prepared (5 mg/ml) and sonicated for 10 min at room temperature. The dispersion was then diluted to a final concentration of 400 µg/ml in distilled water, phosphate buffer saline (PBS) or Eagle's minimum essential medium (EMEM) supplemented with foetal bovine serum (FBS, 20%) and pH was maintained at 7. The diluted solutions were then placed in disposable plastic cuvettes or quartz zeta flow cell for particle size analysis or zeta potential measurements respectively. The particle size and zeta potential measurements were taken using dynamic light scattering (DLS) (Nanoplus, Particulate Systems, USA) at 25 °C. Each DLS measurement consisted of 20 accumulations. For zeta potential measurement, the Smoluchowski equation was employed to convert the electrophoretic mobility to zeta potential as follows:

$$\text{Electrophoretic mobility} = \frac{\epsilon_r \epsilon_0 \zeta}{\eta}$$

Where ϵ_r is relative permittivity/dielectric constant, ϵ_0 is permittivity of vacuum, ζ is zeta potential and η is viscosity at experimental temperature. All measurements were done in triplicates and the data is represented as mean \pm standard deviation (SD)

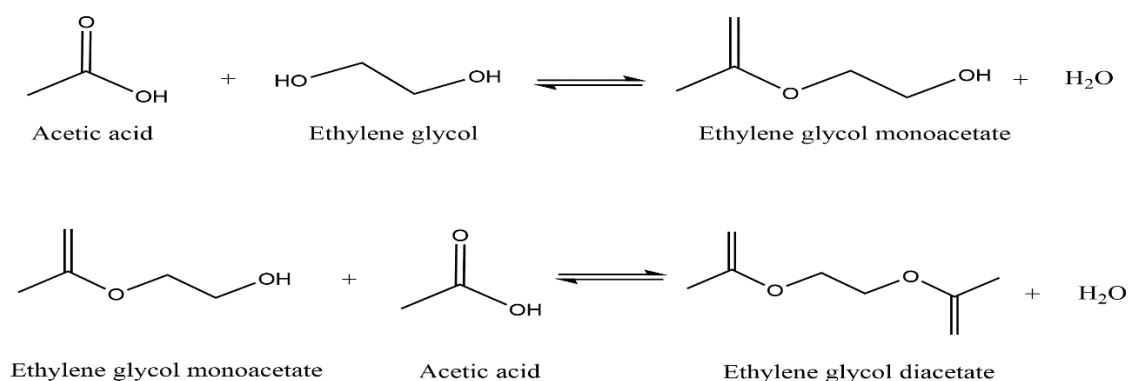
2.2.9 Colloidal stability and sterilisation

The colloidal stability (*i.e.* the resistance of the nanoparticles against precipitation in solution) of EGCNPs and non-coated nanoceria was measured by allowing nanoparticle dispersions (400 µg/ml) to settle over 7 days at room temperature. The concentration of the nanoparticles in the supernatant was measured each day using a spectrophotometer (Cary 8454 UV-Vis, Agilent, USA) at 300 nm. The nanoparticles were sterilised by filtration through 0.22 µm syringe filters (Millipore, USA). The amount of the nanoparticles lost in the filtration process was measured spectrophotometrically at 300 nm.

2.3 Results and discussion

2.3.1 EGCNPs morphology and crystallinity (TEM and XRD)

Ethylene glycol has the ability to complex with Ce^{3+} ions through coordination bonds with the hydroxyl (OH) groups, making the reaction homogenous for the ensuing ammonia precipitation step.^{113,117} Coating nanocerium with ethylene glycol starting from a nitrate precursor has been reported previously to produce relatively large particle sizes (> 10 nm) and significant polydispersity due to aggregation in both water and cell culture media that adversely impact biomedical applications.¹¹³ The ability to produce water dispersible ultra-small (< 5 nm) nanocerium is desirable as the size reduction with concomitant high surface to volume ratio increases both ROS deactivation capacity and regenerative properties of nanocerium.^{100,103} Furthermore, smaller particle size provides better penetration into the cells compared to their larger counterparts.¹¹⁸ To obtain nanoparticles with these desirable properties, a modified synthetic process was employed where cerium(III) acetate hydrate was used as a starting precursor in an alkaline precipitation reaction. In this reaction, the acetate ligands esterified ethylene glycol forming monoacetate and diacetate derivatives as part of the coating according the following equations:



The produced formulation is referred to ethylene glycol and ethylene glycol acetates-coated nanoceria (EGCNPs).

The morphology, particle size and crystallinity of EGCNPs were investigated using a transmission electron microscope (TEM). TEM micrographs of EGCNPs (Figure 2-1a and Figure 2-1b) show the nanoparticles with average core sizes of $4.0 \text{ nm} \pm 0.8 \text{ nm}$ (histogram shown in Figure 2-1d). The images show mosaic-like patterns of monodisperse and well-separated nanoparticles. This is caused by the presence of ethylene glycol which appears as transparent coronae in the TEM images because of its low electron density compared to electron-rich cerium oxide cores. On the other hand, non-coated nanoceria exhibited larger particle sizes (7 – 13 nm) with significant aggregation and lack of uniformity, highlighting the role of ethylene glycol coating in stabilising the synthesis (Figure 2-1c).

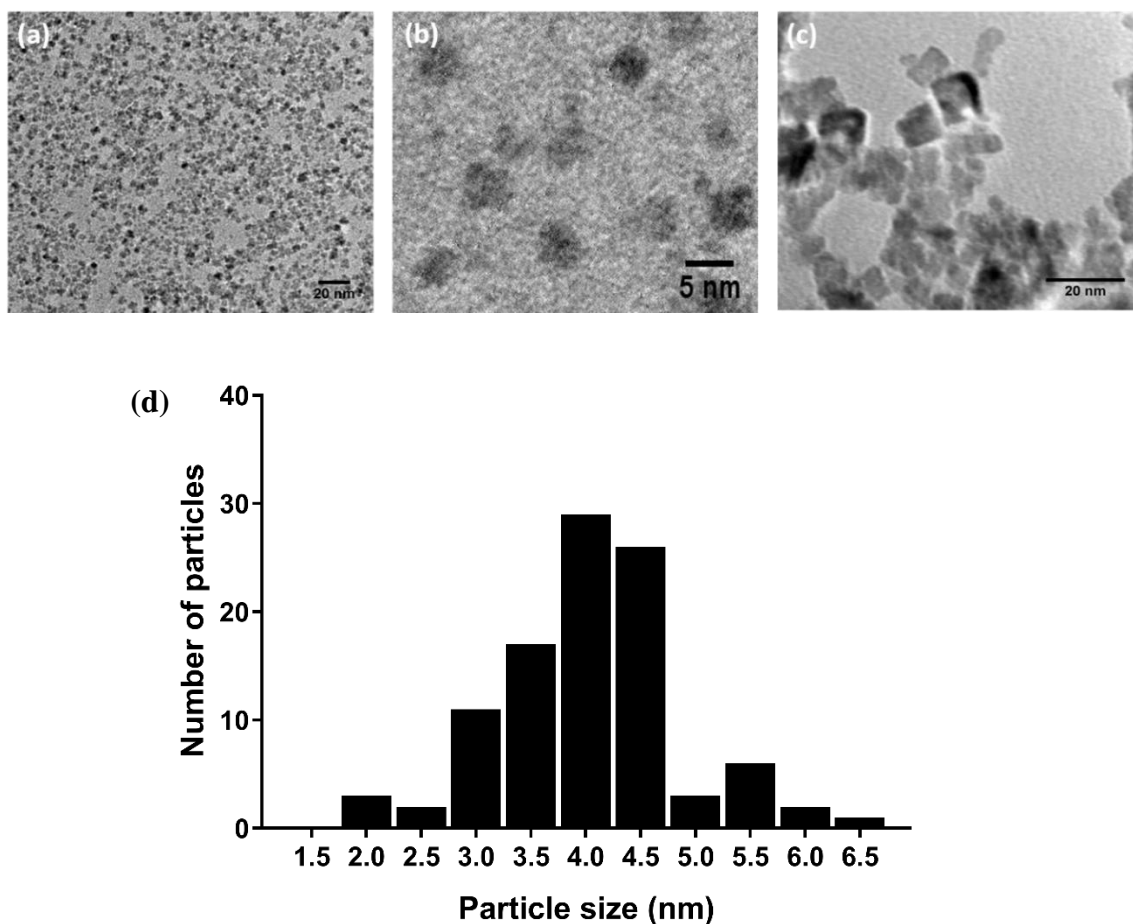


Figure 2-1 Transmission electron microscopic (TEM) images of nanocerium.

(a) ethylene glycol-coated nanocerium (EGCNPs) at 20K and (b) EGCNPs at 100K magnification; both images show that nanoparticles are relatively uniform in size and well separated with near spherical morphology, (c) non-coated nanocerium (at 100k magnification) that exhibit significant clustering, irregularity and polydispersity, (d) A histogram showing size distribution of a hundred EGCNPs nanoparticles measured by TEM.

The crystallinity of EGCNPs was confirmed by the presence of the crystal lattice fringes clearly identified in the high resolution TEM images as shown in Figure 2-2a. A line profile was plotted (Figure 2-2b) from which the d-spacing of the characteristic (111) plane was calculated to be 0.33 nm. This was in a close agreement with the lattice spacing value reported in the literature (0.31 nm) given the resolution limitation of TEM.

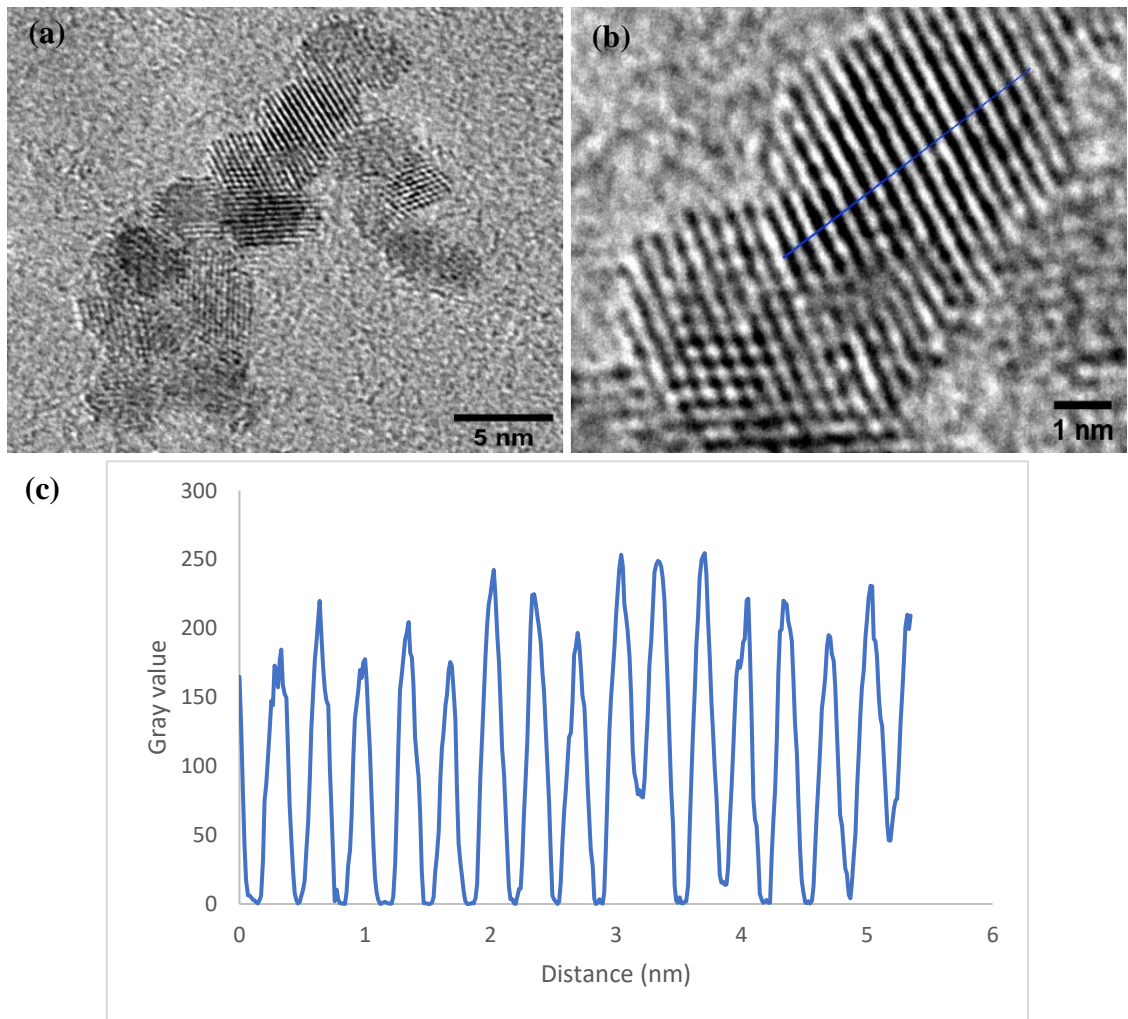


Figure 2-2 High resolution TEM micrographs showing the lattice fringes.

(a) and (b) EGCNPs, (c) A line profile plotting (of the blue line in image b) showing the d-spacing of the characteristic (111) lattice planes where it was measured to be 0.33 nm.

Powder X-ray diffraction (XRD) data further confirmed the cubic fluorite crystalline structure of CeO_2 which was in agreement with the structure reported in the literature (JCPDS No. 75-0390).¹⁰⁹ The characteristic 2θ diffraction peaks at 28.4° , 33.3° , 47.3° , 56.12° correspond to the (111), (200), (220), and (311) planes respectively, and are annotated on the diffractogram (Figure 2-3). The d-spacing values of the aforementioned planes were 3.137, 2.69, 1.91 and 1.63 nm respectively. The diffraction peaks of EGCNPs were significantly broader than those of non-coated nanoceria which is indicative of EGCNPs

smaller crystallite size.¹⁰¹ The crystallite size, calculated by applying the Scherrer equation on (111) diffraction peak was found to be 3.5 nm (a calculation is available in the appendix). This is close to the average particle size calculated from TEM images (4.0 nm). This difference between TEM and XRD measured sizes is expected as a crystallite (measured by XRD) is usually smaller than a particle which may be composed of multiple crystallites.¹¹⁹ Additionally, in the case of a particle being composed of one crystallite, XRD provides more accuracy in measuring the particle size due to the high statistical power involved.¹¹⁹

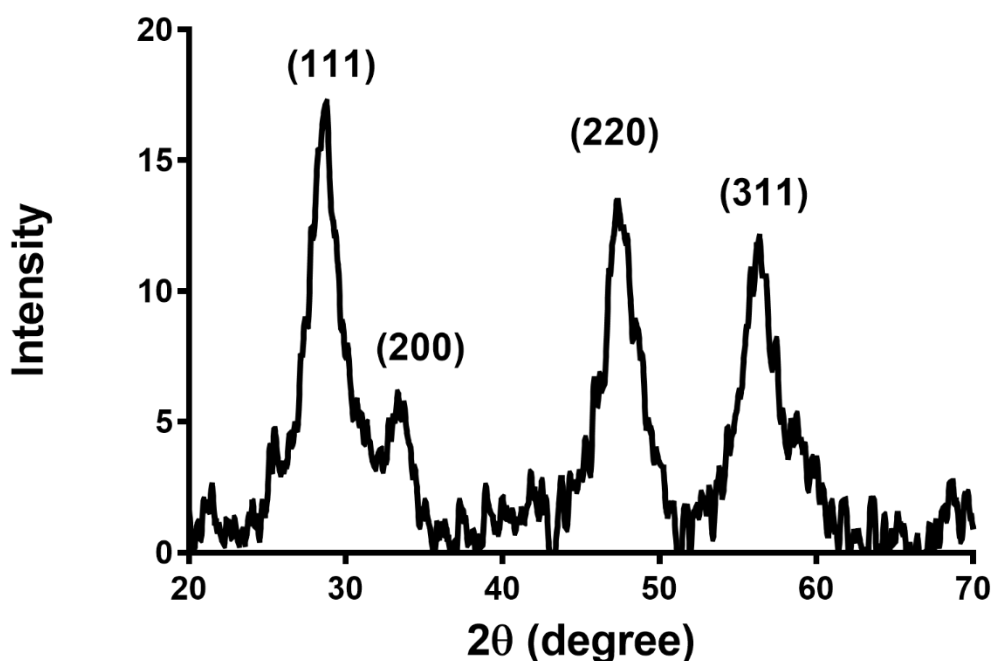


Figure 2-3 X-ray diffractogram displaying characteristic planes (annotated) typical of face-centered cubic fluorite structure of EGCNPs.

2.3.2 FTIR characterisation

FTIR is utilised to identify the various functional groups in a given molecule based on the frequency of IR radiation absorbed by its specific bonds. Hence, the presence or the absence of specific bands and their relative intensities can provide valuable information about the structure of the compounds being studied.¹²⁰ The FTIR spectrum for EGCNPs (Figure 2-4a) confirmed the structure of EGCNPs and this concurs with findings reported in the literature.¹²¹ The presence of ethylene glycol coating was indicated by the presence of two characteristic bands corresponding to methylene (CH₂) stretching at 2950 and 2850 cm⁻¹ and a broad band from 3000 - 3600 cm⁻¹ corresponding to (O-H) stretching.¹¹³ The (O-H) stretching band was significantly prominent compared to a non-coated formulation (Figure 2-4b) indicating that the band pertains to additional (OH) groups from ethylene glycol and does not primarily arise from moisture adsorption on the surface.¹²⁰ The intense band at 1400 cm⁻¹ can be assigned to bending vibration of adsorbed H₂O molecules.¹²² The bands at 1550 cm⁻¹ and 1400 cm⁻¹ correspond to C-H bending of the methylene group and Ce-O stretching respectively.¹²¹

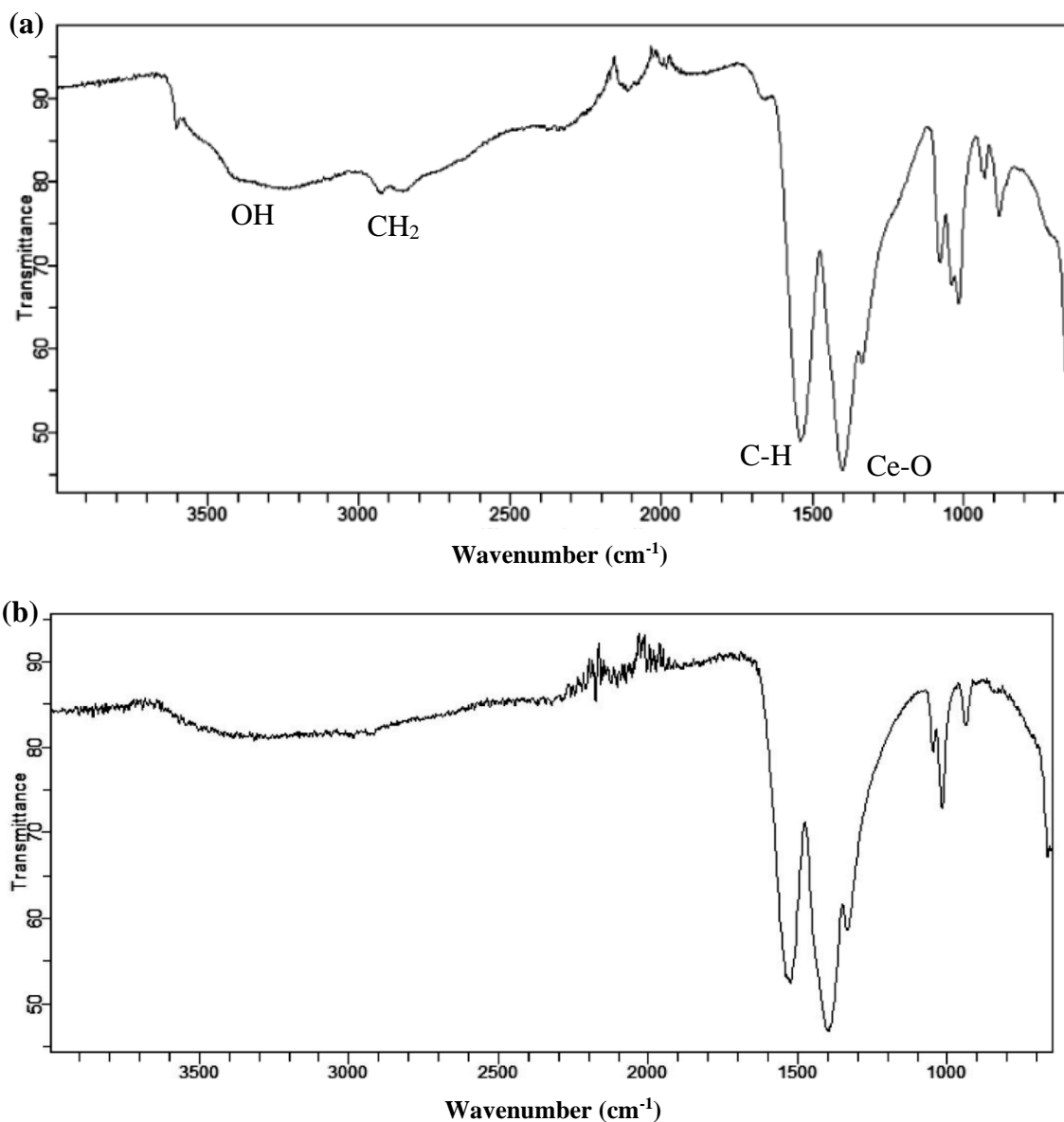


Figure 2-4 FTIR analysis of nanoceria.

(a) EGCNPs FTIR confirming the presence of ethylene glycol and ethylene glycol acetates coating as indicated by the appearance of methylene stretching as two small peaks in the spectra, (b) non-coated nanoceria FTIR showing weak OH stretching and lack of methylene stretching. Transmittance is presented as a percentage.

2.3.3 UV-vis characterisation

The UV-vis spectrum of EGCNPs aqueous dispersion showed two main absorption peaks at 255 nm and 300 nm (Figure 2-5) signifying the presence of mixed state valence. Ce^{3+} is known to absorb light between 230-260 nm while Ce^{4+} absorbs light in the region of 300 – 400 nm.⁸⁸ A typical nanoceria crystal contains cerium predominantly in its oxidized state (Ce^{4+}). As the crystal size decreases, surface defects associated with oxygen vacancies arise, increasing Ce^{3+} at the surface. The co-existence and transition of the cerium ions between the two oxidation states is what endows the nanoparticles with their free radical deactivation ability where the $\text{Ce}^{4+}/\text{Ce}^{3+}$ ratio is critical in determining the mechanism by which they scavenge for ROS.¹⁰³

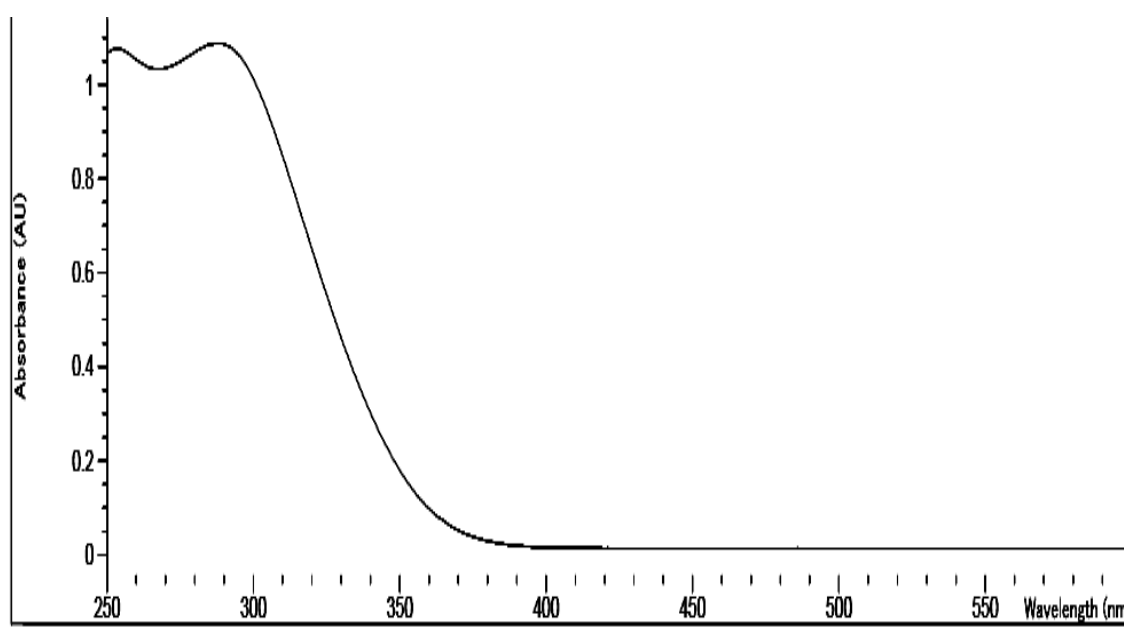


Figure 2-5 UV-visible spectrum of EGCNPs showing absorption at 255 nm and 300 nm confirming the presence of surface Ce^{3+} .

2.3.4 SEM-EDX characterisation

The elemental composition of EGCNPs was confirmed by scanning electron microscopy equipped with energy dispersive X-ray spectroscopy (SEM-EDX). As shown in the EDX spectrum in Figure 2-6, M_{α} and L_{α} characteristic X-ray emission peaks for cerium (^{58}Ce) were observed at 0.88 KeV and 4.83 KeV respectively. K_{α} X-ray emission at 0.52 KeV confirmed the presence of oxygen in the CeO_2 lattice.

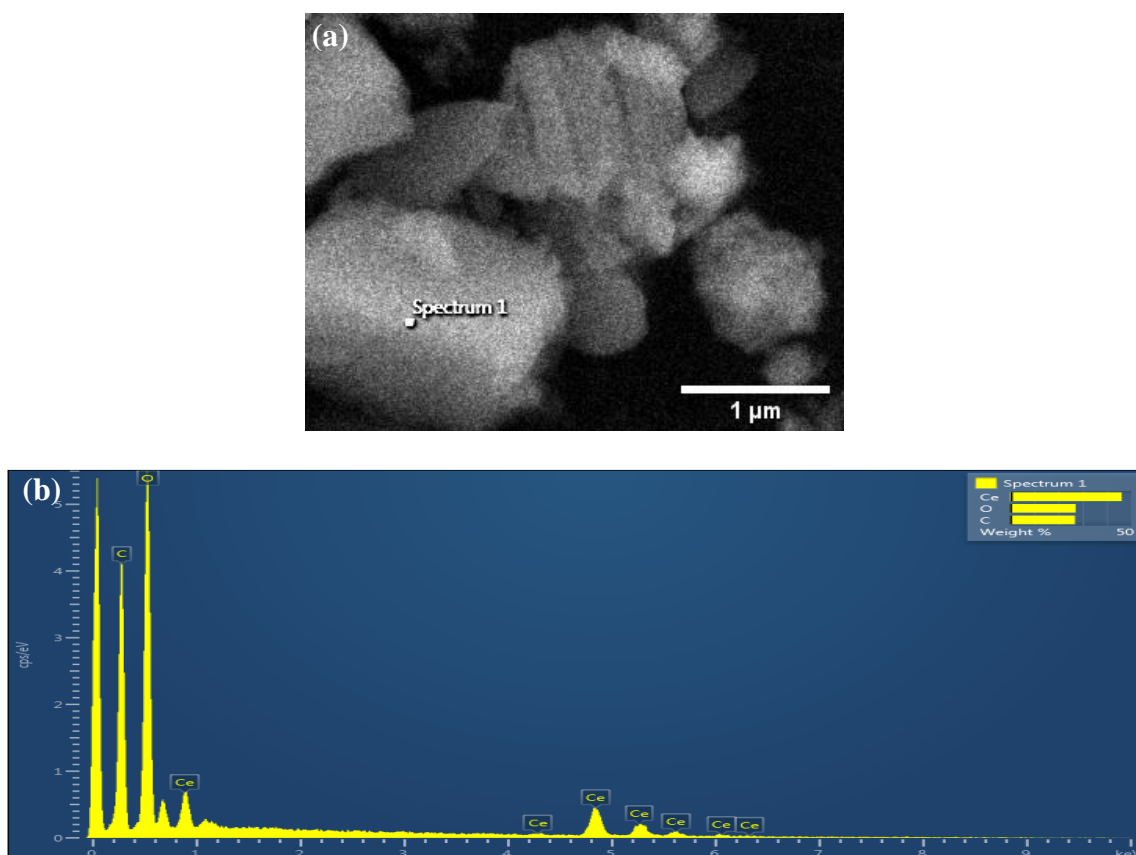


Figure 2-6 SEM-EDX analysis of EGCNPs.

(a) SEM micrograph of a cluster of EGCNPs, (b) EDX spectrum of the point highlighted in the SEM micrograph showing characteristics peaks of cerium and oxygen of CeO_2 .

2.3.5 EGCNPs coating characterisation by TGA-GC-MS

The presence and composition of the surface coating of EGCNPs were confirmed using TGA-GC-MS as shown in Figure 2-7 and Figure 2-8. Two main regions of weight loss were observed. The initial weight loss starting from 100 °C to 150 °C (10%) can be attributed to the loss of residual water and the loosely bound outermost layer of the coating, while the second weight loss (20%) indicated full decomposition of the coating from 200 -700 °C. The components of the vaporised coating were then separated by gas chromatography and analysed by mass spectroscopy. Mass spectrometry data (Figure 2-8) revealed that the coating was a mixture of three compounds; ethylene glycol, ethylene glycol monoacetate and ethylene glycol diacetate. This modified hybrid coating provided the nanoparticles with additional carbonyl groups conferred by the acetate ligands and these are hypothesised to play an important role in the aqueous stability of nanoceria through hydrogen bonding with water molecules. Moreover, the additional ethylene glycol acetate ligands are longer than pure ethylene glycol coating and longer surface ligands are generally associated with enhanced stability of the nanoparticles through the steric hindrance effect.^{123,124}

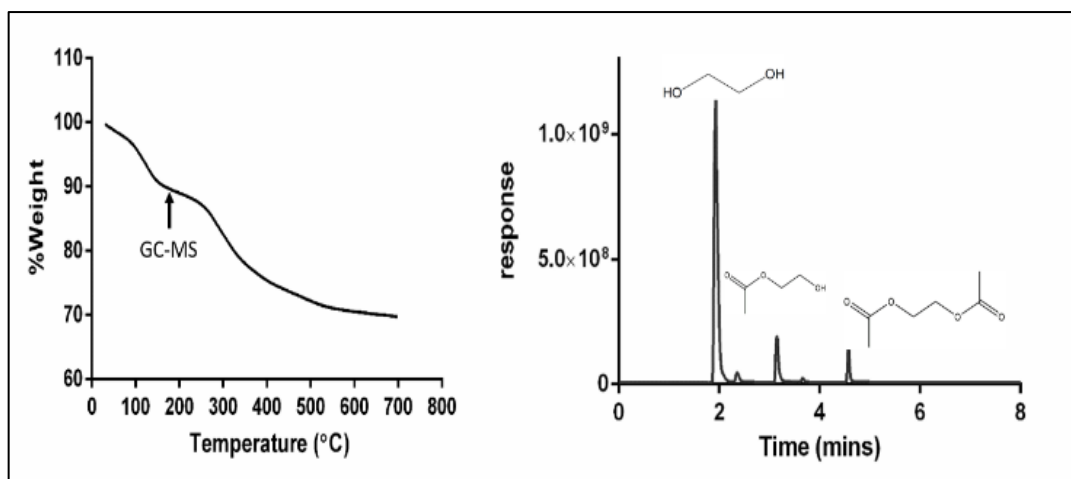


Figure 2-7 Thermogravimetric analysis (TGA) of EGCNPs showing two main weight loss regions.

The decomposed coating was separated by gas chromatography and analysed by mass spectrometry. The arrow indicates the time at which GC-MS analysis was triggered. Chromatogram peaks at 2.1, 3.1 and 4.5 min correspond to ethylene glycol, ethylene glycol monoacetate and ethylene glycol diacetate respectively.

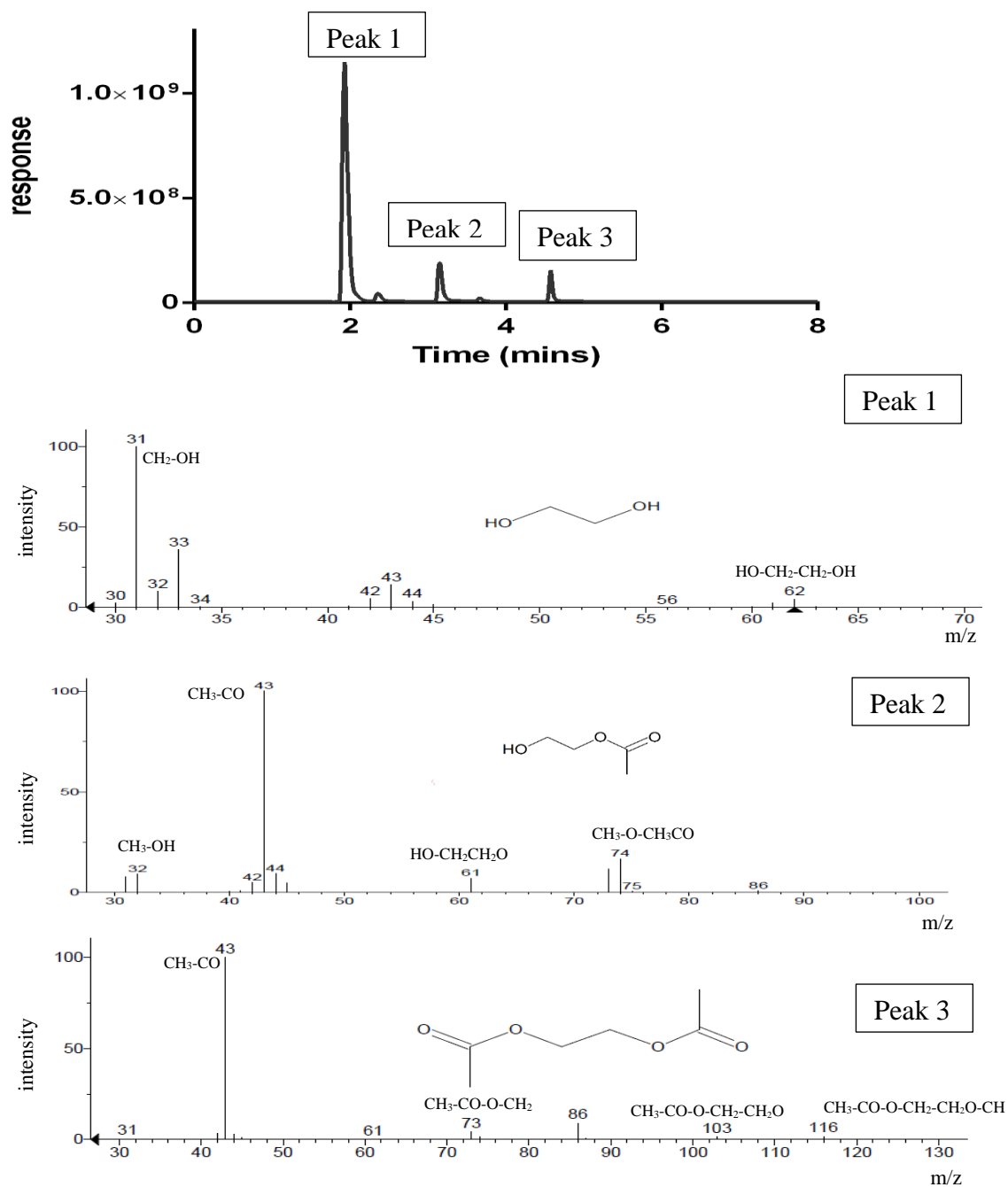


Figure 2-8 Gas chromatography - mass spectrometry analysis (GC-MS) of EGCNPs coating after decomposition in TGA.

The chromatogram is showing the three main peaks separated from the decomposed coating and mass spectra of the peaks are displayed confirming the composition to be ethylene glycol, ethylene glycol acetate and ethylene glycol diacetate. Key m/z values are as follows:

In order to ensure that the presence of the modified ethylene glycol surface coating does not inhibit the antioxidant and auto-regenerative properties of EGCNPs by blocking the access of ROS to the surface cerium oxide cores, a solution of EGCNPs (pH = 7) was treated with H₂O₂ and an immediate colour change from colourless to orange was observed (Figure 2-9). This indicated the oxidation of surface Ce³⁺ (colourless) into Ce⁴⁺ (orange), reducing the hydrogen peroxide in the process.^{81,125} The reduced colourless solution associated with the presence of surface Ce³⁺ was successfully retrieved by either boiling (*ca.* 5 min) or leaving the oxidised solution at ambient conditions (10 days). The retrieved colourless solution (Ce³⁺) was able to react again with freshly added H₂O₂ turning orange.¹²⁵ Such transition between Ce³⁺ to Ce⁴⁺ was further accompanied by a corresponding red shift in the UV-Vis absorbance spectrum as shown in Figure 2-9. Such reversibility in the behaviour of nanocerium is crucial for its biomedical activity where the nanoparticles can alternate between catalase and superoxide dismutase (SOD) like activities depending on the ambient environment.⁸¹ Hence, the results clearly indicate that the acetylated ethylene glycol coating does not interfere with the redox and reversible properties of EGCNPs rendering them promising for *in vitro* studies.

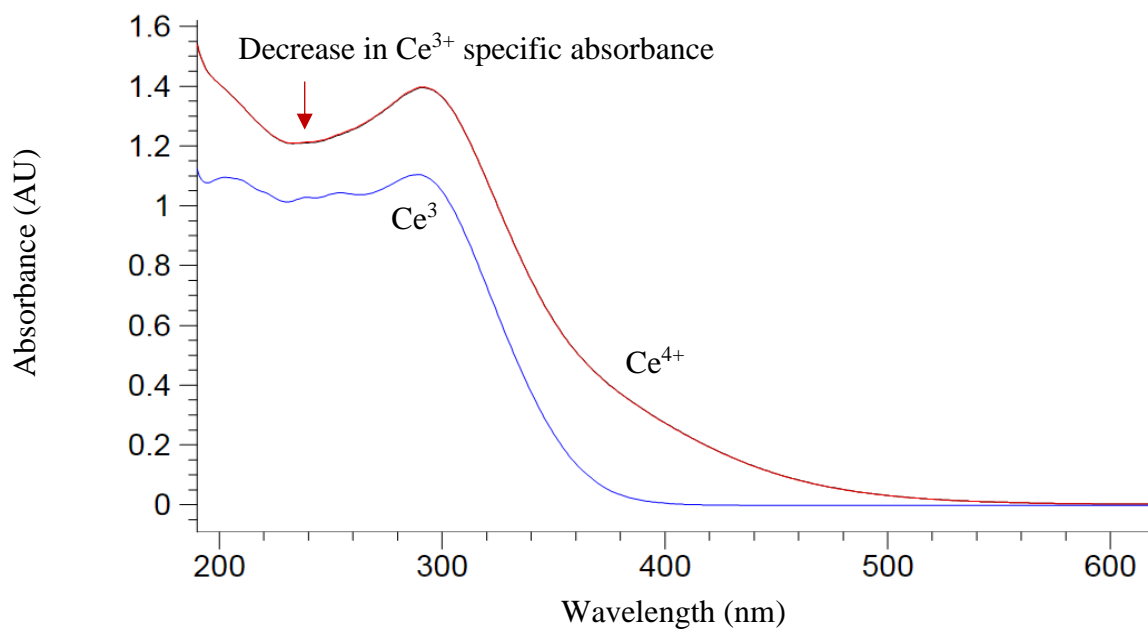
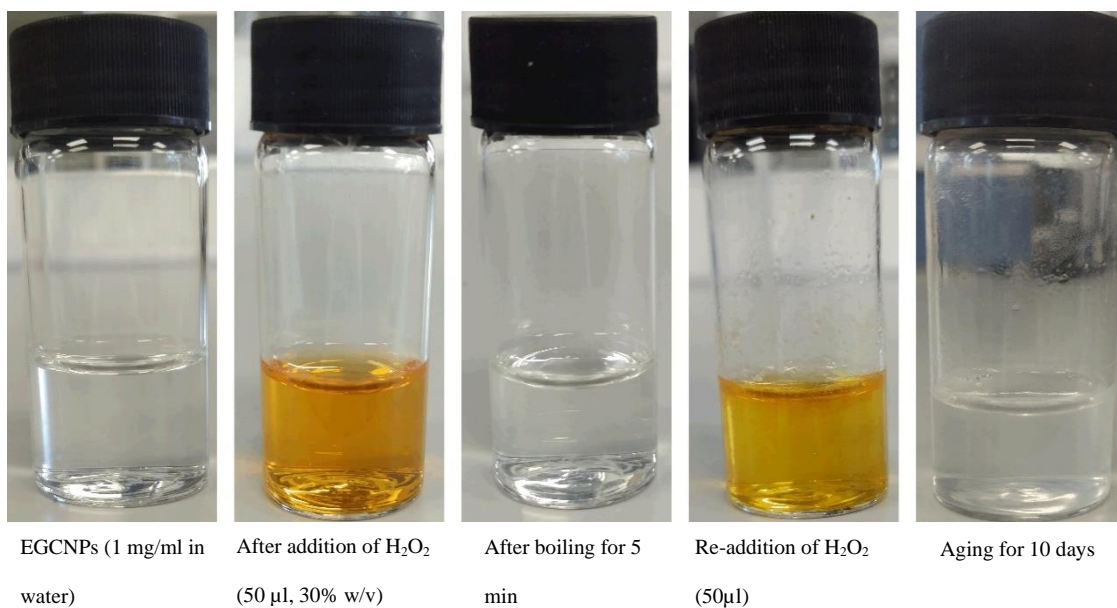


Figure 2-9 Acetylated ethylene glycol coating does not interfere with the antioxidant and regenerative properties of EGCNPs.

Oxidation of Ce⁺³ (colourless) into Ce⁺⁴ (orange) upon hydrogen peroxide addition. A red shift in the UV absorption of the resulting orange solution corresponding with this change was observed; colourless Ce⁺³ (blue spectrum), Ce⁺⁴ (red spectrum). The reduced colourless solution (Ce⁺³) was retrieved by either boiling or leaving the oxidised solution at ambient conditions (10 days). The reduced solution (Ce⁺³) reacted again with freshly added hydrogen peroxide turning orange.

2.3.6 EGCNPs photoluminescence and optical properties

Fluorescence studies revealed that EGCNPs exhibited unique multi-coloured emissions that extended from the UV to the red region of the visible spectrum. Figure 2-10a and Figure 2-10b show EGCNPs emissions in the blue, green and red regions of the visible spectrum when excited with 390, 450 and 513 nm respectively, and Figure 2-10c and Figure 2-10d show the blue and green emissions detected in both dispersion and powder forms when excited with the appropriate wavelengths. The shorter wavelength emission (blue) was relatively broad with the peak tail reaching beyond 600 nm (Figure 2-10a). Both excitation and emission spectra were considerably broad which made the detection of nanoparticles highly tunable in a fashion similar to quantum dots (*i.e.* multiple excitations and emission wavelengths can be used for their detection).¹²⁶ For example, when excited at 270 nm, EGCNPs maximum emission was blue-shifted with maximum emission at 350 nm (Figure 2-11). Such tunability would limit their use in multiplexing experiments where multiple fluorescent probes need to be employed. However, the fluorescence was generally weak and required a strong laser power for excitation which could be problematic during biomedical imaging in complex cellular matrix where difficulty in separating its signal from background cellular autofluorescence may be encountered. In particular, the red fluorescence (> 600 nm) is relatively faint making EGCNPs detection in biosystems challenging since most cell lines strongly auto-fluoresce in the blue and green regions.¹²⁶ Hence, it is preferable for nano-formulations to possess fluorescence in the red region (around and beyond 600 nm) for efficient tracking within cellular matrices.¹²⁶ A strategy to enhance the fluorescent properties of EGCNPs to suit biomedical applications is discussed in Section 2.3.8.

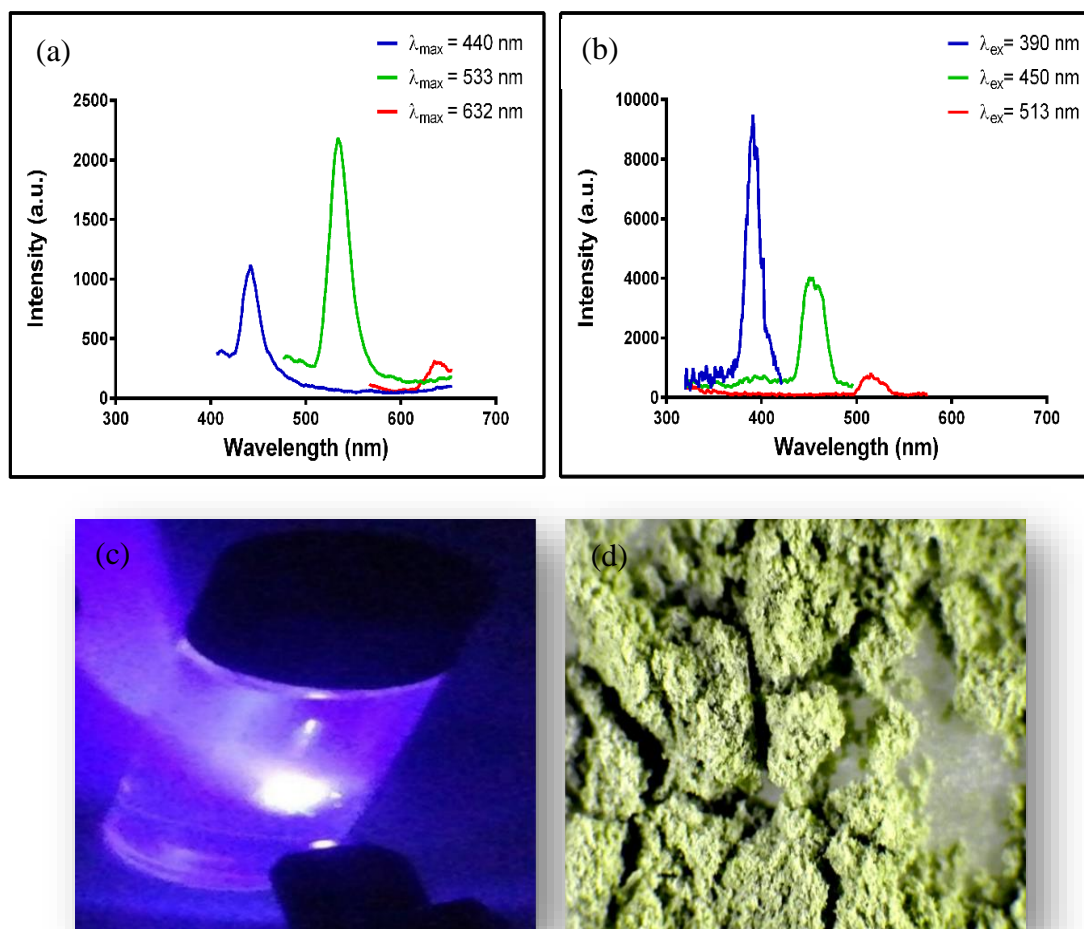


Figure 2-10 Photoluminescent properties of EGCNPs.

(a) Emission spectra showing peaks at 440nm, 533nm and 632 nm when excited with 390 nm, 450 nm, and 513 nm respectively, (b) corresponding excitation spectra with detection bandwidths set at 10 nm, (c) an EGCNPs suspension demonstrating strong blue to violet emission when excited with UV excitation source (380 nm), (d) EGCNPs powder showing broad green emission after blue light excitation.

EGCNPs emission scan (excitation = 270 nm)

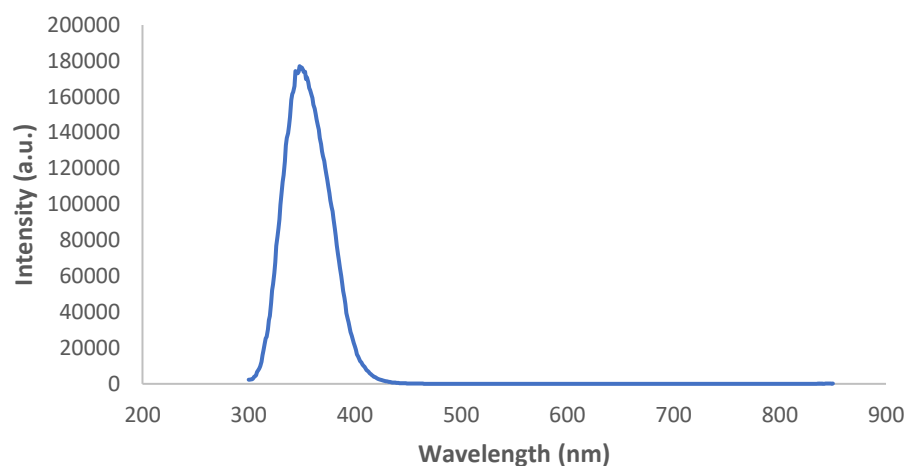


Figure 2-11 EGCNPs maximum emission is blue shifted to 350 nm upon excitation with a wavelength of 270 nm.

When examined with laser scanning confocal microscopy, emissions from EGCNPs dry powder could be detected across the blue, green and red regions using a single excitation wavelength (405 nm) as shown in Figure 2-12. This agrees with the broad emission spectra of EGCNPs upon UV excitation (Figure 2-10a).

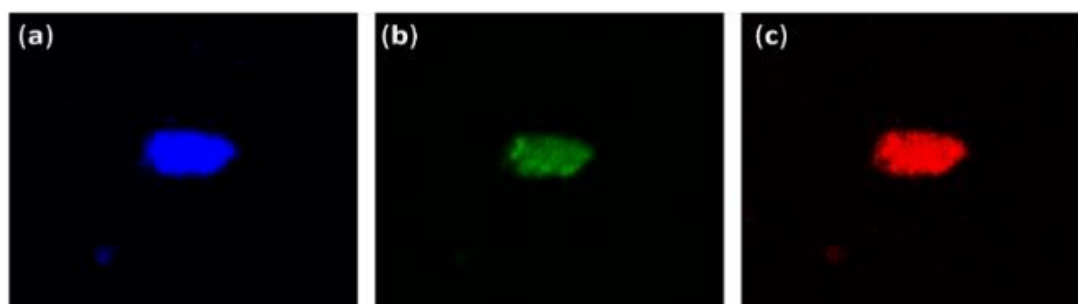


Figure 2-12 Confocal images of a cluster of EGCNPs powder upon 405 nm excitation with emissions detected at (a) 450 nm, (b) 550 nm and (c) 630 nm.

The photoluminescent behaviour of nanoceria has been reported in the literature, but the findings are not consistent. Krishnan *et al.* reported multi-coloured fluorescence of

organophilic 2 – 3 nm oleic acid-coated CeO₂ nanodots (OACNPs) fabricated by solvothermal decomposition.⁹⁵ OACNPs dispersed in toluene exhibited blue ($\lambda_{\text{ex}}= 350$), green ($\lambda_{\text{ex}}= 405$) and red emissions ($\lambda_{\text{ex}}= 532$).⁹⁵ These unique fluorescent properties were attributed to the quantum confinement effect due to the presence of a large number of crystal defects associated with the small nanoparticle size (2 nm) with a higher Ce³⁺ to Ce⁴⁺ ratio.⁹⁵ A CeO₂ film deposited (80 nm) on a silica substrate was reported to have violet to blue luminescence at 380 nm.¹²⁷ Nanocerium (2 nm), coated with a double layer of oleic acid prepared by thermal decomposition, were reported to have a broad spectrum with maximum emission at 515 nm with 400 nm excitation.¹²⁸ As such, this is the first study to report that nanocerium prepared by an aqueous precipitation method can exhibit multi-coloured photoluminescence. Moreover, the ability to detect them with a fluorescent microscope in all visible regions of light spectrum using a single excitation wavelength is reported for the first time.

2.3.7 EGCNPs colloidal stability and sterilisation

After fully characterising EGCNPs, it was crucial to assess their suitability for use in physiologically relevant aqueous media before their use for *in vitro* studies. This should in turn develop an understanding of the role of the modified ethylene glycol coating in stabilising the nanoparticles. To achieve such purposes, dynamic light scattering (DLS), sedimentation over time, and sterilisation studies were carried out. DLS is a standard tool used to measure the hydrodynamic diameter and zeta potential of the nanoparticles in a given colloidal dispersion. The nanoparticles in a colloidal system undergo a Brownian motion by interacting with each other (inter-particle collisions) and with the solvent molecules. When light is shone on the nanoparticles, the light is scattered and the intensity of the scattered light that hit the detector will fluctuate due to the constructive and destructive interferences of the scattered light. By plotting the intensity fluctuations as a function of time (in

microseconds), an autocorrelation function (ACF) can be calculated from which the translational diffusion coefficient (D_t) can be measured from the decay rate of the ACF curve. Smaller nanoparticles have faster Brownian motion and hence loss of correlation in intensity fluctuations is faster. The translation diffusion coefficient (D_t) can then be used to calculate the hydrodynamic diameter using Stokes-Einstein equation:¹²⁹

$$D_t = \frac{TK_B}{6\pi\mu R_H}$$

Where T is temperature, K_B is the Boltzmann constant, μ is viscosity, and R_H is the hydrodynamic radius.

Similarly, the zeta potential of the particles can be measured using DLS by applying an electric field to the dispersed nanoparticles and calculating their electrophoretic mobility. During electrophoresis, the moving nanoparticles scatter light with a frequency different to that of the original incident light. The shift in the frequency is dependent on the speed of the nanoparticles and is called Doppler shift. The scattered beam is compared to a reference beam from which the Doppler shift is measured. The velocity of the nanoparticles is then inferred using the Doppler shift value and the zeta potential is measured by applying multiple mathematical equations.¹²⁹ Together, the hydrodynamic diameter and zeta potential provide information on the stability of the nanoparticles in dispersions.

The intensity weighted mean hydrodynamic diameter (Z-average), polydispersity index (PDI) and zeta potential of EGCNPs were measured in three different aqueous media: water, EMEM supplemented with FBS (20%) and saline (0.9%). EMEM was used since it is one of the most commonly used cell culture media and will be the main media employed in the following chapters. The data are summarised in Table 2-1.

Table 2-1 Particle size, polydispersity index and zeta potential measurements of EGCNPs in different physiological media (pH = 7, 25°C)

Media	Z-average (nm)	PDI	Zeta (mV)
1- Distilled Water	21.8 ± 0.6	0.28	+ 44.1
2- EMEM + FBS (20%)	128.7 ± 9.2	0.17	- 9.7
3- 0.9% saline	158.1 ± 20.6	0.24	+ 14.0

In all tested media, EGCNPs showed unimodal distribution of mean hydrodynamic diameters and no aggregation peaks were observed (Figure 2-13). On the other hand, a non-coated nanoceria formulation showed an aggregation peak in water (>1000 nm) and the hydrodynamic diameter of the main peak was significantly larger at 133 nm (Figure 2-14)

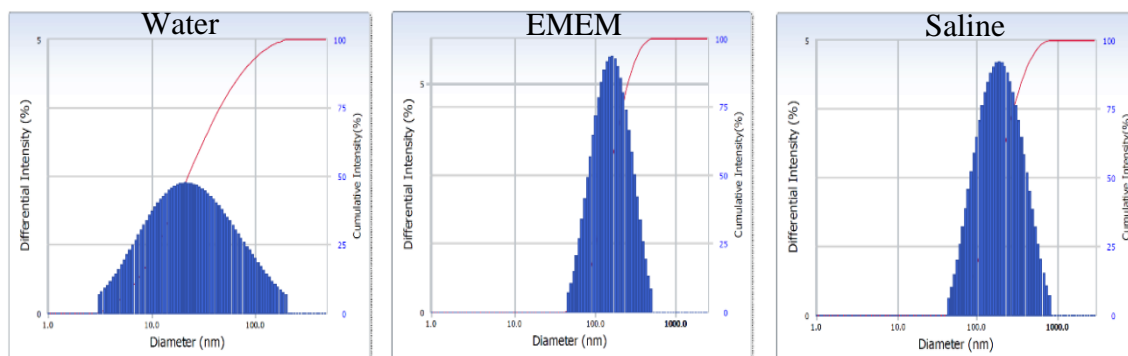


Figure 2-13 Distribution of the intensity-weighted hydrodynamic diameters (Z-average) of EGCNPs in different aqueous media.

The histograms show unimodal distribution of EGCNPs in all media without signs of aggregation.

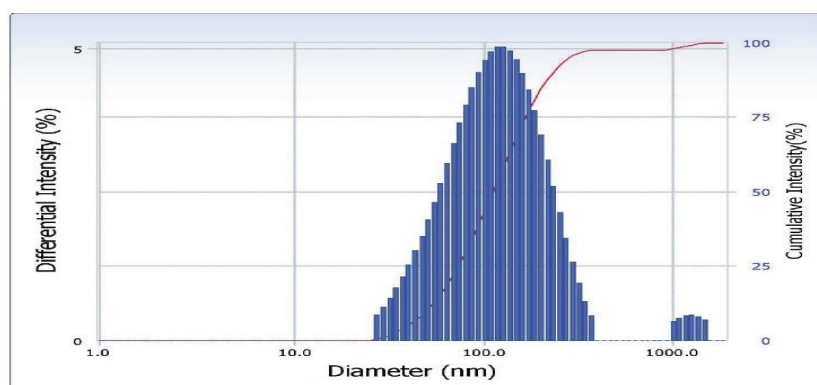


Figure 2-14 The hydrodynamic diameter (Z-average) of non-coated cerium oxide nanoparticles in water showing polydispersity and aggregation.

The hydrodynamic diameter of EGCNPs was the smallest in water (21.86 nm) and increased significantly in other media while maintaining monodispersity. This was demonstrated by small PDI values (Table 2-1). The hydrodynamic diameter measured by DLS is expected to be inherently different from the particle size measured by TEM since the former is based on light scattering of the coating and hydration layer surrounding the particles while the latter is more sensitive to the core size of the particles.⁹⁵ The increase in the hydrodynamic diameter in serum-containing EMEM is caused by the adsorption of a layer of serum proteins on the surface of nanoparticles forming a corona that contributed to its overall measured hydrodynamic diameter.^{130,131} The association of surface proteins was further reflected in the zeta potential value of EGCNPs and its inversion to a negative value.¹³² Serum proteins are predominantly negatively charged at physiological pH and hence their accumulation on the surface of the nanoparticles alters their zeta potential.¹³³ In saline solution, the increase in the hydrodynamic diameter was expected as high salt concentrations are known to shield the electrical field around nanoparticles reducing the electrostatic repulsion and causing agglomeration.¹³⁴ This is clearly manifested in the decrease in positive charge in saline solution compared to the value in water (Table 2-1). Despite that, the nanoparticles remained well dispersed in all media with no signs of precipitation or aggregation.

Since nanoparticles must be sterile for biomedical applications, the small particle size in water permitted easy sterilisation by filtration through 0.22 μm syringe filters with minimal loss of the nanoparticles (less than 6% loss) as confirmed spectrophotometrically at 300 nm. The amount of EGCNPs lost after sterilisation was found to decrease as the volume of filtered solution passing through the same filter increased, suggesting that the loss was due to adsorption on the filter surface. This helped in avoiding high temperatures in autoclaving which may affect the stability of the nanoparticles.

When left to precipitate over one week at room temperature in water, EGCNPs showed a slight loss in the supernatant concentration (6%) over the testing duration. This level of stability was superior to their non-coated counterparts for which a significant loss in supernatant concentration (>35%) was observed after 24 h, highlighting the role of ethylene glycol coating in stabilising the dispersion (Figure 2-15). The previously reported synthesis of ethylene-glycol coated nanoparticles was initiated from a nitrate precursor that resulted in hydrodynamic diameters of 222 nm and 206 nm in water and RPMI + FBS (10%) respectively, and both exhibited significant polydispersity with bimodal size distribution deeming them unsuitable for biomedical applications.¹¹³ Moreover, the colloidal stability study of that formulation showed substantial loss of nanoceria content in the supernatant where 38% were precipitated when a dispersion was left to precipitate over 7 days. Hence, it is shown that by simply synthesising nanoceria from a different precursor (an acetate precursor rather than a nitrate precursor), a noticeable enhancement on the stability of the nanoparticles with ethylene glycol can be achieved. This is attributed to the fact that the extra acetate ligands provided in the reaction mixture reacted with ethylene glycol and formed monoacetate and diacetate ethylene glycol derivatives as previously shown in

Figure 2-7. These modified acetylated ligands are speculated to have provided improved stability via two proposed mechanisms. Firstly, the acetate ligands are longer and hence provided better steric hindrance stability by shielding the inter-particular attractive forces which in turn prevented aggregation.¹³⁴ Secondly, the acetate derivatives provided the coating with additional polar carbonyl groups (C=O) that can form hydrogen bonding in aqueous solvents. It is also noteworthy the zeta potential plays an important role in stabilising the nanoparticles in aqueous media through electrostatic repulsion and usually a balance between steric hindrance and electrostatic forces has to be struck for optimum stability. To the best of the author's knowledge, the EGCNPs described here are the simplest aqueously

stable nanoceria with a well-defined colloidal stability that can be formulated and stored in dry powder form.

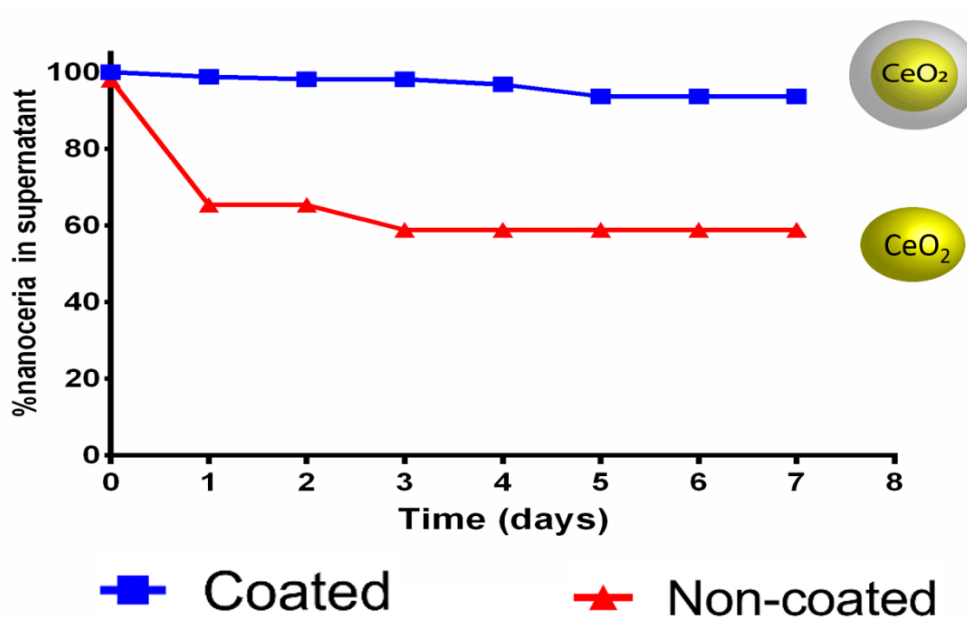


Figure 2-15 Colloidal stability of ethylene glycol-coated nanoceria (EGCNPs) and non-coated nanoceria kept in water at room temperature for a week.

Concentration of nanoceria in the supernatant was determined at one-day intervals spectrophotometrically at 300 nm.

2.3.8 Europium doping to enhance the photoluminescent properties of EGCNPs

Although EGCNPs showed fluorescent properties as discussed in Section 2.3.6, the fluorescence was weak which therefore required further enhancement if the nanoparticles were to be employed in studies where fluorescence imaging in complex biological matrices (*i.e.* cellular monolayers or tissues) is needed. The nanoparticles were synthesised in a similar fashion, where europium ions (Eu^{3+}) were doped inside the crystal lattice of cerium oxide, and the resultant nanoparticles are referred to as europium doped nanoceria (EuCNPs). Europium (Eu) is a rare earth lanthanide which produces a strong red fluorescence when

doped in different crystals.¹¹⁶ Doping with europium was chosen over the traditional attachment of fluorescent tags on the surface of the nanoparticles for several reasons. Firstly, minimal changes to the surface chemistry are induced by doping which is needed for maintaining the biomedical activity of the nanoparticles. Secondly, the bulk size of the nanoparticles remains unchanged.¹¹⁶ Thirdly, lanthanides such as europium have long fluorescence decay times enabling time resolved fluorometry and are resistant to photobleaching.¹²⁶ Finally, the red emission of europium can be obtained when excited with different wavelengths extending from UV to visible light.¹¹⁶

The synthesis of europium doped nanoceria has been previously reported and was shown to enhance the red fluorescence of nanoceria although their use in tracking nanoceria within *in vitro* cell lines was not reported in the literature.¹¹⁶ EuCNPs were characterised as before for EGCNPs and the main data are summarised in Figure 2-16. EuCNPs showed very similar particle size to EGCNPs (4.3 ± 0.8 nm). XRD data revealed the main diffraction peaks pertinent to the cubic fluorite structure of CeO₂ crystal. No additional peaks specific to europium oxide were observed suggesting complete solubility of europium into the cerium oxide lattice. The main diffraction peaks of EuCNPs were slightly shifted to a lower 2θ angle compared to EGCNPs. This is caused by the slight expansion of the lattice parameters as a result of the higher ionic radius of Eu³⁺ ions (0.1066 nm) replacing the Ce⁴⁺ ions (ionic radius = 0.097 nm).¹¹⁶ This replacement leads to the creation of oxygen vacancies to compensate the loss in the positive charge maintaining the charge equilibrium.¹³⁵ Importantly, EuCNPs exhibited typical strong red emission at 612 nm under multiple excitation wavelengths from UV to end of green region (ranging from 350 - 550 nm) rendering them suitable for biomedical imaging studies (Figure 2-16c and Figure 2-16d).¹¹⁶

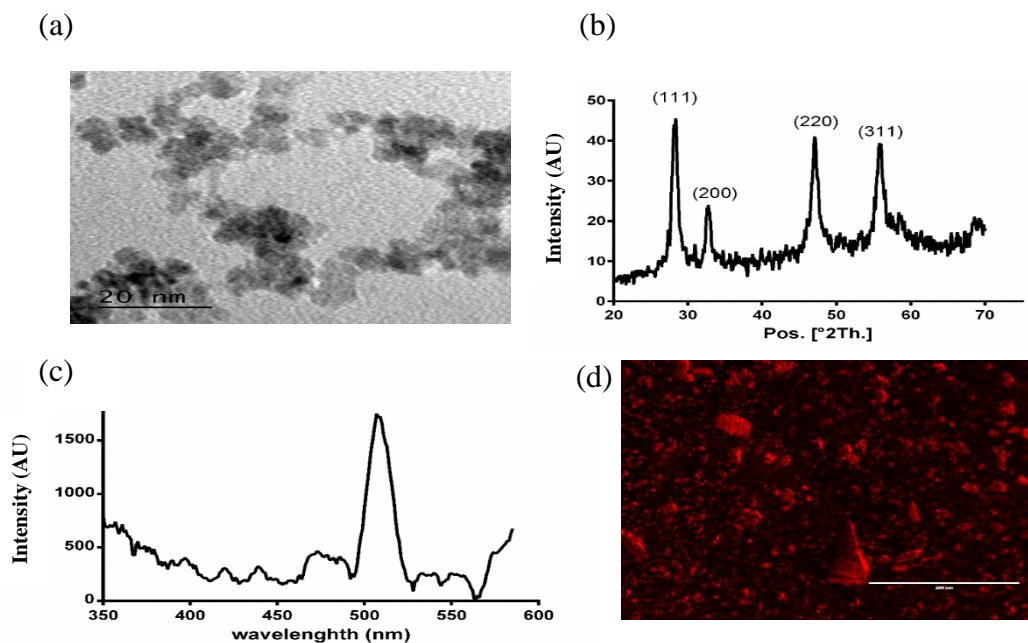


Figure 2-16 Characterisation of europium-doped nanoceria (EuCNPs).

(a) TEM image showing particles average size of 4 nm. (b) XRD analysis typical of nanoceria fcc crystal, (c) Excitation spectrum of EuCNPs with emission detected at 612 nm, multiple excitation wavelengths can be used to detect the particles at that particular emission wavelength, (d) Fluorescent microscope image of EuCNPs powder showing strong red fluorescence. The fluorescence was detected using RFP-compatible settings (excitation at 531 nm/40 nm, emission at 593 nm/40 nm) using a fluorescent microscope.

2.4 Conclusion

A novel nanoceria formulation coated with ethylene glycol and ethylene glycol mono- and di- acetates (EGCNPs) was successfully formulated with an ultra-small particle size (4 nm) using a simple one-pot precipitation reaction starting from cerium acetate as a precursor under mild conditions. The modified synthesis has enabled the use of ethylene glycol as a coating material which was previously reported to induce significant polydispersity. This was not the case for EGCNPs as DLS and colloidal stability studies have shown that they possess superior aqueous stability and monodispersity in different physiologically relevant media paving the way for carrying out biological studies with no sedimentation-induced variabilities. Furthermore, EGCNPs exhibited multi-coloured photoluminescence which was observed for the first time for aqueously prepared nanoceria. Unfortunately, EGCNPs natural fluorescence was relatively weak requiring strong excitation for its detection. Therefore, a similar nanoceria formulation doped with europium (EuCNPs) was synthesised for employing in imaging studies.

3 Toxicity evaluation of EGCNPs in human lens epithelial cells

3.1 Introduction

The use and commercial applications of nanomaterials are rapidly booming in the 21st century. In 2015, it was estimated that nanomaterials global market was valued at approximately \$14.7 billion and is projected to reach more than \$55 billion by 2022 growing at compound annual growth rate of 20.7% during this period.¹³⁶ Nanomaterials possess a very small particle size (usually between 1 - 100 nm in at least one external dimension), and a very large surface to volume ratio.¹³⁷ This provides nanomaterials with unique physical, chemical, and biological characteristics that are different from those of the bulk form.¹³⁸ The different characteristics and large surface area can result in a very high activity of the nanomaterials, which could also potentially lead to toxicity. Despite the exponential rise in the use of new nanomaterials, nanotoxicological evaluation is not carried out with a similarly high rate.¹³⁸ Hence, assessing and evaluating the biocompatibility of nanomaterials are crucial issues for both the public and the scientific community to enable informed decisions regarding their use.

Cerium oxide nanoparticles “nanoceria” are being researched for biomedical and drug delivery applications because of their unique regenerative antioxidant, neuroprotective, radioprotective and anti-inflammatory properties.^{81,88,97,99,139} Additionally, nanoceria are increasingly used for industrial applications as an additive to diesel fuel (commercially available under several trade names such as EnviroxTM) to reduce soot emissions and decrease fuel consumption.^{140,141} This has led to increased exposure to nanoceria which warrants investigation of their toxicological effects and interactions with various eukaryotic

cells. As such, nanoceria was considered a high priority for toxicological evaluation.^{141,142}

The toxicity of nanoceria has been studied in various *in vivo* and *in vitro* models.¹⁴³ However, more investigations into the mechanism of their action are needed.¹⁴² Additionally, many of the toxicological studies have been performed on nanoceria with unknown or poor colloidal stability, a common problem for nanoceria, which gives rise to conflicting toxicological profiles. Although nanoceria are known for their powerful antioxidant properties, some studies have reported their ability to cause oxidative stress.^{142,144,145} Ocular exposure is of particular interest due to the ease for sustained environmental exposure. Although nanoceria have shown promise in treating some ocular diseases such as retinal degeneration,¹⁴⁶ corneal inflammation,¹⁴⁷ and glaucoma,¹⁴⁸ there is a paucity of knowledge about toxicity of nanoceria in the lens.

If nanoceria are to be used for the prevention and treatment of cataract, their safety to the human lens has to be evaluated. The human lens epithelial cell line (HLECs) provides a suitable model for studying the toxicity of nanoceria to the eye lens as these are the lenticular progenitor cells that differentiate into the lens fiber cells forming the bulk of the lens.^{149–151} This transition is accompanied with distinct biochemical and morphological alterations such as the synthesis of lens fiber proteins (β -crystallins and γ -crystallins), cell elongation and loss of cell organelles.^{149–151} Damage to the lens epithelium could disrupt protein expression, differentiation and could lead to aggregation of proteins that causes light scatter and manifests as cataract.¹⁴⁹

The aim of this chapter then was to (1) determine the concentrations of the well-characterised and colloidally stable EGCNPs formulation that can be safely used and tolerated in HLECs for short-term studies, and (2) explore the mechanism of acute toxicity of very high concentrations of EGCNPs in HLECs providing the first mechanistic investigation of

nanoceria toxicity in any ocular tissue. To achieve this, various cellular health indicators have been studied including growth rate, cellular morphology, cell membrane integrity, DNA integrity, mitochondrial morphology, mitochondrial membrane potential, ATP production and key apoptotic and necrotic hallmarks.

3.2 Materials and methods

3.2.1 Cell culture and maintenance

Human lens epithelial cells (HLECs) (B3, ATCC[®] CRL11421[™], UK) were grown in Eagle's minimum essential medium (EMEM, ATCC[®] 30-2003, UK) supplemented with foetal bovine serum (FBS, 20%, Scientific Laboratory Supplies), penicillin (100 IU/ml, Sigma Aldrich, UK) and streptomycin (0.1 mg/ml, Sigma Aldrich, UK). The cells were incubated at 37°C and 5% CO₂ in a humidified environment. Sub-culturing (passaging) of the cells was carried out every three or four days by removing the growth media, washing once with Dulbecco's Phosphate Buffered Saline (D-PBS, 1X, ATCC[®] 30-2200[™], UK) and incubating with trypsin/EDTA solution (0.025%, Lonza, UK) for 1 min at 37 °C. After detaching the cells, trypsin was deactivated by adding FBS-supplemented medium and passaging into new tissue culture flasks was performed using a sub-cultivation ratio of 1:3 or 1:4. Cryopreservation of the cells was done using supplemented growth medium with 5% (v/v) dimethyl sulfoxide (DMSO, Fisher Scientific, UK) and the cells were stored in a liquid nitrogen vapour phase. For cell counting, of cell suspension (10 µl) was mixed with trypan blue solution (10 µl, 0.4%, Thermo Fisher, UK), and counting was performed using LUNA-II[™] Automated Cell Counter (Logos Biosystems, South Korea). The number of viable cells rather than total number of cells was used in all experiments. All experiments were conducted on cells in the logarithmic growth phase.

3.2.2 Cell viability of HLECs after EGCNPs exposure (MTT assay)

EGCNPs effect on HLECs viability was evaluated by MTT assay.¹⁵² HLECs were seeded in 96-well plates with a seeding density of 5000 cells per well in 200 µl growth medium. The cells were left to recover from handling for 24 h before treatment. The medium was then gently aspirated and replaced with fresh medium containing different concentrations of EGCNPs. The tested EGCNPs concentrations were 0, 100, 200, 400, 600, 800, 1000 µg/ml

with four wells used per condition. After the treatment durations (24 h or 48 h), 20 μ l of 3-(4,5-dimethyl-2-thiazolyl)-2,5-diphenyl-2H-tetrazolium bromide (MTT) solution (5 mg/ml in PBS, Sigma Aldrich, UK) were added to each well to reach a final concentration of 0.5 mg/ml, and the cells were incubated at 37°C for 2 h. After incubation, the MTT solution was gently aspirated and DMSO (200 μ l) were added to each well and left on a plate shaker for 10 min protected from light to solubilise the formed formazan crystals. Absorbance readings were taken at 570 nm using a plate reader (Clariostar, BMG Labtech, Germany). EGCNPs were incubated with MTT solution in absence of the cells and no formazan crystals formation was observed.

3.2.3 Proliferation of HLECs after EGCNPs exposure (live cell imaging)

The effect of different EGCNPs concentrations on the proliferation and morphological features of HLECs was observed using real-time live cell analysis. HLECs were seeded in 6-well plates with a seeding density of 1×10^5 cells per well in completed growth medium (5 ml) and immediately treated with different concentrations of EGCNPs (0, 50, 100, 200, 400 μ g/ml). The plates were imaged using the Incucyte[®] S3 Live Cell Analysis System (Essen BioScience, Germany) fitted inside an incubator set at 37 °C and 5% CO₂. Four fields of view were imaged in each well every 3 h with 20x objective over 3 days. Confluence percentages were calculated using the integrated Incucyte[®] S3 software and growth curves were subsequently generated.

3.2.4 Cell membrane integrity of HLECs after EGCNPs exposure (live cell imaging)

The cell membrane integrity, a measure of cellular cytotoxicity, was evaluated in HLECs after exposure to different concentrations of EGCNPs (0, 50, 100, 200, 400 μ g/ml) up to 72 h by means of live cell imaging. This was conducted in the presence of Incucyte[®] Cytotox Red for counting dead cells (250 nM, Essen Bioscience, Germany), a cyanine nucleic acid

dye that only permeates cells with compromised cell membranes. Briefly, HLECs were seeded in 96-well plates with a seeding density of 5000 cells per well in completed growth media (200 μ l) containing Cytotox Red and immediately treated with different concentrations of EGCNPs. Three fields of view were imaged in each well, with a 20x objective every 3 h over three days using the Incucyte[®] S3 Live Cell Analysis System fitted inside an incubator. The cytotoxicity level (cell membrane damage) was measured and expressed as the total fluorescent area of Cytotox Red (μm^2) per image using the integrated Incucyte[®] software.

3.2.5 Basal ROS level measurement (H₂DCFDA assay)

H₂DCFDA probe (2',7'-dichlorodihydrofluorescein diacetate, D399, Thermo Fisher, UK) was employed to measure basal ROS levels as previously reported.¹⁵³ Briefly, HLECs were seeded in 96-well plates in completed EMEM (5000 cells/well) and allowed to recover for 24 h. The media was then removed and replaced with fresh medium containing different EGCNPs concentrations (0, 50, 100, 200 and 400 $\mu\text{g}/\text{ml}$) for 24 h. H₂O₂ (200 μM , Sigma Aldrich, UK) was used as a positive control. After the treatment period, the media was discarded, the cells were washed once with pre-warmed PBS (ATCC[®] 30-2200[™]) and incubated with H₂DCFDA solution (10 μM in PBS) for 30 min at 37 °C. H₂DCFDA solution was then discarded, cell washed with pre-warmed PBS and fresh PBS (200 μ l) was added to each well. Dichlorofluorescein (DCF) fluorescence intensity was measured using a microplate reader (FLUOstar Omega, BMG Labtech, Germany) or a fluorescent microscope (EVOS FL, Thermo Fisher, UK) at excitation/emission of 485/520 nm. Correcting the fluorescence values was performed before data analysis by subtracting the fluorescence of unstained cells from all other values. No fluorescence was observed for cell-free H₂DCFDA/PBS and H₂DCFDA/PBS/ EGCNPs mixtures.

3.2.6 EGCNPs mitochondrial uptake and localisation (SEM-EDX)

HLECs were grown in five T175 flasks until they were approximately 80% confluent. The cells were then treated with EGCNPs (400 µg/ml) for 24 h. The cells were then harvested, pelleted and washed once with full media and once with PBS. The mitochondria were then isolated from the pellet by means of differential centrifugation using the Mitochondria Isolation Kit for Cultured Cells (89874, Thermo Fisher, UK) in accordance with the supplier's instructions. The isolated mitochondria were washed once with PBS, fixed with paraformaldehyde (4%, 5 min, Sigma Aldrich, UK) and dried in pure ethanol (5 min, Fisher Scientific). The mitochondria were then placed on an SEM aluminium stub covered with a carbon tape and the specimens were coated with a gold layer (5 nm) using a sputter coater (Q150R ES, Quorum, UK). The specimens were examined using a scanning electron microscope equipped with an EDX detector (JEOL, JSM-7100f, Japan). EDX spectra and mapping were acquired and processed using Aztec software (Oxford Instruments, UK).

3.2.7 Mitochondrial morphology (confocal microscopy)

HLECs were seeded (5000 cells/well) in black 96-well plates with clear flat bottoms (Falcon® 353219, Corning, USA) and left to establish for 24 h. The following day, the medium was discarded, and the cells were treated with EGCNPs-containing medium (0, 50, 100, 200 and 400 µg/ml) for 24 h. H₂O₂ (200 µM) was used as a positive control. After the treatment period, the medium was removed, and the cells were washed once with pre-warmed PBS. The cells were then incubated with full media containing MitoTracker™ Red CMXRos (200 nM, Thermo Fisher, UK) for 20 min at 37 °C. After staining, the cells were washed once with pre-warmed PBS, fixed in pre-warmed paraformaldehyde solution (4% in PBS) for 10 min at room temperature and permeabilised by incubating in ice-cold acetone (Fischer Scientific, UK) for 5 min. The cells were then counterstained by incubating in PBS containing Hoechst 33342 (2 µg/ml, Thermo Fisher, UK) and ActinGreen™ 488

ReadyProbes™ reagent (100 µl/ml) for 20 min at room temperature. Imaging was carried out using a laser scanning confocal microscope (Leica, Germany) using the following settings: sequential scanning, 20x dry objective, ex/em: Mitotracker: 543/599 nm, ActinGreen: 496/518 nm, Hoechst: 405/461 nm.

3.2.8 Mitochondrial membrane potential (JC-1 staining)

JC-1 probe (Abcam, UK) was employed for mitochondrial membrane potential measurements. HLECs were seeded (5000 cells/well), established and treated with different EGCNPs concentrations (0, 50, 100, 200 and 400 µg/ml) for 24 h. Sodium azide (1 and 2 mM, Sigma Aldrich, UK) was used as a positive control. After the treatment period, the medium was removed, and cells were incubated with JC-1 probe in complete medium (10 µM) for 30 min at 37 °C in dark conditions. The staining solution was removed, the cells were washed with PBS and replaced with phenol red-free complete medium. The wells were then imaged once using Incucyte® S3 high throughput imaging system using the green and red channels (5 wells per treatment condition, three images per each well) and quantification of the red/green ratio was calculated using the integrated software and the experiment was run in triplicate. Qualitative high magnification images were acquired using a laser scanning confocal microscope after nuclear staining with Hoechst 33342. The excitations/emission settings were as follows: Hoechst 33342 (405/461 nm), JC-1 green monomers (488/530 nm), JC-1 red aggregates (543/590 nm).

3.2.9 ATP quantification (Luciferase assay)

Quantification of cellular ATP was carried out using the luminescent luciferase assay (CellTiter-Glo, Promega, USA) in accordance with the supplier's instructions. Briefly, HLECs were established in 96-well plates as before and treated with different EGCNPs concentrations for 24 h and 48 h. After the treatment period, the medium was removed and replaced with fresh medium. An equal volume of CellTiter-Glo reagent was added to each

well to lyse the cells and release a bioluminescent signal proportional to the amount of ATP present. The plate was placed on an orbital shaker for 2 min and then incubated in the dark at room temperature for 10 min to stabilise the signal. The luminescent signal was read using a luminometer (Infinite[®] 200 PRO, TECAN, Japan).

3.2.10 Genotoxicity (immunocytochemistry)

The DNA damage was evaluated using the HCS DNA kit (Thermo Fisher, UK) according to the supplier's instructions. Briefly, HLECs were seeded in a black 96-well plate, established and treated for 24 h with different EGCNPs concentrations (0, 50, 100, 200 and 400 µg/ml) as before. After the treatment period the medium was removed, the cells were fixed in paraformaldehyde solution (4%, 10 min), rinsed with PBS, and permeabilised in 0.2% Triton-X-100 (15 min). The cells were then washed with PBS and then incubated in a blocking buffer (1 %w/v bovine serum albumin in PBS, Melford, UK) for 1 h at room temperature. The blocking buffer was then removed, and the cells were incubated with the primary antibody solution (pH2AX mouse monoclonal antibody) for 1 h. The primary antibody solution was removed, and the cells were washed three times with PBS. The cells were then incubated with the secondary antibody/nuclear stain solution (Alexa Fluor 555 goat anti-mouse IgG/Hoechst 33342) for 1 h. The secondary antibody solution was then removed, the cells were washed three times with PBS and replaced with fresh PBS before proceeding to imaging. Imaging was carried out using a laser scanning confocal microscope using the following settings: (sequential scanning ex/em: pH2AX: 543/565 nm, Hoechst: 405/461 nm). For data analysis, Hoechst staining was used for nuclear segmentation and the DNA damage was measured by the increase in the fluorescence of pH2AX signal in the region defined as the nuclei. The experiment was repeated four times and at least 100 nuclei were analysed in each replicate.

3.2.11 Caspase-3,7 assay (live cell imaging)

HLECs were seeded in 96-well plates (5000 cells per well) and left to establish for 24 h. The cells were then treated with different EGCNPs concentrations (0, 50, 100, 200 and 400 µg/ml) in supplemented EMEM in presence of IncuCyte® Caspase-3/7 Red Apoptosis Assay Reagent (0.5 µM, excitation/emission 630/650 nm). The cells were then imaged every 2 h for 24 h using the Incucyte® S3 live cell imaging system (Essen BioScience, Germany) fitted inside an incubator (5% CO₂, 37 °C). Three fields of view were imaged per each well using a 20x objective. Images were then analysed, and the caspase activity was measured and expressed as the area of red fluorescent caspase signal (µm²) per image. The experiment was performed four times.

3.2.12 Annexin V/Cytotox Red assay (live cell imaging)

The assay was performed on the Incucyte® S3 live cell imaging system as mentioned in Section 3.2.11 but in the presence of double staining with IncuCyte® Annexin V Green Reagent /IncuCyte® Cytotox Red Reagent (250 nM). Excitation/emission maxima for Annexin V and Cytotox Red are 490/515 nm and 612/631 nm respectively.

3.2.13 Statistical analysis

Each experiment was conducted at least three times ($n \geq 3$). Statistical analysis was carried out using GraphPad prism 7 software (USA). Where relevant, analysis of variance one-way or two-way ANOVA followed appropriate post-hoc test was used to compare groups with statistical significance set at $p < 0.05$. Details of statistical analysis are available in the figures' legends. Error bars are presented as means \pm SEM. Asterisks were used to denote statistical significance with the following notation: (*) $p \leq 0.05$, (**) $p \leq 0.01$, (***) $p \leq 0.001$ and (****) $p \leq 0.0001$.

3.3 Results and discussion

3.3.1 Effect of EGCNPs on cell viability, membrane integrity, proliferation and morphology of HLECs

The impact of different concentrations of EGCNPs (0 to 1000 $\mu\text{g/ml}$) on the viability of HLECs, after 24 h and 48 h exposure in culture media was evaluated using the MTT assay and the data is shown in Figure 3-1.

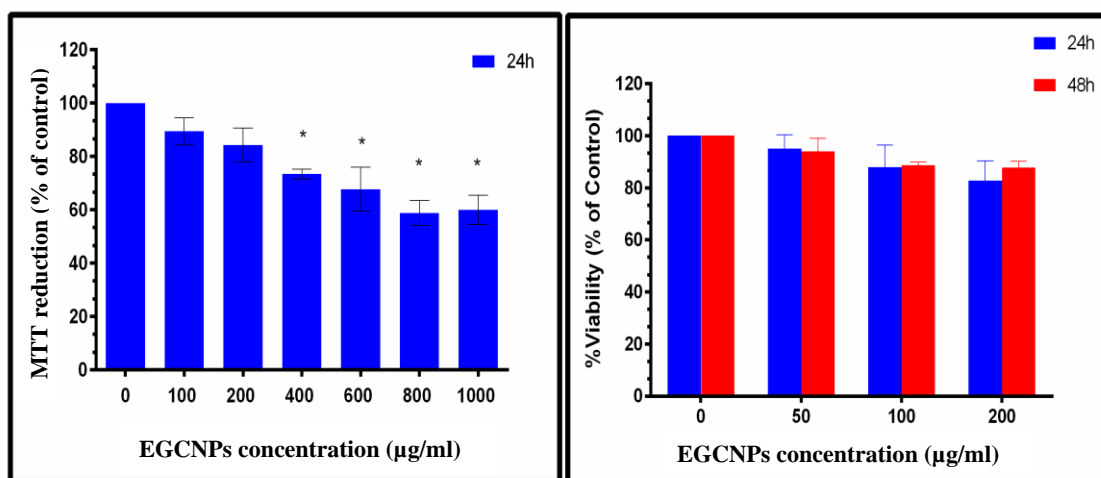


Figure 3-1 MTT reduction assay in HLECs with different EGCNPs concentrations.

Concentrations up to 200 $\mu\text{g/ml}$ are well tolerated by the cells after 48 hours of exposure. At concentrations of 400 $\mu\text{g/ml}$ and beyond, significant decrease in viability was observed after treatment for 24 h. Error bars are presented as mean \pm SEM. Asterisks denote statistically significant difference from the negative control, $n = 3$, one-way ANOVA, Dunnett's multiple comparisons. Error bars are presented as mean \pm SEM.

EGCNPs concentrations up to 200 $\mu\text{g/ml}$ did not have any significant effect on cell viability, when compared to control cells at the two tested time points (p value < 0.05). However, the 24 h exposure to concentrations of 400 $\mu\text{g/ml}$ and beyond resulted in a statistically significant decrease ranging from 27% (at 400 $\mu\text{g/ml}$) to 40% (1000 $\mu\text{g/ml}$). This is the first time to show the MTT cytotoxicity of any nanoceria formulation in HLECs and hence direct comparisons between EGCNPs and other nanoceria formulations are not feasible. However,

it is helpful to shed light on the cytotoxicity profile of similar nanoceria formulations employed *in vitro* in other mammalian cell lines. Previous studies have shown no cytotoxicity or anti-proliferative effect of a negatively charged ethylene glycol-coated nanoceria formulation (11 nm) on Jurkat human T-lymphocytes after three days of exposure to a concentration of 200 µg/ml.¹¹³ However, no uptake studies were conducted and hence the lack of cytotoxicity might have been the result of a lack of uptake of the nanoparticles. This is a serious concern since poor or lack of internalisation of negatively charged nanoceria has been previously found in two normal cell lines; embryonic kidney cells and H9c2 cardiac myocytes.¹⁵⁴ The same study showed significant cytotoxicity of positively charged nanoceria (1 mM, 172 µg/ml) on the same cell lines after 24 hour exposure signifying the critical role the surface charge plays in determining the toxicity profile.¹⁵⁴ It is noteworthy that the positive charges on the surface of nanomaterials promote cellular adhesion and penetration owing to the ionic interactions with negatively charged cell surfaces and hence their cytotoxicity is generally expected to be more pronounced compared to negatively charged nanomaterials.^{155,156} It is possible that the adsorption of negatively charge coronae on the surface of EGCNPs (as discussed in Chapter 2, 2.3.7) reduced their toxicity by mitigating cell membrane damage normally associated with positive charged nanoparticles.¹⁵⁷

Furthermore, the proliferation of HLECs incubated with different EGCNPs concentrations (0 to 400 µg/ml) was observed for three days without medium change. As shown in Figure 3-2, HLECs with different treatments were able to reach 100% confluence following a similar growth pattern to the negative control. Statistically non-significant variation in the early stages of growth were observed as the cellular growth pattern in the four fixed imaged areas in each well can slightly change from one well to another. Additionally, the presence of EGCNPs during Incucyte[®] phase contrast imaging generates some artefacts which can be

misidentified as cells by the Incucyte[®] confluence analysis algorithm causing slight exaggeration of the confluence values in the treated conditions. Nonetheless, careful visual examination of the generated images shows similar growth rates. One interesting finding was that the 400 µg/ml did not adversely affect the proliferation rate over the tested duration. This contrasted with the results from the MTT assay (Figure 3-1) that showed a decrease in viability for cells incubated with EGCNPs with concentrations of 400 µg/ml and beyond which warranted further toxicological evaluation.

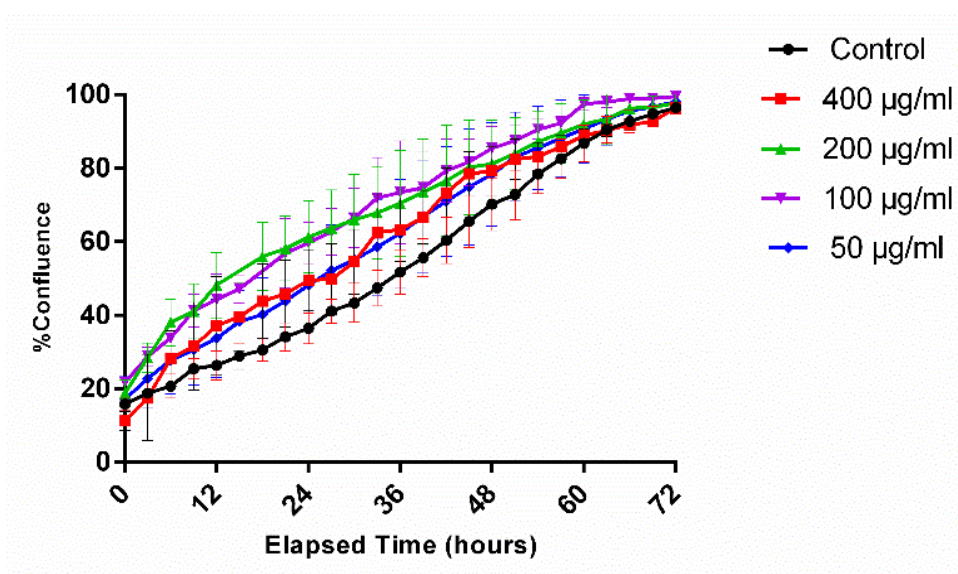


Figure 3-2 Effect of different EGCNPs concentrations on HLECs proliferation.

Cells were imaged in 6-well plates at an interval of 3 hours for 3 days while growing in full growth media using IncuCyte S3 live cell imaging system. Four different spots were imaged in each well. %Confluence was analysed by the integrated IncuCyte software and plotted against elapsed time in hours. Confluence at 0 h indicates the cell density at the point of seeding. All cells reached full confluence by 72 h. Small variations in early stage of growth arise from statistically insignificant variations in the four areas imaged in each well.

The cytotoxicity of EGCNPs in HLECs was further studied over 72 h by means of live cell imaging employing the Incucyte[®] Cytotox Red reagent. Cytotox Red is a cell-impermeable cyanine nucleic acid dye that is non-perturbing to the growth and morphology of growing

cells and has very little of any intrinsic fluorescence.¹⁵⁸ Once the cells die, their cell membrane integrity becomes compromised enabling the dye to enter the cells and intercalate with DNA which is accompanied by 100 - 1000-fold increase in its fluorescence. This allows real-time analysis of cell death in response to various pharmacological agents including EGCNPs the subject of study in this work. As shown in Figure 3-3, no significant cytotoxic effect was observed for EGCNPs concentrations ranging from 50 - 400 $\mu\text{g/ml}$ (compared to negative control) for an exposure duration up to 72 h. The cells maintained similar morphology without significant changes at all the tested concentrations and time points (Figure 3-3). At an EGCNPs concentration of 400 $\mu\text{g/ml}$, the Cytotox Red results were also in contrast with the MTT assay results. The conflicting data (between MTT and Cytotox Red assays at 400 $\mu\text{g/ml}$) suggested that at a concentration of 400 $\mu\text{g/ml}$, there seemed to be a toxic effect of EGCNPs in HLECs that did not manifest itself in the short-term proliferation and cell membrane integrity studies. Since the MTT assay is strongly associated with the mitochondrial activity where mitochondrial dehydrogenases in metabolically active cells reduce the yellow MTT tetrazolium salt to purple formazan crystals,¹⁵⁹ it was hypothesised that the higher concentration of EGCNPs (400 $\mu\text{g/ml}$) could be adversely interfering with the mitochondrial functions which in turn manifested itself in MTT assay rather than the proliferation and cytotoxicity assays. Therefore, detailed investigations of how EGCNPs may affect the mitochondria and other cell health indicators in HLECs were necessary. This was conducted by measuring the effect of EGCNPs (with concentrations ranging from 0 to 400 $\mu\text{g/ml}$) on the basal reactive oxygen species (ROS) levels, mitochondrial morphology, mitochondrial uptake, mitochondrial membrane potential, ATP levels, DNA damage, and apoptotic hallmarks. The results of these investigations are further discussed in the following sections.

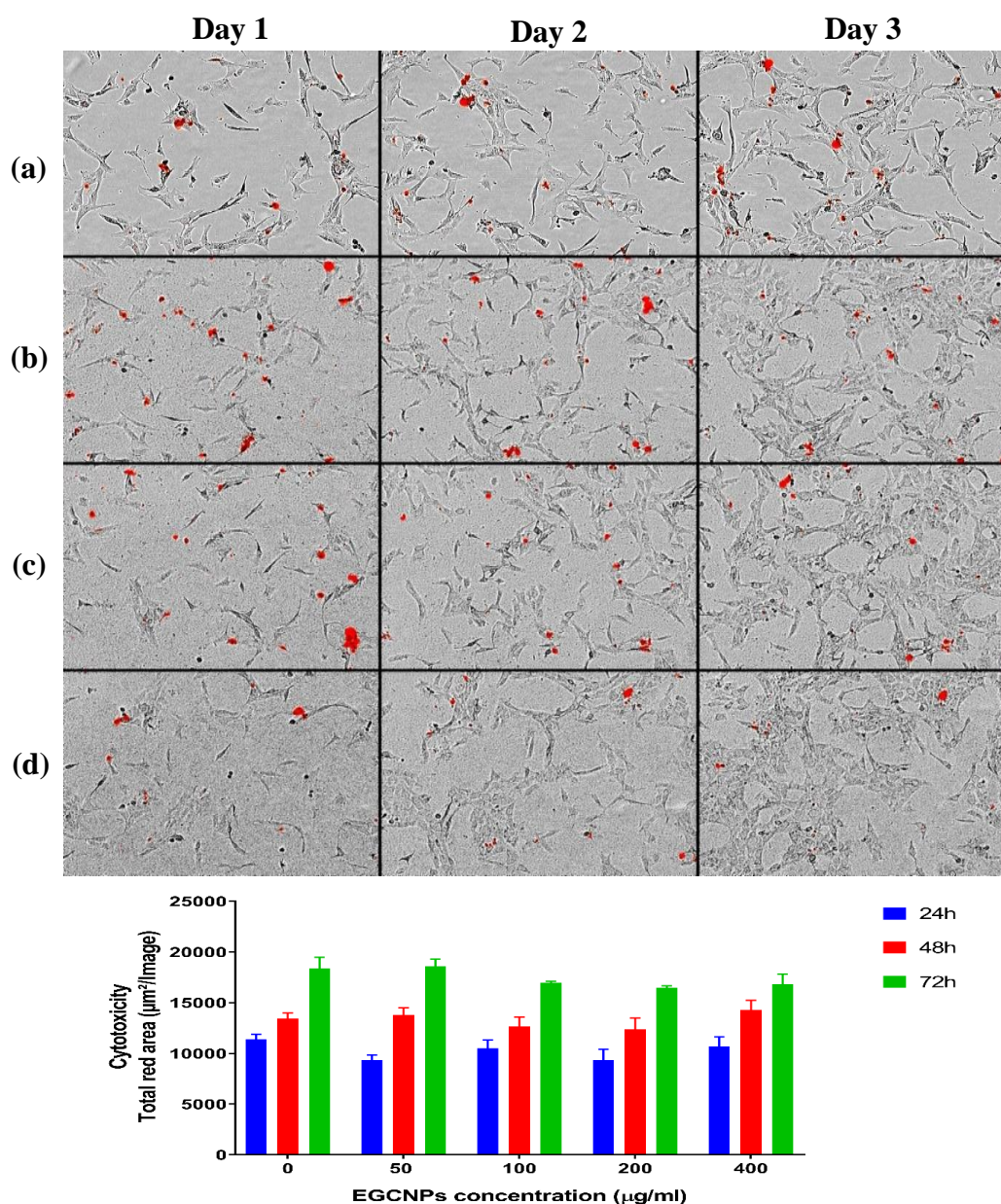


Figure 3-3 Live cell analysis showing cytotoxicity, morphology and proliferation in HLECs upon EGCNPs exposure up to 72 h. No statistically significant cytotoxicity difference (One-way ANOVA) was found between different concentration at each time point.

HLECs were treated with different EGCNPs concentration allowed to proliferate in presence of Cytotox Red dye (250 nM) that binds to the DNA of dead cells and gives red fluorescence. Images were taken using Incucyte S3 live cell imaging system (10x objective). (a) Control cells, (b) treated with 100 µg/ml EGCNPs, (c) treated with 200 µg/ml EGCNPs, (d) treated with 400 µg/ml EGCNPs. Error bars are displayed as mean \pm SEM. No statistically significant difference found between treated and control cells at each time point (one-way ANOVA) indicating that EGCNPs are not cytotoxic at these exposure conditions.

3.3.2 Acute exposure to high EGCNPs concentrations increases basal ROS

Overproduction of ROS is one of the most common pathways involved in nanomaterials toxicity.¹³⁸ ROS are involved in the aetiology and pathogenesis of many diseases and disorders such as; Alzheimer's disease, Parkinson's disease, diabetes and cataract and hence the identification of the effects of new drugs on the redox state of a target cell line/tissue is essential.^{106,107,160,161} Therefore, the basal ROS level in HLECs was measured after 24 h exposure to different EGCNPs concentrations (0 - 400 $\mu\text{g/ml}$) using H₂DCFDA probe. H₂DCFDA is a non-fluorescent cell-permeable dye which is cellularly retained upon internalisation due to deacetylation, and then oxidised by the action of ROS into highly fluorescent DCF enabling relative estimation of ROS levels. As shown in Figure 3-4, EGCNPs concentrations up to 200 $\mu\text{g/ml}$ did not lead to significant alteration to the basal ROS level when compared to control cells ($p>0.05$). This agrees with the aforementioned cell viability and cytotoxicity results. Conversely, when the EGCNPs concentration was increased to 400 $\mu\text{g/ml}$, a significant elevation in ROS level was observed indicating oxidative action exerted by EGCNPs agreeing with MTT assay results shown in Figure 3-1. This shows that even though EGCNPs possess antioxidant and ROS scavenging properties,⁸¹ short-term overexposure to high concentrations can elevate ROS levels. This increase in ROS levels is likely to have been caused by Fenton/Haber Weiss like reactions where reduced metal ions (*e.g.* Ce³⁺) react with cellular hydrogen peroxide (H₂O₂) producing hydroxyl radicals (HO•) that are highly toxic to biomolecules.¹⁶² It was previously shown in Chapter 2 that EGCNPs had surface trivalent cerium (Ce³⁺) and hence the progression of a Fenton-like reaction is expected to occur as reported in the literature according the following equations:¹⁶³

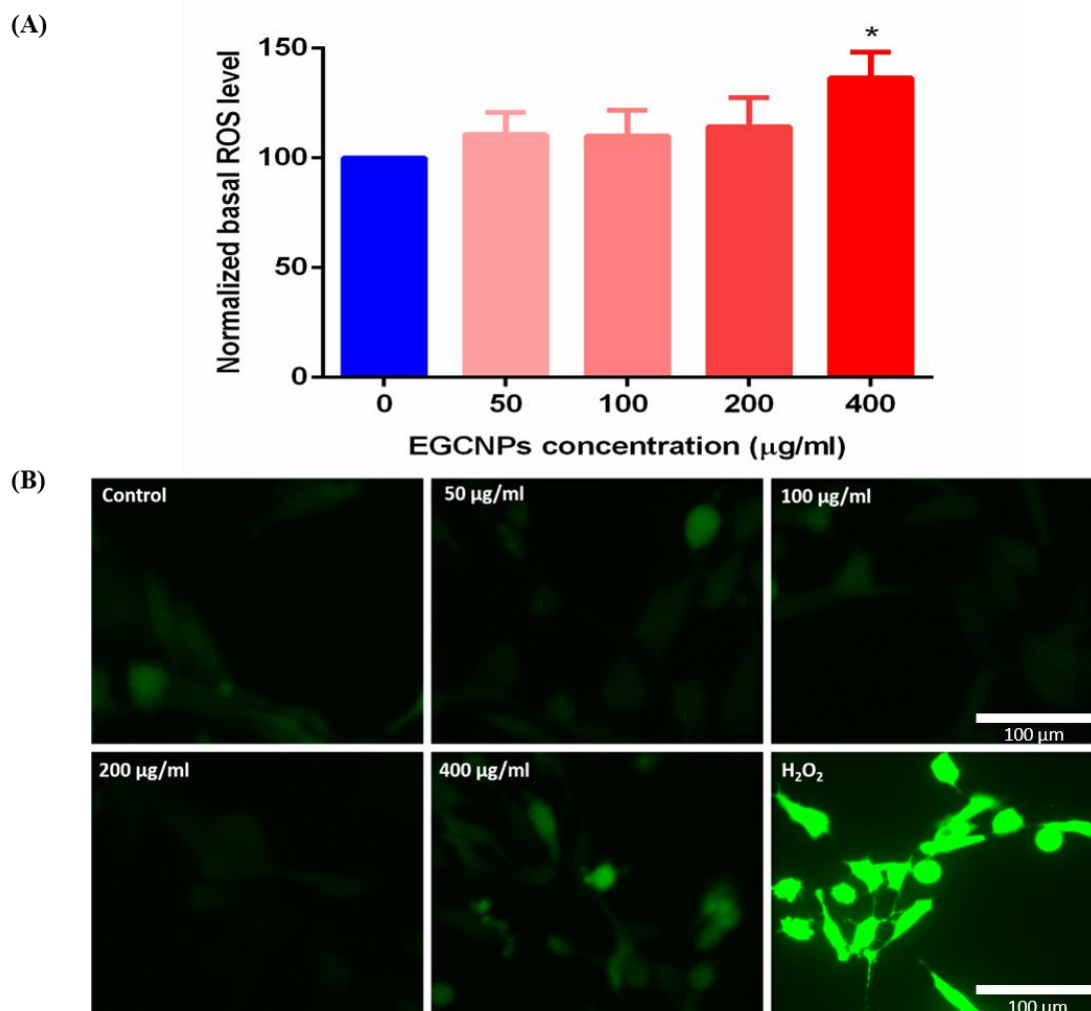
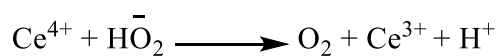
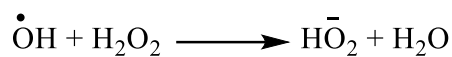
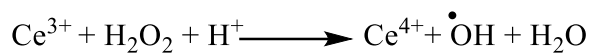


Figure 3-4 Effect of EGCNPs (24 h exposure) on basal ROS level in HLECs employing H₂DCFDA fluorescent probe.

Measurement carried out by (a) a plate reader, (b) a fluorescence microscope. Asterisks denote statistical significance from negative control (0 µg/ml), $n \geq 3$, one-way ANOVA followed by Dunnett's multiple comparisons test, $*p < 0.05$. Error bars are presented as mean \pm SEM.

3.3.3 EGCNPs localise in the mitochondria

Since the mitochondria are the main source of ROS generation,¹³⁸ it was necessary to investigate if EGCNPs exert their impact on ROS levels through becoming localised in the mitochondria. To achieve that, EGCNPs-treated HLECs were harvested and their mitochondria were isolated from the cytosolic fraction by differential centrifugation using a standard mitochondria isolation procedure.¹⁶⁴ The isolated mitochondria were then examined with a scanning electron microscope (SEM) and the presence of cerium was checked for using energy dispersive X-ray spectroscopy (EDX). EDX is a valuable tool enabling the identification of different elements based on their emitted characteristic X-rays after excitation with a high accelerating voltage electron beam.¹⁶⁵ By using this technique, it was feasible to avoid surface functionalisation with fluorescent markers; a common practice in the literature to track the localisation of the nanoparticles which changes the surface properties and in turn could affect the uptake behaviour of nanoparticles.¹⁶⁶ Figure 3-5a shows an SEM micrograph of the isolated mitochondria and its associated cerium EDX map (the red regions are associated with high cerium characteristic X-ray emissions). The full elemental composition of the scanned map is displayed in Figure 3-5b and the M_{α} and L_{α} characteristic X-ray emission peaks for cerium were observed at 0.88 KeV and 4.83 KeV respectively. Furthermore, semi-quantitative EDX elemental analysis shows that cerium was the third most abundant element in the mitochondria following carbon and oxygen. These findings clearly confirm that significant and uptake localisation of EGCNPs in the mitochondria occurs within 24 h of treatment. The mitochondrial localisation of EGCNPs is likely caused by the strong positive charge that EGCNPs carry (+44 mV) making the negatively charged interior of the mitochondria an ideal target.¹⁰⁶ This finding is interesting since it is known from the previous investigation in Chapter 2 that protein coronae is adsorbed on the surface of EGCNPs making them slightly negatively charged (-9.7 mV) in

cell culture media containing foetal bovine serum. Nonetheless, the coronae did not seem to prevent the nanoparticles from entering the mitochondria. The surface charge is known to play a significant role in subcellular localisation of nanocereria which affects both the toxicity and activity profile.¹⁵⁴ For example, it has previously been shown that targeting nanocereria specifically to the mitochondria by surface functionalisation with the mitochondrial targeting cationic ligand triphenylphosphonium suppresses oxidative stress-induced neuronal death in mice.¹⁰⁶ The findings reported herein indicate that this specific functionalisation is not required for mitochondrial uptake in HLECs.

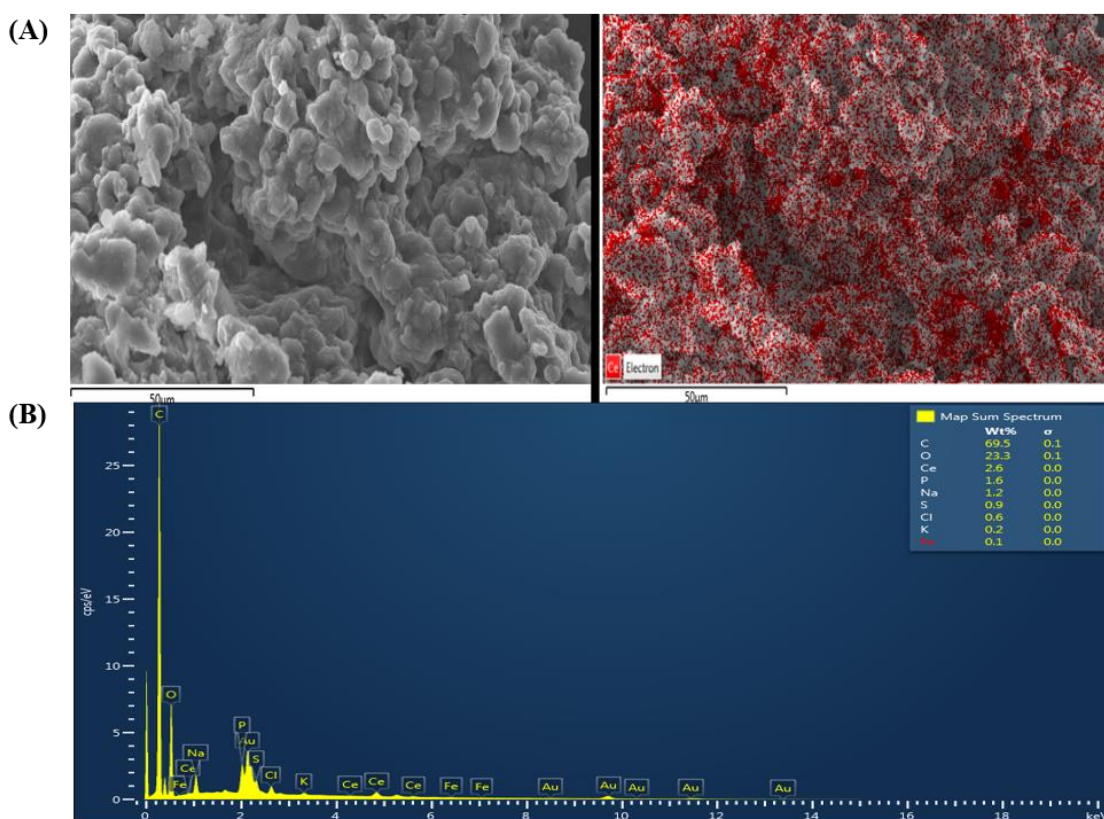


Figure 3-5 SEM-EDX analysis of isolated mitochondria.

(a) SEM micrograph of the mitochondrial enriched fraction isolated from HLECs treated with EGCNPs (left) and its associated cerium EDX mapping (right), (b) EDX spectrum and semi-quantitative full elemental analysis generated from EDX mapping of the mitochondria. The presence of gold (Au) is due to sample coating with gold. Scale bars = 50 μm .

3.3.4 Effect of EGCNPs on the mitochondrial network

Following the confirmation of mitochondrial uptake of EGCNPs, the effect of such uptake on the morphology and network organisation of the mitochondria in HLECs was studied. Staining with the mitochondria-selective stain (MitoTracker™ Red CMXRos) was employed and the cells were examined with a confocal microscope. MitoTracker™ Red CMXRos is a cell permeant dye that specifically accumulates in active mitochondria and permanently binds to mitochondrial thiol groups of cysteine residues owing to presence of reactive chloromethyl group (CH₂Cl) allowing its retention even after cell fixation.¹⁶⁷ As shown in Figure 3-6a, the mitochondria were uniform in shape and organisation when treated with EGCNPs concentrations of up to 400 µg/ml and showed no significant difference from control cells. The mitochondria were short and rod-shaped with organized localisation in the perinuclear region (Figure 3-6b). H₂O₂ used as a positive control caused significant mitochondrial aggregation and diffusion of the mitochondrial network (Figure 3-6). This suggested that at the higher concentration (400 µg/ml) the cells could be undergoing early stage apoptosis where the shape of the mitochondria is known to remain intact during the process.^{168,169} Consequently, some of the key apoptotic hallmarks were further investigated to examine this assumption and further assess the toxicological profile of EGCNPs in HLECs.

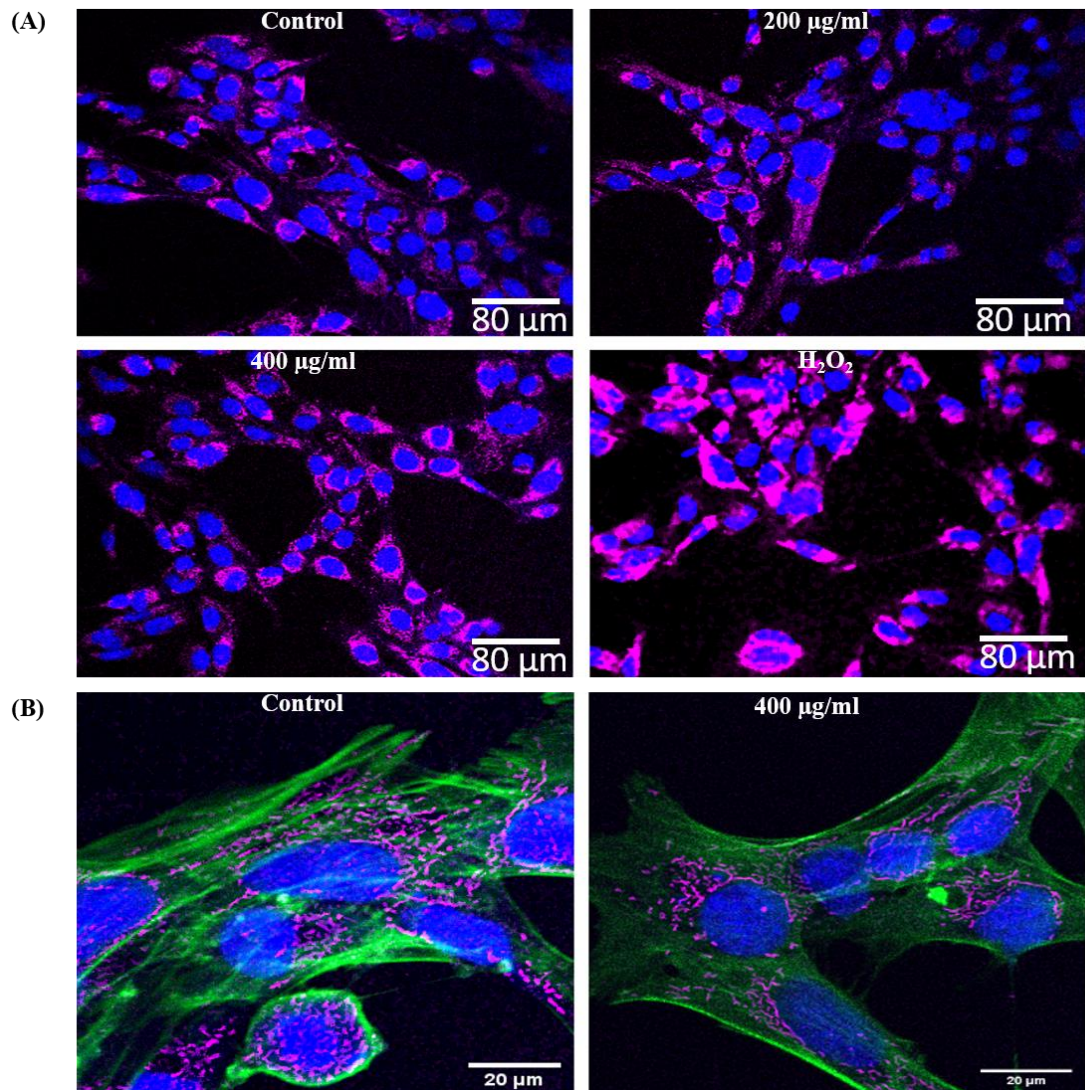


Figure 3-6 Confocal examination of mitochondria in HLECs.

(a) Representative confocal images showing the effect of different EGCNPs concentrations (24 h exposure) on the mitochondrial morphology and organization (magenta) in HLECs. (b) High magnification confocal images of the mitochondria counterstained with cytoskeleton selective stain ActinGreen 488 (green) and Hoechst 33342 (blue). No changes from control were observed up to EGCNPs concentrations of 400 µg/ml. H₂O₂ (400 µM) was used as a positive control which shows significant aggregation of the mitochondria.

3.3.5 Effect of EGCNPs on the mitochondrial membrane potential ($\Delta\Psi_m$)

The integrity of the mitochondrial membrane potential is one of the most critical factors in assessing the function of the mitochondria and its depolarisation (loss of normal charge distribution on both sides of the membrane) is an indicator for early stage apoptosis.^{124,168,170,171} Mitochondrial membrane depolarisation and formation of mitochondrial membrane transition pores allow the release of mitochondrial intermembrane space enzymes (*e.g.* cytochrome *c*) that activate the caspase cascade initiating apoptosis.^{124,172} JC-1 dye was used to differentiate between healthy and depolarised mitochondria based on the change in the dye's fluorescence. In healthy mitochondria, the cationic dye accumulates into the negatively charged interior of mitochondria where it forms J-aggregates shifting the fluorescence from green to red. Consequently, decreased red/green ratio is an indicator for mitochondrial membrane depolarisation.¹⁷³ This ratio is highly accurate as it reports on changes in membrane potential regardless of the shape, size or density of mitochondria.¹⁷³ As shown in Figure 3-7, EGCNPs concentrations up to 200 $\mu\text{g/ml}$ had no significant effect on the ($\Delta\Psi_m$). When the concentration was increased to 400 $\mu\text{g/ml}$, significant decrease in red/green ratio (membrane depolarisation) was observed suggesting that early stage apoptosis was taking place. For comparison, two different concentrations of sodium azide (NaN_3) were used as positive controls since NaN_3 is known to induce mitochondrial depolarisation by blocking complex IV activity in the mitochondrial electron transport chain.¹⁷³ Figure 3-8 shows representative images acquired from high throughput Incucyte[®] S3 imaging system which were used for quantification of JC-1 red/green ratio.

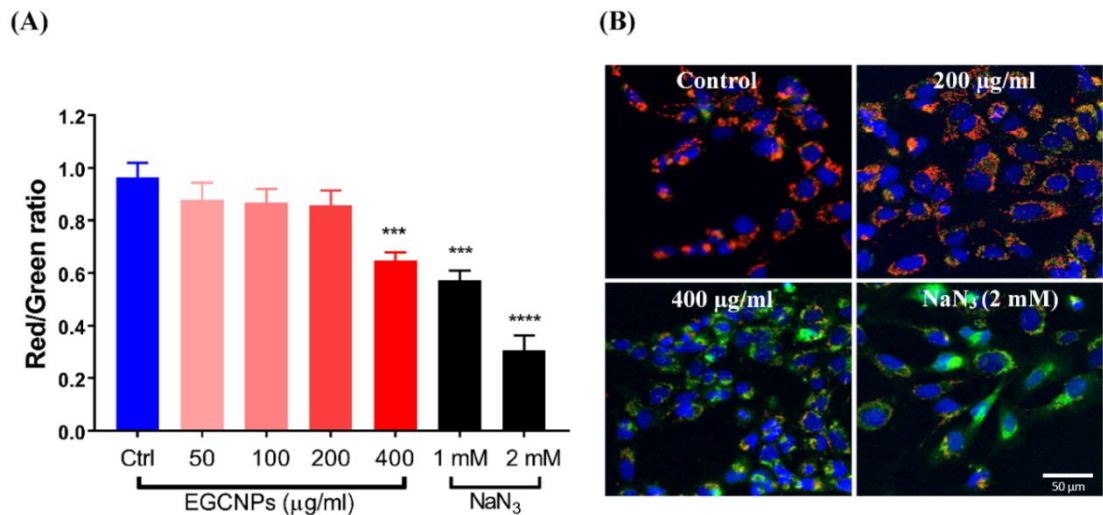


Figure 3-7 Effect of EGCNPs concentrations on mitochondrial membrane potential ($\Delta\Psi_m$) measured using JC-1 staining.

Decrease in red/green ratio indicates depolarisation of the mitochondrial membrane. (a) Quantification of red/green ratio from high throughput Incucyte[®] S3 fluorescent images, (b) Representative high magnification confocal microscopy images with JC-1 staining counterstained with Hoechst 33342 (blue) showing significant increase in green/red ratio (depolarised $\Delta\Psi_m$) at 400 $\mu\text{g/ml}$. Up to 200 $\mu\text{g/ml}$, the red and green had a ratio close to 1 causing them to colocalise. NaN₃ was used as a positive control as it is a known disruptor of ($\Delta\Psi_m$). Asterisks denote statistical significance from control (*** $p \leq 0.001$ and **** $p \leq 0.0001$), $n = 3$, one-way ANOVA, Dunnett's multiple comparisons. Error bars are presented as mean \pm SEM.

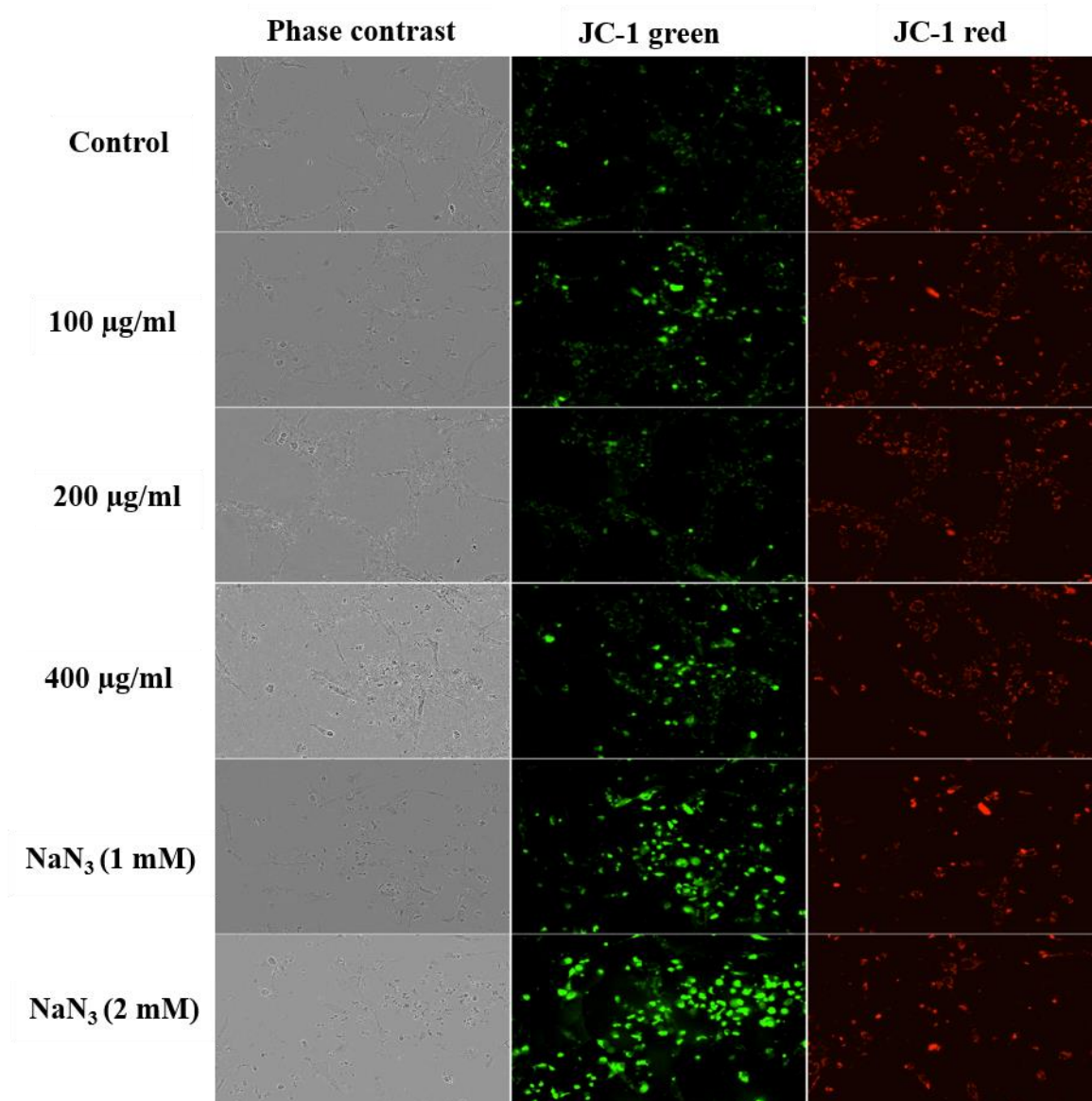
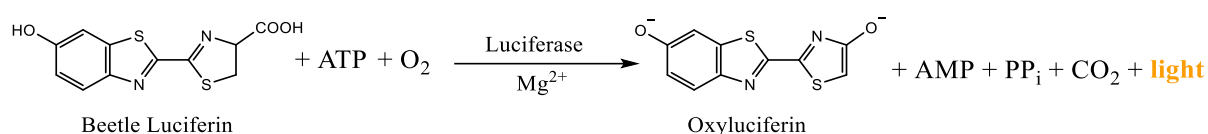


Figure 3-8 Representative Incucyte[®] S3 images used for the quantification of JC-1 red/green ratio in HLECs after treatment with different EGCNPs concentrations.

Three fields of view were imaged in each well (in 96 well plates), at least four wells were used for each treatment condition. The experiment was independently repeated three times (36 images were quantified per each condition).

3.3.6 Effect of EGCNPs on ATP level (luciferase assay)

The intracellular ATP production is considered a well-accepted differentiator between apoptotic and necrotic cell death.^{169,174} Apoptosis is an energy-driven process which requires ATP for its execution. The cells require ATP in order to initiate the controlled apoptotic cell death through various ATP-dependent steps such as caspase activation, nuclear condensation and apoptotic bodies formation.¹⁷⁴ When the ATP level drops significantly, it is an indication of the termination of controlled cell death and necrosis starts to take over. The changes in intracellular ATP production upon exposure to different EGCNPs concentrations were measured based on the bioluminescence produced using the highly sensitive luciferin-luciferase assay according to the following reaction:^{174,175}



As shown in Figure 3-9, no significant decline in ATP level was observed in HLECs treated with EGCNPs concentrations up to 200 $\mu\text{g/ml}$ which agrees with the previous results. Interestingly, no changes in ATP level was observed at 400 $\mu\text{g/ml}$ even though mitochondrial membrane depolarisation does take place at this concentration. The cells were then treated for a longer duration (48 h), and a significant decrease in ATP production was observed at 400 $\mu\text{g/ml}$ (Figure 3-9). This can be attributed to the termination of apoptosis in some of the cells with concomitant ATP depletion which manifested itself in the longer treatment duration. Another interesting finding was the slight increase (significant at 100 and 200 $\mu\text{g/ml}$) in ATP level at low EGCNPs concentrations after 24 h. One possible reason is that the uptake of EGCNPs may have proceeded through energy-dependent clathrin-mediated and caveolae-mediated endocytic pathways, which have been reported as the main uptake mechanism of nanoceria in many mammalian cell lines.^{118,154,166}

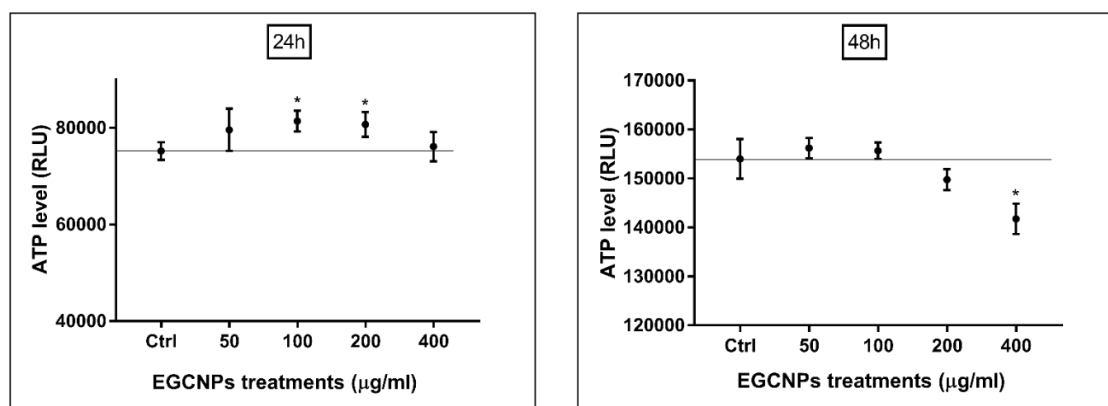


Figure 3-9 Effect of EGCNPs on ATP production in HLECs measured by luciferin-luciferase bioluminescent assay at 24 h and 48 h.

Asterisks denote statistical significance from control, n=3, one-way ANOVA. Error bars are presented as mean \pm SEM.

3.3.7 Genotoxicity (pH2AX immunocytochemistry)

DNA integrity is particularly important if EGCNPs are to be used for cataract treatment and prevention. The eye lens is in continual growth amassing new cell layers on top of the older ones.¹⁰⁹ HLECs are the stem cells of the lens that are found just beneath the anterior lens capsule and they are the initiators of the lens growth. HLECs synthesise the lens proteins (about 35% of the lens weight) and differentiate into lens fibre cells forming the bulk of the eye lens.^{6,109} Consequently, DNA damage in HLECs could lead to impaired protein synthesis, impaired differentiation and disruption of protein organisation which could result in alteration in the lens refractive index, lens opacity and cataract formation.^{6,109,176} EGCNPs induced genotoxicity was evaluated by detecting DNA double strands breaks (DSBs). As a response to DSBs, the histone protein H2AX is phosphorylated (pH2AX) which can be detected and quantified with immunofluorescence.¹⁷⁷ Figure 3-10 shows a summary of main steps followed in the quantification of genotoxicity level in HLECs.

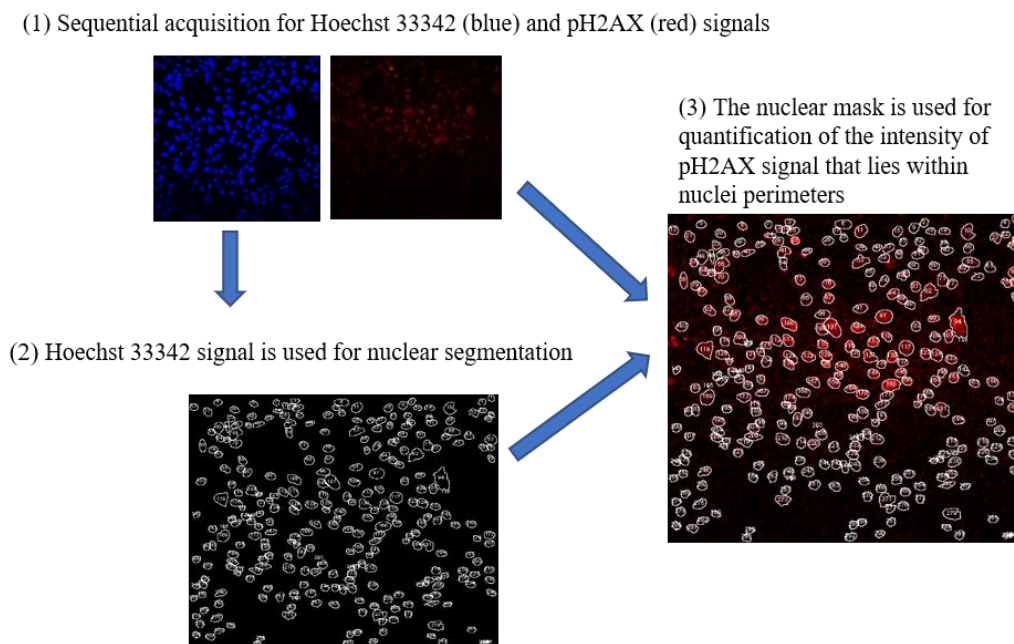


Figure 3-10 Schematic representation of the steps employed for the quantification of DNA damage (genotoxicity) by the detection of phosphorylated histone variant H2AX.

The results show that EGCNPs had no significant genotoxic effect up a concentration of 200 $\mu\text{g/ml}$ (Figure 3-11). However, at 400 $\mu\text{g/ml}$ significant genotoxicity was observed (Figure 3-11). It was shown before that nanoceria coated with 3-phosphonopropionic acid had no adverse effects on DNA health when exposed to a concentration of 10 $\mu\text{g/ml}$ for 24 h.¹⁰⁹ It is demonstrated here that EGCNPs can be tolerated at a 20-fold higher concentration (200 $\mu\text{g/ml}$) for same treatment duration. However, an overdose (400 $\mu\text{g/ml}$) caused significant DNA double strand breaks as shown in Figure 3-11 agreeing with the above results. DNA damage at high EGCNPs concentration is likely caused by increased ROS which attack the DNA causing double strand breaks.¹⁶² Additionally, it is possible that some nuclear uptake of EGCNPs took place promoting genotoxicity.¹⁴⁵ Even though some nanoparticles have poor permeability into the nuclei, their entry into the nuclei is inevitable during mitosis where the nuclear membrane is broken as the cells prepare for division.¹⁷⁸ As such, higher doses of EGCNPs will provide more chance for increased localisation and possibly

aggregation into the nuclei. The uptake and localisation of nanoceria in HLECs will be discussed in the following chapter.

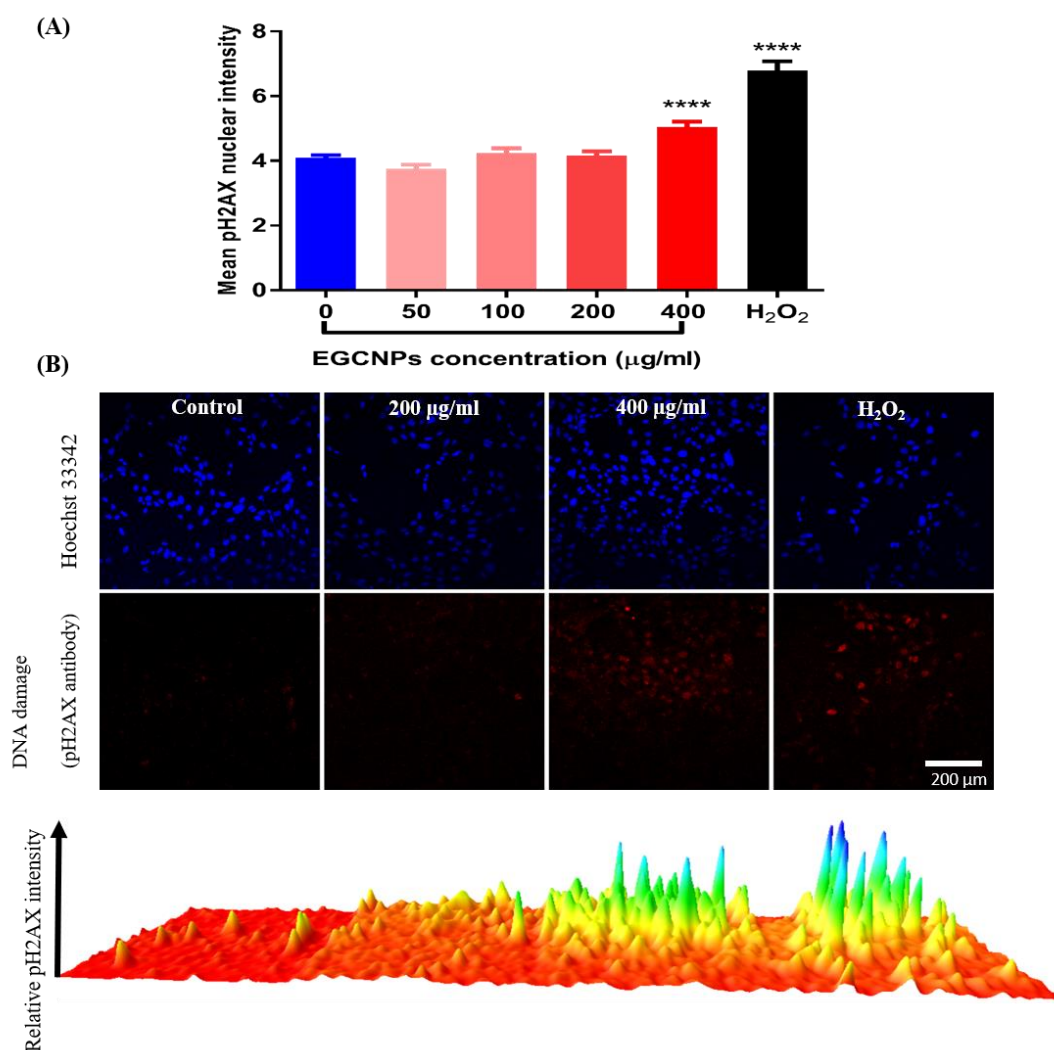


Figure 3-11 Effect of EGCNPs on DNA damage in HLECs (24 h) measured by immunocytochemistry through detection and quantification of pH2AX mean intensity.

(a) quantification of pH2AX fluorescence intensity (only pH2AX signal inside nuclei perimeters) within at least 500 individual nuclei obtained from 4 independent experiments. (b) representative confocal images and 3D surface plotting of relative pH2AX intensity (red). Asterisks denote statistical significance from control (**** $p \leq 0.0001$), one-way ANOVA, Dunnett's multiple comparisons. Error bars are presented as mean \pm SEM.

3.3.8 Effect of EGCNPs on caspase-3,7 activity

The previous results suggested that very high EGCNPs concentrations ($\geq 400 \mu\text{g/ml}$) may be causing apoptosis in HLECs after short-term exposure (24 h) and hence some of the main

indicators of apoptosis were investigated to confirm this inference. Activation of caspases is a key indicator of cells irrevocably committing to apoptotic death.¹⁷² The activation of caspases 3 and 7 (effector caspases in mammals) in HLECs upon EGCNPs treatment was detected over 24 h by means of live cell imaging using the IncuCyte[®] Caspase-3/7 Red apoptosis assay reagent. The reagent consists of a red fluorophore (NucView[™]633) attached to an activated caspase recognition motif (DEVD). Upon binding with activated caspases, the motif is cleaved, and the fluorophore is liberated then intercalates with DNA giving red fluorescence proportional to caspase activity that can be quantified over time. Figure 3-12 shows that EGCNPs do not result in significant caspase activation up to concentrations of 200 µg/ml compared to control cells. Overexposure to EGCNPs (400 µg/ml) caused significant caspase activation as soon as 12 h from the treatment. This agrees with the JC-1 data (Figure 3-7) where loss of membrane potential was observed only at 400 µg/ml. It is well known that mitochondrial membrane depolarisation results in the release of cytochrome c from the mitochondrial intermembrane space into the cytoplasm where it activates apoptotic protease activating factor 1 (Apaf-1).¹⁷² The cytochrome c-Apaf-1 complex binds to ATP (which was shown to be amply present at 400 µg/ml) forming a complex known as apoptosome.¹⁷² The apoptosome then activates caspase 9 (an initiator caspase in mammalian cells) which in turn activates caspase 3 and caspase 7 to execute the apoptotic process.¹⁷² It should be noted that there was a systematic increase in caspase activation for each EGCNPs concentration (including control) over time which can be attributed to normal controlled death as cells grow in a confined area.

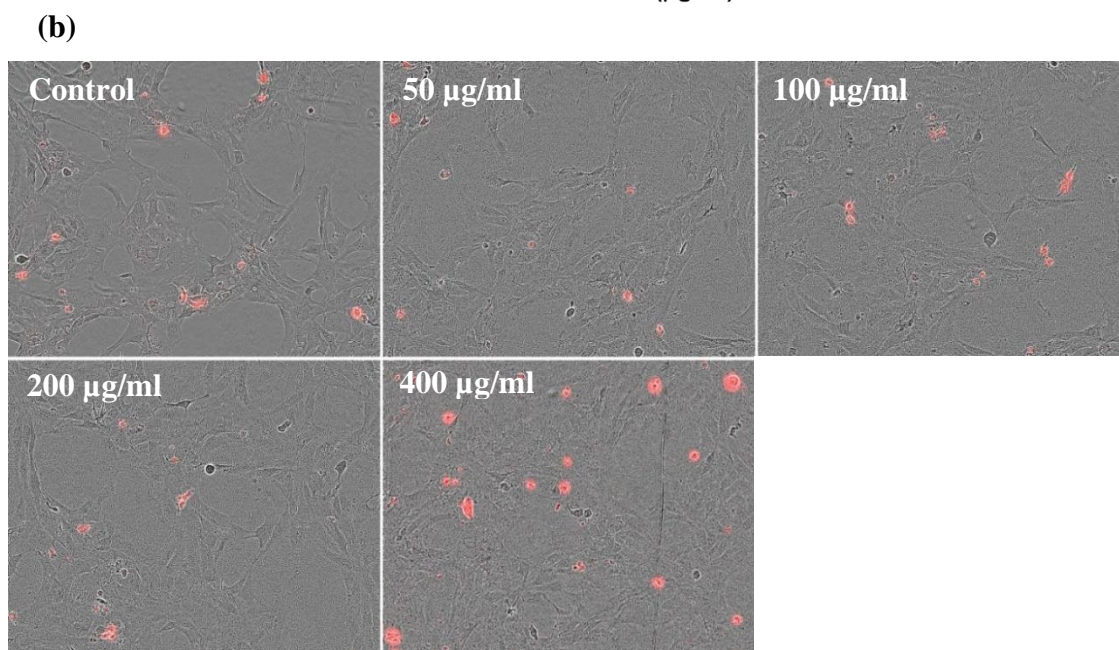
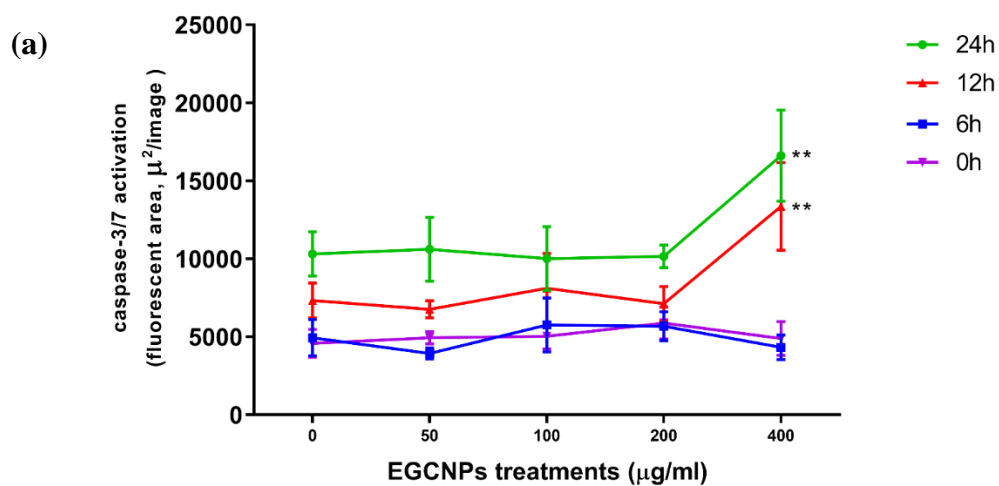


Figure 3-12 (a) Effect of different EGCNPs concentrations on caspase-3,7 activity in HLECs.

No significant caspase activation was observed up to 200 μg/ml. At 400 μg/ml, significant caspase activity was observed as soon as 12 h of treatment, (b) representative Incucyte® images used for measurement and quantification of caspase-3,7 activity in HLECs after treatment with different EGCNPs concentrations (0 - 400 μg/ml) for 24 h. Asterisks denote statistical significance from control in same time group (** $p \leq 0.01$), $n=4$, two-way ANOVA. Error bars are presented as mean \pm SEM.

3.3.9 Annexin V/Cytotox Red assay

To further confirm cell commitment to the apoptotic rather than the necrotic pathway, at an EGCNPs concentration of 400 μg/ml, the cells were double stained with annexin V

green/Cytotox Red and observed by means of live cell imaging using Incucyte[®] S3 live imaging system. The cell membrane of healthy cells can be characterised by asymmetrical distribution of the anionic phospholipid phosphatidylserine (PS) where it is restricted to the inner leaflet of the cell membrane.^{179,180} During apoptosis, the asymmetry is disturbed and PS is externalised to the outer leaflet of the cell membrane.^{179,180} The activation of caspases has been linked in the literature to this externalisation process which allows the recognition of apoptotic bodies by adjacent cells.¹⁶⁸ Annexin V is a protein (36 KDa) that binds to externalised PS in presence of Ca²⁺ and hence can be used to identify apoptotic cells by using a fluorescently labelled annexin V.¹⁷⁹ Apoptotic cells only show annexin V labelling (green) while late apoptotic or necrotic cells are double labelled with both annexin V/Cytotox Red. Figure 3-13a shows that the 400 µg/ml concentration caused a significant increase in cells labelled with annexin V, when compared to negative control after treatments durations of 6 h, 12 h and 24 h supporting the caspase-3,7 data. No significant change was observed in the number of necrotic cells (labelled with Cytotox Red) over the same treatment durations (Figure 3-13b). Together, these findings indicate that apoptosis is the main mechanism of cell death in HLECs upon short-term overexposure (≥ 400 µg/ml) to EGCNPs.

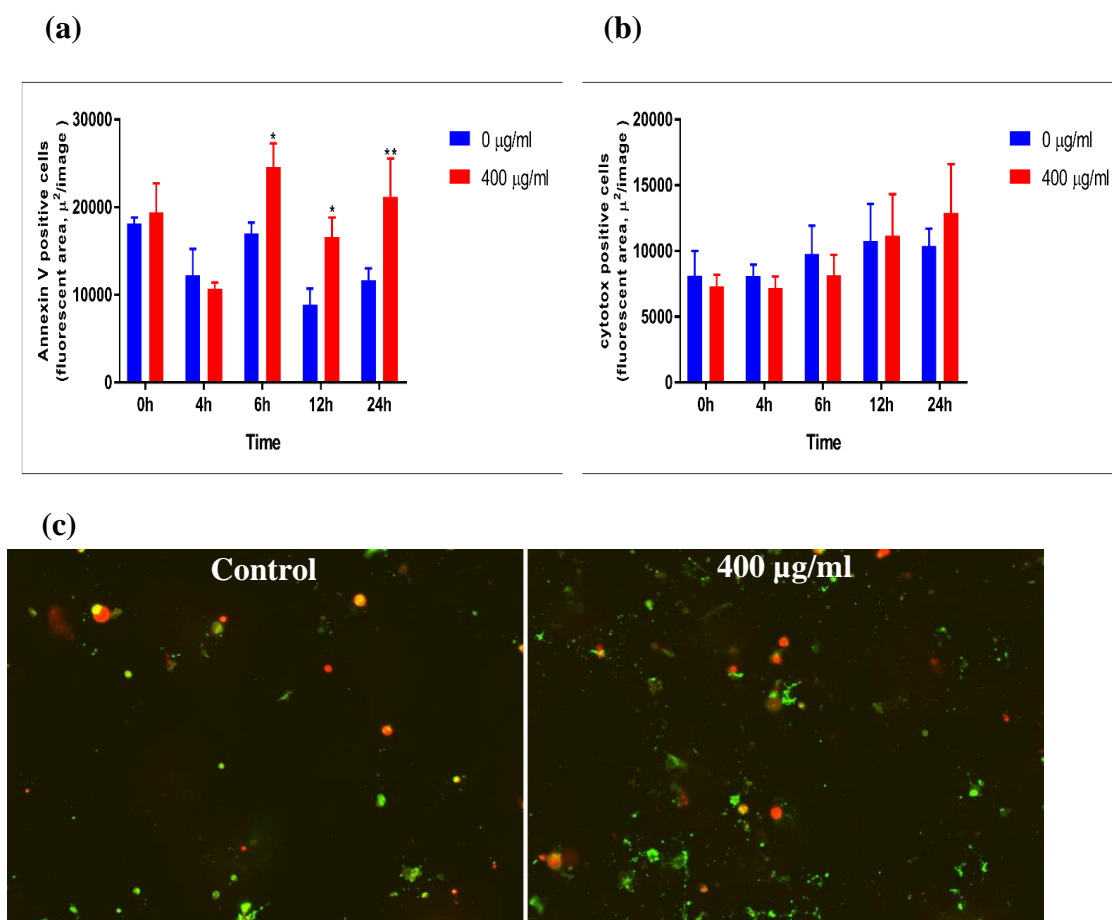


Figure 3-13 Annexin V/Cytotox Red assay comparing non-treated (0 μg/ml) and EGCNPs-treated (400 μg/ml) HLECs over 24 h.

(a) quantification of apoptotic cells that only show annexin V staining, (b) quantification of necrotic or late apoptotic cells that show Cytotox Red staining, (c) representative Incucyte images of Annexin V green/Cytotox Red staining in HLECs comparing control and EGCNPs treated cells (24 h). Treated cells showed marked increase in annexin V labelling (apoptotic cells) without increase in number of necrotic cells (Cytotox Red). Asterisks denote statistical significance from control at the same time point ($*p \leq 0.05$ and $**p \leq 0.01$), $n=4$, two-way ANOVA. Error bars are presented as mean \pm SEM.

The toxicity of nanoceria has been studied *in vitro* using a range of cell lines (reviewed in Gagnon and Fromm, 2015),¹⁴³ but the data are not comparable given the varying characteristics of nanoceria used including the shape, size, colloidal stability, zeta potential, surface valence, surface functionality and the range of nanoceria fabrication methods. There are still inconsistencies in the literature regarding the mechanism of nanoceria toxicity.¹⁴²

The results of the present study show, in a dose-dependent manner, the toxicity mechanism of well characterized nanoceria (EGCNPs) in human lens epithelium. To conclude, when considering nanoceria toxicity, and given their redox active characteristics, emphasis must be on the evaluation of the mitochondrial functionality as an early indicator for cell health as it can reveal significant effects that can be easily overlooked in short-term proliferation and standard toxicological studies.

3.4 Conclusion

EGCNPs toxicity in HLECs was evaluated by studying varying cellular health indicators. The results show that EGCNPs had no cytotoxic or genotoxic effects up to concentrations of 200 $\mu\text{g/ml}$ and hence can be safely used for biomedical applications below that threshold. At a higher dose (400 $\mu\text{g/ml}$), EGCNPs induced ROS generation which mediated cellular apoptosis. It was clearly demonstrated that the cell death was driven by the mitochondrial apoptotic pathway, wherein ROS-mediated mitochondrial membrane depolarisation is followed by DNA damage and caspase cascade activation. To date, this is the first report on the mechanism of nanoceria toxicity in lens cells. To conclude, when considering nanoceria toxicity, emphasis must be on the evaluation of mitochondrial functionality as an early indicator for cell health; often overlooked in short-term proliferation studies.

4 Uptake, localisation and anti-cataract properties of EGCNPs in human lens epithelium

4.1 Introduction

A major cause of chronic diseases that are exacerbated by ageing, are changes in protein structure that lead to malfunction of tissues, organs and ultimately, to the system. These are conditions such as diabetes, Alzheimer's disease and cataract.^{161,181} The latter can occur as solely ocular, or as a secondary manifestation of a systemic condition.²² This presents the opportunity of using cataract as a model for investigating the causal factors of visual impairment and to gain insight into causal factors that underpin systemic protein-based diseases. Cataract is an opacification of the eye lens that prevents light from reaching the retina by either scattering or absorbing traversing rays. It is the leading cause of blindness worldwide with over 24 million cases in the United States reported in 2010 which is expected to double by 2050.¹⁸² Cataract is a multifactorial disease with oxidative stress considered to be one of the major factors contributing to its development.^{22,26,183–186} The human lens possesses natural defence mechanisms against reactive oxygen species (ROS) including the presence of reduced glutathione and antioxidant enzymes such as superoxide dismutase and catalase.¹⁸⁶ With ageing, such defences weaken, rendering the cells prone to oxidative insult that can lead to post-translational modifications and aggregation of lens proteins (crystallins) eventually causing cataract.^{22,26,186} Human lens epithelial cells (HLECs) are the stem cells of the lens that differentiate into fibre cells forming the lens body. Oxidative stress induced damage to the lens epithelial cells would result in faulty protein synthesis and aggregation that eventually would cause lens opacity.⁶ As such the use of HLECs as an *in-vitro* model has become important to draw conclusion on cataract progression. Currently, surgical

extraction of the cataractous lenses and replacement by intraocular implants is the only approved treatment. This comes with limitations such as accessibility in the developing world and the associated perioperative and postoperative complications.¹ Additionally, to date there is no single implant model that can replicate the image quality and the capacity to alter focus that the biological lens can.⁵¹

In the previous two chapters, the effective synthesis of a novel nanoceria formulation (EGCNPs) was achieved and its safety has been established in HLECs. In this chapter, the aim of research described in this chapter is to study whether EGCNPs can enter HLECs at the established safe concentrations, and if such entry will provide anti-cataract actions. For the purpose of the discussion of this chapter, anti-cataract actions are defined as the general ability of a therapeutic to protect against oxidative stress, improve natural enzymatic defence system in HLECs, and block one of the most common post-translational modifications in the human lens namely glycation.

4.2 Materials and methods

4.2.1 Time-dependent uptake of EGCNPs in HLECs (ICP-MS studies)

The cellular uptake of EGCNPs over time was measured employing inductively-coupled plasma mass spectroscopy (ICP-MS). HLECs were seeded in 6-well plates in complete EMEM (50000 cell/well) and allowed to establish for 24 h. The medium was then removed and replaced with fresh medium containing EGCNPs (200 µg/ml). Different plates were used to test the following EGCNPs incubation times: 0 min, 15 min, 1 h, 2 h and 4 h. After the specific incubation period with EGCNPs, the medium was removed, and the cells were rinsed three times with PBS to remove any surface bound EGCNPs. The washed cells were harvested using 500 µL trypsin-EDTA (0.25%) and collected in 20 ml Falcon tubes (3 tubes/replicates per each time point). The number of collected cells in each tube was counted using LUNA-II™ Automated Cell Counter (Logos Biosystems, South Korea). The cells in each tube were then digested by adding concentrated nitric acid (HNO₃, 2 ml, 70%) to each tube and left for three days to ensure complete digestion of EGCNPs. After digestion, the solutions were diluted to a known volume (12 ml) using 1% HNO₃ and the insoluble material were removed by means of filtration. The concentration of cerium ions in each solution was calculated using ICP-MS (PerkinElmer NexION 1000, USA). A cerium standard for ICP (TraceCERT®, 1000 ppm Ce in nitric acid, Sigma Aldrich, UK) was serially diluted in 1% HNO₃ to make the following concentrations: 1000, 500, 250, 125, 62.5, 31.25 ppb, and a calibration curve was subsequently generated (available in the appendix). For accurate determination of cerium content in the cells, the amount of cerium in each condition (tube) was normalised to the counted number of digested cells and the results were expressed as cerium amount (ng) per 10000 cells.

4.2.2 Mechanism of EGCNPs uptake in HLECs

To determine if the uptake of EGCNPs in HLECs proceeds mainly by passive uptake mechanism or energy-dependent endocytosis, two ways of measuring endocytosis inhibition were employed. Briefly, HLECs were seeded in 6-well plates as above and treated with chemical endocytosis inhibitors NaN_3 (10 mM, Sigma Aldrich, UK) and 2-deoxy-D-glucose (2-DOG, 50 mM, Sigma Aldrich, UK) for 30 min. After the treatment period, EGCNPs (200 $\mu\text{g/ml}$) were added to the cells and left for 3 h. The cells were then rinsed with PBS, and digestion and ICP-MS analysis were carried out as mentioned above. In a separate set of experiments, endocytosis inhibition was carried out by incubating the cells with EGCNPs (200 $\mu\text{g/ml}$) for 4 h at 4 °C instead of using chemical endocytosis inhibitors. All experiments were run in triplicate (n=3).

4.2.3 Localisation of EGCNPs and EuCNPs in HLECs (SEM-EDX studies)

HLECs were grown to 70% confluence in full growth medium on cover slips in 6-well plates and then treated with EGCNPs (200 $\mu\text{g/ml}$) and incubated for one minute, 4 h and 24 h. After each treatment duration, the medium was aspirated, and the cell monolayers were washed with serum free medium followed by fixation in paraformaldehyde in PBS buffer (4%) for 15 minutes. The cells were then washed three times with PBS and dehydrated in graded alcohol solutions (50%, 60%, 70%, 80%, 90% and 100% ethanol) for five minutes each. The specimens were coated with layer of gold (5 nm) using a sputter coater (Q150R ES, Quorum, UK) and visualised under SEM (JEOL, JSM-7100f, Japan) with accelerating voltage of 10 kV and probe current of 10 mA. EDX spectra were collected in at least ten different cell compartments using Aztec software (Oxford Instruments, UK). A contrast-sensitive pseudo-colour was applied to the SEM images using imageJ (National Institutes of Health, USA) .

4.2.4 Localisation of EGCNPs and EuCNPs in HLECs (confocal studies)

HLECs were seeded in black 96-well plates with clear bottoms (Corning 353219, USA) and established for 24 h. The cells were then incubated with 200 µg/ml EGCNPs or EuCNPs for 24 h, fixed with paraformaldehyde (4 %w/v, 10 min) then permeabilised with Triton™ X-100 (0.2 %v/v, 10 min, Fisher Scientific, UK). The cells were counterstained with Hoechst 33342 (2 µg/ml in PBS, 10 min, Thermo Fisher, UK), washed with PBS (1X) and visualised using a TCS SP5 confocal laser scanning microscope (Leica, Germany). Fluorescent signals from both the nanoparticles and the nuclear stain were collected sequentially at same focal plane using a 20x dry objective (numerical aperture = 0.4) and a pinhole size of 0.9 AU. For EGCNPs detection, the cellular autofluorescence was first photobleached using a high intensity laser power for 2 min, and EGCNPs were detected at (530-560 nm) using 488 nm excitation laser line. In the case of EuCNPs, their fluorescence signal was strong enough compared to cellular autofluorescence to be detected and the nanoparticles were viewed directly at 612 nm using 514 nm excitation laser line.

4.2.5 Protective effect of EGCNPs against oxidative stress in HLECs

The protective effect of EGCNPs on oxidative stress levels in HLECs after H₂O₂ exposure was investigated using 2',7'-dichlorodihydrofluorescein diacetate (H₂DCFDA) staining (D399, Thermo Fisher, UK) according to the supplier's instructions. Briefly, HLECs were seeded in 96-well plates, established for 24 h, then pre-treated with different EGCNPs concentrations (0, 50 and 100 µg/ml) for 24 h. After the treatment period, the medium was removed, and the cells were washed once with PBS and replaced with complete medium containing H₂O₂ (100 µM) for 1 h. After 1 h, the medium was removed, washed once with PBS and the cells were incubated in H₂DCFDA solution (10 µM in PBS) for 30 min at 37 °C. The cells were washed with PBS and PBS (200 µl) was finally added to each well. DCF fluorescence intensity was measured using a plate reader (TECAN infinite 200 PRO, Japan)

at excitation 495 nm/emission 529 nm. The experiment was run in triplicate. For qualitative images, the experiment was repeated, and DCF fluorescence was imaged in FITC channel using a widefield epi-fluorescent microscope (EVOS FL, Thermo Fisher, UK).

4.2.6 The effect of EGCNPs pre-treatment and co-treatment on HLECs viability and proliferation when exposed to oxidative stress (live cell imaging)

HLECs proliferation in presence of oxidative insult induced by H₂O₂ was observed for three days under two conditions: (1) pre-treatment: the cells were pre-treated with EGCNPs for 24 h before addition of H₂O₂ (100 µM), and (2) co-treatment: the cells were simultaneously treated with EGCNPs and H₂O₂. Briefly, HLECs were seeded in 96-well plates as described above and left to establish for 24 h. The cells were then pre-treated with medium containing EGCNPs with different concentrations; 50, 100 and 200 µg/ml for further 24 hours. After the treatment period, the media was aspirated, the cells were washed with PBS, and replaced with fresh medium containing H₂O₂ (100 µM). The proliferation of EGCNPs-treated and non-treated HLECs was then observed for three days using the Incucyte[®] S3 live cell imaging system as described previously. For co-treatment experiments, the same steps were repeated excluding the EGCNPs pre-treatment step: EGCNPs were simultaneously added with H₂O₂ after the cells were established.

4.2.7 Catalase mimetic activity of EGCNPs in HLECs

To determine if EGCNPs protect HLECs against oxidative stress by exerting catalase-like actions, the catalase inhibitor 3-amino-1,2,4-triazole (3-AT, Sigma Aldrich, UK) was employed as reported in the literature with modifications.^{100,187} HLECs were seeded in complete EMEM in 96-well plates (5000 cells/well) and allowed to recover for 24 h. The cells were then preincubated with medium containing EGCNPs (50 µg/ml) for 24 h. A

negative control (no treatments) and a positive control (3-AT only) were also used. After the treatment period, the medium was aspirated, and cells were washed once with PBS and incubated with the catalase inhibitor 3-AT (100 mM) for 24 h. After the treatment period, the medium was aspirated, the cells were washed once with PBS and the viability of the cells was determined using the MTT assay as described previously. Cell viability was expressed as % of negative control. The experiment was repeated in triplicate.

4.2.8 Effect of EGCNPs on GSH/GSSG ratio

The effect of EGCNPs on the ratio between reduced and oxidised glutathione (GSH/GSSG) in HLECs was determined using GSH/GSSG ratio detection assay kit (fluorometric green, ab138881, Abcam, UK) according to the supplier's instructions. HLECs were seeded in 6-well plates in complete EMEM with a seeding density of 50000 cells/well and left to establish for 48 h in an incubator set at 37 °C and 5% CO₂. The medium was then removed and replaced with fresh medium containing EGCNPs (50 µg/ml) and the cells were treated for 48 h. A negative control (medium alone) was used for comparison. After the treatment duration, the cells were washed with cold PBS, lysed in radioimmunoprecipitation (RIPA) lysing buffer (200 µl, Thermo Fisher, UK) and homogenised in the lysing buffer by tilting the plate back and forth. The cell lysates were then collected in 2 ml prelabelled Eppendorf tubes and centrifuged at 22000 g for 15 min at 4 °C to remove insoluble cell material. The clear supernatants were then collected and transferred to clean Eppendorf tubes kept on ice. Since the lysates may contain enzymes that can interfere with the analysis, deproteinisation of the samples was carried out by adding 40 µl of trichloroacetic acid (TCA, 100% (w/v), Sigma Aldrich, UK) to all the samples and incubating on ice for 5 min. The samples were then centrifuged at 12000 g for 5 min at 4 °C, and the supernatants were transferred to clean Eppendorf tubes. The samples were then neutralised by slowly adding NaHCO₃ (120 µl, 10%, Fisher Scientific) making sure the pH does not exceed 7 as GSH can be easily oxidised

at pH > 7. The samples were centrifuged again as before, and the deproteinised and neutralised lysates were collected in fresh Eppendorf tubes. To make a calibration curve, GSH standards were prepared by serially diluting a stock solution (10 μ M) in the supplied assay buffer (Abcam, UK). To measure reduced GSH concentrations, GSH assay mixture (thiol green solution) (50 μ l) was added to an equivalent volume of samples and GSH standards in 96-well plates and left to incubate in the dark at room temperature for 1 h. The fluorescence was then read at ex/em = 490/520 nm using a plate reader (TECAN infinite 200 PRO, Japan). Similarly, total glutathione concentrations (GSH + GSSG) was measured but in this case GSSG was reduced first to GSH using the supplied GSSG probe (Abcam, UK). GSSG concentration was calculated by subtracting GSH concentration from total glutathione concentration and GSH/GSSG ratio could be determined for all the samples. Each individual sample and standard were assayed in duplicate and their fluorescence were first corrected by subtracting the blank fluorescence from it. The experiment was repeated five times (n = 5).

4.2.9 Measuring Antiglycation properties of EGCNPs

The ability of EGCNPs to prevent protein glycation was determined by measuring the distinctive fluorescence of advanced glycation end products (AGEs) as previously reported in the literature.⁴² Briefly, two solutions of bovine serum albumin (BSA, 10 mg/ml) D-glucose (10 mg/ml) were separately made in PBS (pH = 7). Sodium azide was added to each solution (0.02%) as a preservative. Equal volumes of BSA and glucose solution were mixed in 2 ml Eppendorf tubes with or without treatments. The treatments were as follows: EGCNPs (50, 100, and 200 μ g/ml) and aminoguanidine as an anti-glycating agent (10 and 20 mM). The samples were incubated for three days at 40 °C. After the incubation period, aliquots were taken from all samples (100 μ l) and placed in the wells of F-bottom black 96-well plates (Greiner). The fluorescence intensity of AGEs was measured at ex/em: 300-9 nm/400-20 nm using a plate reader (TECAN infinite 200 PRO, Japan). The same steps were

repeated using α -crystallin (1 mg/ml) and glucose (5 mg/ml) to check for protection against glycation in a lens protein. All experiments were run in triplicate.

4.3 Results and discussion

4.3.1 Time dependent uptake of EGCNPs in HLECs and its mechanism

Studying the interactions between nanomaterials and biological systems is crucial in understanding how the nanomaterials affect system function, and in turn, serves as a basis for improving the design of the nanomaterials to achieve the desired purpose. Biological systems are complex in nature making it challenging to predict the behaviour of a certain material in any given system.¹¹⁸ Nano-systems present extra challenges caused by their multi-faceted properties (*e.g.* size, charge, and aggregation state) which can dramatically change their physicochemical properties and hence their uptake in and interactions with biosystems.¹¹⁸ For example, it was reported in various studies that nanoparticles (specifically larger ones) can cause cell membrane rupture and deformation based on how they are uptaken.^{188,189} Additionally, for a nanomaterial to work as drug delivery system, a therapeutic or a diagnostic agent, it has to be able to pass through the cell membranes without causing damage. Nanomaterials can be erroneously claimed to be safe based on toxicological studies that have not correlated them with their cellular uptake. The lack of toxicity may be simply due to the lack of uptake and hence it is of paramount importance to associate them. Therefore, studying the uptake of nanomaterials is an integral part of understanding their activity and toxicity profiles.

In this work, EGCNPs uptake in HLECs was studied in a time-dependent manner. The amount of cerium oxide internalised by the cells was accurately measured using ICP-MS. Before the analysis, the number of cells in different conditions were counted before preparatory digestion for ICP-MS to ensure highly accurate representation of the results, and to negate any variability that can be caused by slightly different growth pattern in different wells or plates. The predetermined highest safe EGCNPs concentration (200 µg/ml, see

chapter 3 for toxicological studies) was used in these experiments to ensure the availability of the nanoparticles in the growth medium throughout the specified experiment time. As shown in Figure 4-1, EGCNPs were rapidly internalised by the cells within only 15 min of incubation (4.8 ng of cerium per 10^4 cells). The uptake thereafter was shown to be time-dependent increasing to 8.9, 17 and 26.4 nanograms of cerium per 10^4 cells after 1 h, 2 h and 4 h respectively.

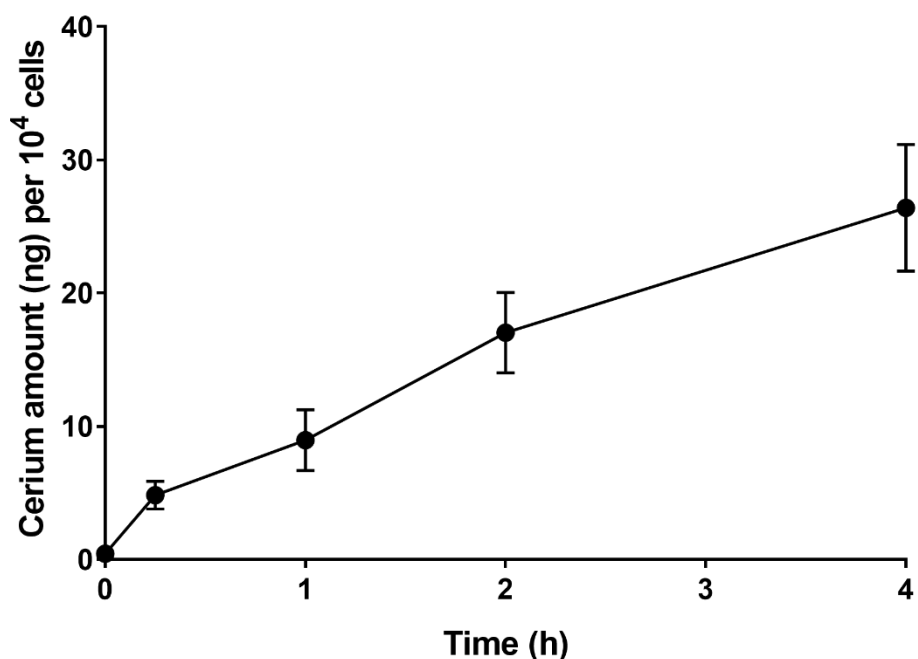


Figure 4-1 Time dependent uptake of EGCNPs in HLECs.

HLECs were incubated with EGCNPs for 0 min, 15 min, 1 h, 2 h and 4 h and the level of internalised cerium in the cells was measured by ICP-MS. The experiments were run in triplicate for each time point and the data are expressed as mean \pm standard deviation (SD).

To further understand the mechanism of EGCNPs uptake, the cells were incubated with EGCNPs under two different conditions intended to suppress the endocytic pathway. Endocytosis is a main cellular internalisation mechanism for macromolecules, nanoparticles and solutes where a given material is surrounded by a membrane-bound vesicle before being engulfed by the plasma membrane.¹¹⁸ Contrary to passive cellular pathway, endocytosis is an energy-dependent process for which ATP is needed to proceed.^{118,166} Endocytosis can also be subclassified into two key categories: phagocytosis (*i.e.* cell eating for large particles) and pinocytosis (*i.e.* cell drinking for liquids and solutes).^{118,166} After internalisation, molecules are transported to different cell compartments based on a multitude of factors such as charge, size, and interactions with other cellular macromolecules.¹⁶⁶ The first condition was to inhibit endocytosis chemically using sodium azide (NaN₃) and 2-deoxyglucose (2-DOG) before adding the nanoparticles. These two chemicals deplete the cellular ATP level blocking the energy-dependent process.¹⁹⁰ The second condition was to incubate the cells at 4 °C which causes the cell membrane to become more rigid blocking the endocytic process.¹⁶⁶ As shown in Figure 4-2, significant inhibition of EGCNPs uptake was observed under the two conditions when compared to negative control (*i.e.* no endocytosis inhibition). These results clearly indicate that energy-dependent endocytosis is required for efficient uptake of EGCNPs in HLECs. The results may also explain the previous data (reported in chapter 3, Figure 3-9) where slight increase in ATP level in HLECs was observed in the presence of different safe concentrations of EGCNPs corroborating the hypothesis that endocytosis was the drive for such an increase. It is noteworthy to emphasise that EGCNPs are also internalised to some extent in the presence of endocytosis-inhibiting conditions (Figure 4-2) which may suggest that even though endocytosis is the main uptake mechanism, other mechanisms such passive uptake pathway may be in action. A similar observation was

reported for carbon nanotubes where their uptake in multiple cell lines (such as A549, HeLa and Jurkat cell lines) was not predominately dependent on a single pathway.¹⁸⁹

The results herein present the first reported elucidation of nanoceria's time-dependent uptake and its mechanism in HLECs. Therefore, one can only contrast the results with the uptake behaviour of similar formulations tested in different cell lines. Asati *et al.* studied the uptake of polymer coated nanoceria (3-4 nm) carrying different surface charges in multiple cell lines (cardiac myocytes H9c2, human embryonic kidney HEK293, lung cancer A549 and breast cancer MCF-7).¹⁵⁴ The results showed that positively charged nanoceria were efficiently internalised by all the tested cell lines after 3 h of incubation. However, negatively charged nanoceria were poorly uptaken by HEK293, and did not enter H9c2 and MCF-7 cell lines.¹⁵⁴ Confocal studies (which are semi-quantitative compared to ICP-MS) also showed that endocytosis was the main mechanism uptake.¹⁵⁴ Since EGCNPs carry a strong positive charge, it is also likely that this plays a role in its strong uptake by HLECs. Nonetheless, the uptake behaviour of different formulations should be assessed on an individual basis for a given formulation in the cell line of interest given the multitude of the factors that can affect it.

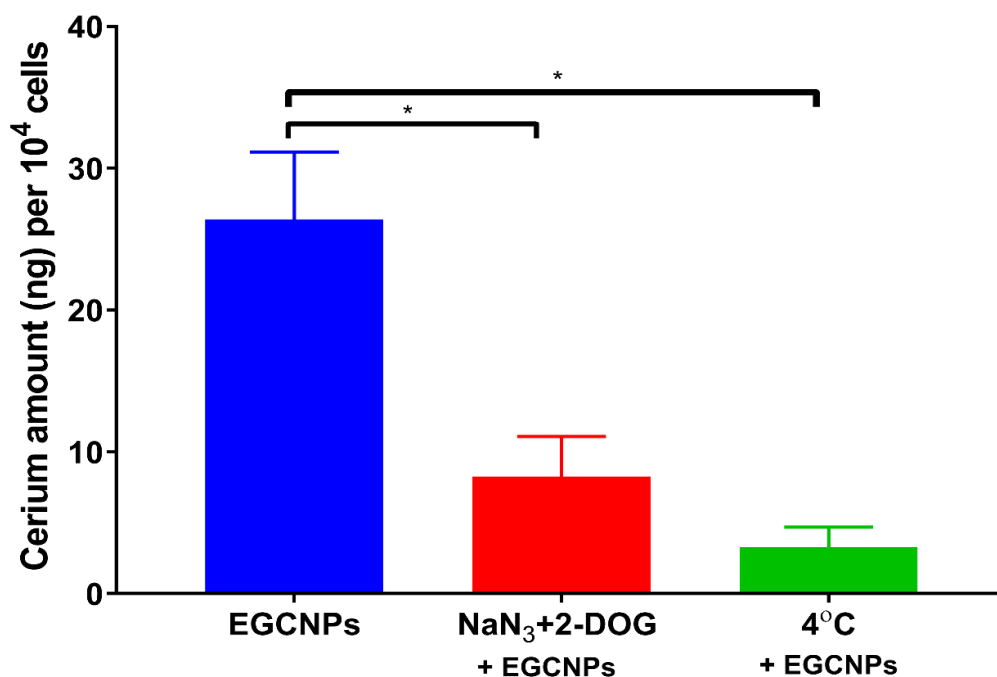


Figure 4-2 EGCNPs uptake in HLECs is endocytosis-dependent.

HLECs were treated with EGCNPs (200 $\mu\text{g/ml}$) for 4 h with or without endocytosis inhibition. Two different ways to inhibit endocytosis were used; chemical inhibition ($\text{NaN}_3 + 2\text{-deoxy-glucose}$) or by incubating the cells at 4 $^\circ\text{C}$. In both cases, significant inhibition of EGCNPs internalisation was observed indicating that endocytosis is the main uptake mechanism. Asterisks denote statistical significance ($n=3$, $p<0.05$, one-way ANOVA). Error bars are presented as means \pm SD.

4.3.2 Localisation of EGCNPs and EuCNPs in HLECs

The cellular localisation of nanoparticles plays an important role in their overall toxicity and activity.¹⁹¹ Many factors impact on the uptake of nanoparticles such as particle size, polydispersity, zeta potential and surface coating. Cerium is a lanthanide element that does not naturally occur in human cells. Therefore, it was feasible to observe the localisation of the nanoparticles employing a scanning electron microscope equipped with energy dispersive x-ray spectroscopy (SEM-EDX). EDX is an elemental analysis tool that enables the detection of characteristic x-ray energy emitted from different elements (*e.g.* cerium)

after excitation with an accelerated electron beam. By examining different cell compartments, the presence or absence of cerium oxide can be confirmed.

Figure 4-3 shows control cells (Figure 4-3a) and the uptake and localisation of EGCNPs in HLECs after incubation for 4 h (Figure 4-3b) and 24 h (Figure 4-3c). EGCNPs entered the cells at significant levels for both tested time points agreeing with ICP-MS results. The nanoparticles were heavily localised in the cytoplasm, mainly in perinuclear regions (Figure 4-3b and Figure 4-3c). This supports the results in the previous chapter where significant mitochondrial localisation was detected. Minimal amounts of EGCNPs have been detected in the nuclei as confirmed by EDX spectra. The amount of nanoparticles that entered the nucleus was slightly higher in the 24 h incubation period but the majority of the nanoparticles were retained in the cytoplasm. The cellular compartments with the most EGCNPs localisation were very distinct in the SEM images owing to the atomic number contrast. Heavy elements (*e.g.* cerium, atomic number = 58) backscatter electron strongly compared to the lighter elements that make up most of biological specimens, and hence appear brighter in the SEM images.¹⁹² By virtue of this phenomenon, a contrast sensitive pseudo-colour was applied to all the SEM images highlighting EGCNPs-containing compartments with a green colour (Figure 4-3). To ensure that the detected EGCNPs were not originating from poorly washed out nanoparticles, an experiment was carried out by incubating the cells for less than 1 min with EGCNPs, washed and fixed as other treated conditions. Under such condition, EGCNPs could not be detected by EDX (Figure 4-3). Representative EDX spectra confirming the presence of EGCNPs are shown in Figure 4-4.

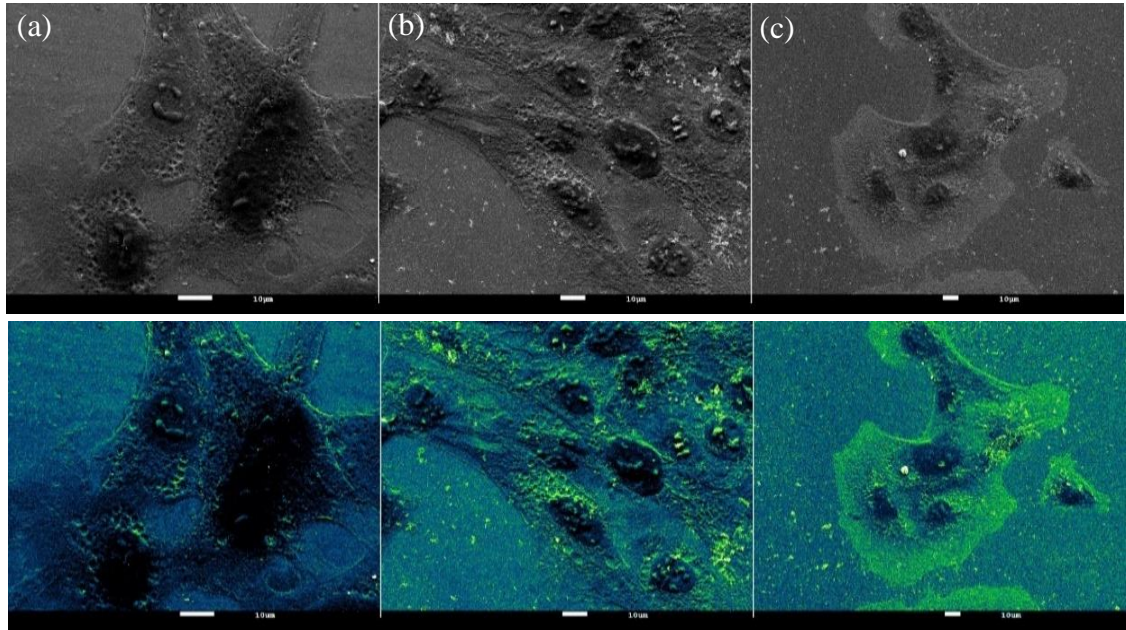


Figure 4-3 SEM images showing uptake and localisation of EGCNPs in HLECs at different time points.

(a) 1 min incubation showing no uptake of EGCNPs, (b) EGCNPs uptake and localization after 4 h incubation, (c) EGCNPs uptake and localization after 24 h incubation. Strong uptake was detected at 4 h and 24 h time points with heavy localisation around the nuclei as detected by EDX. Areas with most nanoceria localization are distinguished by brightness arising from atomic number contrast of cerium element (Ce atomic number = 58) and hence it produces more secondary and backscattered electrons. Contrast sensitive pseudocolour was applied simultaneously to the images highlighting nanoceria localisation as bright green. Scale bars = 10 μm .

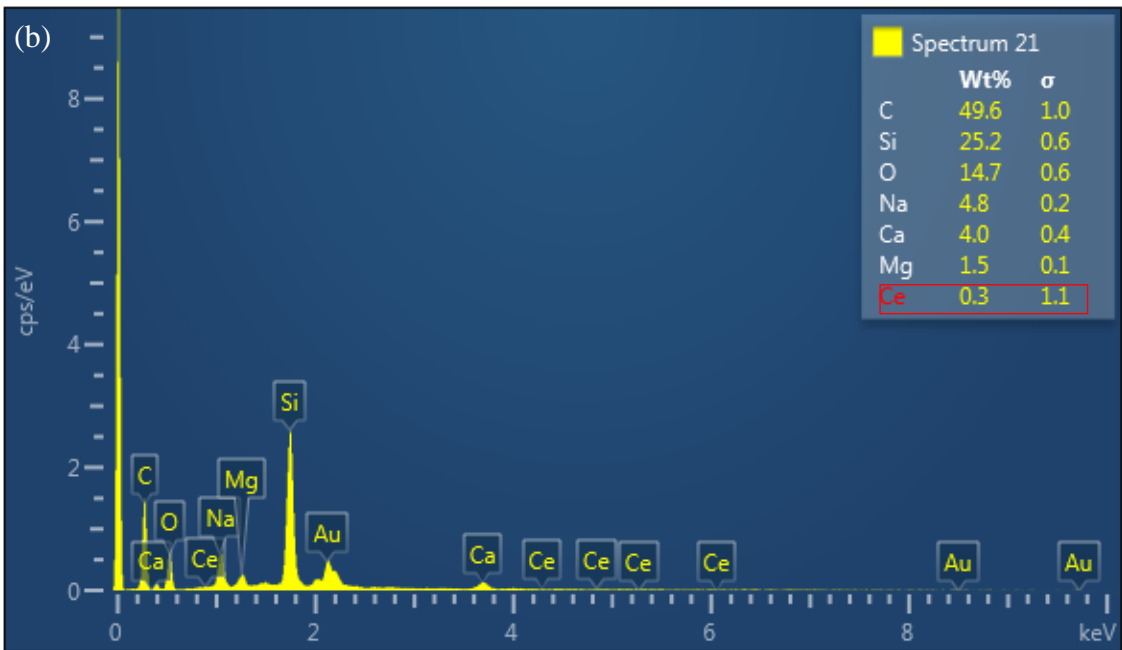
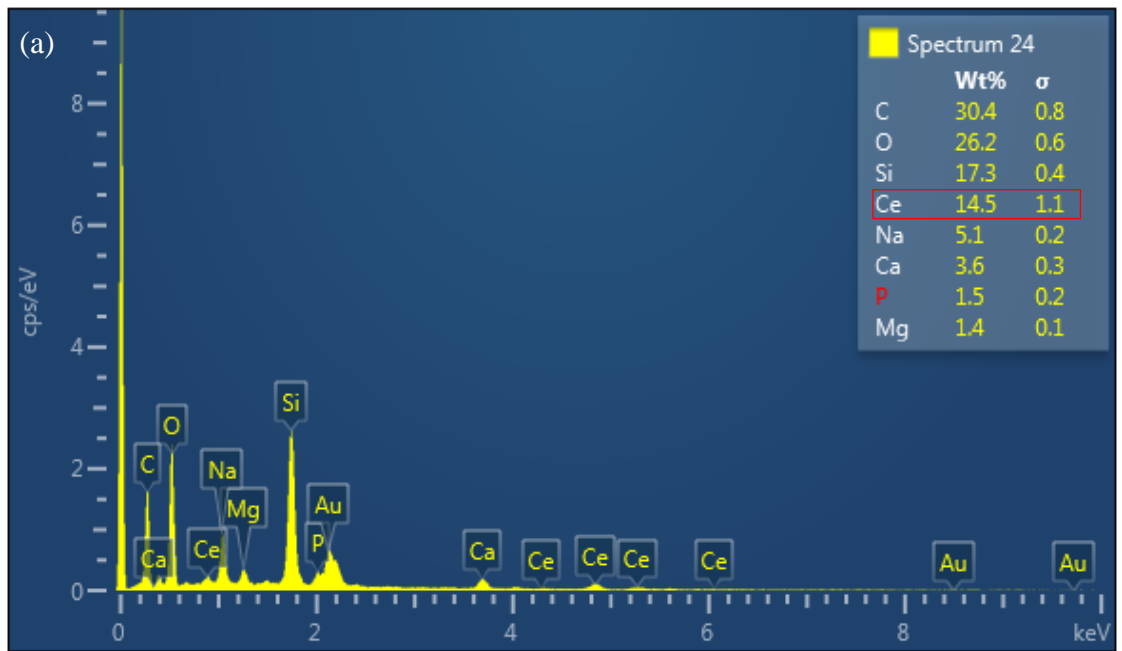


Figure 4-4 EDX analysis in HLECs compartments.

(a) a sample spectrum from the cytoplasm (perinuclear region) showing significant uptake of cerium (Ce) that was autodetected. (b) a sample spectrum from the nucleus with no or negligible cerium, in this case cerium was not autodetected and was manually input for comparison. Silica (Si) is present in both samples because of mounting on glass cover slips.

For further validation of EGCNPs uptake and localisation obtained by SEM-EDX, confocal microscopy experiments were conducted. As shown in Figure 4-5, HLECs exhibited strong autofluorescence in the blue and green regions when excited with a 405 nm laser line.

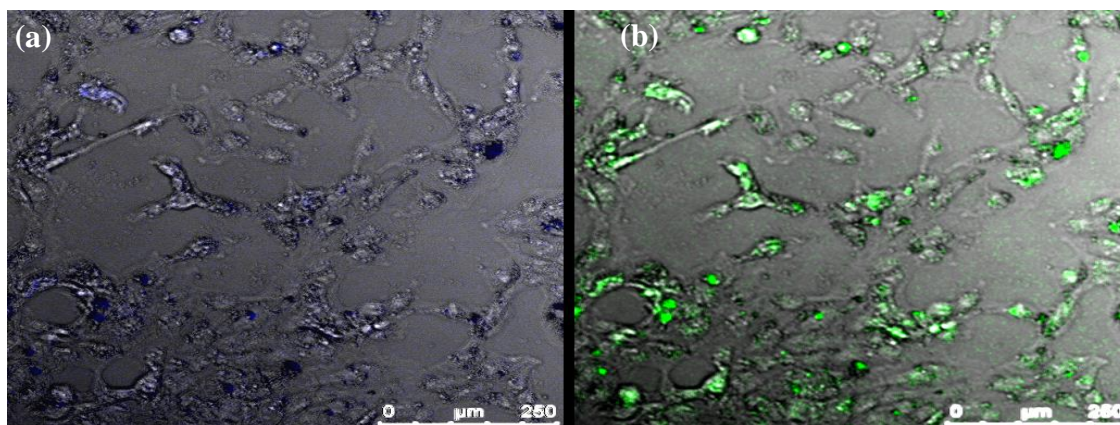


Figure 4-5 Confocal images showing autofluorescence of human lens epithelial cells.

(a) blue emission and (b) green emission after excitation with 405 nm.

This presented a challenge for detecting EGCNPs fluorescence since it was relatively weak as discussed in chapter 2. This means that in order to detect EGCNPs natural fluorescence a strong excitation wavelength must be used which leads to simultaneous increase in cellular autofluorescence that masks EGCNPs fluorescence. By taking advantage of the ability of the lanthanide elements (*e.g.* cerium) to resist photobleaching,¹²⁶ it was possible to track EGCNPs inside HLECs. This was achieved by photobleaching the cellular autofluorescence using a strong laser power minimising its interference with EGCNPs signal. As shown in Figure 4-6a and Figure 4-6b, EGCNPs were confirmed to be mainly localised in the cytoplasm corroborating SEM-EDX data. To the knowledge of the author, this is the first time unlabelled pure nanocerium have been successfully tracked inside any cell line employing fluorescent studies.

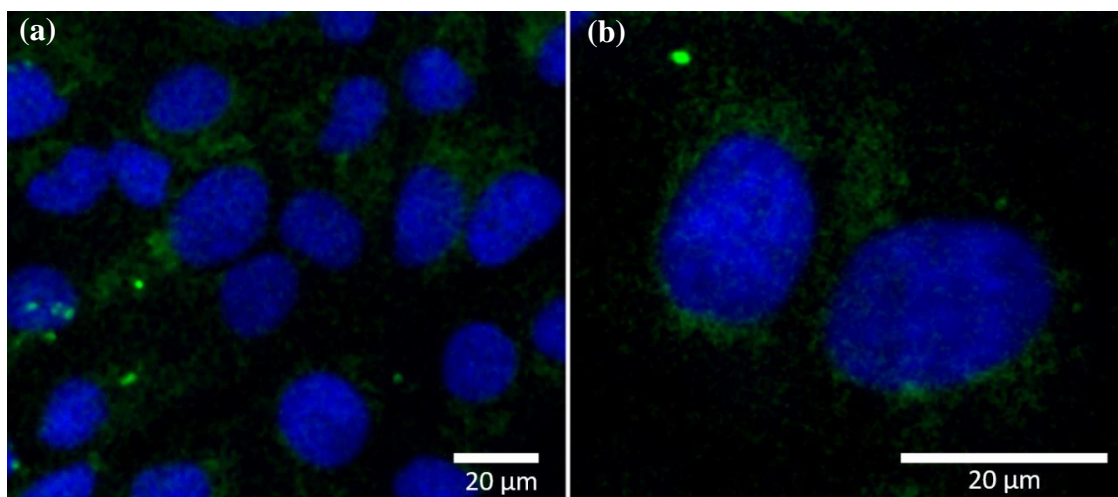


Figure 4-6 Uptake and perinuclear localisation of unlabelled EGCNPs in HLECs.

(a) low magnification and (b) high magnification confocal images showing cytoplasmic localisation of EGCNPs (green) in HLECs (excitation 488 nm/emission 530 nm). Hoechst 33342 (blue) was used for nuclear staining. A negative control image is available in the appendix.

To avoid interference with cellular autofluorescence, it is preferable for the nanoparticles to possess emissions at wavelengths above 600 nm where cellular autofluorescence is significantly minimised.¹²⁶ In order to achieve significant emission in the longer wavelength end of the visible spectrum, a nanoceria formulation doped with europium (EuCNPs) was prepared and subsequently employed in confocal imaging. As discussed in chapter 2, the doped nanoceria (EuCNPs) exhibited typical strong emission at 612 nm under multiple excitation wavelengths from UV to end of green region (ranging from 350 - 550 nm).¹¹⁶ Additionally, similar particle size (5 nm) and surface charge (+34.49 mV) to EGCNPs were achieved. Doping with europium was chosen over attachment of traditional fluorescent dyes since the latter involves surface modifications that could affect the behaviour of the nanoparticles uptake.¹⁹³ After 24 h incubation with HLECs, As shown in Figure 4-7a, EuCNPs were found in the cytoplasm mainly in the perinuclear region corroborating the previous data. Additionally, EuCNPs showed a similar localisation pattern to EGCNPs when

examined by SEM-EDX (Figure 4-7b). Single point EDX elemental analysis showed the presence of both cerium and europium in the cytoplasm confirming the uptake of the europium doped nanoceria (Figure 4-7c). It is therefore concluded that SEM imaging coupled with EDX spectroscopy is a potentially reliable technique for studying uptake and localisation of nanoceria in lens epithelial cells. It provides the convenience of not having to label the nanoparticles post synthesis in order to confirm their uptake. Nonetheless, EuCNPs do not seem to alter the uptake and localisation behaviour in HLECs and hence can be employed in multiplexing and colocalisation studies where multiple fluorescent probes need to be used simultaneously. This is possible as EuCNPs exhibit a sufficient fluorescence signal that, contrary to pure nanoceria, can be reliably distinguished from cellular autofluorescence (Figure 4-7a).

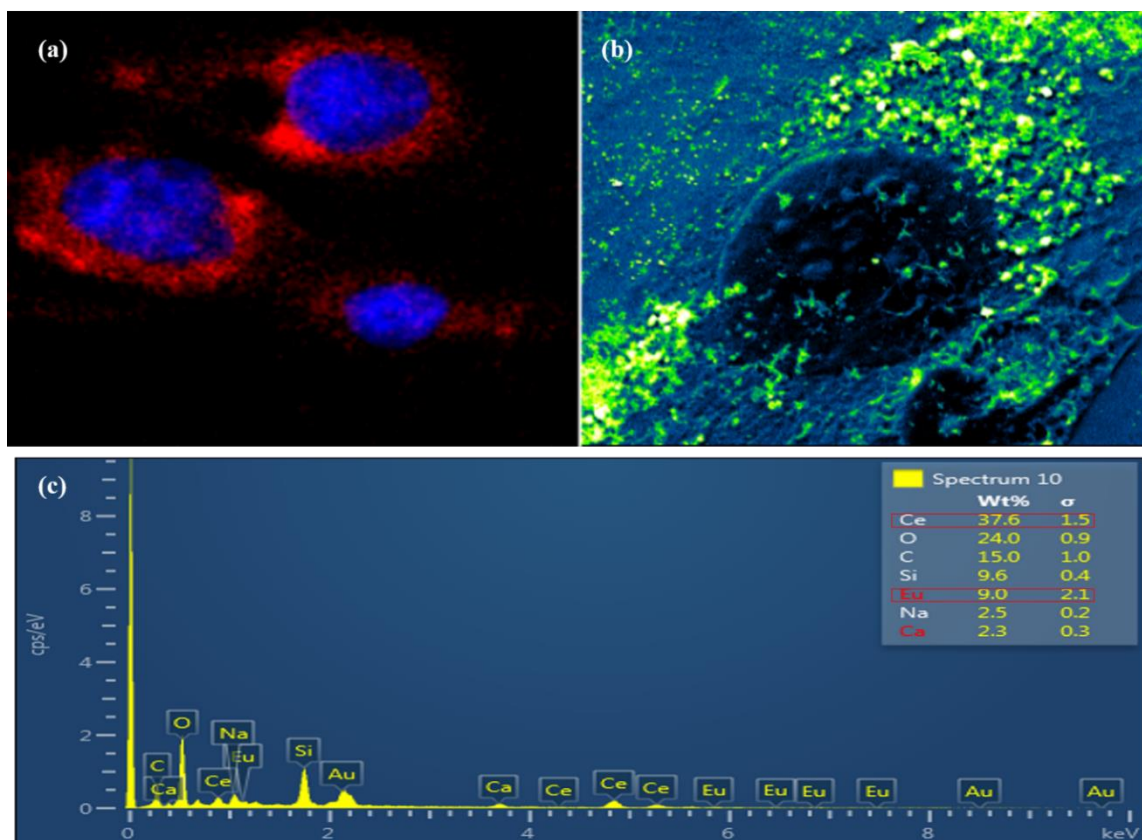


Figure 4-7 Uptake and perinuclear localisation of EuCNPs in HLECs.

(a) a confocal microscopy image showing cytoplasmic localisation of nanoceria doped with europium (EuCNPs) in HLECs, EuCNPs showed similar localisation pattern to EGCNPs, (b) A SEM image showing cytoplasmic localisation of EuCNPs (green areas), (c) EDX analysis of the cytoplasm showing the presence of Ce and Eu confirming the cytoplasmic localisation of EuCNPs in HLECs.

It was reported in chapter 3 that EGCNPs localise in the mitochondria which was revealed in SEM-EDX studies. To further confirm these results, the fluorescent properties of EuCNPs were employed in confocal microscopy studies where the mitochondria of HLECs were stained with the mitochondrial specific stain MitoTracker™ Red CMXRos. The colocalisation of the fluorescent signals from both EuCNPs and Mitotracker were subsequently studied to check for the presence of EuCNPs in the mitochondria. One issue was that both Mitotracker Red and EuCNPs possessed strong red emissions at 612 nm when excited using their maximum excitation wavelengths (579 nm and 508 nm respectively), and

hence it was not possible to separate their signal based on their emission. Fortunately, EuCNPs red emission can be acquired at different excitation wavelengths as previously reported in chapter 2. Therefore, the fluorescent signals of both compounds were distinguished by selectively exciting EuCNPs at 476 nm at which Mitotracker fluorescence is negated. As shown in Figure 4-8, EuCNPs colocalised with mitochondria which is shown in the merged image. This confirms previous SEM-EDX results and the suitability of europium doping to track nanoceria in fluorescence studies.

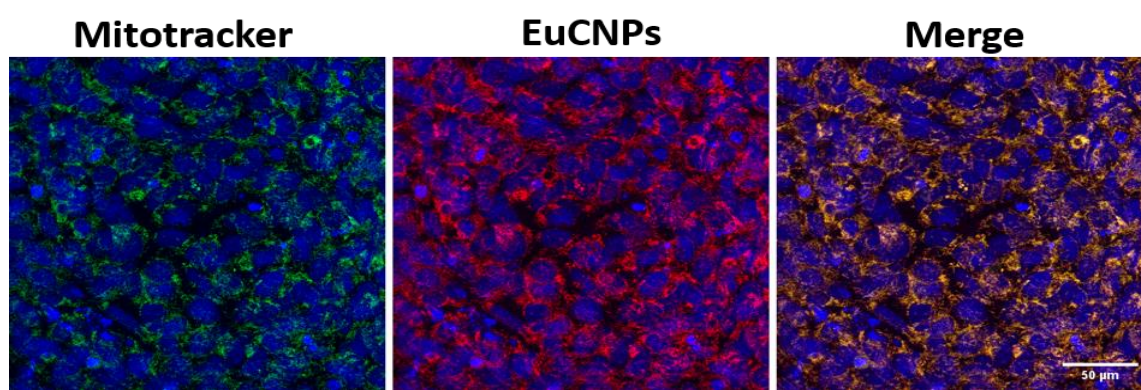


Figure 4-8 Mitochondrial localisation of EuCNPs observed by confocal microscopy.

HLECs were incubated with EuCNPs and co-labelled with Mitotracker. Both Mitotracker and EuCNPs emissions were detected in the red region (612 nm) using different excitation wavelengths (543 nm and 476 nm respectively). Although Mitotracker emission is effectively in the red region, it was pseudo-coloured with green colour to allow visualisation of the merge image. The orange colour in the merge image indicates the areas where both Mitotracker (green) and EuCNPs (red) colocalise. Nuclei (blue) were stained with Hoechst 33342.

Since it is well known that the mitochondria are the dominant hub for ROS generation (approximately 90% of ROS generation),¹⁹⁴ the results reported herein show great potential for nanoceria in the treatment of age-related including cataract. This will be explored further in the upcoming studies to evaluate nanoceria's efficacy in protecting the human lens epithelium from ROS-mediated injury.

4.3.3 EGCNPs protect the normal proliferation of HLECs when exposed to oxidative stress

After establishing the efficient entry of EGCNPs into HLECs, the next step was to study if they can provide protection against one of the main cataract inducers namely; oxidative stress. Oxidative environment in the lens can lead to colouration, protein insolubilisation, denaturation and crosslinking.²⁶ Oxidative stress takes place when the production of oxidative species outweighs the ability of the cellular natural anti-oxidant system to neutralise or degrade them.¹⁹⁵ In the mitochondria and as part of the electron transport chain for energy production, full four-electron reduction of molecular oxygen (O_2) into water (H_2O) takes place.¹⁹⁵ However, partial reduction of oxygen can also take place producing free radicals and ROS such as H_2O_2 , hydroxyl radicals, and superoxide.¹⁹⁵ The source of free radical and ROS can also be exogenous from diet, radiation, sun exposure, smoking, and air contaminants.¹⁹⁵

EGCNPs with predetermined safe concentrations (100 and 200 $\mu g/ml$) were tested for their ability to protect the proliferation of HLECs from oxidative damage induced by H_2O_2 . Two experimental conditions were tested; co-treatment (cells were subjected to oxidative stress simultaneously with EGCNPs) and pre-treatment (cells were incubated with EGCNPs for 24 h and then subjected to oxidative stress in nanoceria-free medium). The proliferation of the cells in both conditions was observed for three days by means of live cell imaging. In the co-treatment condition, the two tested concentrations of EGCNPs exhibited a noticeable protective effect against H_2O_2 compared to non-EGCNPs treated cells. This was manifested in higher proliferation rate of the cells over the tested duration. The higher concentration of EGCNPs did not seem to provide further protection compared to the lower concentration (Figure 4-9). The results indicate the EGCNPs can easily deactivate H_2O_2 in growth medium.

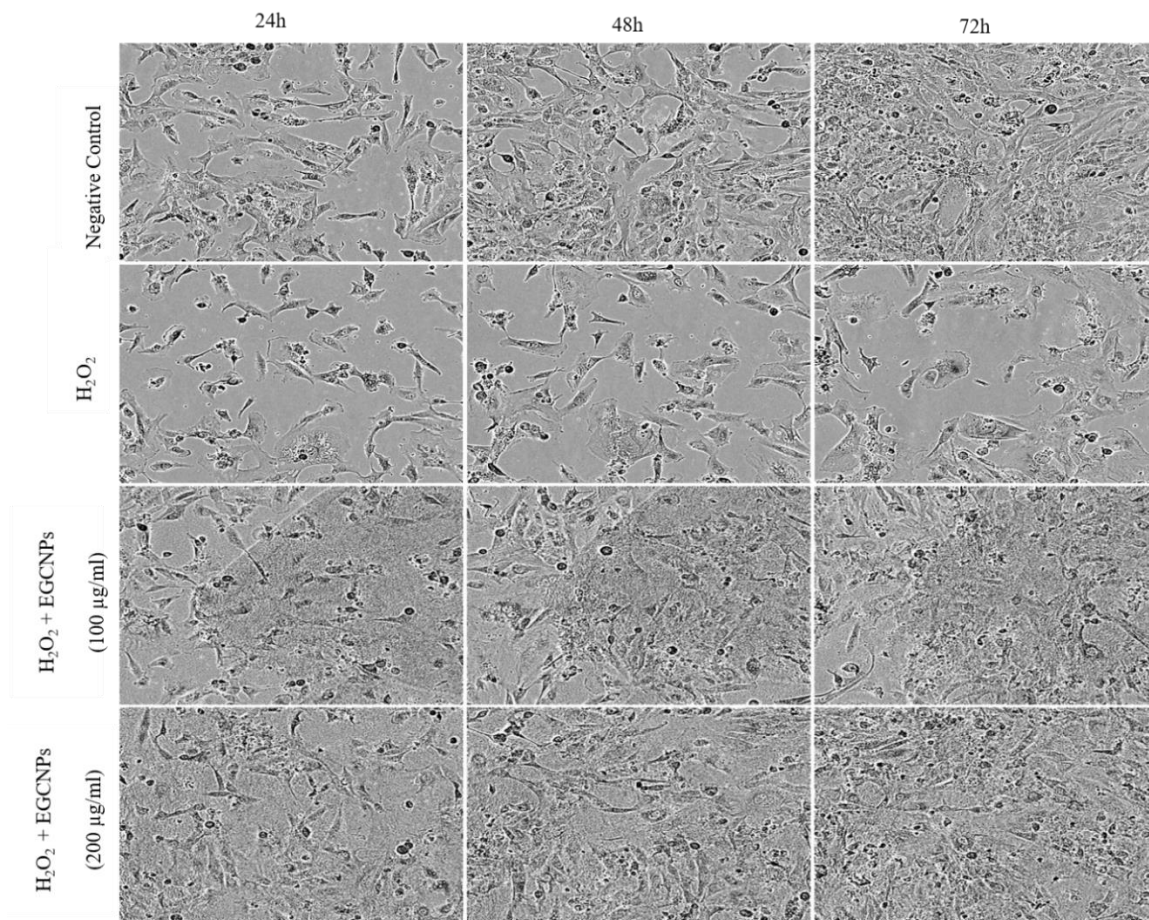


Figure 4-9 Live cell analysis of HLECs growth showing protective effect of EGCNPs against oxidative stress induced by H₂O₂.

The cells were incubated with H₂O₂ (100 µM) with or without EGCNPs treatments (co-treatment) and allowed to proliferate for three days at 37 °C, 5% CO₂. Images were taken every 2 h using the Incucyte[®] S3 system. EGCNPs-treated cells were able to reach full confluency within three days while the growth of non-treated cells (H₂O₂ only) was significantly inhibited by H₂O₂.

In the pre-incubation condition (Figure 4-10), the tested concentrations showed similar protection against H₂O₂. The protection level was slightly higher in the co-treatment condition compared to pre-treatment conditions. In the former condition EGCNPs may have had direct contact with H₂O₂ in medium allowing for more efficient hydrogen peroxide deactivation. It is also noteworthy that the concentration of H₂O₂ used was considerably higher compared to that routinely used in other studies.^{183,185,196}

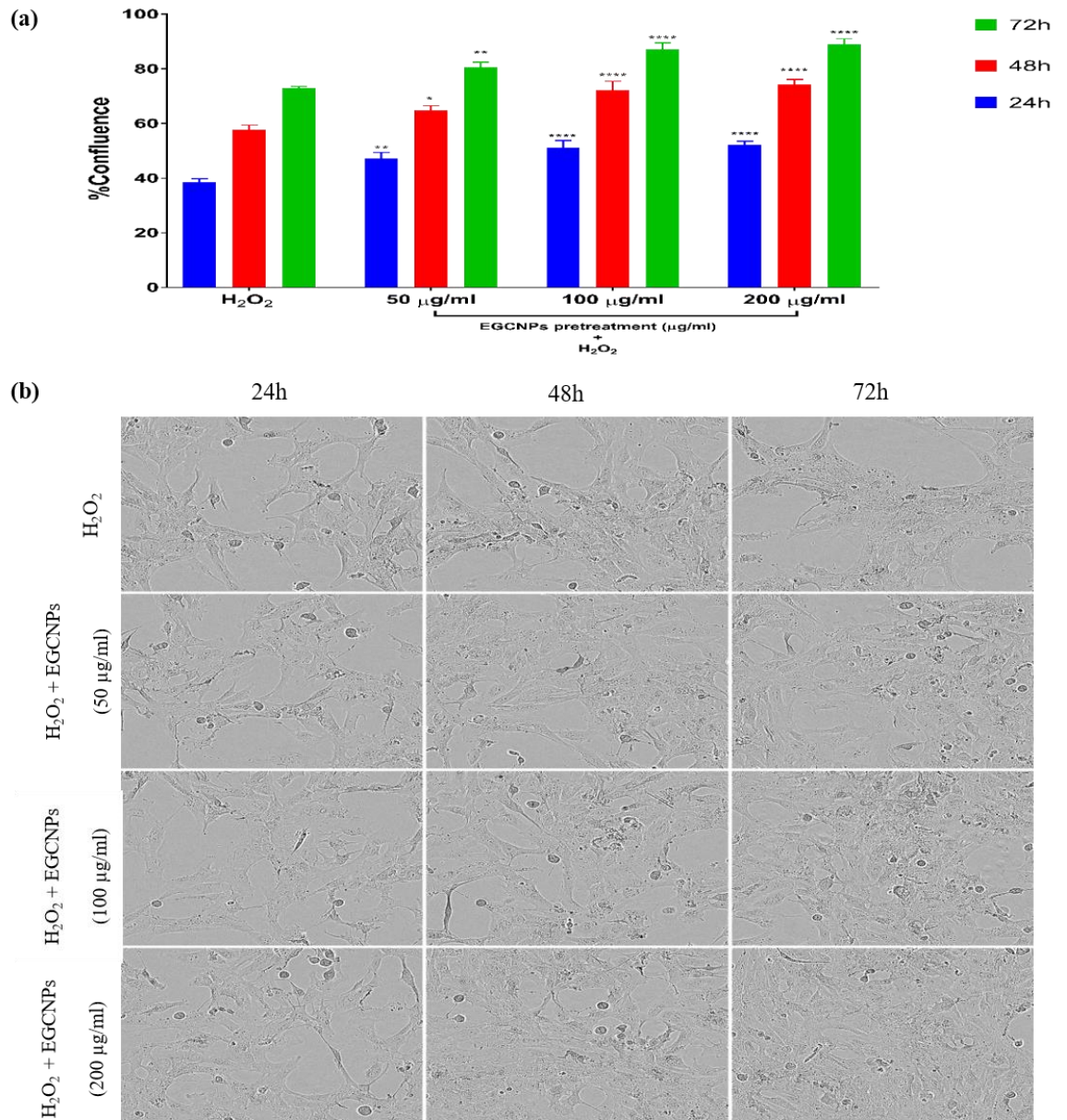


Figure 4-10 Live cell analysis of HLECs pre-treated with EGCNPs for 24 h then treated with H₂O₂ for 72 h.

(a) confluence quantification, (b) representative images at different time points under different conditions. Images were taken every 2 h using the Incucyte[®] S3 system. EGCNPs-treated cells were able to reach full confluency within three days while non-treated cells (H₂O₂ only) proliferation was significantly inhibited. Asterisks denote statistical significance ($n=3$, $*p \leq 0.05$, $**p \leq 0.01$, $***p \leq 0.001$ and $****p \leq 0.0001$, one-way ANOVA). Error bars are presented as means \pm SEM.

4.3.4 EGCNPs protect against oxidative stress (H₂DCFDA staining)

EGCNPs, with predetermined safe concentrations (50, 100 and 200 µg/ml), were tested for their ability to protect HLECs from oxidative damage induced by H₂O₂ using H₂DCFDA staining. H₂DCFDA is a non-fluorescent cell-permeable dye which is cellularly retained upon internalisation due to deacetylation, and then oxidised by the action of ROS into highly fluorescent DCF enabling relative estimation of ROS levels. As shown in Figure 4-11, the tested EGCNPs concentrations exhibited a significant protective effect compared to non-EGCNPs treated cells demonstrated by the low fluorescence levels in cells pre-treated with EGCNPs. All of the tested concentrations showed a similar level of protection against H₂O₂-induced oxidative stress. Such protective effects suggest that EGCNPs inside the HLECs can exert catalase-like activity where excess H₂O₂ was deactivated.¹⁰⁰ This mechanism will be investigated in the following study.

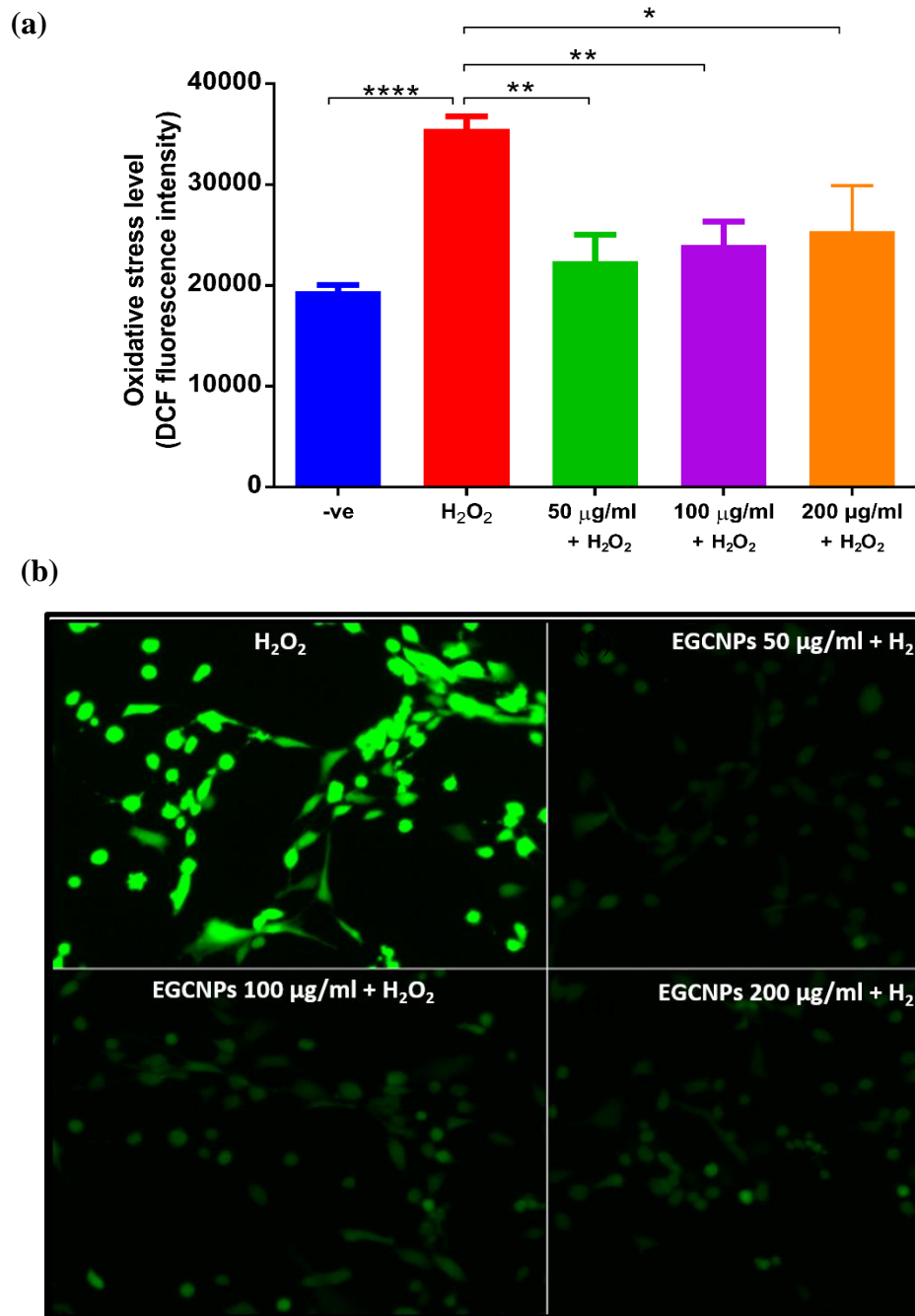


Figure 4-11 EGCNPs protect against H₂O₂-induced oxidative stress in human lens epithelial cells (H₂DCFDA staining).

HLECs were pre-treated with EGCNPs for 24 h, and then exposed to H₂O₂ (100 µM) for 1 h in EGCNPs-free medium. Oxidative stress levels were determined by measuring DCF fluorescence intensity using (a) a plate reader, (b) a fluorescence microscope. Asterisks denote statistical significance (n=3, **p* ≤ 0.05, ***p* ≤ 0.01, ****p* ≤ 0.001 and *****p* ≤ 0.0001, one-way ANOVA). Error bars are presented as means ± SEM.

4.3.5 Catalase-like activity of EGCNPs in HLECs

Catalase is a naturally occurring enzyme in the human lens epithelium.¹⁸⁵ This provides a natural defence mechanism against H₂O₂ breaking it down into water and oxygen. When the lens ages, depletion of catalases takes place which in turn increases the propensity of the lens to oxidative insult that can lead to protein post-translational modifications and cataract formation.¹⁸⁵ It was reported that transfecting mice lenses with catalase targeted only to the mitochondria led to significant delay in age-related cataract progression.¹⁹⁷ This provides an incredible opportunity for EGCNPs to act as a catalase mimetic for cataract prevention since they were shown to localise significantly in the mitochondria of HLECs as discussed in the previous results. 3-AT (Figure 4-12) is a well-known catalase blocker causing cellular accumulation of intracellular H₂O₂ and cellular death.¹⁰⁰ This anti-catalase activity has been shown to exacerbate various oxidative stress related conditions such as Alzheimer's, inflammatory diseases and liver dysfunction in both *in-vitro* and *in-vivo* models.^{100,187,198} Therefore, in this study 3-AT was employed to irreversibly block the catalase activity in HLECs and determine the ability of EGCNPs to replace the activity of the inhibited catalase.

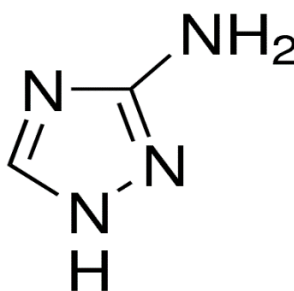


Figure 4-12 Chemical structure of the catalase inhibitor 3-amino-1,2,4-triazole (3-AT).

First, the effect of two concentrations of 3-AT (100 and 200 mM) on the viability of HLECs was studied at two time points; 4 h and 24 h. As shown in Figure 4-13, no decrease in cell viability was observed after 4 h exposure to both concentrations. At 24 h, however, both

concentrations (100 and 200 mM) significantly decreased cell viability by 37% and 76% respectively. Since the lower 3-AT concentration (100 mM) provided a significant viability reduction after 24 h exposure ($p < 0.0001$), it was deemed suitable to use that concentration and exposure duration in studying the catalase mimetic activity of EGCNPs.

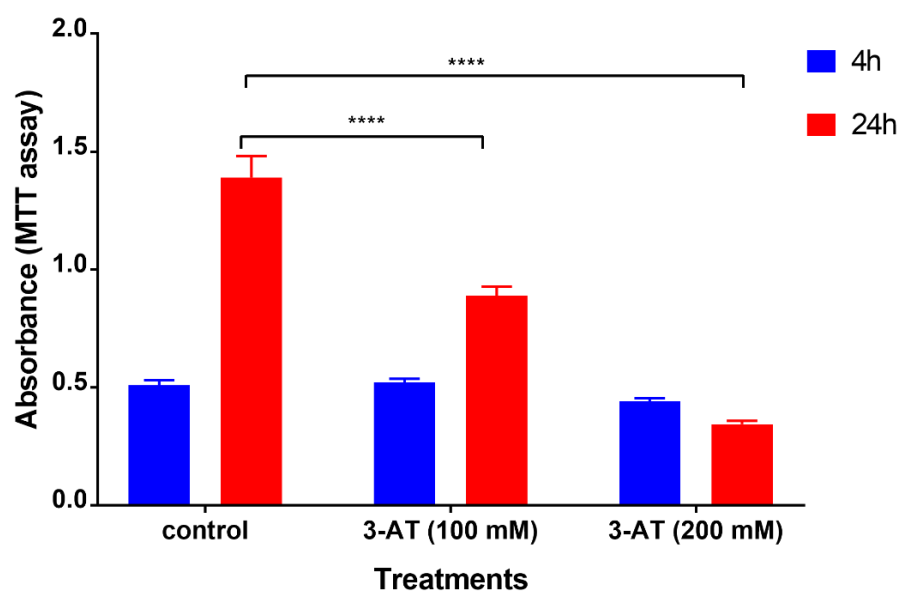


Figure 4-13 Dose and time dependent effect of the catalase inhibitor 3-AT on HLECs viability measured by the MTT assay.

Asterisks denote statistical significance from the negative control (two-way ANOVA followed by Tukey's multiple comparisons test, $n=3$, **** $p \leq 0.0001$). Error bars are presented as means \pm SEM.

In a subsequent experiment, HLECs were pre-treated with EGCNPs for 24 h before exposure to 3-AT. The results show that HLECs pre-treated with EGCNPs exerted a significant protection against the cytotoxic effect of catalase depletion induced by 3-AT manifested in the increase in viability by 14% for the EGCNPs treated cells (Figure 4-14). This indicated that EGCNPs can act as a nanozyme exhibiting catalase-like activity in HLECs making them a promising mitochondrial targeted anti-cataract therapy. This concurs with the previous

observations in the proliferation studies of HLECs where EGCNPs provided protection against the oxidative insult induced by H₂O₂.

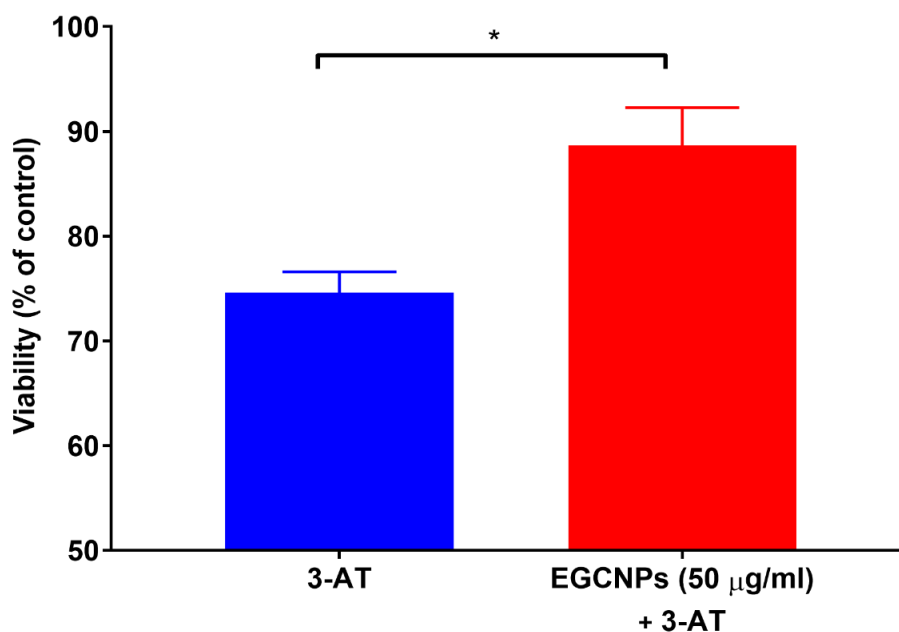


Figure 4-14 Catalase-mimetic activity of EGCNPs in HLECs. EGCNPs protect against damage induced by the catalase inhibitor 3-AT (100 mM).

The asterisk denotes statistical significance ($n=3$, $p<0.05$, Student's t-test). Error bars are presented as means \pm SEM.

4.3.6 Effect of EGCNPs on GSH/GSSG ratio

Glutathione (GSH) is a tripeptide (γ -glutamyl-cysteine-glycine) that plays an important role in the defence system of the human lens against oxidative stress-induced damage.^{29,186} The eye lens naturally contains a high concentration of glutathione in its reduced form (GSH) in addition to high content of thiol-containing proteins (protein-SH). The crosslinking between such proteins through the formation of disulphide linkages (protein-S-S-protein) is implied in cataract formation.¹⁸⁶ The presence of reduced GSH in the eye lens protects the thiol content from such crosslinking maintaining the lens transparency through the oxidation of the reduced GSH to its oxidised form GSSG.¹⁸⁶ GSH levels in the lens decrease with age

with a concomitant increase in disulphide glutathione GSSG.²⁹ This is reported to be one of the most characteristic features of nuclear cataract formation.^{26,195} This loss is also observed in the majority of experimentally induced cataracts.^{26,199} Therefore, it was suggested that maintaining high levels of GSH in the eye lens can play an important role in the prevention of cataract formation.

In this study, the effect of EGCNPs on GSH/GSSG ratio in HLECs was investigated after 48 h exposure to the nanoparticles. This was achieved using a sensitive one-step fluorometric assay to quantify reduced GSH content and total glutathione content (GSH + GSSG) from which GSSG content was calculated. The assay employs a non-fluorescent probe that reacts with GSH emitting strong fluorescence that can be quantified using a spectrofluorometer. The total glutathione concentration was measured by enzymatically reducing GSSG to GSH and using the same probe for quantification. From a calibration curve plotted using GSH standards (Figure 4-15a), the content of GSH can be accurately calculated and compared across different samples. As shown in Figure 4-15b, HLECs treated with EGCNPs (50 µg/ml) showed significant improvement ($p < 0.05$) of GSH/GSSG ratio compared to the negative control.

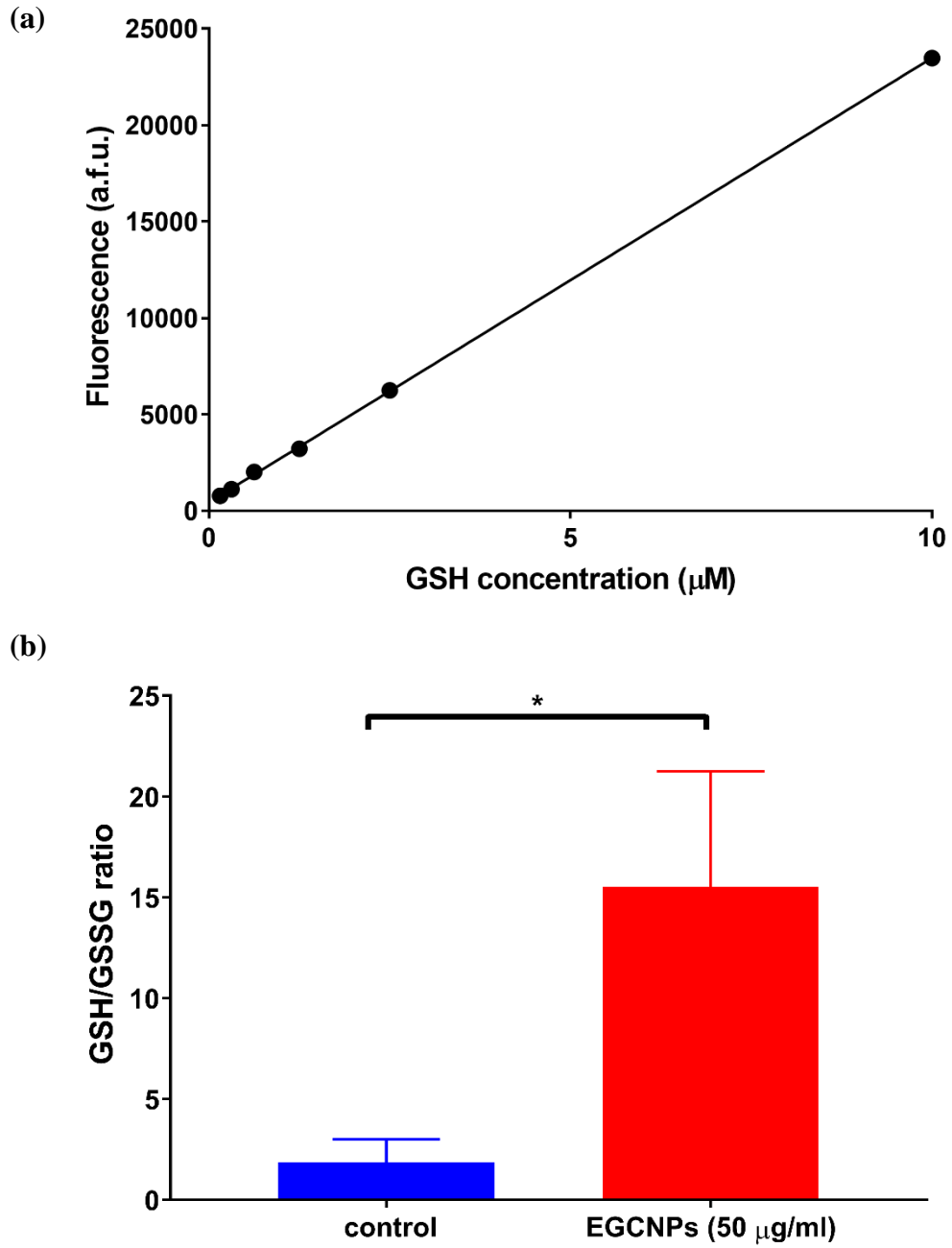


Figure 4-15 Effect of EGCNPs on GSH/GSSG ratio in HLECs.

(a) GSH standards calibration curve (R^2 is 0.9999) generated using a spectrofluorometer at ex/em = 490/520 nm, (b) 48 h exposure to EGCNPs (50 $\mu\text{g/ml}$) significantly increase GSH/GSSG ratio compared to negative control. The asterisk denotes statistical significance ($n=5$, $p<0.05$, Student's t -test). Error bars are presented as means \pm SEM.

As shown in Figure 4-16, the increase in GSH/GSSG ratio can be primarily attributed to increased content of GSH in EGCNPs-treated cells. Additionally, GSSG concentration in treated cells was slightly lower but non-significant compared to control cells. This finding is the first of its kind for showing the impact cerium oxide nanoparticles on GSH/GSSG in HLECs. It has been previously reported that cerium chloride loaded mesoporous silica ($\text{CeCl}_3@m\text{SiO}_2$) nanoparticles increase GSH content in diabetic rat lenses after eight weeks of exposure.²⁰⁰ This may suggest that cerium, as an element, may play a role in promoting the cellular synthesis of GSH which is worthy of further investigation. Together, these results indicate great potential for EGCNPs in cataract prevention not only because of their direct antioxidant properties but also for their GSH promoting effect.

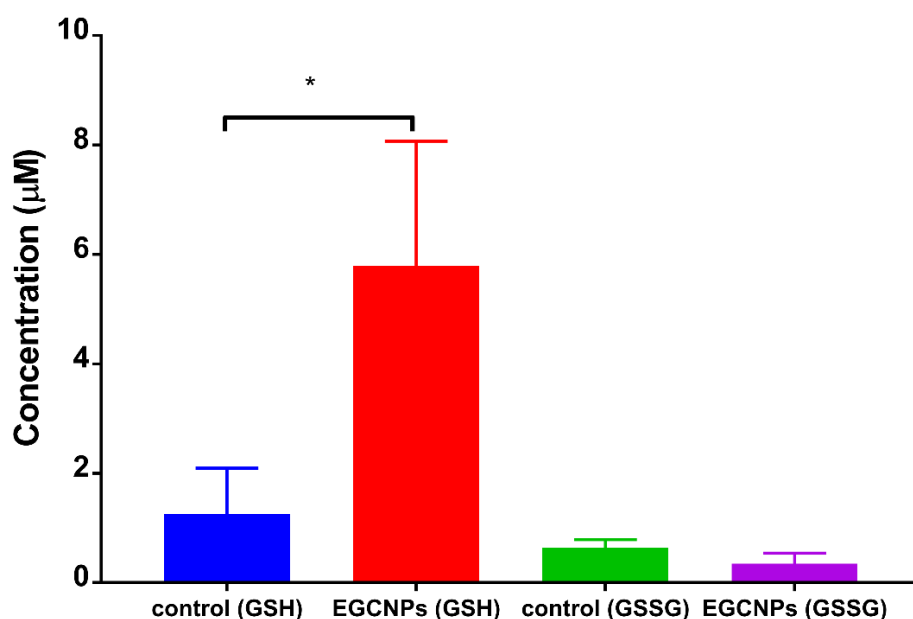


Figure 4-16 Effect of EGCNPs (50 µg/ml) on GSH and GSSG concentrations in HLECs after 48 h exposure.

The asterisk denotes statistical significance ($n=5$, $p<0.05$, Student's t-test). Error bars are presented as means \pm SEM.

4.3.7 Effect of EGCNPs on protein glycation

Protein glycation is one form protein post-translational modifications where sugars and proteins react non-enzymatically leading to the formation of advanced glycation end products (AGEs).^{201,202} The glycation process proceeds very slowly over a period of weeks through a series of reactions between the amino groups of proteins and reducing sugars such as glucose.²⁰³ The reactions start with rapid formation of Schiff base adducts followed by slow Amadori rearrangement and finally AGEs formation in a complex process known as the Maillard reaction.²⁰² This makes crystallins an ideal target for glycation due to the lack of protein turnover in the lens.²² The formation of AGEs were shown to be strongly implicated in many pathologies including Alzheimer's, diabetes, retinopathy, nephropathy, atherosclerosis and cataract formation.^{22,202,204} Glycation of the lens proteins has been previously shown to induce protein conformational changes, crosslinking, yellowing and aggregation that are more pronounced with diabetes.²² In addition to the direct damage to crystallins, sugars can deactivate enzymes including the natural anti-oxidant defence system in the lens (*e.g.* catalase, superoxide dismutase, glutathione and glutathione reductase) which can lead to the build-up of oxidative stress; a major cause of cataract development.³⁵ Since oxidative stress is also known to expedite and promote the glycation process, this creates a vicious cycle between AGEs and ROS.

The ability of EGCNPs to prevent protein glycation was tested *in-vitro* by measuring the inhibitory effect of the nanoparticles on the formation AGEs of a model protein (BSA) when incubated with glucose. BSA was chosen for preliminary testing because of its low cost and the availability of previous glycation studies carried out on it in the literature.²⁰⁴ Fluorescence studies were employed to measure AGEs formation owing to AGEs characteristic fluorescence.²⁰⁴ High fluorescence intensity of protein and sugar mixtures is usually indicative of higher degree of protein glycation.^{204,205} Three EGCNPs concentrations

(50, 100 and 200 $\mu\text{g/ml}$) were tested and the antiglycation effect was compared to two concentrations of the standard antiglycation agent aminoguanidine (10 and 20 mM). As shown in Figure 4-17, all of the tested EGCNPs concentrations showed highly significant inhibition of protein glycation ($****p < 0.0001$) when compared to the non-treated protein/glucose mixture.

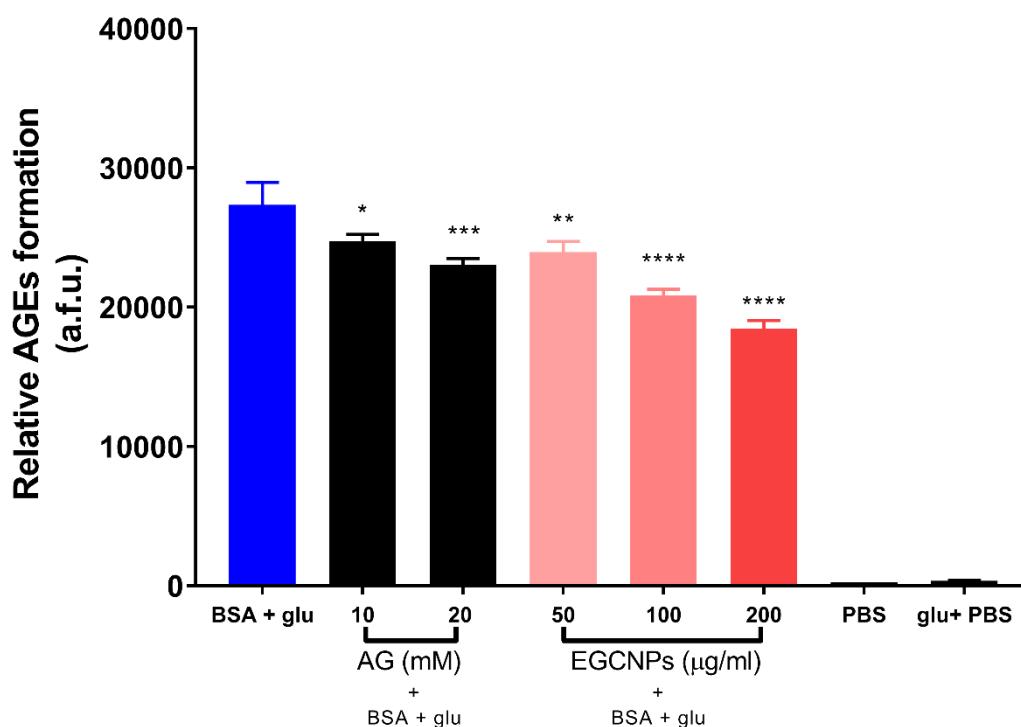


Figure 4-17 Effect of EGCNPs on the inhibition of the formation of advanced glycation end products (AGEs) for bovine serum albumin (BSA) when incubated with glucose (glu) for 72 h.

For comparison, two concentrations of aminoguanidine (AG) were used as it is known for its antiglycation actions. AGEs formation was measured spectrofluorometrically using a plate reader at $\text{ex/em} = 300/400 \text{ nm}$. Asterisks denote statistical significance from BSA + glu, ($n=3$, $*p \leq 0.05$, $**p \leq 0.01$, $***p \leq 0.001$ and $****p \leq 0.0001$, one-way ANOVA). Error bars are presented as means \pm SEM.

The anti-glycating effect EGCNPs was concentration dependent with a decrease in AGEs formation by 13%, 24% and 33% at EGCNPs concentrations of 50, 100 and 200 $\mu\text{g/ml}$ respectively. The percentage decrease in AGEs formation for aminoguanidine was 10% and

16% at 10 mM and 20 mM respectively. The results clearly demonstrate that EGCNPs can act as a potent anti-glycating agent. It is noteworthy that the glucose concentration employed in this study was significantly higher than the concentration that is naturally found in normal and diabetic lens (0.7–2.2 mM and 3–4.5 mM respectively).²⁰⁶

Building on the previous results, it was necessary to investigate if EGCNPs could have similar anti-glycating effects on the eye lens proteins (*i.e.* crystallin). For that, bovine α -crystallin was chosen for testing EGCNPs effects. Not only is α -crystallin one of the main structural lens proteins, but it also functions as a molecular chaperone that protects other lens proteins and enzymes from aggregation.³⁵ In addition, α -crystallin is known to be among proteins prone to glycation in presence of sugars.²⁰⁷ It was shown that α -crystallin protects other proteins such as glutathione reductase and catalase against protein glycation over several days.³⁵ Such protection was exerted regardless of the species of α -crystallin (bovine or human).^{208,209} Moreover, α -crystallin protects against protein inactivation caused by glucocorticoids, which are a known risk factor for cataract development.^{35,210} For example, bovine α -crystallin was reported to fully protect against catalase inactivation induced by six day incubation with prednisolone-21-hemisuccinate; a protective effect that was only specific to α -crystallin compared to other control proteins.²¹¹ For the aforementioned reasons, α -crystallin was chosen for studying EGCNPs anti-glycating effect.

As shown in Figure 4-18, EGCNPs exhibited significant protective effects against the glycation of α -crystallin upon incubation with glucose for three days. This is shown to decrease AGEs fluorescence in all treated conditions compared to non-treated protein and glucose mixture (Figure 4-18). Similar to BSA glycation data, EGCNPs protected α -crystallin in a concentration dependent manner where mean AGEs formation was decreased by 15%, 26% and 34% at EGCNPs concentrations of 50, 100 and 200 μ g/ml respectively.

Aminoguanidine (AG) also decreased mean AGEs formation in α -crystallin by 5% and 7% respectively although, unlike the BSA data, the anti-glycating effect of the lower AG

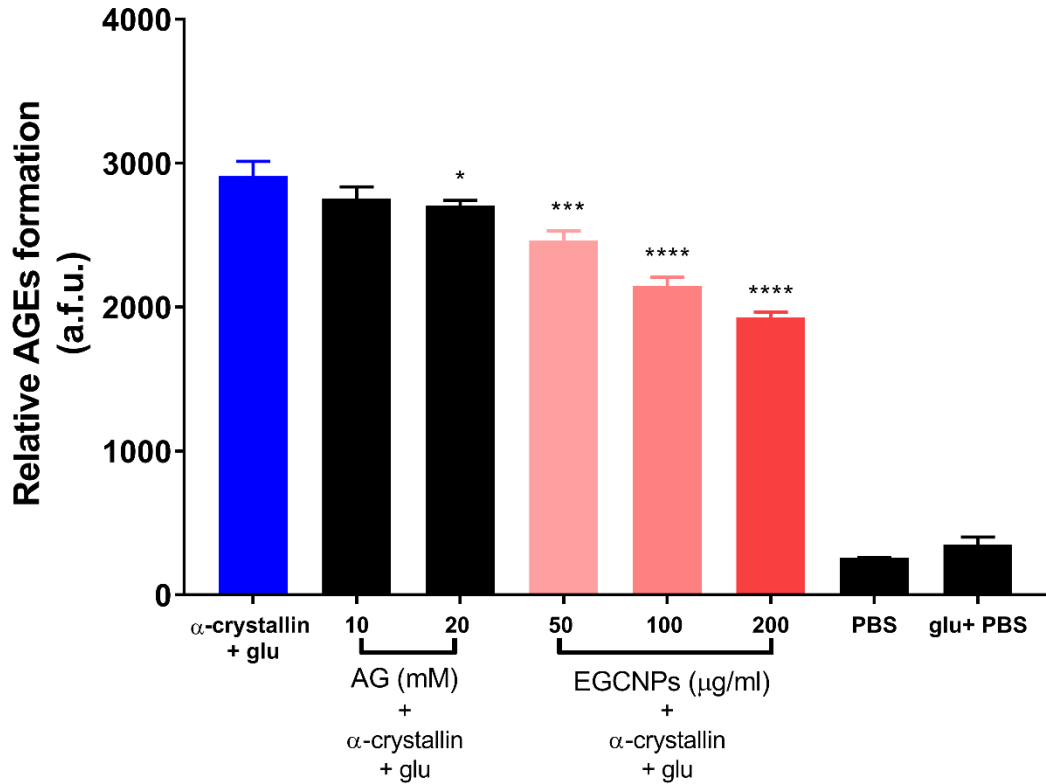


Figure 4-18 Effect of EGCNPs on the inhibition of the formation of advanced glycation end products (AGEs) for bovine α -crystallin when incubated with glucose (glu) for 72 h.

For comparison, two concentrations of aminoguanidine (AG) were used as it is known for its antiglycation actions. AGEs formation was measured spectrofluorometrically using a plate reader at $ex/em = 300/400$ nm. Asterisks denote statistical significance from BSA + glu, ($n=3$, $*p \leq 0.05$, $**p \leq 0.01$, $***p \leq 0.001$ and $****p \leq 0.0001$, one-way ANOVA). Error bars are presented as means \pm SEM.

concentration was not statistically significant ($p=0.09$). This could be attributed to the higher glucose/crystallin ratio used compared to glucose/BSA ratio. Nonetheless, AG (20 mM) showed significant inhibition of AGEs formation. Importantly, all tested EGCNPs concentrations exhibited stronger anti-glycation actions compared to the highest AG concentration. It was previously shown that AG slows cataract formation in moderately diabetic rats (plasma glucose < 350 mg/dl), but its actions were overwhelmed in severely

diabetic rats (plasma glucose < 350 mg/dl).²¹² It was also suggested that protection against glycation is not enough on its own to resist severe diabetes.¹⁹⁵ The results from different reports in literature suggest that a drug possessing both antioxidant and anti-glycating activities would be more effective than a drug that possess only one of them.^{195,213} The data shown here suggest that EGCNPs may present a more preferable alternative given the nanoparticles' additional beneficial protective effects. Together these results show that EGCNPs have potential in protecting against glucose-induced deactivation of one of the abundant crystallin classes. Preserving α -crystallin activity will in turn provide further protection of the other lens structural proteins and the lens antioxidant enzymes due its chaperone activity. The results also may predict that EGCNPs can protect against the glycation of other structural lens proteins (β -crystallin and γ -crystallin) given their structural similarity.²¹⁴ The mechanism by which cerium oxide nanoparticles prevent protein glycation could be ascribed to the activity of surface Ce^{3+} towards many functional groups such as the free amino groups (NH_2) of α -crystallin that constitute the main targets of glycation.²⁰¹ Another possible explanation is that the antioxidant capability of the nanoparticles helped to decrease glycation-promoting free radical in the protein/sugar mixtures. To the best knowledge of the author, this is the first report of cerium oxide nanoparticles (CeO_2) possessing protective actions against glucose-induced α -crystallin glycation.

4.4 Conclusion

In this chapter, the uptake mechanism and localisation of nanocerium (EGCNPs) have been elucidated for the first time in HLECs. It was demonstrated that safe concentrations of EGCNPs enter HLECs very quickly (as short as 15 min), and in a time-dependent manner. The uptake proceeded mainly through energy-dependent endocytosis. SEM-EDX and confocal studies have demonstrated that the nanoparticles localise primarily in the cytoplasm of the cells particularly in the mitochondria. This efficient entry of EGCNPs in HLECs allowed the nanoparticles to exert anticataract actions that were demonstrated in: (1) their ability to protect the cells against external oxidative stress manifested in normal proliferation and total ROS in treated cells, (2) their ability to replace the activity of the catalase enzyme, (3) improving the ratio between reduced and oxidised glutathione (GSH/GSSG), and finally (4) their ability to provide a significant protection against the glycation of lens proteins which is one of the major causes of cataract particularly in diabetics. Given the multifactorial nature of cataract where no one single cause is solely responsible for its progression, EGCNPs demonstrated varied actions providing a highly promising alternative for non-surgical intervention.

5 General discussion, conclusions and recommendations for future work

5.1 Discussion and conclusions

The work presented in this thesis provides new hope for finding an alternative for cataract surgery. To date, surgery is the only effective treatment for cataract, but it is costly, not easily accessible to patients particularly in the developing world and comes with perioperative and postoperative complications. The way to creating a new dawn for cataract treatment is contingent on finding therapeutics that can either delay, halt or reverse the disease process. Identifying a therapeutic intervention that is successful in reversing or preventing cataracts may have applications for other chronic diseases of protein misfolding, such as diabetes and Alzheimer's disease as these have similar causation factors, notably oxidative stress.^{161,181}

In this work, cerium oxide nanoparticles “nanoceria” were proposed as a potential anti-cataract non-surgical treatment because of their inherent antioxidant, radioprotective, enzyme mimetic and recyclable properties. Given the cumulative evidence associating oxidative stress with cataract development and progression,²⁶ testing if these nanoparticles have benefit for cataract seemed to be a logical and unexplored research direction. Although cataract is primarily age-related, the causes behind its development are multi-faceted. Therefore, the use of nanoparticles that can offer protection against multiple potential causes is an attractive strategy for cataract treatment. Many conventional antioxidants such as vitamin C, vitamin E and L-carnosine have shown potential for cataract prevention, but the proposed cerium oxide nanoparticles are superior to these compounds for two main reasons.

Firstly, cerium oxide can deactivate free radicals without being transformed into a free radical itself.⁸¹ Secondly, the particles can recycle themselves in an ambient environment regenerating their antioxidant properties in the process.⁸¹ The latter is a very attractive attribute for chronic diseases since it can significantly decrease dosage frequency and increase patient compliance. The use of nanotechnology offers additional advantages as well in terms of the ability to enhance and optimise drug penetration, release, targeting and the ability to combine multiple therapeutics in a single entity.²¹⁵

The start of this project aimed to formulate cerium oxide nanoparticles with several concerns in mind before proceeding to biological testing. These were:

- 1- The particle size should be very small preferably below 5 nm. This was needed to obtain a high surface-to-volume ratio which increases the activity of the nanoparticles and decrease the required dosage. Additionally, smaller nanoparticles are known for their enhanced cellular penetration with less cell membrane damage which is beneficial.¹¹⁸
- 2- A simple synthetic method preferably in aqueous conditions is needed. The use of organic synthetic methods is costly and produces nanoparticles with toxicity concerns.¹¹³ The simplicity of the synthetic method will positively reflect on the reproducibility of the method, the potential for scale-up and the commercial translation.
- 3- The colloidal stability of cerium oxide nanoparticles is often overlooked in the literature. This partly explains the discrepancies often found in the data reported. Therefore, it was of utmost importance to produce nanoparticles that stay suspended without aggregation or sedimentation in the physiological media intended for biological testing. Coating the nanoparticles is a common strategy for achieving good colloidal stability.

Ethylene glycol is known for its biocompatibility and hydrophilicity, and therefore its choice for aqueous coating of nanocerium was considered.¹¹³ However, in one study ethylene glycol was reported to produce nanoparticles with significant polydispersity and sedimentation. This clearly excludes it from being useful in biomedical applications.¹¹³ In the work carried out in this thesis, however, a novel strategy for the synthesis of the nanoparticles has made it possible to use ethylene glycol and produce monodisperse nanoparticles with an ultra-small particle size (2-5 nm). This was conducted by simply changing the starting cerium precursor from a nitrate to an acetate. The acetate ligands introduced to the reaction partially modified ethylene glycol and produced a hybrid coat of ethylene glycol and mono- and di-acetate derivatives endowing the nanoparticles (EGCNPs) with superior colloidal stability and monodispersity in various physiological media. One concern was that such coating may block the surface antioxidant activity of the nanoparticles, but it was demonstrated that they retain their activity in presence of such coating. The strategy described in this work can also be expanded to enhance the colloidal stability and monodispersity of other types of inorganic nanoparticles without adding to the complexity of the synthetic route.

Fluorescent labelling of the nanoparticles was needed in order to use them for imaging studies. In the literature, it is common practice to label the surfaces of the nanoparticles with fluorescent probes such as FITC or rhodamine. However, this significantly changes the surface properties of the nanoparticles and poses the risk of changing their behaviour.¹¹⁶ In the work described in this thesis, this was addressed by doping the nanoparticles with europium which resulted in the formation of nanoparticles with similar surface properties. Even though doping with europium is not a novel strategy per se, the successful tracking of europium doped cerium oxide nanoparticles (EuCNPs) in any cell line is reported for the first in the work described in this thesis. It was feasible to obtain strong fluorescent emissions in the red region of the light spectrum where cellular autofluorescence is minimal. It should

be noted that the natural weak fluorescence of unlabelled pure nanocerium was also successfully detected in the cells for the first time utilising the ability of cerium oxide to resist photobleaching. This further validated europium doping not altering the localisation pattern of the nanoparticles.

Having obtained cerium oxide nanoparticles with required particle size, monodispersity, colloidal stability, and fluorescent properties, the way was paved to employ them in biological testing. The first thing that needed to be investigated was to assess the formulation safety in HLECs. These are the stem cells of the lens where the majority of the metabolic activities takes place including crystallin synthesis and differentiation into fibre cells that make up the bulk of the lens body. The effect of the nanoparticles on several cellular parameters were assessed in a dose-dependent manner. These parameters included studying the effects of the nanoparticles on the mitochondrial morphology, mitochondrial membrane potential, ATP level, cell proliferation, cell membrane integrity and apoptosis. The results of these investigations showed that these nanoparticles were highly safe even when used at very high concentrations ($\leq 200 \mu\text{g/ml}$) with no signs of decreased proliferation or mitochondrial damage. This level of safety at such a high concentration is unprecedented where another nanocerium formulation showed genotoxic effect in HLECs at half this concentration ($100 \mu\text{g/ml}$).⁶ The reported safe concentrations of nanocerium tested on different cell lines were also much lower.⁶ It is possible that the superior colloidal stability is behind this jump in the tolerability of nanoparticles where sedimentation and aggregation are known causes of increased toxicity. The nanoparticles were also synthesised at a low temperature ($40 \text{ }^\circ\text{C}$) which is reported in the literature to produce less toxic and more antioxidative nanoparticles.²¹⁶ This emphasises the need to test the colloidal stability of any new formulation before employing them in biological experiments. It is worthy of note that many other factors play a role in the toxicity profile including $\text{Ce}^{4+}/\text{Ce}^{3+}$ ratio, particle size, the

morphology, the purity, the starting precursor, the adsorption of protein coronae, the zeta potential, and the used cell line.¹⁴³ Therefore, the safety level of a formulation always needs to be assessed on a case by case basis.

No matter how safe a formulation is, an overdose risks generating toxic or undesirable effects. There was a lack of understanding about the mechanism of the cytotoxic and genotoxic effects of nanoceria when used at higher concentrations. In the work described in this thesis, the mechanism of nanoceria toxicity was investigated after 24-hour exposure in HLECs. At high nanoceria concentrations (400 µg/ml), intracellular levels of ROS were increased and the HLECs exhibited classical hallmarks of apoptosis. These findings concur with the cells maintaining normal ATP levels necessary to execute the apoptotic process. These results highlight the need for nanoceria dose-effect studies on a range of cells and tissues to identify therapeutic concentrations *in-vitro* or *in-vivo*.

When the safe level of nanoceria was determined in HLECs, testing if they provide protective action against oxidative stress was set as the next objective. It could be argued that these nanoparticles are already known for their antioxidant properties, so they are guaranteed to protect against oxidative stress. However, this is not always the case where nanoceria tested in some cell lines were previously reported in the literature not to have any protective effects against oxidative stress.¹⁴³ In other cell lines, nanoceria could not enter the cells and hence they could not protect the cells either.¹⁵⁴ So testing the uptake, localisation and the actions of the nanoparticles needed to be assessed for EGCNPs in HLECs. The results described in this thesis show extensive uptake of EGCNPs. Importantly, most of these nanoparticles localised in the mitochondria which was very promising given that these are the organelles where the majority of ROS are generated. It was subsequently found through a series of studies, that such localisation leads to the protection of HLECs against induced oxidative stress and nanoparticles exerted *in-vitro* catalase mimetic action in cells with

inhibited catalases. The nanoparticles actions did not stop there as it was found that GSH/GSSG ratio increased dramatically in EGCNPs treated cells. This is a remarkable finding given the strong association between decreased GSH/GSSG ratio and cataract progression in nearly all cataract models.²⁶ The work in this thesis was concluded by showing that EGCNPs not only provide antioxidative actions, but they can also provide protection against the glycation of lens proteins. To the best knowledge of the author, this is the first single drug entity that has been demonstrated to collectively provide antioxidative, anti-glycating, GSH promoting and catalase mimetic effects in HLECs. Given the multifactorial nature of cataracts and the potential to add more functionalities to the nanoparticles, EGCNPs have great potential for cataract treatments and should be tested *in-vivo*.

5.2 Recommendations for future work

The research carried out in this thesis has opened new avenues for future work:

- 1- EGCNPs should be tested in *ex-vivo* and *in-vivo* models to study if their protective actions can be replicated. These studies should include protection against glycation, oxidative stress and glutathione depletion. *Ex-vivo* studies on porcine lenses would be a suitable start because of the similarity of protein content compared to the human lenses. The ability of the nanoparticles to pass through the lens capsule into the lens epithelium needs to be assessed.
- 2- The need for more representative *in-vitro* cellular models of the human lens epithelium is desirable. Culturing HLECs on three dimensional (3D) substrates should be investigated.
- 3- It is not yet known by which mechanism EGCNPs protect against protein glycation and if it is the only PTM it protects against. Recent advances in mass spectrometry facilitate the identification and characterisation of various PTMs. This needs further work.
- 4- An ideal formulation for cataract would have to be administered topically. Corneal permeability of EGCNPs need to be assessed and enhanced if needed. The encapsulation of EGCNPs in various kinds of polymeric or lipidic nanoparticles is a possible strategy if needed. Injection of a formulation into the aqueous humour is a possible strategy but not preferred as it will not be convenient for patients.
- 5- Europium-doped nanoceria (EuCNPs) seem to have an extraordinary capability of targeting the mitochondria. TEM studies are required for precise determination of EGCNPs localisation in various organelles including the mitochondria. SEM-EDX is a convenient and quick tool. However, the purity of the mitochondrial fractions should be assessed before analysis by checking for marker enzymes. Given their characteristic

excitation/emission properties, low cost and ease of synthesis, EuCNPs have a great potential to act as mitochondrial probes replacing the less versatile and more expensive Mitotracker™ dyes. This needs optimisation and testing in various cell lines. The safety and antioxidant activity of the doped nanoparticles should also be studied.

6 References

1. Abdelkader, H., Alany, R. G. & Pierscionek, B. Age-related cataract and drug therapy: Opportunities and challenges for topical antioxidant delivery to the lens. *J. Pharm. Pharmacol.* **67**, 537–550 (2015).
2. Hejtmancik, J. F. & Shiels, A. *Overview of the Lens. Progress in Molecular Biology and Translational Science* **134**, (2015).
3. Benedek, G. B. Theory of Transparency of the Eye. *Appl. Opt.* **10**, 459–73 (1971).
4. Duncan, G., Michael Wormstone, I. & Davies, P. D. The aging human lens: Structure, growth, and physiological behaviour. *Br. J. Ophthalmol.* **81**, 818–823 (1997).
5. Eye anatomy vector | Free Vector. Available at: [https://www.freepik.com/free-vector/eye-anatomy-vector_760161.htm#page=1&query=eye anatomy&position=13](https://www.freepik.com/free-vector/eye-anatomy-vector_760161.htm#page=1&query=eye%20anatomy&position=13). (Accessed: 16th February 2020)
6. Pierscionek, B. K., Li, Y., Schachar, R. A. & Chen, W. The effect of high concentration and exposure duration of nanoceria on human lens epithelial cells. *Nanomedicine Nanotechnology, Biol. Med.* **8**, 383–390 (2012).
7. Harding, J. J., Rixon, K. C. & Marriott, F. H. Men have heavier lenses than women of the same age. *Exp. Eye Res.* **25**, 651 (1977).
8. Danysh, B. P. & Duncan, M. K. The lens capsule. *Exp. Eye Res.* **88**, 151–164 (2009).
9. Croft, M. A., Heatley, G., McDonald, J. P., Katz, A. & Kaufman, P. L. Accommodative movements of the lens/capsule and the strand that extends between the posterior vitreous zonule insertion zone & the lens equator, in relation to the vitreous face and aging. *Ophthalmic Physiol. Opt.* **36**, 21–32 (2016).

10. Koretz, J. F. & Handelman, G. H. How the human eye focuses. *Sci. Am.* **259**, 92–99 (1988).
11. Bhat, S. P. The ocular lens epithelium. *Biosci. Rep.* **21**, 537–563 (2001).
12. Sugiyama, Y., Prescott, A. R., Tholozan, F. M. D., Ohno, S. & Quinlan, R. A. Expression and localisation of apical junctional complex proteins in lens epithelial cells. *Exp. Eye Res.* **87**, 64–70 (2008).
13. Davies, M. J. & Truscott, R. J. W. Photo-oxidation of proteins and its role in cataractogenesis. *J. Photochem. Photobiol. B Biol.* **63**, 114–25 (2001).
14. Kuszak, J. R., Zoltoski, R. K. & Sivertson, C. Fibre cell organization in crystalline lenses. *Exp. Eye Res.* **78**, 673–687 (2004).
15. Wistow, G. *et al.* X-ray analysis of the eye lens protein gamma-II crystallin at 1.9 Å resolution. *J. Mol. Biol.* **170**, 175–202 (1983).
16. Bloemendal, H. The vertebrate eye lens. *Science.* **197**, 127–138 (1977).
17. Bloemendal, H. *et al.* Ageing and vision: Structure, stability and function of lens crystallins. *Progress in Biophysics and Molecular Biology* **86**, 407–485 (2004).
18. Clark, A. R., Lubsen, N. H. & Slingsby, C. SHSP in the eye lens: Crystallin mutations, cataract and proteostasis. *Int. J. Biochem. Cell Biol.* **44**, 1687–1697 (2012).
19. Augusteyn, R. C. On the growth and internal structure of the human lens. *Exp. Eye Res.* **90**, 643–654 (2010).
20. Ray, N. J. Biophysical chemistry of the ageing eye lens. *Biophysical Reviews* **7**, 353–368 (2015).
21. Vinson, J. A. Oxidative stress in cataracts. *Pathophysiology* **13**, 151–162 (2006).

22. Harding, J. J. Viewing molecular mechanisms of ageing through a lens. *Ageing Res. Rev.* **1**, 465–479 (2002).
23. Yool, A. J. & Campbell, E. M. Structure, function and translational relevance of aquaporin dual water and ion channels. *Molecular Aspects of Medicine* **33**, 553–561 (2012).
24. Fan, X., Monnier, V. M. & Whitson, J. Lens glutathione homeostasis: Discrepancies and gaps in knowledge standing in the way of novel therapeutic approaches. *Experimental Eye Research* **156**, 103–111 (2017).
25. Umapathy, A., Donaldson, P. & Lim, J. Antioxidant delivery pathways in the anterior eye. *BioMed Research International* **2013**, (2013).
26. Truscott, R. J. W. Age-related nuclear cataract - Oxidation is the key. *Exp. Eye Res.* **80**, 709–725 (2005).
27. Toh, T. Y., Morton, J., Coxon, J. & Elder, M. J. Medical treatment of cataract. *Clin. Exp. Ophthalmol.* **35**, 664–671 (2007).
28. Klein, B. E. K., Klein, R. & Linton, K. L. P. Prevalence of Age-related Lens Opacities in a Population: The Beaver Dam Eye Study. *Ophthalmology* **99**, 546–552 (1992).
29. Thrimawithana, T. R. *et al.* Drug delivery to the lens for the management of cataracts. *Advanced Drug Delivery Reviews* **126**, 185–194 (2018).
30. Park, S. & Choi, N. K. Hepatitis virus infection and age-related cataract. *Sci. Rep.* **7**, 13089 (2017).
31. Pichi, F., Lembo, A., Serafino, M. & Nucci, P. Genetics of congenital cataract. *Dev. Ophthalmol.* **57**, 1–14 (2016).

32. Sparrow, J. M., Bron, A. J., Brown, N. A. P., Ayliffe, W. & Hill, A. R. The Oxford Clinical Cataract Classification and Grading System. *Int. Ophthalmol.* **9**, 207–225 (1986).
33. Moreau, K. L. & King, J. A. Protein misfolding and aggregation in cataract disease and prospects for prevention. *Trends Mol. Med.* **18**, 273–282 (2012).
34. Truscott, R. J. W. & Friedrich, M. G. The etiology of human age-related cataract. Proteins don't last forever. *Biochim. Biophys. Acta - Gen. Subj.* **1860**, 192–198 (2016).
35. Hook, D. W. A. & Harding, J. J. Protection of enzymes by α -crystallin acting as a molecular chaperone. *Int. J. Biol. Macromol.* **22**, 295–306 (1998).
36. Cobb, B. A. & Petrush, J. M. α -crystallin chaperone-like activity and membrane binding in age-related cataracts. *Biochemistry* **41**, 483–490 (2002).
37. Andley, U. P. The lens epithelium: Focus on the expression and function of the α -crystallin chaperones. *Int. J. Biochem. Cell Biol.* **40**, 317–323 (2008).
38. Berthoud, V. M. & Beyer, E. C. Oxidative stress, lens gap junctions, and cataracts. *Antioxidants and Redox Signaling* **11**, 339–353 (2009).
39. Roberts, J. E. Ultraviolet radiation as a risk factor for cataract and macular degeneration. *Eye and Contact Lens* **37**, 246–249 (2011).
40. Harding, J. J., Harding, R. S. & Egerton, M. Risk factors for cataract in Oxfordshire: diabetes, peripheral neuropathy, myopia, glaucoma and diarrhoea. *Acta Ophthalmol.* **67**, 510–517 (2009).
41. Ji, L. *et al.* A simple and stable galactosemic cataract model for rats. *Int. J. Clin. Exp. Med.* **8**, 12874–12881 (2015).

42. Abdelkader, H., Longman, M., Alany, R. G. & Pierscionek, B. On the Anticataractogenic Effects of L-Carnosine: Is It Best Described as an Antioxidant, Metal-Chelating Agent or Glycation Inhibitor? *Oxid. Med. Cell. Longev.* **2016**, (2016).
43. Kisic, B., Miric, D., Zoric, L., Ilic, A. & Dragojevic, I. Antioxidant capacity of lenses with age-related cataract. *Oxid. Med. Cell. Longev.* **2012**, (2012).
44. Eaton, J. W. Is the lens canned? *Free Radic. Biol. Med.* **11**, 207–213 (1991).
45. Palmquist, B. M., Philipson, B. & Barr, P. O. Nuclear cataract and myopia during hyperbaric oxygen therapy. *Br. J. Ophthalmol.* **68**, 113–117 (1984).
46. Cataract Statistics & Resources | Laser Eye Surgery Hub. Available at: <https://www.lasereyesurgeryhub.co.uk/cataract-statistics/>. (Accessed: 13th February 2020)
47. The Way Forward Resources - The Royal College of Ophthalmologists. Available at: <https://www.rcophth.ac.uk/standards-publications-research/the-way-forward/>. (Accessed: 13th February 2020)
48. Khairallah, M. *et al.* Number of people blind or visually impaired by cataract worldwide and in world regions, 1990 to 2010. *Investig. Ophthalmol. Vis. Sci.* **56**, 6762–6769 (2015).
49. Davis, G. The Evolution of Cataract Surgery. *Mo. Med.* **113**, 58–62 (2016).
50. Raj, S. M., Vasavada, A. R., Johar, S. R. K., Vasavada, V. A. & Vasavada, V. A. Post-operative capsular opacification: a review. *Int. J. Biomed. Sci.* **3**, 237–50 (2007).
51. Wang, K. & Pierscionek, B. K. Biomechanics of the human lens and accommodative system: Functional relevance to physiological states. *Progress in Retinal and Eye Research* **71**, 114–131 (2019).

52. Quinlan, R. A. A new dawn for cataracts. *Science*. **350**, 636 LP – 637 (2015).
53. Brian, G. & Taylor, H. Cataract blindness - Challenges for the 21st century. *Bull. World Health Organ.* **79**, 249–256 (2001).
54. Abdelkader, H., Longman, M. R., Alany, R. G. & Pierscionek, B. Phytosome-hyaluronic acid systems for ocular delivery of L-carnosine. *Int. J. Nanomedicine* **11**, 2815–2827 (2016).
55. Babizhayev, M. A., Burke, L., Micans, P. & Richer, S. P. N-acetylcarnosine sustained drug delivery eye drops to control the signs of ageless vision: Glare sensitivity, cataract amelioration and quality of vision currently available treatment for the challenging 50,000-patient population. *Clin. Interv. Aging* **4**, 31–50 (2009).
56. Babizhayev, M. A., Deyev, A. I., Yermakova, V. N., Brikman, I. V. & Bours, J. Lipid peroxidation and cataracts: N-Acetylcarnosine as a therapeutic tool to manage age-related cataracts in human and in canine eyes. *Drugs in R and D* **5**, 125–139 (2004).
57. Babizhayev, M. A. *et al.* Efficacy of N-acetylcarnosine in the treatment of cataracts. *Drugs R D* **3**, 87–103 (2002).
58. Varma, S. D. & Richards, R. D. Ascorbic acid and the eye lens. *Ophthalmic Res.* **20**, 164–173 (1988).
59. Robertson, J. M., Donner, A. P. & Trevithick, J. R. A possible role for vitamins C and E in cataract prevention. in *American Journal of Clinical Nutrition* **53**, 346S-351S (1991).
60. Seddon, J. M. *et al.* The use of vitamin supplements and the risk of cataract among US male physicians. *Am. J. Public Health* **84**, 788–792 (1994).
61. Chylack, L. T. *et al.* The Roche European American Cataract Trial (react): A

- randomized clinical trial to investigate the efficacy of an oral antioxidant micronutrient mixture to slow progression of age-related cataract. *Ophthalmic Epidemiol.* **9**, 49–80 (2002).
62. McNeil, J. J. *et al.* Vitamin E Supplementation and Cataract: Randomized Controlled Trial. *Ophthalmology* **111**, 75–84 (2004).
 63. Cotlier, E. Aspirin effect on cataract formation in patients with rheumatoid arthritis alone or combined with diabetes. *Int. Ophthalmol.* **3**, 173–7 (1981).
 64. Crompton, M., Rixon, K. C. & Harding, J. J. Aspirin prevents carbamylation of soluble lens proteins and prevents cyanate-induced phase separation opacities in vitro: A possible mechanism by which aspirin could prevent cataract. *Exp. Eye Res.* **40**, 297–311 (1985).
 65. Gupta, P. P. *et al.* Aspirin in experimental cataractogenesis. *Indian J. Med. Res.* **80**, 703–7 (1984).
 66. Blakytyn, R. & Harding, J. J. Prevention of cataract in diabetic rats by aspirin, paracetamol (acetaminophen) and ibuprofen. *Exp. Eye Res.* **54**, 509–18 (1992).
 67. Van Heyningen, R. & Harding, J. J. A case-control study of cataract in Oxfordshire: Some risk factors. *Br. J. Ophthalmol.* **72**, 804–808 (1988).
 68. West, S. K., Muñoz, B. E., Newland, H. S., Emmett, E. A. & Taylor, H. R. Lack of Evidence for Aspirin use and Prevention of Cataracts. *Arch. Ophthalmol.* **105**, 1229–1231 (1987).
 69. Kim, S. J., Flach, A. J. & Jampol, L. M. Nonsteroidal Anti-inflammatory Drugs in Ophthalmology. *Survey of Ophthalmology* **55**, 108–133 (2010).
 70. Bekendam, P. D., Narváez, J. & Agarwal, M. Case of corneal melting associated with

- the use of topical Nepafenac. *Cornea* **26**, 1002–1003 (2007).
71. Harding, J. J. Can cataract be prevented? *Eye* **13**, 454–456 (1999).
 72. Zhao, L. *et al.* Lanosterol reverses protein aggregation in cataracts. *Nature* **523**, 607–611 (2015).
 73. Makley, L. N. *et al.* Pharmacological chaperone for α -crystallin partially restores transparency in cataract models. *Science*. **350**, 674–677 (2015).
 74. Qi, L. B. *et al.* Cataract-causing mutation S228P promotes β B1-crystallin aggregation and degradation by separating two interacting loops in C-terminal domain. *Protein Cell* **7**, 501–515 (2016).
 75. Leng, X. Y. *et al.* Congenital microcornea-cataract syndrome-causing mutation X253R increases β b1-crystallin hydrophobicity to promote aggregate formation. *Biochem. J.* **473**, 2087–2096 (2016).
 76. Shanmugam, P. M. *et al.* Effect of lanosterol on human cataract nucleus. *Indian J. Ophthalmol.* **63**, 888–890 (2015).
 77. Felici, A., Mengato, D., Falciani, M. & Bertelli, E. Lanosterol Eye Drops in a Human Juvenile Nuclear Cataract. *Arch Clin Med Case Rep* **2**, 12–15 (2018).
 78. Daszynski, D. M. *et al.* Failure of Oxysterols Such as Lanosterol to Restore Lens Clarity from Cataracts. *Sci. Rep.* **9**, (2019).
 79. Patel, A. Ocular drug delivery systems: An overview. *World J. Pharmacol.* **2**, 47 (2013).
 80. Cetinel, S. & Montemagno, C. Nanotechnology for the prevention and treatment of cataract. *Asia-Pacific J. Ophthalmol.* **4**, 381–387 (2015).

81. Xu, C. & Qu, X. Cerium oxide nanoparticle: A remarkably versatile rare earth nanomaterial for biological applications. *NPG Asia Mater.* **6**, e90-16 (2014).
82. Bouzigues, C., Gacoin, T. & Alexandrou, A. Biological applications of rare-earth based nanoparticles. *ACS Nano* **5**, 8488–8505 (2011).
83. Corma, A., Atienzar, P., García, H. & Chane-Ching, J. Y. Hierarchically mesostructured doped CeO₂ with potential for solar-cell use. *Nat. Mater.* **3**, 394–397 (2004).
84. Izu, N., Shin, W., Matsubara, I. & Murayama, N. Development of resistive oxygen sensors based on cerium oxide thick film. *J. Electroceramics* **13**, 703–706 (2004).
85. Montini, T., Melchionna, M., Monai, M. & Fornasiero, P. Fundamentals and Catalytic Applications of CeO₂-Based Materials. *Chem. Rev.* **116**, 5987–6041 (2016).
86. Yabe, S. & Sato, T. Cerium oxide for sunscreen cosmetics. in *Journal of Solid State Chemistry* **171**, 7–11 (Academic Press Inc., 2003).
87. Kosynkin, V. D. *et al.* The study of process production of polishing powder based on cerium dioxide. *J. Alloys Compd.* **303–304**, 421–425 (2000).
88. Alpaslan, E., Yazici, H., Golshan, N. H., Ziemer, K. S. & Webster, T. J. PH-Dependent Activity of Dextran-Coated Cerium Oxide Nanoparticles on Prohibiting Osteosarcoma Cell Proliferation. *ACS Biomater. Sci. Eng.* **1**, 1096–1103 (2015).
89. Hirst, S. M. *et al.* Anti-inflammatory properties of cerium oxide nanoparticles. *Small* **5**, 2848–2856 (2009).
90. Naz, S. *et al.* Cerium oxide nanoparticles: A ‘radical’ approach to neurodegenerative disease treatment. *Nanomedicine* **12**, 545–553 (2017).

91. Chen, J., Patil, S., Seal, S. & McGinnis, J. F. Nanoceria particles prevent roi-induced blindness. *Adv. Exp. Med. Biol.* **613**, 53–59 (2008).
92. Pagliari, F. *et al.* Cerium oxide nanoparticles protect cardiac progenitor cells from oxidative stress. *ACS Nano* **6**, 3767–3775 (2012).
93. Liu, X., Chen, S. & Wang, X. Synthesis and photoluminescence of CeO₂:Eu³⁺ phosphor powders. *J. Lumin.* **127**, 650–654 (2007).
94. Calvache-Muñoz, J., Prado, F. A. & Rodríguez-Páez, J. E. Cerium oxide nanoparticles: Synthesis, characterization and tentative mechanism of particle formation. *Colloids Surfaces A Physicochem. Eng. Asp.* **529**, 146–159 (2017).
95. Krishnan, A., Sreeremya, T. S., Murray, E. & Ghosh, S. One-pot synthesis of ultra-small cerium oxide nanodots exhibiting multi-colored fluorescence. *J. Colloid Interface Sci.* **389**, 16–22 (2013).
96. Chen, H. I. & Chang, H. Y. Synthesis of nanocrystalline cerium oxide particles by the precipitation method. *Ceram. Int.* **31**, 795–802 (2005).
97. Li, C. *et al.* Hot Topics and Challenges of Regenerative Nanoceria in Application of Antioxidant Therapy. *J. Nanomater.* **2018**, 1–12 (2018).
98. Mullins, D. R. The surface chemistry of cerium oxide. *Surface Science Reports* **70**, 42–85 (2015).
99. He, L., Su, Y., Lanhong, J. & Shi, S. Recent advances of cerium oxide nanoparticles in synthesis, luminescence and biomedical studies: a review. *J. Rare Earths* **33**, 791–799 (2015).
100. Singh, R. & Singh, S. Redox-dependent catalase mimetic cerium oxide-based nanozyme protect human hepatic cells from 3-AT induced acatalasemia. *Colloids*

Surfaces B Biointerfaces **175**, 625–635 (2019).

101. Korsvik, C., Patil, S., Seal, S. & Self, W. T. Superoxide dismutase mimetic properties exhibited by vacancy engineered ceria nanoparticles. *Chem. Commun.* **2007**, 1056–1058 (2007).
102. Celardo, I., Pedersen, J. Z., Traversa, E. & Ghibelli, L. Pharmacological potential of cerium oxide nanoparticles. *Nanoscale* **3**, 1411–1420 (2011).
103. Pirmohamed, T. *et al.* Nanoceria exhibit redox state-dependent catalase mimetic activity. *Chem. Commun.* **46**, 2736–2738 (2010).
104. Lipinski, B. Hydroxyl radical and its scavengers in health and disease. *Oxid. Med. Cell. Longev.* **2011**, (2011).
105. Singh, S. *et al.* A phosphate-dependent shift in redox state of cerium oxide nanoparticles and its effects on catalytic properties. *Biomaterials* **32**, 6745–6753 (2011).
106. Kwon, H. J. *et al.* Mitochondria-Targeting Ceria Nanoparticles as Antioxidants for Alzheimer's Disease. *ACS Nano* **10**, 2860–2870 (2016).
107. Pinna, A. *et al.* Ceria nanoparticles for the treatment of Parkinson-like diseases induced by chronic manganese intoxication. *RSC Adv.* **5**, 20432–20439 (2015).
108. Chen, J., Patil, S., Seal, S. & McGinnis, J. F. Rare earth nanoparticles prevent retinal degeneration induced by intracellular peroxides. *Nat. Nanotechnol.* **1**, 142–150 (2006).
109. Pierscionek, B. K. *et al.* Nanoceria have no genotoxic effect on human lens epithelial cells. *Nanotechnology* **21**, (2010).

110. Caputo, F. *et al.* Cerium oxide nanoparticles, combining antioxidant and UV shielding properties, prevent UV-induced cell damage and mutagenesis. *Nanoscale* **7**, 15643–15656 (2015).
111. Skorodumova, N. V., Simak, S. I., Lundqvist, B. I., Abrikosov, I. A. & Johansson, B. Quantum origin of the oxygen storage capability of ceria. *Phys. Rev. Lett.* **89**, 166601 (2002).
112. Lee, S. S. *et al.* Antioxidant properties of cerium oxide nanocrystals as a function of nanocrystal diameter and surface coating. *ACS Nano* **7**, 9693–9703 (2013).
113. Caputo, F. *et al.* A novel synthetic approach of cerium oxide nanoparticles with improved biomedical activity. *Sci. Rep.* **7**, 1–14 (2017).
114. Cho, E. C., Zhang, Q. & Xia, Y. The effect of sedimentation and diffusion on cellular uptake of gold nanoparticles. *Nat. Nanotechnol.* **6**, 385–391 (2011).
115. Karakoti, A. S. *et al.* *Nanoceria as antioxidant: Synthesis and biomedical applications.* *JOM* **60**, 33–37 (2008).
116. Kumar, A., Babu, S., Karakoti, A. S., Schulte, A. & Seal, S. Luminescence properties of europium-doped cerium oxide nanoparticles: Role of vacancy and oxidation states. *Langmuir* **25**, 10998–11007 (2009).
117. Hall, A. *et al.* Towards MRI microarrays. *Chem. Commun.* **46**, 2420–2422 (2010).
118. Singh, S. *et al.* Cerium oxide nanoparticles at the nano-bio interface: size-dependent cellular uptake. *Artif. Cells, Nanomedicine Biotechnol.* **46**, S956–S963 (2018).
119. Li, Q. *et al.* Correlation between particle size/domain structure and magnetic properties of highly crystalline Fe₃O₄ nanoparticles. *Sci. Rep.* **7**, 1–4 (2017).

120. Coates, J. Interpretation of Infrared Spectra, A Practical Approach. in *Encyclopedia of Analytical Chemistry* 10815 – 10837 (2006). doi:10.1002/9780470027318.a5606
121. De Marzi, L. *et al.* Cytotoxicity and genotoxicity of ceria nanoparticles on different cell lines in vitro. *Int. J. Mol. Sci.* **14**, 3065–3077 (2013).
122. Faisal, M. *et al.* Role of ZnO-CeO₂ Nanostructures as a Photo-catalyst and Chemi-sensor. *J. Mater. Sci. Technol.* **27**, 594–600 (2011).
123. Karakoti, A. S., Kuchibhatla, S. V. N. T., Babu, K. S. & Seal, S. Direct synthesis of nanoceria in aqueous polyhydroxyl solutions. *J. Phys. Chem. C* **111**, 17232–17240 (2007).
124. Lovrić, J., Cho, S. J., Winnik, F. M. & Maysinger, D. Unmodified cadmium telluride quantum dots induce reactive oxygen species formation leading to multiple organelle damage and cell death. *Chem. Biol.* **12**, 1227–1234 (2005).
125. Perez, J. M., Asati, A., Nath, S. & Kaittanis, C. Synthesis of biocompatible dextran-coated nanoceria with pH-dependent antioxidant properties. *Small* **4**, 552–556 (2008).
126. Wolfbeis, O. S. An overview of nanoparticles commonly used in fluorescent bioimaging. *Chem. Soc. Rev.* **44**, 4743–4768 (2015).
127. Gao, F. *et al.* Growth and photoluminescence of epitaxial CeO₂film on Si (111) substrate. *Chinese Phys. Lett.* **18**, 443–448 (2001).
128. Krishnan, A., Sreeremya, T. S. & Ghosh, S. Size-tunable hydrophilic cerium oxide nanoparticles as a ‘turn-on’ fluorescence sensor for the rapid detection of ultralow concentrations of Vitamin C. *RSC Adv.* **6**, 53550–53559 (2016).
129. Bhattacharjee, S. DLS and zeta potential - What they are and what they are not? *Journal of Controlled Release* **235**, 337–351 (2016).

130. Pino, P. Del *et al.* Protein corona formation around nanoparticles - From the past to the future. *Mater. Horizons* **1**, 301–313 (2014).
131. Cedervall, T. *et al.* Understanding the nanoparticle-protein corona using methods to quantify exchange rates and affinities of proteins for nanoparticles. *Proc. Natl. Acad. Sci.* **104**, 2050–2055 (2007).
132. Konduru, N. V. *et al.* Protein corona: Implications for nanoparticle interactions with pulmonary cells. *Part. Fibre Toxicol.* **14**, 42 (2017).
133. Gräfe, C. *et al.* Intentional formation of a protein corona on nanoparticles: Serum concentration affects protein corona mass, surface charge, and nanoparticle-cell interaction. *Int. J. Biochem. Cell Biol.* **75**, 196–202 (2016).
134. Sperling, R. A. & Parak, W. J. Surface modification, functionalization and bioconjugation of colloidal Inorganic nanoparticles. *Philos. Trans. R. Soc. A Math. Phys. Eng. Sci.* **368**, 1333–1383 (2010).
135. Min, P., Zhang, S., Xu, Y. & Li, R. Enhanced oxygen storage capacity of CeO₂ with doping-induced unstable crystal structure. *Appl. Surf. Sci.* **448**, 435–443 (2018).
136. Inshakova, E. & Inshakov, O. World market for nanomaterials: Structure and trends. in *MATEC Web of Conferences* **129**, 02013 (EDP Sciences, 2017).
137. Commission Recommendation. On the definition of nanomaterial. *Off. J. Eur. Union* **L 275**, 2010–2012 (2011).
138. Fu, P. P., Xia, Q., Hwang, H. M., Ray, P. C. & Yu, H. Mechanisms of nanotoxicity: Generation of reactive oxygen species. *J. Food Drug Anal.* **22**, 64–75 (2014).
139. von Montfort, C., Alili, L., Teuber-Hanselmann, S. & Brenneisen, P. Redox-active cerium oxide nanoparticles protect human dermal fibroblasts from PQ-induced

- damage. *Redox Biol.* **4**, 1–5 (2015).
140. Gantt, B. *et al.* Factors affecting the ambient physicochemical properties of cerium-containing particles generated by nanoparticle diesel fuel additive use. *Aerosol Sci. Technol.* **49**, 371–380 (2015).
141. Hussain, S. *et al.* Cerium dioxide nanoparticles induce apoptosis and autophagy in human peripheral blood monocytes. *ACS Nano* **6**, 5820–5829 (2012).
142. Yokel, R. A. *et al.* The yin: An adverse health perspective of nanoceria: Uptake, distribution, accumulation, and mechanisms of its toxicity. *Environ. Sci. Nano* **1**, 406–428 (2014).
143. Gagnon, J. & Fromm, K. M. Toxicity and Protective Effects of Cerium Oxide Nanoparticles (Nanoceria) Depending on Their Preparation Method, Particle Size, Cell Type, and Exposure Route. *Eur. J. Inorg. Chem.* **2015**, 4510–4517 (2015).
144. Auffan, M. *et al.* CeO₂ nanoparticles induce DNA damage towards human dermal fibroblasts in vitro. *Nanotoxicology* **3**, 161–171 (2009).
145. Benameur, L. *et al.* DNA damage and oxidative stress induced by CeO₂ nanoparticles in human dermal fibroblasts: Evidence of a clastogenic effect as a mechanism of genotoxicity. *Nanotoxicology* **9**, 696–705 (2015).
146. Chen, J., Patil, S., Seal, S. & McGinnis, J. F. Rare earth nanoparticles prevent retinal degeneration induced by intracellular peroxides. *Nat. Nanotechnol.* **1**, 142–150 (2006).
147. Zheng, Q. *et al.* Cytocompatible cerium oxide-mediated antioxidative stress in inhibiting ocular inflammation-Associated corneal neovascularization. *J. Mater. Chem. B* **7**, 6759–6769 (2019).

148. Patil, S., Reshetnikov, S., Haldar, M. K., Seal, S. & Mallik, S. Surface-derivatized nanoceria with human carbonic anhydrase II inhibitors and fluorophores: A potential drug delivery device. *J. Phys. Chem. C* **111**, 8437–8442 (2007).
149. Andley, U. P., Rhim, J. S., Chylack, L. T. & Fleming, T. P. Propagation and immortalization of human lens epithelial cells in culture. *Investig. Ophthalmol. Vis. Sci.* **35**, 3094–3102 (1994).
150. Usha P. Andley; Timothy P. Fleming. Immortalized epithelial cell lines, US Patent 5,643,782 (1997).
151. Fleming, T. P., Song, Z. & Andley, U. P. Expression of Growth Control and Differentiation Genes in Human Lens Epithelial Cells with Extended Life Span. *Investig. Ophthalmol. Vis. Sci.* **8**, 1387–1392 (1998).
152. Stockert, J. C., Horobin, R. W., Colombo, L. L. & Blázquez-Castro, A. Tetrazolium salts and formazan products in Cell Biology: Viability assessment, fluorescence imaging, and labeling perspectives. *Acta Histochem.* **120**, 159–167 (2018).
153. Hanafy, B. I., Cave, G. W. V., Barnett, Y. & Pierscionek, B. Ethylene glycol coated nanoceria protects against oxidative stress in human lens epithelium. *RSC Adv.* **9**, 16596–16605 (2019).
154. Asati, A., Santra, S., Kaittanis, C. & Perez, J. M. Surface-charge-dependent cell localization and cytotoxicity of cerium oxide nanoparticles. *ACS Nano* **4**, 5321–5331 (2010).
155. Jiang, X., Du, B., Huang, Y. & Zheng, J. Ultrasmall noble metal nanoparticles: Breakthroughs and biomedical implications. *Nano Today* **21**, 106–125 (2018).
156. Li, B., Agarwal, V., Ho, D., Vede, J. P. & Iyer, K. S. Systematic assessment of surface

- functionality on nanoscale patterns for topographic contact guidance of cells. *New J. Chem.* **42**, 7237–7240 (2018).
157. Hu, W. *et al.* Protein corona-mediated mitigation of cytotoxicity of graphene oxide. *ACS Nano* **5**, 3693–3700 (2011).
158. Incucyte® Cytotox Red Reagent for counting dead cells – Incucyte eShop. Available at: <https://shop.essenbioscience.com/products/cytotox-red-reagent-for-counting-dead-cells>. (Accessed: 15th August 2020)
159. Rai, Y. *et al.* Mitochondrial biogenesis and metabolic hyperactivation limits the application of MTT assay in the estimation of radiation induced growth inhibition. *Sci. Rep.* **8**, 1531 (2018).
160. Volpe, C. M. O., Villar-Delfino, P. H., Dos Anjos, P. M. F. & Nogueira-Machado, J. A. Cellular death, reactive oxygen species (ROS) and diabetic complications review-Article. *Cell Death Dis.* **9**, 119 (2018).
161. Pollreisz, A. & Schmidt-Erfurth, U. Diabetic Cataract—Pathogenesis, Epidemiology and Treatment. *J. Ophthalmol.* **2010**, (2010).
162. Dayem, A. A. *et al.* The role of reactive oxygen species (ROS) in the biological activities of metallic nanoparticles. *Int. J. Mol. Sci.* **18**, 120 (2017).
163. Heckert, E. G., Seal, S. & Self, W. T. Fenton-like reaction catalyzed by the rare earth inner transition metal cerium. *Environ. Sci. Technol.* **42**, 5014–5019 (2008).
164. Zhang, Q. *et al.* Circulating mitochondrial DAMPs cause inflammatory responses to injury. *Nature* **464**, 104–107 (2010).
165. Nasrazadani, S. & Hassani, S. Modern analytical techniques in failure analysis of aerospace, chemical, and oil and gas industries. in *Handbook of Materials Failure*

Analysis with Case Studies from the Oil and Gas Industry 39–54 (Butterworth-Heinemann, 2015). doi:10.1016/B978-0-08-100117-2.00010-8

166. Singh, S., Kumar, A., Karakoti, A., Seal, S. & Self, W. T. Unveiling the mechanism of uptake and sub-cellular distribution of cerium oxide nanoparticles. *Mol. Biosyst.* **6**, 1813–1820 (2010).
167. Chazotte, B. Labeling Mitochondria with MitoTracker Dyes. *Cold Spring Harb. Protoc.* **2011**.
168. Saraste, A. & Pulkki, K. Morphologic and biochemical hallmarks of apoptosis. *Cardiovasc. Res.* **45**, 528–537 (2000).
169. Richter, C., Schweizer, M., Cossarizza, A. & Franceschi, C. Control of apoptosis by the cellular ATP level. *FEBS Lett.* **378**, 107–110 (1996).
170. Jana, S. K., Banerjee, P., Das, S., Seal, S. & Chaudhury, K. Redox-active nanoceria depolarize mitochondrial membrane of human colon cancer cells. *J. Nanoparticle Res.* **16**, 2441 (2014).
171. Doll, R. Prospects for prevention. *Br. Med. J. (Clin. Res. Ed.)* **286**, 445–453 (1983).
172. Shi, Y. Caspase activation, inhibition, and reactivation: A mechanistic view. *Protein Sci.* **13**, 1979–1987 (2004).
173. Keil, V. C., Funke, F., Zeug, A., Schild, D. & Müller, M. Ratiometric high-resolution imaging of JC-1 fluorescence reveals the subcellular heterogeneity of astrocytic mitochondria. *Pflugers Arch. Eur. J. Physiol.* **462**, 693–708 (2011).
174. Zamaraeva, M. V *et al.* Cells die with increased cytosolic ATP during apoptosis: A bioluminescence study with intracellular luciferase. *Cell Death Differ.* **12**, 1390–1397 (2005).

175. Mofford, D. M., Reddy, G. R. & Miller, S. C. Latent luciferase activity in the fruit fly revealed by a synthetic luciferin. *Proc. Natl. Acad. Sci. U. S. A.* **111**, 4443–8 (2014).
176. Kleiman, N. J. & Spector, A. DNA single strand breaks in human lens epithelial cells from patients with cataract. *Curr. Eye Res.* **12**, 423–431 (1993).
177. Wilson, A. J. *et al.* The DNA damage mark pH2AX differentiates the cytotoxic effects of small molecule HDAC inhibitors in ovarian cancer cells. *Cancer Biol. Ther.* **12**, 484–493 (2011).
178. Fröhlich, E. The role of surface charge in cellular uptake and cytotoxicity of medical nanoparticles. *Int. J. Nanomedicine* **7**, 5577–5591 (2012).
179. Crowley, L. C., Marfell, B. J., Scott, A. P. & Waterhouse, N. J. Quantitation of apoptosis and necrosis by annexin V binding, propidium iodide uptake, and flow cytometry. *Cold Spring Harb. Protoc.* **2016**, 953–957 (2016).
180. Fadok, V. A. *et al.* Exposure of phosphatidylserine on the surface of apoptotic lymphocytes triggers specific recognition and removal by macrophages. *J. Immunol.* (1992).
181. Mukherjee, A., Morales-Scheihing, D., Butler, P. C. & Soto, C. Type 2 diabetes as a protein misfolding disease. *Trends Mol. Med.* **21**, 439–449 (2015).
182. NEI charts a clearer future for cataract prevention and treatment | National Eye Institute. *Nei.nih.gov* Available at: <https://nei.nih.gov/content/nei-charts-clearer-future-cataract-prevention-and-treatment>. (Accessed: 15th November 2018)
183. Bai J, Zheng Y, Wang G, L. P. Protective Effect of D-Limonene against Oxidative Stress-Induced Cell Damage in Human Lens Epithelial Cells via the p38 Pathway. *Oxid Med Cell Longev* Article ID 5962832, (2016).

184. Gupta, S. K. *et al.* Lycopene attenuates oxidative stress induced experimental cataract development: An in vitro and in vivo study. *Nutrition* **19**, 794–799 (2003).
185. Zheng, Y. *et al.* Resveratrol protects human lens epithelial cells against H₂O₂-induced oxidative stress by increasing catalase, SOD-1, and HO-1 expression. *Mol. Vis.* **16**, 1467–1474 (2010).
186. Ganea, E. & Harding, J. J. Glutathione-related enzymes and the eye. *Curr. Eye Res.* **31**, 1–11 (2006).
187. Ruiz-Ojeda, F. J., Gomez-Llorente, C., Aguilera, C. M., Gil, A. & Rupérez, A. I. Impact of 3-Amino-1,2,4-Triazole (3-AT)-Derived Increase in Hydrogen Peroxide Levels on Inflammation and Metabolism in Human Differentiated Adipocytes. *PLoS One* **11**, e0152550 (2016).
188. Leroueil, P. R. *et al.* Wide varieties of cationic nanoparticles induce defects in supported lipid bilayers. *Nano Lett.* **8**, 420–424 (2008).
189. Kostarelos, K. *et al.* Cellular uptake of functionalized carbon nanotubes is independent of functional group and cell type. *Nat. Nanotechnol.* **2**, 108–113 (2007).
190. Letoha, T. *et al.* Cell-penetrating peptide exploited syndecans. *Biochim. Biophys. Acta - Biomembr.* **1798**, 2258–2265 (2010).
191. Atul Asati, Santimukul Santra, Charalambos Kaittanis, and J. M. P. Localization, Surface-charge-dependent Cell Nanoparticles, Cerium Oxide. *ACS Nano* **4**, 5321–5331 (2011).
192. Lloyd, G. E. Atomic number and crystallographic contrast images with the SEM: a review of backscattered electron techniques. *Mineral. Mag.* **51**, 3–19 (1987).
193. Ostrowski, A. *et al.* Overview about the localization of nanoparticles in tissue and

- cellular context by different imaging techniques. *Beilstein J. Nanotechnol.* **6**, 263–280 (2015).
194. Balaban, R. S., Nemoto, S. & Finkel, T. Mitochondria, oxidants, and aging. *Cell* **120**, 483–495 (2005).
195. Vinson, J. A. Oxidative stress in cataracts. *Pathophysiology* **13**, 151–162 (2006).
196. Ohguro, N., Fukuda, M., Sasabe, T. & Tano, Y. Concentration dependent effects of hydrogen peroxide on lens epithelial cells. *Br. J. Ophthalmol.* **83**, 1064–8 (1999).
197. Wolf, N. *et al.* Age-related cataract progression in five mouse models for anti-oxidant protection or hormonal influence. *Exp. Eye Res.* **81**, 276–285 (2005).
198. Bagnyukova, T. V., Vasylykiv, O. Y., Storey, K. B. & Lushchak, V. I. Catalase inhibition by amino triazole induces oxidative stress in goldfish brain. *Brain Res.* **1052**, 180–186 (2005).
199. Padgaonkar, V., Giblin, F. J. & Reddy, V. N. Disulfide cross-linking of urea-insoluble proteins in rabbit lenses treated with hyperbaric oxygen. *Exp. Eye Res.* **49**, 887–899 (1989).
200. Yang, J. *et al.* Potential of CeCl₃@mSiO₂nanoparticles in alleviating diabetic cataract development and progression. *Nanomedicine Nanotechnology, Biol. Med.* **13**, 1147–1155 (2017).
201. Yang, J. *et al.* Silica-based cerium (III) chloride nanoparticles prevent the fructose-induced glycation of α -crystallin and H₂O₂-induced oxidative stress in human lens epithelial cells. *Arch. Pharm. Res.* **37**, 404–411 (2014).
202. Zhu, Y. *et al.* Tea flavanols block advanced glycation of lens crystallins induced by dehydroascorbic acid. *Chem. Res. Toxicol.* **28**, 135–143 (2015).

203. Singh, R., Barden, A., Mori, T. & Beilin, L. Advanced glycation end-products: A review. *Diabetologia* **44**, 129–146 (2001).
204. Schmitt, A., Schmitt, J., Münch, G. & Gasic-Milencovic, J. Characterization of advanced glycation end products for biochemical studies: Side chain modifications and fluorescence characteristics. *Anal. Biochem.* **338**, 201–215 (2005).
205. Leclère, J. & Birlouez-Aragon, I. The Fluorescence of Advanced Maillard Products Is a Good Indicator of Lysine Damage during the Maillard Reaction. *J. Agric. Food Chem.* **49**, 4682–4687 (2001).
206. Jedziniak, J. A. *et al.* The sorbitol pathway in the human lens: Aldose reductase and polyol dehydrogenase. *Investig. Ophthalmol. Vis. Sci.* **20**, 314–326 (1981).
207. Beswick, H. T. & Harding, J. J. Conformational changes induced in lens alpha- and gamma-crystallins by modification with glucose 6-phosphate. Implications for cataract. *Biochem. J.* **246**, 761–769 (1987).
208. Blakytyn, R. & Harding, J. J. Prevention of the inactivation of glutathione reductase by fructation using human α -crystallin. *Biochem. Soc. Trans.* **23**, 610S (1995).
209. Blakytyn, R. & Harding, J. J. Prevention of the fructation-Induced inactivation of glutathione reductase by bovine α -crystallin acting as a molecular chaperone. *Ophthalmic Res.* **28**, 19–22 (1996).
210. Dickerson, J. E., Dotzel, E. & Clark, A. F. Steroid-Induced cataract: New perspectives from in vitro and lens culture studies. *Exp. Eye Res.* **65**, 507–516 (1997).
211. Hook, D. W. A. & Harding, J. J. Alpha-crystallin acting as a molecular chaperone protects catalase against steroid-induced inactivation. *FEBS Lett.* **18**, 281–284 (1996).
212. Swamy-Mruthinti, S., Green, K. & Abraham, E. C. Inhibition of cataracts in

- moderately diabetic rats by aminoguanidine. *Exp. Eye Res.* **62**, 505–510 (1996).
213. Agardh, E., Hultberg, B. & Agardh, C. D. Effects of inhibition of glycation and oxidative stress on the development of cataract and retinal vessel abnormalities in diabetic rats. *Curr. Eye Res.* **21**, 543–549 (2000).
214. Greiling, T. M. S. & Clark, J. I. New Insights into the Mechanism of Lens Development Using Zebra Fish. in *International Review of Cell and Molecular Biology* **296**, 1–61 (Elsevier Inc., 2012).
215. Suri, S. S., Fenniri, H. & Singh, B. Nanotechnology-based drug delivery systems. *J. Occup. Med. Toxicol.* **2**, 16 (2007).
216. Karakoti, A. S. *et al.* Preparation and characterization challenges to understanding environmental and biological impacts of ceria nanoparticles. in *Surface and Interface Analysis* **44**, 882–889 (NIH Public Access, 2012).

Publication 1



Cite this: *RSC Adv.*, 2019, 9, 16596

Ethylene glycol coated nanoceria protects against oxidative stress in human lens epithelium†

Belal I. Hanafy,¹ Gareth W. V. Cave,² Yvonne Barnett¹ and Barbara Pierscionek¹*

Chronic diseases are rising in incidence and prevalence because of increases in life expectancy in many parts of the world coupled with advances in medicine which manage disease progression, rather than curing and alleviating the causes. Cataract is one such chronic condition. Identifying a therapeutic intervention that is successful in reversing or preventing cataracts may have applications for other chronic diseases of protein misfolding, such as diabetes and Alzheimer's disease as these have similar causation factors, notably oxidative stress and/or glycation. Cerium oxide nanoparticles (nanoceria) which have antioxidant, radioprotective and enzyme-mimetic properties have the potential to lead to an effective non-surgical treatment. However, nanoceria stability in physiological media is poor thus hindering their effective use in biomedical applications. Here we report a highly efficient one-pot synthesis of nanoceria (2–5 nm) coated with ethylene glycol, that is colloidal stable in physiological media and exhibits multiwavelength photoluminescence. The formulation, up to concentrations of 200 $\mu\text{g ml}^{-1}$, was not toxic to human lens epithelial cells and had no adverse effect on the cellular morphology or proliferation rate. More significantly, these nanoceria showed protective effects against oxidative stress induced by hydrogen peroxide in lens epithelial cells. Electron microscopy studies show the internalization and cytoplasmic localization of the nanoceria was found to be largely in the perinuclear region.

Received 18th February 2019
Accepted 17th May 2019

DOI: 10.1039/c9ra01252d

rsc.li/rsc-advances

Introduction

A major cause of chronic diseases that are exacerbated by ageing are changes in protein structure that lead to malfunction of tissues, organs and, ultimately, the organism. These are conditions such as diabetes, Alzheimer's disease and cataracts.^{1,2} The latter can occur as solely ocular, or as a secondary manifestation of a systemic condition.³ This presents the opportunity of using cataracts as a model for investigating the causal factors of visual impairment and to gain insight into causal factors that underpin systemic protein-based diseases. Cataract is an opacification of the eye lens that prevents light from reaching the retina by either scattering or absorbing traversing rays. It is the leading cause of blindness worldwide with over 24 million cases in the United States reported in 2010 which is expected to double by 2050.⁴ Cataracts is a multifactorial disease with oxidative stress considered to be one of the major factors contributing to its development.^{3,5–9} The human lens possesses natural defence mechanisms against reactive oxygen species (ROS) including the presence of reduced glutathione and antioxidant enzymes such as superoxide dismutase

and catalase.⁸ With ageing, such defences weaken, rendering the cells prone to oxidative insult that can lead to post-translational modifications and aggregation of lens proteins (crystallins) eventually causing cataracts.^{3,8,9} Human lens epithelial cells (HLECs) are the stem cells of the lens that differentiate into fibre cells forming the lens body. Oxidative stress induced damage to the lens epithelial cells would result in faulty protein synthesis and aggregation that eventually would cause lens opacity.¹⁰ As such the use of HLECs as an *in vitro* model has become important to draw conclusions on cataracts progression. Currently, surgical extraction of the cataractous lenses and replacement by intraocular implants is the only approved treatment. This comes with limitations such as accessibility in the developing world and the associated perioperative and postoperative complications.¹¹ Additionally, to date there is no single implant model that can replicate the image quality and the capacity to alter focus of the biological lens.¹² The annual cost associated with cataracts surgeries in the US is estimated to be around \$6.8 billion. This is expected to increase as the average population age increases.¹³ As such, there is a growing interest in developing a therapeutic means of reversing, or at least halting, the progression of cataracts.

Cerium oxide is a rare earth metal oxide with multiple applications in diverse products such as solar cells,¹⁴ oxygen sensors,¹⁵ catalysis,¹⁶ UV filters,¹⁷ and polishing.¹⁸ Cerium oxide (CeO_2) nanoparticles or “nanoceria”, have shown potential for

School of Science and Technology, Nottingham Trent University, Clifton Lane, Nottingham NG11 8NS, UK. E-mail: barbara.pierscionek@ntu.ac.uk

† Electronic supplementary information (ESI) available. See DOI: 10.1039/c9ra01252d



different concentrations of EGCNPs (0, 50, 100, 200, 400 $\mu\text{g ml}^{-1}$). This was conducted in the presence of Incucyte Cytotox red for counting dead cells (250 nM, Essen Bioscience), a cyanine nucleic acid dye that only permeates cells with compromised cell membranes. Three fields of view were imaged in each well, with a $10\times$ objective every three hours over four days using the Incucyte S3 Live Cell Analysis System (Essen BioScience) fitted inside an incubator. Confluence percentages and cytotoxicity levels were calculated using the integrated Incucyte S3 software.

Cell viability of human lens epithelial cell line after EGCNPs exposure (MTT assay)

HLECs were seeded in 96-well plates with a seeding density of 5000 cells per well in 200 μl growth media. The cells were left to recover from handling for 24 hours before treatment. Media were then gently aspirated and replaced with fresh media containing different concentrations of EGCNPs. The tested EGCNPs concentrations were 0, 100, 200, 400, 600, 800, 1000 $\mu\text{g ml}^{-1}$ with four wells per condition. After treatment durations (24 h or 48 h), 20 μl of MTT solution 3-(4,5-dimethylthiazol-2-yl)-2,5-diphenyltetrazolium bromide, 5 mg ml^{-1} in PBS (Sigma Aldrich) were added to each well to reach a final concentration of 0.5 mg ml^{-1} and cells were incubated at 37 $^{\circ}\text{C}$ for 2 hours. After incubation, the MTT solution was gently aspirated and 200 μl dimethyl sulfoxide (DMSO) were added to each well and left on a plate shaker for 10 minutes protected from light to solubilize the formazan crystals. Absorbance readings were taken at 570 nm using a plate reader (Clariostar, BMG LABTECH).

Protective effect against oxidative stress

The effect of EGCNPs on oxidative stress levels in HLECs after H_2O_2 exposure was investigated using 2',7'-dichlorodihydrofluorescein diacetate (H_2DCFDA) staining (D399, ThermoFisher) according to supplier's instructions. Briefly, cells were seeded in 96-well plates as before, established for 24 h, then pretreated with different EGCNPs concentration (0, 50 and 100 $\mu\text{g ml}^{-1}$) for 24 h. After treatment period, media was removed, and cells were washed with PBS and replaced with complete media containing H_2O_2 (100 μM) for 1 h. Media was then removed, washed once with PBS, and cells were incubated in H_2DCFDA solution (10 μM in PBS) for 30 min at 37 $^{\circ}\text{C}$. Cells were then washed with PBS and 200 μl PBS was added to each well. DCF fluorescence intensity was measured using a plate reader (TECAN infinite 200 PRO) at excitation 495 nm/emission 529 nm.

Uptake and localization studies

Cells were grown to 70% confluence in full growth media on cover slips in 6-well plates and then treated with 200 $\mu\text{g ml}^{-1}$ EGCNPs and incubated for one minute, 4 and 24 hours. After each treatment duration, media were aspirated, and the cell monolayers washed with serum free media followed by fixation in 4% paraformaldehyde in PBS buffer for 15 minutes. Cells were then washed three times with PBS and dehydrated in graded alcohol solutions (50%, 60%, 70%, 80%, 90% and 100%

ethanol) for five minutes each. The specimens were coated with gold (5 nm) using a sputter coater (Q150R ES, Quorum) and visualized under SEM (JEOL, JSM-7100f) with accelerating voltage (10 kV) and probe current (10 mA). EDX spectra were collected in at least ten different cell compartments using Aztec software (Oxford Instruments). Details of confocal imaging of EGCNPs and EuCNPs are available in ESL†

Statistical analysis

Each experiment was conducted at least three times ($n \geq 3$). Statistical analysis was carried out using GraphPad prism 7 software. Where relevant, analysis of variance (one-way ANOVA) followed by Dunnett's multiple comparisons test was used to compare groups with statistical significance set at $p < 0.05$.

Results & discussion

EGCNPs characterization

Ethylene glycol has the ability to complex with Ce^{3+} ions, making the reaction homogenous for the ensuing ammonia precipitation step.^{33,38} Coating nanoceria with ethylene glycol starting from a nitrate was previously reported to produce relatively large particle sizes (>10 nm) and significant polydispersity due to aggregation in both water and cell media that adversely impact biomedical applications.³³ The ability to produce water dispersible ultra-small (<5 nm) nanoceria is desirable as size reduction increases ROS deactivation capacity and regenerative properties^{29,39} and provides better penetration into the cells than larger sized particles.⁴⁰

Electron microscopic images (Fig. 1a and b) show the nanoparticles to be crystalline with core sizes ranging from 2–5 nm and an average size of $4.0 \text{ nm} \pm 0.8 \text{ nm}$. The images show mosaic-like patterns of monodisperse and well-separated nanoparticles. This is caused by the presence of ethylene glycol which appears as transparent coronae in the TEM image because of its low electron density compared to electron-rich cerium oxide cores. Non-coated nanoceria exhibited larger particle sizes (7–13 nm) with significant aggregation and lack of uniformity, highlighting the role of ethylene glycol coating in stabilizing the synthesis (Fig. 1c). Powder XRD data confirmed the cubic fluorite crystalline structure of cerium(IV) oxide (CeO_2) which was in agreement with the structure reported in the

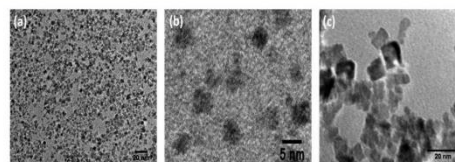


Fig. 1 Transmission electron microscopic (TEM) images of nanoceria showing (a) ethylene glycol-coated nanoceria (EGCNPs) at 20k and (b) EGCNPs at 100k magnification; both images show that particles are relatively uniform in size and well separated with polygonal morphology, (c) non-coated nanoceria (at 100k magnification) that exhibit significant clustering and polydispersity.



literature (JCPDS 75-0390). The characteristic 2θ diffraction peaks at 28.4, 33.3, 47.3, 56.12 correspond to the (111), (200), (220), and (311) planes respectively, and are annotated on the diffractogram (Fig S1a, ESI†). The peaks were significantly broader than non-coated nanoceria which is indicative of smaller crystallite size.²⁸ The crystallite size, calculated by applying the Scherrer equation on (111) diffraction peak, was 3.5 nm. This is close to the average particle size calculated from TEM images (4 nm).

The nature of the surface coating is shown in Fig. 2. Two main regions of weight loss were observed. The initial weight loss (10%) detected at 150 °C was attributed to loss of residual water and the outermost layer of the coating, while the second weight loss (20%) indicated full decomposition of the coating from 200–700 °C. Mass spectroscopic data revealed that the coating was a mixture of three compounds; ethylene glycol, ethylene glycol monoacetate and ethylene glycol diacetate. The additional carbonyl groups conferred by the acetate ligands on the surface of the nanoparticles play an important role in the aqueous stability of nanoceria through hydrogen bonding with water molecules. Additionally, longer surface ligands are generally associated with enhanced stability of the nanoparticles through the steric hindrance effect.^{41,42}

The presence of ethylene glycol surface coating was confirmed not to interfere with the antioxidant and autoregenerative properties of nanoceria by testing EGCNPs reactivity with H_2O_2 . Transitions between Ce^{3+} and Ce^{4+} were marked by colour change of EGCNPs solution and a corresponding shift in UV absorbance spectra (Fig S5, ESI†).^{25,27}

FTIR spectra (Fig S1b, ESI†) confirmed the structure of EGCNPs and this concurs with findings reported in the literature.⁴³ The presence of ethylene glycol coating was indicated by the presence of two characteristic peaks corresponding to methylene (CH_2) stretching at 2950 and 2850 cm^{-1} and a very broad peak at 3400 cm^{-1} corresponding to (O-H) stretching.³³ The (O-H) stretching band was significantly prominent compared to a non-coated formulation indicating that the band pertains to additional (OH) groups from ethylene glycol and

does not primarily arise from moisture adsorption on the surface.⁴⁴ The UV-vis spectrum for EGCNPs aqueous dispersion showed a strong absorption peak at <299 nm (Fig. S1c, ESI†) signifying the presence of Ce^{3+} the surface of the nanoparticles. Ce^{3+} is known to absorb light between 230–260 nm while Ce^{4+} absorbs light in the region of 300–400 nm.¹⁹ A typical nanoceria crystal contains cerium predominantly in its oxidized state (Ce^{4+}). As the crystal size decreases, surface defects associated with oxygen vacancies arise, increasing Ce^{3+} at the surface. The $\text{Ce}^{4+}/\text{Ce}^{3+}$ ratio is critical in determining the mechanism by which nanoceria scavenge for ROS.²⁹ The elemental composition of EGCNPs was confirmed by energy dispersive X-ray spectroscopy (EDX) (Fig. S1d, ESI†).

Colloidal stability and sterilization

The intensity weighted mean hydrodynamic diameter (Z-average), polydispersity index (PDI) and zeta potential of EGCNPs are summarized in Table 1.

In all tested media, EGCNPs showed unimodal distribution of mean hydrodynamic diameters. The hydrodynamic diameter was the smallest in water (21.86 nm) and increased significantly in other media while maintaining monodispersity. This was demonstrated by small PDI values (Table 1). The increase in hydrodynamic diameter in serum-containing DMEM can be attributed to the adsorption of a thin layer of serum proteins on the surface of particles forming a corona that contributes to its overall measured hydrodynamic diameter.^{45,46} The association of surface proteins was reflected in the surface charge of the

Table 1 Particle size, polydispersity index and zeta potential measurements of EGCNPs in different physiological media (pH = 7, 25 °C)

Media	Z-average (nm)	PDI	Zeta (mV)
(1) Distilled water	21.8 ± 0.6	0.28	+44.1
(2) DMEM + FBS (20%)	128.7 ± 9.2	0.17	-9.7
(3) 0.9% saline	158.1 ± 20.6	0.24	+14.0

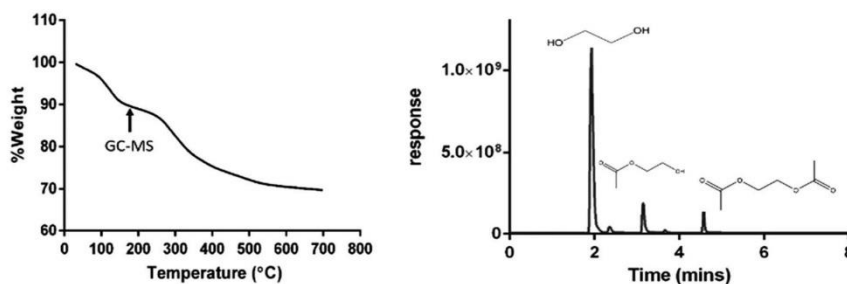


Fig. 2 Thermogravimetric analysis (TGA) of EGCNPs showing two main weight loss regions. The decomposed coating was separated by gas chromatography and analysed by mass spectrometry. The arrow indicates the time at which GC-MS analysis was triggered. Chromatogram peaks at 2.1, 3.1 and 4.5 min correspond to ethylene glycol, ethylene glycol monoacetate and ethylene glycol diacetate respectively (mass spectra are available in ESI†).



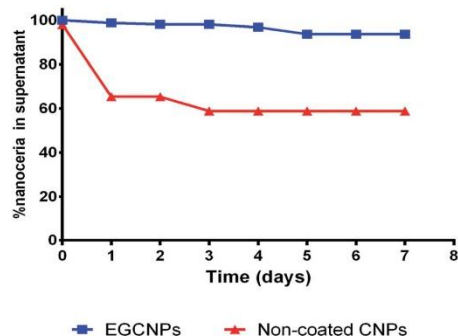


Fig. 3 Colloidal stability of ethylene glycol-coated nanoceria (EGCNPs) and non-coated nanoceria kept in water at room temperature for a week. Concentration of nanoceria in the supernatant was determined at one-day intervals spectrophotometrically at 300 nm.

nanoceria and its inversion to a negative value.⁴⁷ Serum proteins are negatively charged at physiological pH and hence their accumulation on the surface alters the nanoparticle zeta potential.⁴⁸ In saline solution, the increase in hydrodynamic

diameter was expected as high salt concentrations are known to shield the electrical field around nanoparticles reducing the electrostatic repulsion and causing agglomeration.⁴⁹ This is clearly manifested in the decrease in positive charge in saline solution compared to the value in water (Table 1). Despite that, the nanoparticles remained well dispersed in all media with no signs of precipitation. The small particle size in water permitted sterilization by filtration through 0.22 μm filters with minimal loss of the nanoparticles (less than 6% loss) as confirmed spectrophotometrically at 300 nm. The amount of EGCNPs lost after sterilization was found to decrease as the volume of filtered solution passing through the same filter increased, suggesting that the loss was due to adsorption on the filter surface.

When left to precipitate over one week at room temperature in water, EGCNPs showed a slight loss in the supernatant concentration (6%) over the testing duration. This level of stability was superior to their non-coated counterparts for which a significant loss in supernatant concentration (>35%) was observed after 24 h, highlighting the role of ethylene glycol coating in stabilizing the dispersion (Fig. 3). The previously reported synthesis of ethylene-glycol coated nanoparticles from a nitrate precursor resulted in hydrodynamic diameters of 222 nm and 206 nm in water and RPMI + FBS (10%) respectively, and both exhibited significant polydispersity with bimodal size

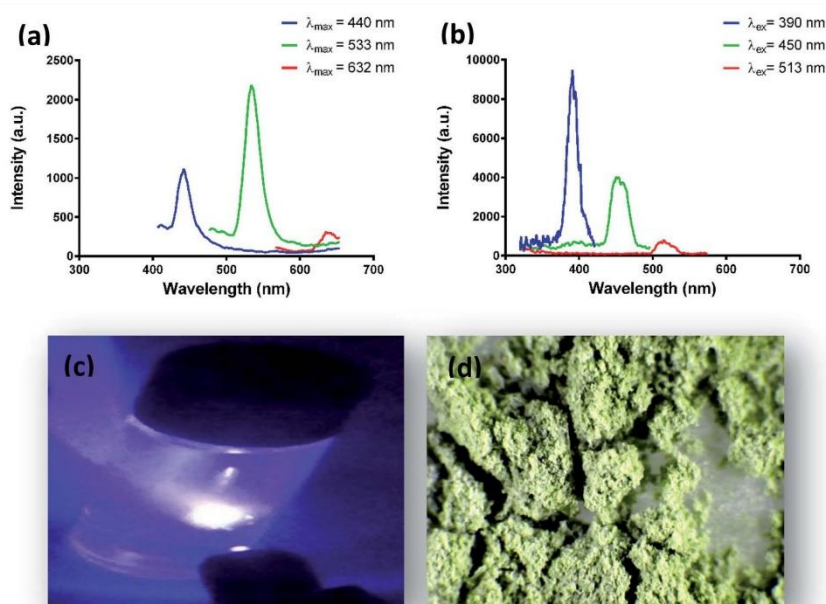


Fig. 4 (a) Emission spectra of EGCNPs suspended in water showing peaks at 440 nm, 533 nm and 632 nm when excited with 390 nm, 450 nm, and 513 nm respectively, (b) corresponding excitation spectra with detection bandwidths set at 10 nm, (c) EGCNPs suspension demonstrating strong blue to violet emission when excited with UV excitation source (380 nm), (d) EGCNPs powder showing broad green emission after blue light excitation.



Paper

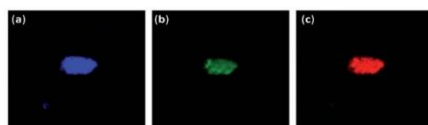


Fig. 5 Confocal images of a cluster of EGCNPs powder upon 405 nm excitation with emissions detected at (a) 450 nm, (b) 550 nm and (c) 630 nm.

distribution.³³ Moreover, the colloidal stability study of that formulation showed 38% loss of nanoceria content in the supernatant when a dispersion was left to precipitate for 7 days. This could be attributed to better stability and monodispersity of EGCNPs to the reaction initiation from an acetate precursor (as opposed to a nitrate precursor) that reacted with ethylene glycol and formed monoacetate and diacetate ethylene glycol derivatives. These ligands were more stable because steric hindrance prevented aggregation. Additionally, the acetate derivatives provided the coating with carbonyl groups that can form hydrogen bonding in aqueous solvents. To the best of our knowledge, the EGCNPs described here are the simplest aqueously stable nanoceria with a well-defined colloidal stability that can be formulated and stored in a dry powder form.

Photoluminescence and optical properties

EGCNPs exhibited multi-coloured emissions that extend from the UV to the long wavelength region of the visible spectrum. Fig. 4a and b show the EGCNPs emissions in the short, medium and long wavelength ranges of the visible spectrum when excited with 390, 450 and 513 nm respectively. The short wavelength emission was broad with the peak tail reaching beyond 600 nm (Fig. 4a). Both excitation and emission spectra have sufficient breadth, rendering the detection of nanoparticles highly tunable. In general, the fluorescence is relatively faint and requires strong laser power for excitation. Blue and green emissions were detected in both dispersion and powder forms when excited with the appropriate wavelengths (Fig. 4c and d).

When examined with laser scanning confocal microscopy, emissions from EGCNPs powder were detected across the visible spectrum using a single excitation wavelength of 405 nm as shown in Fig. 5. This agrees with the broad emission spectra of EGCNPs after UV excitation (Fig. 4a).

The photoluminescent behaviour of nanoceria has been reported in the literature, but findings are not consistent. Krishnan *et al.* reported multi-coloured fluorescence of organophilic 2–3 nm oleic acid-coated CeO₂ nanodots (OACNPs) fabricated by solvothermal decomposition.⁵⁰ OACNPs dispersed in toluene exhibited blue ($\lambda_{\text{ex}} = 350$), green ($\lambda_{\text{ex}} = 405$) and red emissions ($\lambda_{\text{ex}} = 532$).⁵⁰ These unique fluorescent properties were attributed to a large number of crystal defects associated with nanoparticle size (2 nm) with a higher Ce³⁺ to Ce⁴⁺ ratio.⁵⁰ A CeO₂ film deposited (80 nm) on a silica substrate was reported to have violet to blue luminescence at 380 nm.⁵¹ Nanoceria (2 nm), coated with a double layer of oleic acid prepared by thermal decomposition, were reported to have a broad spectrum with maximum emission at 515 nm with 400 nm excitation.⁵² To our knowledge, no other study has found that nanoceria prepared by an aqueous precipitation method can exhibit such multi-coloured photoluminescence, nor that nanoceria can be detected using a fluorescent microscope in all visible regions of light spectrum using a single excitation wavelength.

Cell viability, proliferation and morphology

The impact of different concentrations of EGCNPs (0 to 1000 $\mu\text{g ml}^{-1}$) on cultured HLECs, after 24 h and 48 h exposure in culture media is shown in Fig. 6. EGCNPs with concentrations up to 200 $\mu\text{g ml}^{-1}$ did not have any significant effect on cell viability, when compared to control cells at the two tested time points (p value < 0.05). However, the 24 h exposure to concentrations of 400 $\mu\text{g ml}^{-1}$ or higher resulted in a statistically significant decrease in viability ranging from 27% (at 400 $\mu\text{g ml}^{-1}$) to 40% (1000 $\mu\text{g ml}^{-1}$). The genotoxicity of negatively charged nanoceria have been previously investigated on HLECs – the durations were longer than in this study but the concentrations were not as high.^{10,32} Previous studies have shown no cytotoxicity of negatively charged ethylene glycol-coated

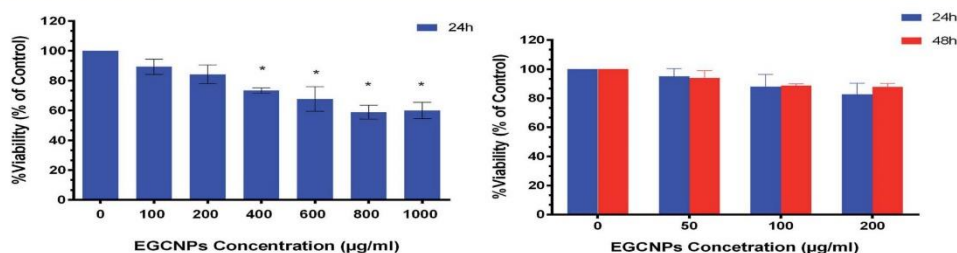


Fig. 6 MTT cell viability assay in HLECs with different EGCNPs concentrations. Concentrations up to 200 $\mu\text{g ml}^{-1}$ are well tolerated by the cells after 48 hours of exposure. Error bars are represented as mean \pm SEM. Asterisks denote statistically significant difference from the negative control (p value < 0.05).



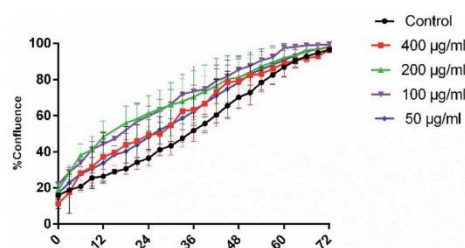


Fig. 7 Effect of different EGCNPs concentrations on HLECs proliferation. Cells were imaged in 6-well plates at an interval of 3 hours for 3 days while growing in full growth media using IncuCyte S3 live cell imaging system. Four different spots were imaged in each well. % Confluence was analysed by the integrated IncuCyte software and plotted against elapsed time in hours. Confluence at 0 h indicates the cell density at the point of seeding. All cells reached full confluence by 72 h. Small variations in early stage of growth arise from statistically insignificant variations in the four areas imaged in each well. A time lapse movie of cell growth over 4 days is available in the ESI.†

nanoceria on Jurkat human T-lymphocytes after three days of exposure.³³ However, no uptake studies were conducted and hence the lack of cytotoxicity might have been the result of a lack of uptake of the nanoparticles. Poor or lack of internalization of negatively charged nanoceria has been previously found in two normal cell lines; embryonic kidney cells and H9c2 cardiac myocytes.³³ The same study showed significant cytotoxicity of positively charged nanoceria (1 mM , $172 \mu\text{g ml}^{-1}$) on the same cell lines after 24 hour exposure.³³ It is noteworthy that the positive charges on the surface of nanomaterials promote cellular adhesion and penetration owing to the ionic interactions with negatively charged cell surfaces and hence their cytotoxicity is generally expected to be more pronounced compared to negatively charged nanomaterials.^{54,55} It is possible that the adsorption of negatively charge coronae on the surface of EGCNPs reduced their toxicity by mitigating cell membrane damage normally associated with positive charged nanoparticles.⁵⁶

Fig. 7 shows the proliferation of HLECs incubated with different EGCNPs concentrations (0 to $400 \mu\text{g ml}^{-1}$) for three

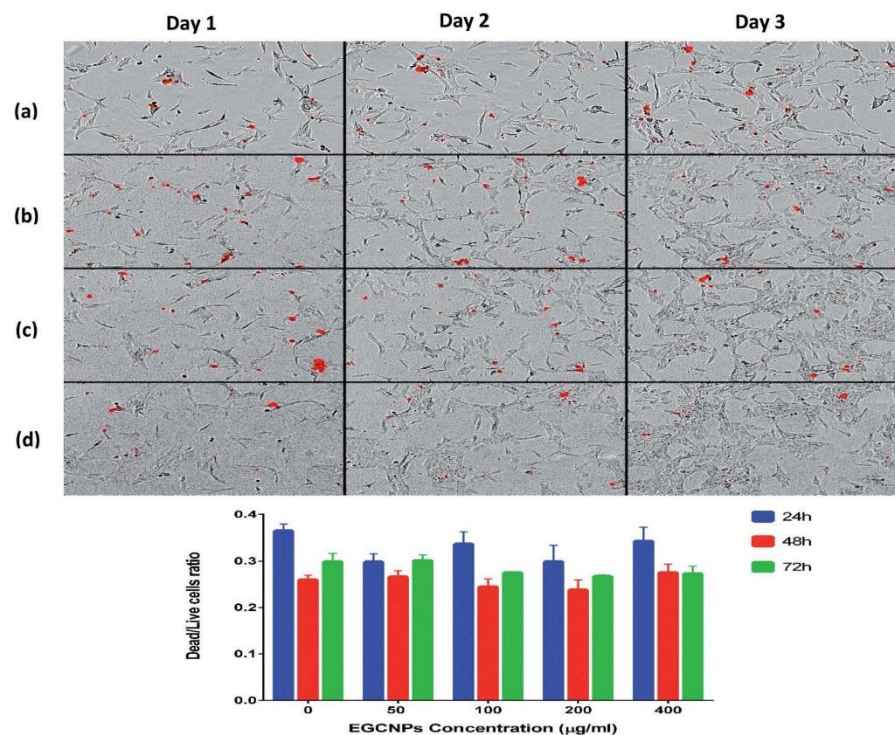


Fig. 8 Live cell analysis showing cytotoxicity, morphology and proliferation in HLECs upon EGCNPs exposure up to 72 h. Cells were treated with different EGCNPs concentration and allowed to proliferate in presence of Cytotox Red dye (250 nM) that binds to the DNA of dead cells and gives red fluorescence. Images were taken using IncuCyte S3 live cell imaging system ($10\times$ objective). (a) Control cells, (b) treated with $100 \mu\text{g ml}^{-1}$ EGCNPs, (c) treated with $200 \mu\text{g ml}^{-1}$ EGCNPs, (d) treated with $400 \mu\text{g ml}^{-1}$ EGCNPs. Error bars are displayed as mean \pm SEM. No statistically significant difference was found between treated and control cells at each time point (one-way ANOVA) indicating that EGCNPs are not cytotoxic at these exposure conditions.



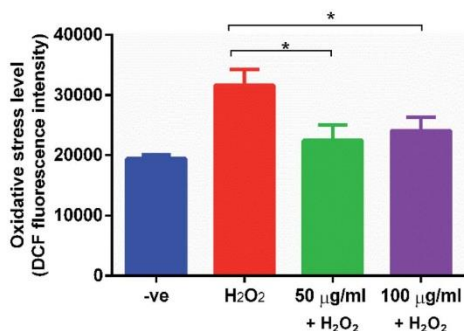


Fig. 9 EGCNPs protect against H₂O₂-induced oxidative stress in human lens epithelial cells (H₂DCFDA assay). Cells were pre-treated with EGCNPs for 24 h, and then exposed to H₂O₂ (100 µM) for 1 h in EGCNPs-free media. Oxidative stress levels were determined by measuring DCF fluorescence intensity using a plate reader. Asterisks denote statistical significance ($n = 3$, $p < 0.05$, ANOVA followed by Dunnett's test). Error bars are displayed as mean \pm SEM.

days without media change. All cells with different treatments were able to reach 100% confluence following a similar growth pattern to negative controls. This contrasted with results from the MTT assay that showed a decrease in viability for cells incubated with EGCNPs (400 µg ml⁻¹). The results of further investigation with nucleic acid staining are shown in Fig. 8. No cytotoxicity was observed for concentrations (50–400 µg ml⁻¹) for exposure durations up to 72 h. This could be a result of the 400 µg ml⁻¹ concentration interfering with mitochondrial activity which could in turn have affected the MTT viability.³⁷ Nonetheless, we conclude that EGCNPs concentrations, from 50 to 200 µg ml⁻¹ were safe and had no harmful effect on the

morphology, proliferation, and cell membrane integrity of the HLECs after 72 h exposure.

Protective effects of EGCNPs against ROS in lens cells

EGCNPs, with predetermined safe concentrations (50 and 100 µg ml⁻¹), were tested for their ability to protect HLECs from oxidative damage induced by H₂O₂ using H₂DCFDA probe. As shown in Fig. 9, the tested EGCNPs concentrations exhibited a significant protective effect compared to non-EGCNPs treated cells demonstrated by the low fluorescence levels in cells pre-treated with EGCNPs. Both concentrations showed a similar level of protection against H₂O₂-induced oxidative stress. Such protective effect shows that EGCNPs inside the HLECs can exert catalase-like activity where excess H₂O₂ was deactivated.³⁹ Moreover, cultured cells that were exposed to EGCNPs were able to reach full confluence after three days compared to the positive control in which cell proliferation was significantly halted supporting H₂DCFDA assay findings (Fig S6, ESI†).

Uptake and localization of EGCNPs in human lens epithelial cells

The cellular localization of nanoparticles plays an important role in their overall toxicity and activity.³⁸ Many factors impact on the uptake of nanoparticles such as particle size, polydispersity, zeta potential and surface coating.

Fig. 10 shows the uptake and localization of EGCNPs in HLECs after incubation for 4 h (Fig. 10b) and 24 h (Fig. 10c). EGCNPs entered the cells at significant levels for both tested time points. The nanoparticles were heavily localized in the cytoplasm, mainly in perinuclear regions (Fig. 10b and c). Minimal amounts of nanocerium were detected in the nuclei as confirmed by EDX spectra (Fig S4, ESI†).

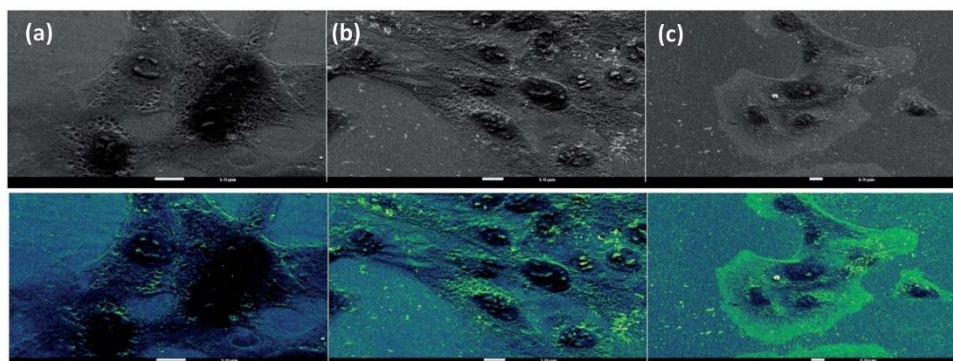


Fig. 10 SEM images showing uptake and localization of EGCNPs in HLECs at different time points: (a) 1 min incubation showing no uptake of EGCNPs, (b) EGCNPs uptake and localization after 4 h incubation, (c) EGCNPs uptake and localization after 24 h incubation. Strong uptake was detected at 4 h and 24 h time points with heavy localization around the nuclei as detected by EDX. Areas with most nanocerium localization are distinguished by brightness arising from atomic number contrast of cerium element (Ce atomic number = 58) and hence it gives off more secondary and backscattered electrons. Contrast sensitive pseudocolour was applied simultaneously to the images highlighting nanocerium localization as bright green. EDX spectra are available in the ESI.†



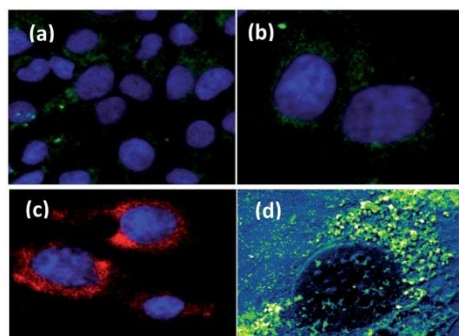


Fig. 11 Uptake and perinuclear localisation of EGCNPs and EuCNPs in HLECs. (a) and (b) Confocal images showing cytoplasmic localisation of EGCNPs in HLECs (excitation 488 nm/emission 530 nm). (c) a confocal microscopy image showing localisation of nanocereria doped with europium (EuCNPs). (d) SEM images showing cytoplasmic localisation of EuCNPs (green areas).

For further validation of SEM-EDX uptake and localization, confocal microscopy experiments were conducted. HLECs exhibited strong autofluorescence in the blue and green regions. Even though the fluorescence of EGCNPs is relatively weak compared to cellular autofluorescence, it can still be tracked inside the cells by taking advantage of the lanthanides ability to resist photobleaching.⁵⁹ Fig. 11a and b confirm that EGCNPs are predominantly localised in the cytoplasm, specifically in the perinuclear regions. This concurs with SEM data. The images show that some nanoparticles penetrate the nucleus. Such minimal nuclear uptake is likely to have taken place during mitosis where nuclear membrane breaks down.⁶⁰ To our knowledge this the first time unlabelled nanocereria have been tracked inside the cells.

The EuCNPs exhibited typical strong red emission at 612 nm under multiple excitation wavelengths from UV to end of green region (ranging from 350–550 nm);⁶¹ particle size (5 nm) and surface charge (+34.49 mV in water, –2.4 mV in media) were similar to those of EGCNPs. Doping with Europium is preferred over attachment of traditional fluorescent dyes since the latter involves surface modifications that could affect the behaviour of the nanoparticle uptake.⁶² Characterization of EuCNPs is available in the ESI (Fig S2†). After 24 hour incubation with HLECs, EuCNPs were found in the cytoplasm mainly in the perinuclear region corroborating the previous findings (Fig. 11c). EuCNPs also showed a similar localization pattern to EGCNPs when examined by SEM-EDX (Fig. 11b). It remains to be investigated whether surface charge manipulation may have an impact on the uptake and localization of nanocereria in HLECs cells and its relationship to cytotoxicity and protective behaviour.

Uptake studies show that EGCNPs preferentially reside in the cytoplasm surrounding the nuclei. Such localisation resulted in no cytotoxicity to HLECs and the nanoparticles showed protection against oxidative stress.

Conclusions

A nanocereria formulation coated with ethylene glycol and ethylene glycol acetates (EGCNPs) was successfully formulated using a simple precipitation reaction starting from cerium acetate as the precursor. The formulation has superior aqueous stability and monodispersity in different physiological media allowing for more reliable biological studies with no sedimentation-induced variabilities. EGCNPs were found to be heavily localised in the cytoplasm and provided protection in human lens epithelial cells from H₂O₂-induced oxidative stress, rendering these particles a potential candidate for an anti-cataracts therapy. Future work is needed to elucidate the mechanism and mode of action of nanocereria within the cellular organelles and their regenerative antioxidant properties if these are to be effective for the treatment of cataracts.

Conflicts of interest

There are no conflicts to declare.

Acknowledgements

The authors would like to thank Kathryn Kroon for the technical assistance with electron microscopy, and BH acknowledges PhD studentship from Nottingham Trent University.

Notes and references

- 1 A. Pollreis and U. Schmidt-Erfurth, *J. Ophthalmol.*, 2010, 1–8.
- 2 A. Mukherjee, D. Morales-Scheihing, P. C. Butler and C. Soto, *Trends Mol. Med.*, 2015, **21**, 439–449.
- 3 J. J. Harding, *Ageing Res. Rev.*, 2002, **1**, 465–479.
- 4 NEI charts a clearer future for cataract prevention and treatment, National Eye Institute, <https://nei.nih.gov/content/nei-charts-clearer-future-cataract-prevention-and-treatment>, accessed 15 November 2018.
- 5 J. Bai, Y. Zheng, G. Wang and P. Liu, *Oxid. Med. Cell. Longevity*, 2016, 1–12.
- 6 S. K. Gupta, D. Trivedi, S. Srivastava, S. Joshi, N. Halder and S. D. Verma, *Nutrition*, 2003, **19**, 794–799.
- 7 Y. Zheng, Y. Liu, J. Ge, X. Wang, L. Liu, Z. Bu and P. Liu, *Mol. Vision*, 2010, **16**, 1467–1474.
- 8 E. Ganea and J. J. Harding, *Curr. Eye Res.*, 2006, **31**, 1–11.
- 9 R. J. W. Truscott, *Exp. Eye Res.*, 2005, **80**, 709–725.
- 10 B. K. Pierscionek, Y. Li, R. A. Schachar and W. Chen, *Nanomedicine*, 2012, **8**, 383–390.
- 11 H. Abdelkader, R. G. Alany and B. Pierscionek, *J. Pharm. Pharmacol.*, 2015, **67**, 537–550.
- 12 K. Wang and B. K. Pierscionek, *Prog. Retinal Eye Res.*, 2018, DOI: 10.1016/j.preteyeres.2018.11.004.
- 13 H. E. Golligly, D. O. Hodge, J. L. St. Sauver and J. C. Erie, *J. Cataract Refractive Surg.*, 2013, **39**, 1383–1389.
- 14 A. Corma, P. Atienzar, H. Garcia and J. Y. Chane-Ching, *Nat. Mater.*, 2004, **3**, 394–397.



- 15 N. Izu, W. Shin, I. Matsubara and N. Murayama, *J. Electroceram.*, 2004, **13**, 703–706.
- 16 T. Montini, M. Melchionna, M. Monai and P. Fornasiero, *Chem. Rev.*, 2016, **116**, 5987–6041.
- 17 F. Caputo, M. De Nicola, A. Sienkiewicz, A. Giovanetti, I. Bejarano, S. Licocchia, E. Traversa and L. Ghibelli, *Nanoscale*, 2015, **7**, 15643–15656.
- 18 V. D. Kosynkin, A. A. Arzgatkina, E. N. Ivanov, M. G. Chtoutsu, A. I. Grabko, A. V. Kardapolov and N. A. Sysina, *J. Alloys Compd.*, 2000, **303–304**, 421–425.
- 19 E. Alpaslan, H. Yazici, N. H. Golshan, K. S. Ziemer and T. J. Webster, *ACS Biomater. Sci. Eng.*, 2015, **1**, 1096–1103.
- 20 S. M. Hirst, A. S. Karakoti, R. D. Tyler, N. Srinanganathan, S. Seal and C. M. Reilly, *Small*, 2009, **5**, 2848–2856.
- 21 S. Naz, J. Beach, B. Heckert, T. Tummala, O. Pashchenko, T. Banerjee and S. Santra, *Nanomedicine*, 2017.
- 22 J. Chen, S. Patil, S. Seal and J. F. McGinnis, *Adv. Exp. Med. Biol.*, 2008, **53–59**.
- 23 F. Pagliari, C. Mandoli, G. Forte, E. Magnani, S. Pagliari, G. Nardone, S. Licocchia, M. Minieri, P. Di Nardo and E. Traversa, *ACS Nano*, 2012, **6**, 3767–3775.
- 24 C. von Montfort, L. Alili, S. Teuber-Hanselmann and P. Brenneisen, *Redox Biol.*, 2015, **4**, 1–5.
- 25 C. Xu and X. Qu, *NPG Asia Mater.*, 2014, **6**, e90.
- 26 N. V. Skorodumova, S. I. Simak, B. I. Lundqvist, I. A. Abrikosov and B. Johansson, *Phys. Rev. Lett.*, 2002, **89**, DOI: 10.1103/PhysRevLett.89.166601.
- 27 J. M. Perez, A. Asati, S. Nath and C. Kaittanis, *Small*, 2008, **4**, 552–556.
- 28 C. Korsvik, S. Patil, S. Seal and W. T. Self, *Chem. Commun.*, 2007, 1056–1058.
- 29 T. Pirmohamed, J. M. Dowling, S. Singh, B. Wasserman, E. Heckert, A. S. Karakoti, J. E. S. King, S. Seal and W. T. Self, *Chem. Commun.*, 2010, **46**, 2736–2738.
- 30 C. Li, X. Shi, Q. Shen, C. Guo, Z. Hou and J. Zhang, *J. Nanomater.*, 2018, **2018**, 1–12.
- 31 J. Chen, S. Patil, S. Seal and J. F. McGinnis, *Nat. Nanotechnol.*, 2006, **1**, 142–150.
- 32 B. K. Pierscionek, Y. Li, A. A. Yasseen, L. M. Colhoun, R. A. Schachar and W. Chen, *Nanotechnology*, 2009, **21**, 035102.
- 33 F. Caputo, M. Mameli, A. Sienkiewicz, S. Licocchia, F. Stellacci, L. Ghibelli and E. Traversa, *Sci. Rep.*, 2017, **7**, 1–14.
- 34 E. C. Cho, Q. Zhang and Y. Xia, *Nat. Nanotechnol.*, 2011, **6**, 385–391.
- 35 A. S. Karakoti, N. A. Monteiro-Riviere, R. Aggarwal, J. P. Davis, R. J. Narayan, W. T. Seif, J. McGinnis and S. Seal, *Nanoceria as antioxidant: Synthesis and biomedical applications*, 2008, vol. 60.
- 36 G. W. V. Cave, *US Pat.*, 20180280910-A1, 2018.
- 37 A. Kumar, S. Babu, A. S. Karakoti, A. Schulte and S. Seal, *Langmuir*, 2009, **25**, 10998–11007.
- 38 A. Hall, V. J. Mundell, C. Blanco-Andujar, M. Bencsik, G. McHale, M. I. Newton and G. W. V. Cave, *Chem. Commun.*, 2010, **46**, 2420.
- 39 R. Singh and S. Singh, *Colloids Surf., B*, 2019, **175**, 625–635.
- 40 S. Singh, A. Ly, S. Das, T. S. Sakthivel, S. Barkam and S. Seal, *Artif. Cells, Nanomed., Biotechnol.*, 2018, **46**, S956–S963.
- 41 A. S. Karakoti, S. V. N. T. Kuchibhatla, K. S. Babu and S. Seal, *J. Phys. Chem. C*, 2007, **111**, 17232–17240.
- 42 J. Lovrić, S. J. Cho, F. M. Winnik and D. Maysinger, *Chem. Biol.*, 2005, **12**, 1227–1234.
- 43 L. De Marzi, A. Monaco, J. De Lapuente, D. Ramos, M. Borrás, M. Di Gioacchino, S. Santucci and A. Poma, *Int. J. Mol. Sci.*, 2013, **14**, 3065–3077.
- 44 J. Coates, in *Encyclopedia of Analytical Chemistry*, 2006.
- 45 P. Del Pino, B. Pelaz, Q. Zhang, P. Maffre, G. U. Nienhaus and W. J. Parak, *Mater. Horiz.*, 2014, **1**, 301–313.
- 46 T. Cedervall, I. Lynch, S. Lindman, T. Berggard, E. Thulin, H. Nilsson, K. A. Dawson and S. Linse, *Proc. Natl. Acad. Sci. U. S. A.*, 2007, **104**, 2050–2055.
- 47 N. V. Konduru, R. M. Molina, A. Swami, F. Damiani, P. Pyrgiotakis, P. Lin, P. Andreozzi, T. C. Donaghey, P. Demokritou, S. Krol, W. Kreyling and J. D. Brain, *Part. Fibre Toxicol.*, 2017, **14**, DOI: 10.1186/s12989-017-0223-3.
- 48 C. Gräfe, A. Weidner, M. V. D. Lühe, C. Bergemann, F. H. Schacher, J. H. Clement and S. Dutz, *Int. J. Biochem. Cell Biol.*, 2016, **75**, 196–202.
- 49 R. A. Sperling and W. J. Parak, *Philos. Trans. R. Soc., A*, 2010, **368**, 1333–1383.
- 50 A. Krishnan, T. S. Sreeremya, E. Murray and S. Ghosh, *J. Colloid Interface Sci.*, 2013, **389**, 16–22.
- 51 F. Gao, G. H. Li, J. H. Zhang, F. G. Qin, Z. Y. Yao, Z. K. Liu, Z. G. Wang and L. Y. Lin, *Chin. Phys. Lett.*, 2001, **18**, 443–448.
- 52 A. Krishnan, T. S. Sreeremya and S. Ghosh, *RSC Adv.*, 2016, **6**, 53550–53559.
- 53 A. Asati, S. Santra, C. Kaittanis and J. M. Perez, *ACS Nano*, 2010, **4**, 5321–5331.
- 54 X. Jiang, B. Du, Y. Huang and J. Zheng, *Nano Today*, 2018, **21**, 106–125.
- 55 B. Li, V. Agarwal, D. Ho, J. P. Vede and K. S. Iyer, *New J. Chem.*, 2018, **42**, 7237–7240.
- 56 W. Hu, C. Peng, M. Lv, X. Li, Y. Zhang, N. Chen, C. Fan and Q. Huang, *ACS Nano*, 2011, **5**, 3693–3700.
- 57 S. K. Jana, P. Banerjee, S. Das, S. Seal and K. Chaudhury, *J. Nanopart. Res.*, 2014, **16**, DOI: 10.1007/s11051-014-2441-z.
- 58 A. Asati, S. Santra, C. Kaittanis and J. M. Perez, *ACS Nano*, 2010, **4**, 5321–5331.
- 59 O. S. Wolfbeis, *Chem. Soc. Rev.*, 2015, **44**, 4743–4768.
- 60 E. Fröhlich, *Int. J. Nanomed.*, 2012, **7**, 5577–5591.
- 61 A. Kumar, S. Babu, A. S. Karakoti, A. Schulte and S. Seal, *Langmuir*, 2009, **25**, 10998–11007.
- 62 A. Ostrowski, D. Nordmeyer, A. Boreham, C. Holzhausen, L. Mundhenk, C. Graf, M. C. Meinke, A. Vogt, S. Hadam, J. Lademann, E. Ruhl, U. Alexiev and A. D. Gruber, *Beilstein J. Nanotechnol.*, 2015, **6**, 263–280.



Publication 2

Article

Treatment of Human Lens Epithelium with High Levels of Nanoceria Leads to Reactive Oxygen Species Mediated Apoptosis

Belal I. Hanafy ¹, Gareth W. V. Cave ¹, Yvonne Barnett ^{1,2} and Barbara Pierscionek ^{1,3,*}

¹ School of Science and Technology, Nottingham Trent University, Clifton Lane, Nottingham NG11 8NS, UK; belal.hanafy2017@my.ntu.ac.uk (B.I.H.); gareth.cave@ntu.ac.uk (G.W.V.C.); Yvonne.barnett@anglia.ac.uk (Y.B.)

² Faculty of Science and Technology, Anglia Ruskin University, East Road, Cambridgeshire CB1 1PT, UK

³ School of Life Science and Education, Staffordshire University College Road, Stafford ST4 2DE, UK

* Correspondence: barbara.pierscionek@staffs.ac.uk; Tel.: +447952248455

Received: 20 December 2019; Accepted: 16 January 2020; Published: 21 January 2020



Abstract: Nanoceria (cerium oxide nanoparticles) have been shown to protect human lens epithelial cells (HLECs) from oxidative stress when used at low concentrations. However, there is a lack of understanding about the mechanism of the cytotoxic and genotoxic effects of nanoceria when used at higher concentrations. Here, we investigated the impact of 24-hour exposure to nanoceria in HLECs. Nanoceria's effects on basal reactive oxygen species (ROS), mitochondrial morphology, membrane potential, ATP, genotoxicity, caspase activation and apoptotic hallmarks were investigated. Scanning electron microscopy-energy dispersive X-ray spectroscopy (SEM-EDX) studies on isolated mitochondria revealed significant uptake and localization of nanoceria in the mitochondria. At high nanoceria concentrations (400 $\mu\text{g mL}^{-1}$), intracellular levels of ROS were increased and the HLECs exhibited classical hallmarks of apoptosis. These findings concur with the cells maintaining normal ATP levels necessary to execute the apoptotic process. These results highlight the need for nanoceria dose-effect studies on a range of cells and tissues to identify therapeutic concentrations in vitro or in vivo.

Keywords: apoptosis; genotoxicity; reactive oxygen species; cerium oxide; mitochondria

1. Introduction

Nanoparticles offer great potential as medical devices due to their unique physicochemical properties [1–3]. For example, cerium oxide nanoparticles “nanoceria” are extensively researched for biomedical and drug delivery applications because of their unique recyclable antioxidant, neuroprotective, radioprotective and anti-inflammatory properties [4–8]. These properties arise from the ability of cerium ions to co-exist and transition between trivalent and tetravalent oxidation states (Ce^{3+} , Ce^{4+}) at the surface defects present in the CeO_2 crystalline structure allowing nanoceria to release or acquire oxygen depending on the ambient environment [9,10]. Additionally, nanoceria are increasingly used for industrial applications such as an additive to diesel fuel (commercially available under several trade names such as Envirox™) to reduce soot emissions and decrease fuel consumption [11,12]. This has led to increased exposure to nanoceria which warrants investigation of their toxicological effects and interactions with various eukaryotic cells. As such, nanoceria was considered a high priority for toxicological evaluation [12,13].

Despite the exponential rise in the use of new nanomaterials, nanotoxicological evaluation is not carried out with a similarly high rate [14]. Hence, assessing and evaluating the biocompatibility of nanomaterials are crucial issues for both the public and the scientific community to enable informed

decisions to be made regarding their use. Various studies have focused on the toxicity mechanism of different types of nanoparticles, such as Ag, Zn, and Si, in different cell lines in investigations of oxidative stress as a cause of toxicity [3]. Cerium oxide nanoparticles are unique as they possess inherent antioxidant properties and hence, studying their ability to induce oxidative stress presents a novel and crucial perspective on their potential function and application. The toxicity of nanoceria has been studied in various *in vivo* and *in vitro* models and more investigations into the mechanism of their action are needed [13]. Additionally, many of the toxicological studies are performed on nanoceria with unknown or poor colloidal stability, a common problem for nanoceria, which gives rise to conflicting toxicological profiles. Although nanoceria are known for their powerful antioxidant properties, some studies have reported their ability to cause oxidative stress [13,15,16]. Ocular exposure is of particular interest due to the ease for sustained environmental exposure. Although nanoceria have shown promise in treating some ocular diseases such as retinal degeneration [17], corneal inflammation [18], glaucoma [19], and cataracts [20], there is a paucity of knowledge about toxicity mechanism of nanoceria in any ocular tissue. The human lens epithelial cell line (HLEC) provides a suitable model for studying toxicity of nanoceria on the eye lens, as these cells are the lenticular stem cells from which the lens fiber cells differentiate. Damage to the lens epithelium disrupts protein expression and could lead to aggregation of proteins that causes light scatter and manifests as cataract [21].

Recently, it has been shown that highly stable and well characterized monodisperse cerium oxide nanoparticles (4 nm) coated with ethylene glycol and its acetate derivatives, ie ethylene glycol coated nanoparticles (EGCNPs) can protect HLECs from oxidative stress when used in concentrations as low as $50 \mu\text{g mL}^{-1}$, and the nanoparticles were non-cytotoxic up to $200 \mu\text{g mL}^{-1}$ [20]. When the concentration of nanoceria was increased to $400 \mu\text{g mL}^{-1}$, a decrease in viability, measured by MTT assay, was observed. However, the cells were still able to proliferate normally for over three days without signs of necrotic damage [20]. This suggest that the nanoparticles at this concentration could interfere with mitochondrial functions and this has warranted further investigation.

In this study, we investigated the mechanism of toxicity caused by short-term exposure to different doses of EGCNPs. Here, we report the effect of different EGCNPs concentrations on various cellular parameters. The results show that although nanoceria have antioxidant properties at low doses ($< 200 \mu\text{g mL}^{-1}$) and do not interfere with basal ROS that are needed for normal cell signaling and metabolic functions [22]. At a higher dose ($400 \mu\text{g mL}^{-1}$) they induce reactive oxygen species (ROS) generation that mediates cellular apoptosis. It is clearly demonstrated that cell death is driven by the mitochondrial apoptotic pathway, wherein ROS-mediated mitochondrial membrane depolarization is followed by DNA damage and caspase cascade activation. To date, this is the first report on the mechanism of nanoceria toxicity in lens cells.

2. Results

EGCNPs Characterization

EGCNPs were thoroughly characterized in our previous work using transmission electron microscopy, powder X-ray diffraction, dynamic light scattering, thermogravimetric analysis, gas chromatography-mass spectroscopy, Fourier transform infrared spectroscopy (FTIR), UV-Vis spectroscopy [20]. Briefly, EGCNPs were spherical in shape with a core size (TEM) of $4.0 \pm 0.8 \text{ nm}$ (Figure 1) and crystallite size (XRD, Scherrer formula) of 3.5 nm. EGCNPs were stable in aqueous media for at least seven days with minimum sedimentation. The zeta potential was +44 mV in water and -9.7 mV in cell culture media due to protein coronae formation. EGCNPs were monodisperse with unimodal distribution of intensity-weighted mean hydrodynamic diameters as was demonstrated by DLS [20].

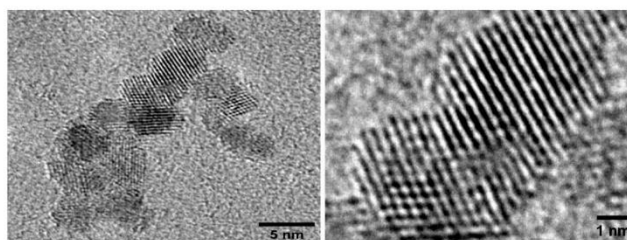


Figure 1. TEM micrographs of ethylene glycol coated nanoparticles EGCNPs showing the spherical, monodisperse and crystalline nature of the nanoparticles.

Acute Exposure to High EGCNPs Concentrations Increases Basal ROS

Overproduction of reactive oxygen species (ROS) is one of the most common pathways involved in nanomaterial toxicity [14]. Therefore, the basal ROS level in HLECs was measured after 24 h exposure to different EGCNPs concentrations (0, 50, 100, 200, and 400 $\mu\text{g mL}^{-1}$) using the H₂DCFDA probe. H₂DCFDA is a non-fluorescent cell-permeable probe which is cellularly retained upon internalization due to deacetylation, and then oxidized by the action of ROS into highly fluorescent DCF enabling the estimation of ROS levels. As shown in Figure 2, EGCNPs concentrations up to 200 $\mu\text{g mL}^{-1}$ did not lead to any significant alteration to the basal ROS level when compared to control cells ($p > 0.05$). Conversely, when the concentration was increased to 400 $\mu\text{g mL}^{-1}$, a significant elevation in ROS level was observed.

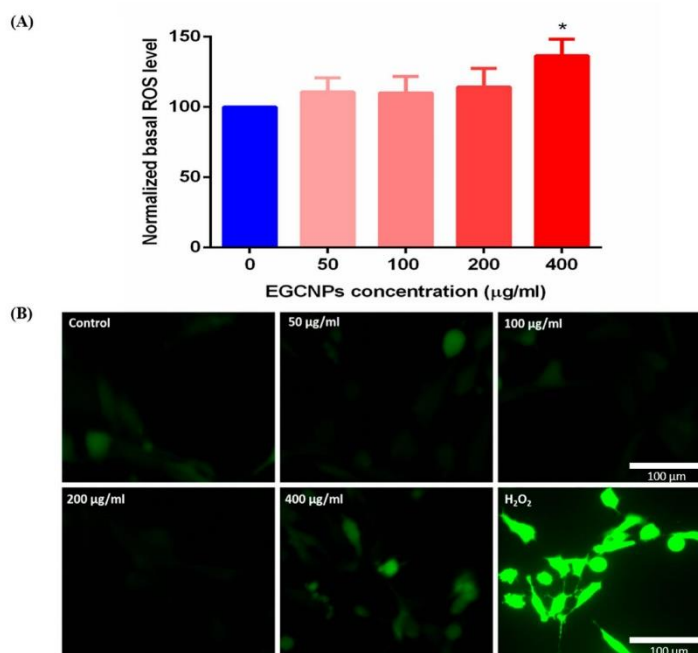


Figure 2. (A) Effect of EGCNPs (24 h exposure) on basal ROS level in HLECs measured by H₂DCFDA fluorescent probe using a plate reader. The asterisk denotes statistical significance ($p < 0.05$)

from negative control ($0 \mu\text{g mL}^{-1}$), $n \geq 3$ where n is the number of replicates using ANOVA followed by Dunnett's multiple comparisons test. Error bars are presented as mean \pm standard error of the mean (SEM) (B) Fluorescent microscope images after H_2DCFDA staining of HLECs treated with different EGCNPs concentrations for 24 h. H_2O_2 (200 μM) was used as a positive control. Images were taken using a fluorescent microscope (Evos FL) using the same intensity power (20%) with minimal exposure duration to avoid auto-oxidation of the probe.

EGCNPs Localize in the Mitochondria

Since the mitochondria are the main source of ROS generation [14], it was necessary to investigate if EGCNPs exert their impact on ROS levels through their localization in the mitochondria. EGCNPs-treated HLECs were harvested and their mitochondria were isolated from the cytosolic fraction by differential centrifugation using a standard mitochondria isolation procedure [23]. The isolated mitochondria were then examined with a scanning electron microscope (SEM) and the presence of cerium was checked for using energy dispersive X-ray spectroscopy (EDX). EDX is a valuable tool enabling the identification of different elements based on their emitted characteristic X-rays after excitation with a high accelerating voltage electron beam [24]. Figure 3A shows an SEM micrograph of the isolated mitochondria (left) and its associated cerium EDX map (right) (the red regions are associated with high cerium characteristic X-ray emissions). The full elemental composition of the scanned map is displayed in Figure 3B and the $\text{M}\alpha$ and $\text{L}\alpha$ characteristic X-ray emission peaks for cerium were observed at 0.88 KeV and 4.83 KeV respectively. Furthermore, semi-quantitative EDX elemental analysis shows that cerium was the third most abundant element in the mitochondria following carbon and oxygen. These findings clearly confirm that significant localization of EGCNPs in the mitochondria occurs within 24 h of treatment.

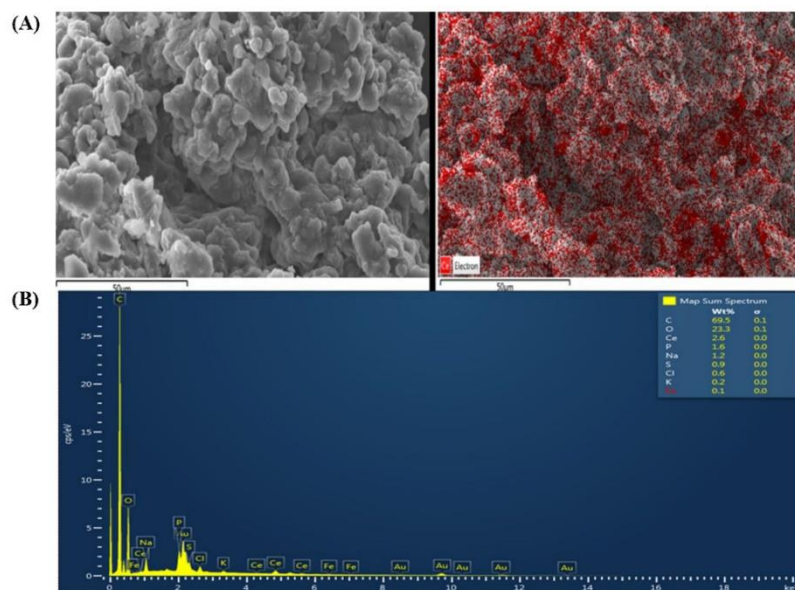


Figure 3. (A) SEM micrograph of the mitochondria isolated from HLECs treated with EGCNPs (left) and its associated cerium EDX mapping (right), (B) EDX spectrum and semi-quantitative full elemental

analysis generated from EDX mapping of the mitochondria. The presence of gold (Au) is due to sample coating with gold. Scale bar = 50 μm .

Effect of EGCNPs on the Mitochondrial Network

To examine the effect of EGCNPs on the mitochondrial morphology and network organization, staining with the mitochondria-selective stain (Mitotracker™ Red CMXRos) was employed. The mitochondria were uniform in shape and organization when treated with EGCNPs concentrations of up to $400 \mu\text{g mL}^{-1}$ and showed no significant difference from control cells (Figure 4A). The mitochondria were short and rod-shaped with organized localization in the perinuclear region (Figure 4B). H_2O_2 (positive control) caused significant mitochondrial aggregation and diffusion of the mitochondrial network was observed.

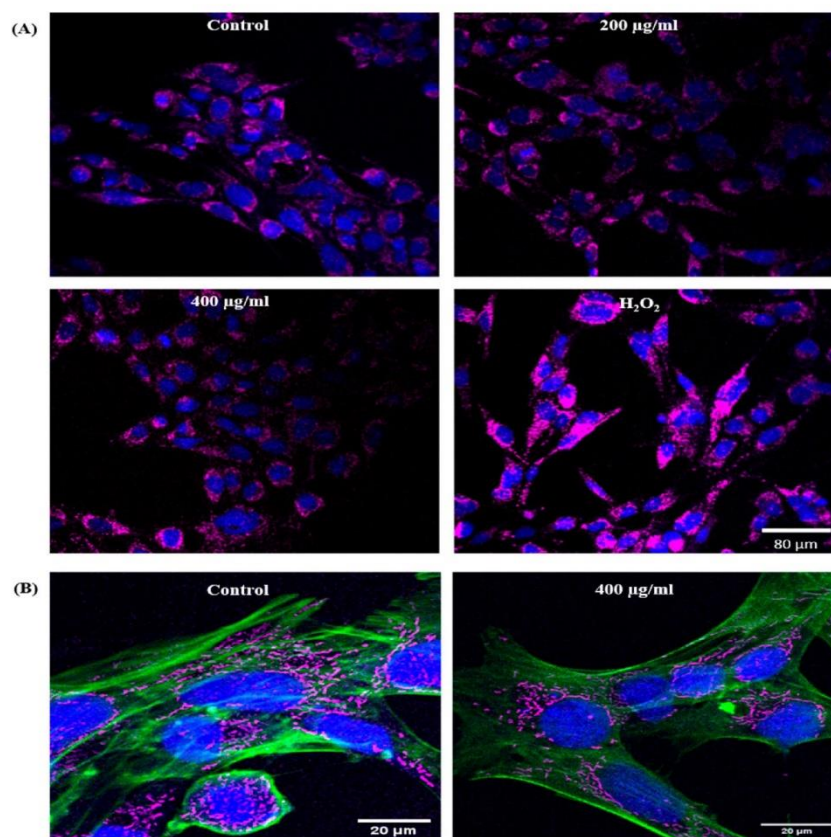


Figure 4. (A) Representative confocal images showing the effect of different EGCNPs concentrations (24 h exposure) on the mitochondrial morphology and organization (magenta) in HLECs, nuclei are stained with Hoechst 33,342 (blue) (B) High magnification confocal images of the mitochondria counterstained with cytoskeleton selective stain ActinGreen 488 (green) and Hoechst 33,342 (blue). No significant changes from control were observed up to EGCNPs concentrations of $400 \mu\text{g mL}^{-1}$. H_2O_2 (400 μM) was used as a positive control which shows significant aggregation of the mitochondria.

EGCNPs Overdose Disrupts Mitochondrial Membrane Potential ($\Delta\Psi_m$)

The integrity of the mitochondrial membrane potential is one of the most critical factors in assessing the function of the mitochondria; its depolarization (loss of normal charge distribution on both sides of the membrane) is an indicator for early stage apoptosis [25–27]. JC-1 dye was used to differentiate between healthy and depolarized mitochondria based on the change in the fluorescence of the dye. In healthy mitochondria, the cationic dye accumulates into the negatively charged interior of mitochondria where it forms J-aggregates shifting the fluorescence from green to red. Consequently, decreased red/green ratio is an indicator for mitochondrial membrane depolarization [28]. This ratio is highly accurate as it reports on changes in membrane potential regardless of the shape, size or density of the mitochondria [28]. As shown in Figure 5, EGCNPs concentrations up to 200 $\mu\text{g mL}^{-1}$ had no significant effect on the ($\Delta\Psi_m$). When the concentration was increased to 400 $\mu\text{g mL}^{-1}$, significant depolarization was observed suggesting that early stage apoptosis was taking place. For comparison, two different concentrations of sodium azide (NaN_3) were used as positive controls since it is known to induce mitochondrial depolarization by blocking complex IV in the mitochondrial electron transport chain [28].

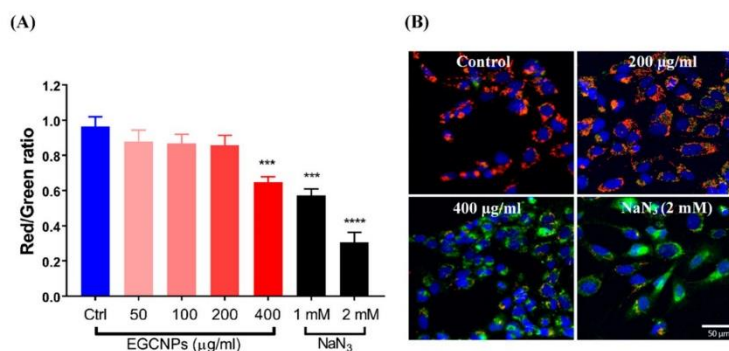


Figure 5. Effect of EGCNPs concentrations on mitochondrial membrane potential ($\Delta\Psi_m$) measured using JC-1 staining. Decrease in red/green ratio indicates depolarization of the mitochondrial membrane. (A) Quantification of red/green ratio from high throughput Incucyte S3 fluorescent images (images available in the SI), (B) Representative high magnification confocal microscopy images with JC-1 staining counterstained with Hoechst 33,342 (blue) showing significant increase in green/red ratio (depolarized $\Delta\Psi_m$) at 400 $\mu\text{g mL}^{-1}$. Up to 200 $\mu\text{g mL}^{-1}$, the red and green had a ratio close to 1 causing them to colocalize. NaN_3 was used as a positive control as it is a known disruptor of $\Delta\Psi_m$. Asterisks denote statistical significance (***) $p \leq 0.001$ and (****) $p \leq 0.0001$ from control, $n = 3$, using one-way ANOVA, Dunnett's multiple comparisons. Error bars are presented as mean \pm SEM.

ATP Level (Luciferase Assay)

The intracellular ATP production is considered a well-accepted differentiator between apoptotic and necrotic cell death [29,30]. Apoptosis is an energy-driven process that requires ATP for its execution such as in the breakdown of macromolecules [30]. When the ATP level drops significantly, it is an indication of the termination of controlled cell death and necrosis starts to take over. The changes in intracellular ATP production upon exposure to different EGCNPs concentrations were measured based on the bioluminescence produced using the highly sensitive luciferin-luciferase assay [29]. Up to 200 $\mu\text{g mL}^{-1}$, no significant decline in ATP level was observed as expected from the aforementioned results (Figure 6). Interestingly, no significant change in ATP level was observed at 400 $\mu\text{g mL}^{-1}$ even though mitochondrial membrane depolarization does take place at this concentration. The cells were then treated for a longer duration (48 h), and a significant decrease in ATP production was observed

at $400 \mu\text{g mL}^{-1}$ (Figure 6). Another notable finding was the slight but significant increase in ATP levels at 100 and $200 \mu\text{g mL}^{-1}$ EGCNP concentrations after 24 h.

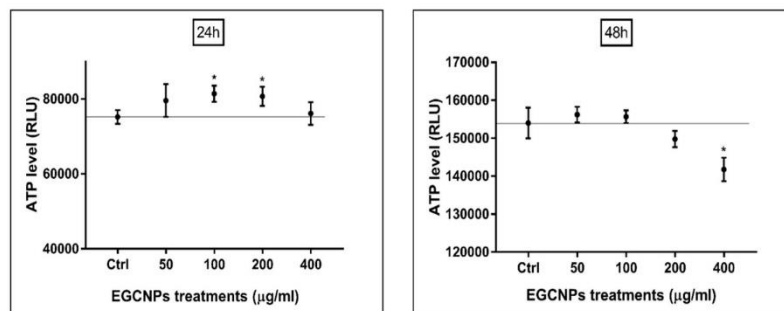


Figure 6. Effect of EGCNPs on ATP production in HLECs measured by luciferin-luciferase bioluminescent assay at 24 h and 48 h. Asterisks denote statistical significance from control ($p < 0.05$), $n = 3$ using one-way ANOVA. Error bars are presented as mean \pm SEM.

Genotoxicity (pH2AX Immunocytochemistry Assay)

DNA integrity in HLECs is particularly important as its damage could lead to impaired protein synthesis, impaired differentiation and consequently cataract formation [31]. Since DNA is a common target of ROS [32], EGCNP induced genotoxicity was evaluated by detecting DNA double strands breaks (DSBs). As a response to DSBs, the histone protein H2AX is phosphorylated (pH2AX) and this can be detected with immunocytochemistry. The results in Figure 7 show that increased ROS was accompanied with increased DNA damage at $400 \mu\text{g mL}^{-1}$ whereas, at low concentrations, no genotoxicity was observed.

Effect of EGCNPs on Caspase-3,7 Activity

Activation of caspases is a key indicator of cells irrevocably submitting to apoptotic death [33]. The activation of caspases 3 and 7 (effector caspases in mammals) in HLECs upon EGCNPs treatment was detected over 24 h by means of live cell imaging using the IncuCyte® Caspase-3/7 Red apoptosis assay reagent. The reagent consists of a red fluorophore (NucView™633) attached to an activated caspase recognition motif (DEVD). Upon binding with activated caspases, the motif is cleaved, and the fluorophore that is liberated intercalates with DNA giving red fluorescence proportional to caspase activity that can be quantified over time. Figure 8A shows that EGCNPs do not result in significant caspase activation up to concentrations of $200 \mu\text{g mL}^{-1}$ compared to control cells. Overexposure to EGCNPs ($400 \mu\text{g mL}^{-1}$) caused significant caspase activation as early as 12 h from the treatment commencing. This agrees with the JC-1 data (Figure 5) where loss of membrane potential was observed only at $400 \mu\text{g mL}^{-1}$.

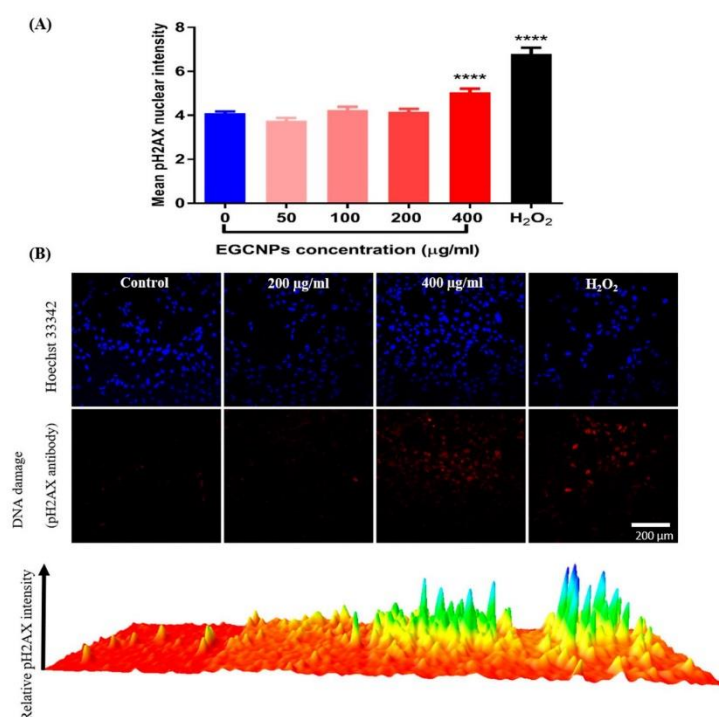


Figure 7. Effect of EGCNPs on DNA damage (genotoxicity) measured by immunocytochemistry through detection of pH2AX mean intensity. (A) quantification of pH2AX fluorescence intensity (only pH2AX signal inside nuclei perimeters) within at least 500 individual nuclei obtained from 4 independent experiments. (B) representative confocal images and 3D surface plotting of relative pH2AX intensity (red). Asterisks denote statistical significance from control ($p < 0.05$) using one-way ANOVA, Dunnett's multiple comparisons. Error bars are presented as mean \pm SEM. A schematic showing DNA damage quantification steps is shown in the Supplementary Information.

Annexin V/Cytotox Red Assay

To confirm whether cells undergo apoptosis rather than necrosis at EGCNP concentration of $400 \mu\text{g mL}^{-1}$, the cells were double stained with annexin V green/Cytotox Red and observed by means of live cell imaging using Incucyte S3 live imaging system. Apoptotic cells only show annexin V labelling (green) while late apoptotic or necrotic cells are double labelled with both stains. Figure 8B shows that the $400 \mu\text{g mL}^{-1}$ concentration caused a significant increase in cells labelled with annexin V, when compared to negative control after treatment durations of 6 h, 12 h and 24 h. No significant change was found in the number of necrotic cells (labelled with Cytotox Red) over the same treatment durations (Figure 8C). These findings indicate that apoptosis is the main mechanism of cell death in HLECs with acute overexposure to EGCNPs.

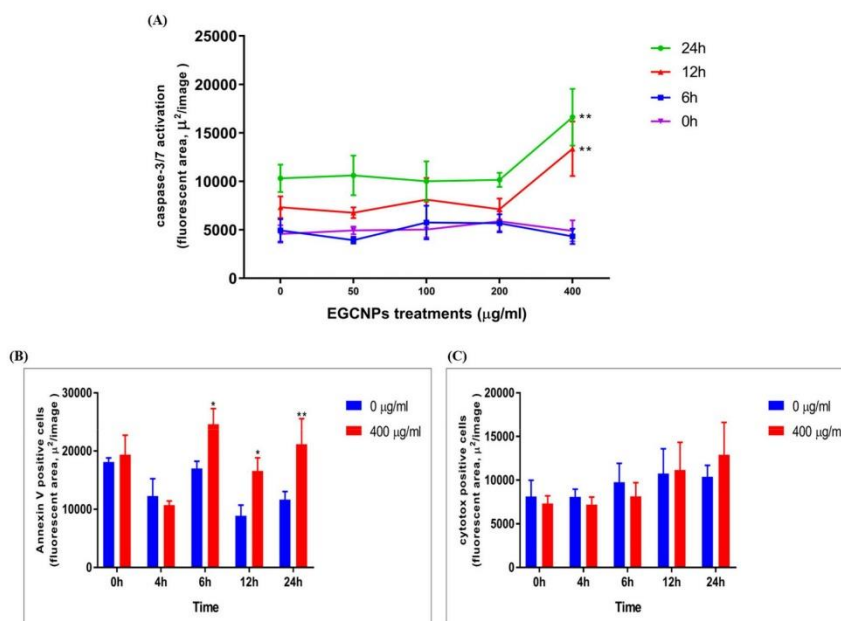


Figure 8. Effect of different EGCNPs concentrations on (A) caspase-3,7 activity, (B) Annexin V binding after 24 h, (C) Cytotox Red staining after 24 h in HLECs. No significant caspase activation was observed up to 200 $\mu\text{g mL}^{-1}$. At 400 $\mu\text{g mL}^{-1}$, significant caspase activity was observed after 12 h of treatment. Asterisks (*) $p \leq 0.05$ and (**) $p \leq 0.01$ denote statistical significance from control in same time group, $n = 4$ where n is the number of replicates, using two-way ANOVA. Error bars are presented as mean \pm standard error of the mean (SEM). Representative images that were used for quantification are available in the Supplementary Information.

3. Discussion

Cerium oxide nanoparticles have shown antioxidant activities in different mammalian cell lines because of their ability to scavenge for different ROS in an enzyme-mimetic fashion [4,17,34]. They have shown promise in the treatment of many ocular diseases such as retinal injury [17]. Additionally, we have recently reported that a novel ultra-small (4 nm) and well characterized monodisperse nanoceria formulation coated with modified ethylene glycol can protect HLECs from oxidative stress induced by H_2O_2 when used at concentrations as low as 50 $\mu\text{g mL}^{-1}$, indicating that nanoceria may have potential as an anticataract treatment [20]. Interestingly, it was found that HLECs can proliferate normally with the same rate when treated with EGCNPs concentrations up to 400 $\mu\text{g mL}^{-1}$ for three days. However, a significant decrease in viability measured by MTT assay was observed at 24 h suggesting that the mitochondria may be affected with nanoceria treatment since the MTT assay assesses the viability based on the activity of mitochondrial succinate dehydrogenase [35]. Consequently, in this study, the aim was to elucidate the biological consequences of the interaction between EGCNPs at 400 $\mu\text{g mL}^{-1}$ and mitochondria in HLECs. Concentrations above 400 $\mu\text{g mL}^{-1}$ caused a marked decrease in proliferation and cell membrane damage (necrosis) and were not subject to further study.

The overproduction of ROS is involved in the etiology and pathogenesis of many diseases and disorders such as Alzheimer's, Parkinson's, diabetes, and cataract. The identification and effects of new drugs on the redox state of a target cell line/cell/tissue is essential [36–39]. In this study, the basal ROS level in HLECs was not affected at low concentrations of EGCNPs. However, a significant

increase in basal ROS was seen when the concentration was increased to $400 \mu\text{g mL}^{-1}$ (Figure 2). This shows that even though EGCNPs possess antioxidant and ROS scavenging properties, short-term overexposure can elevate ROS levels. This increase in ROS levels is likely to have been caused by Fenton like reactions where reduced metal ions (e.g., Ce^{3+}) react with cellular hydrogen peroxide (H_2O_2), producing hydroxyl radicals ($\text{HO}\bullet$) that are highly toxic to biomolecules [32]. It was previously shown that EGCNPs had surface trivalent cerium and hence the progression of a Fenton-like reaction is expected to progress as reported in the literature [40]. It is of significant importance that therapeutic doses of EGCNPs ($< 200 \mu\text{g mL}^{-1}$) do not alter the basal ROS level which is needed to maintain normal metabolic functions and signaling pathways [22]. Our previous work showed that EGCNPs used at $50 \mu\text{g mL}^{-1}$, scavenge for ROS induced by H_2O_2 in HLECs. Considering the results shown here, this suggests that at low concentrations, EGCNPs only exert their ROS lowering capability in the presence of external ROS stimuli without diminishing the cellular benefits of basal ROS.

Since the mitochondria are the major sites for ROS generation [14], it was speculated that their properties and function would be altered with acute exposure to EGCNPs. EGCNPs have been shown to localize mainly in the cytoplasm of HLECs, however, organelle-specific localization was not identified [20]. In this study, the mitochondrial localization of EGCNPs was confirmed by examining isolated mitochondria from EGCNPs-treated HLECs using SEM-EDX (Figure 3). By using this technique, it was feasible to avoid surface functionalization with fluorescent markers; a common practice in the literature to track the nanoparticles that changes the surface properties and in turn could affect the uptake behavior of nanoparticles [41]. The mitochondrial localization of EGCNPs is likely to be caused by the strong positive zeta potential value that EGCNPs carry ($+44 \text{ mV}$) making the negatively charged interior of the mitochondria an ideal target [36]. This finding is interesting since it is known from our previous investigation that protein coronae are adsorbed on the surface of EGCNPs making the zeta potential value slightly negative (-9.7 mV) in cell culture media containing fetal bovine serum. Nonetheless, the coronae do not appear to prevent the nanoparticles from entering the mitochondria. The zeta potential is known to play a significant role in subcellular localization of nanocerium which affects both the toxicity and activity profile [42]. It has previously been shown that targeting nanocerium specifically to mitochondria by surface functionalization with the mitochondrial-targeting cationic ligand (triphenylphosphonium, TPP), suppresses oxidative stress-induced neuronal death in mice [36]. Our findings indicate that this specific functionalization is not required for mitochondrial uptake in HLECs. Following the confirmation of mitochondrial uptake of EGCNPs, the effect of such uptake on the morphology and network organization of the mitochondria was studied using confocal microscopy and was found to be similar up to $400 \mu\text{g mL}^{-1}$ (Figure 4). This suggested that at the higher concentration ($400 \mu\text{g mL}^{-1}$) the cells could be undergoing early stage apoptosis, in which the shape of the mitochondria remains intact [25,30]. Hence, some of the key apoptotic hallmarks were further investigated.

One of the key indicators of early stage apoptosis is the loss of mitochondrial membrane potential where membrane depolarization and formation of mitochondrial membrane transition pores allow the release of mitochondrial intermembrane space enzymes (e.g., cytochrome c) that activate the caspase cascade initiating apoptosis [26,33]. Indeed, significant mitochondrial membrane depolarization at the higher dose of EGCNPs was observed and this indicated that apoptosis was taking place (Figure 5). To support these findings, the ATP level in EGCNPs treated HLECs was measured. Since apoptosis is an energy-dependent process, it was expected that the ATP level should remain relatively the same during the initial stages of apoptosis. Various studies have shown that ATP levels do not change during the initial stages of apoptosis [29]. This was the case in EGCNPs-treated HLECs as the $400 \mu\text{g mL}^{-1}$ concentration showed no significant difference in ATP level from control cells or those treated with lower concentrations of nanocerium (Figure 5). This could be explained by the fact that cells require ATP in order to initiate the controlled apoptotic cell death through various ATP-dependent steps such as caspase activation, nuclear condensation and apoptotic body formation [29]. To further test this assumption, the cells were treated for a longer duration (48 h), and indeed a small but significant decrease, in ATP at $400 \mu\text{g mL}^{-1}$ was observed, indicating the termination of apoptosis in some of

the cells with concomitant ATP depletion. It is noteworthy that at 24 h, safe EGCNPs concentrations ($\leq 200 \mu\text{g mL}^{-1}$) caused a slight increase in ATP levels. One possible reason is that the uptake of EGCNPs may have proceeded through energy-dependent clathrin-mediated and caveolae-mediated endocytic pathways, which have been reported as the main uptake mechanism of nanoceria in many cell lines [41–43].

DNA integrity is of particular interest in HLECs since the cells are continually synthesizing lens proteins (crystallins), and hence damage could lead to disrupted protein expression and eventually lead to cataract formation [44]. It was shown before that nanoceria coated with 3-phosphonopropionic acid have no adverse effect on DNA health when exposed to a concentration of $10 \mu\text{g mL}^{-1}$ for 24 h [45]. It was demonstrated that EGCNPs can be tolerated at a 20-fold higher concentration ($200 \mu\text{g mL}^{-1}$) for the same treatment duration. However, a dose of $400 \mu\text{g mL}^{-1}$ caused significant DNA double strand breaks (as shown in Figure 7). DNA damage is likely to be caused by increased ROS that attack the DNA, causing double strand breaks. It was reported that some nuclear uptake of EGCNPs take place at therapeutic concentrations (less $200 \mu\text{g mL}^{-1}$) [20]. This nuclear uptake is likely to have been increased at $400 \mu\text{g mL}^{-1}$ causing EGCNPs to aggregate inside the nuclei promoting genotoxicity [16]. Even though some nanoparticles have poor permeability into the nuclei, their entry is inevitable during mitosis where the nuclear membrane is broken as the cells prepare for division [46]. As such, higher doses of EGCNPs will provide more opportunity for increased localization and possibly aggregation into the nuclei. The aforementioned events are likely to have led to the activation of caspases at ($400 \mu\text{g mL}^{-1}$) which are the key causes of apoptosis (Figure 8) [33]. Additionally, annexin V/Cytotox Red assay conclusively demonstrated that apoptosis is the main driver for cell death, where an increase in annexin V binding was observed without concomitant increase necrosis-specific Cytotox Red labelling (Figure 8). Together these results demonstrate that the main mechanism of cerium oxide toxicity in HLECs proceeds through a mitochondrial apoptotic pathway mediated by elevated ROS and DNA damage.

The toxicity of nanoceria has been studied *in vitro* using a range of cell lines (reviewed in Gagnon and Fromm, 2015) but the data are not comparable given the varying characteristics of nanoceria used including the shape, size, colloidal stability, zeta potential, surface valence, surface functionality and the range of nanoceria fabrication methods. There are still inconsistencies in the literature regarding the mechanism of nanoceria toxicity [13]. Our results show, in a dose-dependent manner, the toxicity mechanism of well characterized nanoceria (EGCNPs) in human lens epithelium. To conclude, when considering nanoceria toxicity, and given their redox active characteristics, emphasis must be on the evaluation of the mitochondrial functionality as an early indicator for cell health as it can reveal significant effects that can be easily overlooked in short-term proliferation and standard toxicological studies.

4. Materials and Methods

Synthesis of Ethylene Glycol-Coated Cerium Oxide Nanoparticles (EGCNPs)

Cerium oxide nanoparticles coated with ethylene glycol and ethylene glycol mono- and diacetates (EGCNPs) were synthesized in aqueous conditions using the ammonia precipitation method as reported previously [20].

Cell Culture

Human lens epithelial cells (HLECs) (B3, ATCC[®] CRL11421[™]) were cultured in Eagle's minimum essential media (EMEM) (ATCC[®] 30–2003) supplemented with fetal bovine serum (20%, Scientific Lab Supplies), penicillin (100 units/mL, Sigma Aldrich) and streptomycin (0.1 mg/mL, Sigma Aldrich). The cells were incubated at 37 °C and 5% CO₂ in a humidified environment (95% RH). The experiments were carried out on HLECs in the log growth phase.

Basal ROS Level

H₂DCFDA probe (2',7'-dichlorodihydrofluorescein diacetate, D399, ThermoFisher) was employed to measure basal ROS levels as previously reported [20]. Briefly, HLECs were seeded in 96-well plates in complete EMEM (5000 cells/well) and allowed to recover for 24 h. The media were then removed and replaced with fresh media containing different EGCNPs concentrations (0, 50, 100, 200, and 400 µg mL⁻¹) for 24 h. A maximum of 400 µg mL⁻¹ was previously reported as the highest concentration beyond which a marked decrease in proliferation is observed [20]. H₂O₂ (200 µM, Sigma Aldrich) was used as a positive control. After the treatment period, the media were discarded, cells were washed once with pre-warmed PBS (ATCC® 30-2200™) and incubated with H2DCFDA solution (10 µM in PBS) for 30 min at 37 °C. H2DCFDA solution was then discarded, cell washed with pre-warmed PBS and fresh PBS (200 µL) was added to each well. DCF fluorescence intensity was measured using a microplate reader (FLUOstar Omega, BMG LABTECH, Ortenberg, Germany) at excitation/emission of 485/520 nm. Correcting the fluorescence values was performed before analysis by subtracting the fluorescence of unstained cells from all other values. No fluorescence was observed for cell-free H2DCFDA/PBS and H2DCFDA/PBS/EGCNPs mixtures.

EGCNPs Mitochondrial Uptake and Localization (SEM-EDX Studies)

HLECs were grown in five T175 flasks until they reached approximately 80% confluence. The cells were then treated with EGCNPs (400 µg mL⁻¹) for 24 h and subsequently harvested, pelleted and washed once with full media and once with PBS. The mitochondria were then isolated from the pellet using the Mitochondria Isolation Kit for Cultured Cells (89874, ThermoFisher, Paisley, UK) in accordance with the supplier's instructions. The isolated mitochondria were washed once with PBS, fixed with paraformaldehyde (4%, 5 min) and dried in pure ethanol (5 min). The mitochondria were placed on a SEM aluminum stub covered with a carbon tape and the specimens were coated with a gold layer (5 nm) using a sputter coater (Q150R ES, Quorum Technologies Ltd, East Sussex, UK). The specimens were examined using a scanning electron microscope equipped with an EDX detector (JEOL, JSM-7100f, Tokyo, Japan). EDX spectra and mapping were acquired and processed using Aztec software (v.2011, Oxford Instruments, Abingdon, UK).

Mitochondrial Morphology (Confocal Studies)

HLECs were seeded (5000 cells/well) in black 96-well plates with clear flat bottom (Falcon® 353219, Corning, New York, US) and left to establish for 24 h. The following day, the media were discarded, and the cells were treated with EGCNPs-containing media (0, 50, 100, 200 and 400 µg mL⁻¹) for 24 h. After the treatment period, the media were removed, and the cells were washed once with pre-warmed PBS. The cells were then incubated with full media containing MitoTracker™ Red CMXRos (200 nM, ThermoFisher, Paisley, UK) for 20 min at 37 °C. After staining, the cells were washed once with pre-warmed PBS, fixed in pre-warmed paraformaldehyde solution (4% in PBS) for 10 min at room temperature and permeabilized by incubating in ice-cold acetone for 5 min. The cells were then counterstained by incubating in PBS containing Hoechst 33,342 (2 µg/mL, ThermoFisher, Paisley, UK) for 20 min at room temperature. Imaging was carried out using a confocal laser scanning microscope (Leica, Wetzlar, Germany) using the following settings: sequential scanning, 20x dry objective, ex/em: Mitotracker: 543/599 nm, Hoechst: 405/461 nm.

Mitochondrial Membrane Potential (JC-1 Staining)

JC-1 probe (Abcam) was employed for mitochondrial membrane potential measurements. HLECs were seeded, established and treated with different EGCNPs concentrations (0, 50, 100, 200 and 400 µg mL⁻¹) as before and sodium azide (1 and 2 mM, Sigma Aldrich, Gillingham, UK) was used as a positive control. After the treatment period, the media were removed, and cells incubated with JC-1 probe in complete media (10 µM) for 30 min at 37 °C in dark conditions. The staining

solution was removed, cells washed with PBS and replaced with phenol red-free complete media. The wells were then imaged using Incucyte S3 high throughput imaging system using the green and red channels (5 wells per treatment condition, three images per well) and quantification of the red/green ratio was calculated using the integrated software by dividing the fluorescence area of the red channel over the fluorescence area of the green channel. Other software (e.g., ImageJ (version 2, NIH, Maryland, US) can be employed for such calculations by thresholding the red and green fluorescence and subsequently calculating their corresponding areas. The experiment was run in triplicate. Qualitative high magnification images were acquired using a confocal microscope after nuclear staining with Hoechst 33342. The excitations/emission settings were as follows: Hoechst 33,342 (405/461 nm), JC-1 green monomers (488/530 nm), JC-1 red aggregates (543/590 nm).

ATP Quantification (Luciferase Assay)

The quantification of cellular ATP was carried out using the luminescent luciferase assay (CellTiter-Glo, Promega) in accordance with the supplier's instructions. Briefly, HLECs were established in 96-well plates as before and treated with different EGCNPs concentrations for 24 h and 48 h. After the treatment period, the media were removed and replaced with fresh media. An equal volume of CellTiter-Glo reagent was added to each well to lyse the cells and release a luminescent signal proportional to the amount of ATP present. The plate was placed on an orbital shaker for 2 min and then incubated in the dark at room temperature for 10 min to stabilize the signal. The luminescent signal was read using a luminometer (Infinite[®] 200 PRO, TECAN, Männedorf, Switzerland).

Genotoxicity (Immunocytochemistry)

The DNA damage was evaluated using the HCS DNA kit (ThermoFisher) according to the supplier's instructions. Briefly, HLECs were seeded in a black 96-well plate, established and treated for 24 h with different EGCNPs concentrations (0, 50, 100, 200 and 400 $\mu\text{g mL}^{-1}$) as before. After the treatment period, the media was removed, the cells were fixed in paraformaldehyde solution (4%, 10 min), rinsed with PBS, and permeabilized in 0.2% Triton-X-100 (15 min). The cells were washed with PBS and then incubated in a blocking buffer (bovine serum albumin in PBS, 1%) for 1 h at room temperature. The blocking buffer was removed, and the cells were incubated with the primary antibody solution (pH2AX mouse monoclonal antibody) for 1 h. The primary antibody solution was then removed, and the cells were washed three times with PBS and incubated with the secondary antibody/nuclear stain solution (Alexa Fluor 555 goat anti-mouse IgG/Hoechst 33342) for 1 h. The secondary antibody solution was then removed, the cells were washed three times with PBS, and replaced with fresh PBS before proceeding to imaging. Imaging was carried out using a confocal laser scanning microscope using the following settings (sequential scanning ex/em: pH2AX: 543/565 nm, Hoechst: 405/461 nm). For data analysis, Hoechst staining was used for nuclear segmentation and the DNA damage was measured by the increase in the fluorescence of pH2AX signal in the region defined as the nuclei. The experiment was repeated four times and at least 100 nuclei were analyzed in each replicate.

Caspase-3,7 Assay (Live Cell Imaging)

HLECs were seeded in 96-well plates (5000 cells per well) and left to establish for 24 h. The cells were then treated with different EGCNPs concentration (0, 50, 100, 200 and 400 $\mu\text{g mL}^{-1}$) in supplemented EMEM in presence of IncuCyte[®] Caspase-3/7 Red Apoptosis Assay Reagent (0.5 μM , excitation/emission 630/650 nm). The cells were imaged every 2 h for 24 h using the Incucyte S3 live cell imaging system (Essen BioScience, Welwyn Garden City, UK) fitted inside an incubator (5% CO_2 , 37 °C). Three fields of view were imaged per well using the 20 \times objective. Images were then analyzed, and caspase activity was expressed as the area of red fluorescent caspase signal per image. The experiment was performed four times.

Annexin V/Cytotox Red Assay (Live Cell Imaging)

The assay was performed on the Incucyte S3 live cell imaging system as described above but in the presence of double staining IncuCyte® Annexin V Green Reagent/IncuCyte™ Cytotox Red Reagent (250 nM). Excitation/emission maxima for Annexin V and Cytotox Red are 490/515 nm and 612/631 nm respectively.

5. Conclusions

The antioxidant properties of nanoceria are dose dependent with oxidative actions triggered if the concentration is increased beyond a certain threshold. Nanoceria manifest no cytotoxic or genotoxic effects in human lens epithelial cells when concentrations are up to 200 µg mL⁻¹. At 400 µg mL⁻¹, these nanoparticles induced ROS generation which mediated cellular apoptosis driven by the mitochondrial apoptotic pathway. Potential biomedical applications need to take this threshold into consideration. Further work is needed to determine thresholds for other cell and tissue types.

Supplementary Materials: The following are available online at <http://www.mdpi.com/1420-3049/25/3/441/s1>, Figure S1: Representative Incucyte images used for the quantification of JC-1 red/green ratio in HLECs after treatment with different EGCNPs concentrations, Figure S2: Representative Incucyte images used for measurement of caspase-3,7 activity in HLECs after treatment with different EGCNPs concentrations (0–400 µg mL⁻¹) for 24 h, Figure S3: Representative Incucyte images of Annexin V green/Cytotox Red staining in HLECs comparing control and EGCNPs treated cells (24 h), Figure S4: Schematic representation of the steps employed for the quantification of DNA damage.

Author Contributions: All authors have read and agree to the published version of the manuscript. All authors contributed to experimental design, B.H. conducted the experiments, all authors contributed to analysis of results and writing the manuscript.

Funding: This research has been funded by Nottingham Trent University VC studentship scheme.

Acknowledgments: The authors would like to thank Charlotte Howard for her valuable insights on the Mitotracker and JC-1 mitochondrial studies.

Conflicts of Interest: The authors declare no conflict of interest.

References

- De Matteis, V.; Cascione, M.; Toma, C.C.; Leporatti, S. Morphomechanical and organelle perturbation induced by silver nanoparticle exposure. *J. Nanoparticle Res.* **2018**, *20*, 73. [CrossRef]
- Pandurangan, M.; Kim, D.H. In vitro toxicity of zinc oxide nanoparticles: A review. *J. Nanoparticle Res.* **2015**, *17*, 158. [CrossRef]
- Manke, A.; Wang, L.; Rojanasakul, Y. Mechanisms of nanoparticle-induced oxidative stress and toxicity. *Biomed. Res. Int.* **2013**, *2013*. [CrossRef] [PubMed]
- Xu, C.; Qu, X. Cerium oxide nanoparticle: A remarkably versatile rare earth nanomaterial for biological applications. *NPG Asia Mater.* **2014**, *6*, e90. [CrossRef]
- Li, C.; Shi, X.; Shen, Q.; Guo, C.; Hou, Z.; Zhang, J. Hot Topics and Challenges of Regenerative Nanoceria in Application of Antioxidant Therapy. *J. Nanomater.* **2018**, *2018*, 1–12. [CrossRef]
- Alpaslan, E.; Yazici, H.; Golshan, N.H.; Ziemer, K.S.; Webster, T.J. PH-Dependent Activity of Dextran-Coated Cerium Oxide Nanoparticles on Prohibiting Osteosarcoma Cell Proliferation. *ACS Biomater. Sci. Eng.* **2015**, *1*, 1096–1103. [CrossRef]
- Von Montfort, C.; Alili, L.; Teuber-Hanselmann, S.; Brenneisen, P. Redox-active cerium oxide nanoparticles protect human dermal fibroblasts from PQ-induced damage. *Redox Biol.* **2015**, *4*, 1–5. [CrossRef]
- He, L.; Su, Y.; Lanhong, J.; Shi, S. Recent advances of cerium oxide nanoparticles in synthesis, luminescence and biomedical studies: A review. *J. Rare Earths* **2015**, *33*, 791–799. [CrossRef]
- Pirmohamed, T.; Dowding, J.M.; Singh, S.; Wasserman, B.; Heckert, E.; Karakoti, A.S.; King, J.E.S.; Seal, S.; Self, W.T. Nanoceria exhibit redox state-dependent catalase mimetic activity. *Chem. Commun.* **2010**, *46*, 2736–2738. [CrossRef]
- Korsvik, C.; Patil, S.; Seal, S.; Self, W.T. Superoxide dismutase mimetic properties exhibited by vacancy engineered ceria nanoparticles. *Chem. Commun.* **2007**, *10*, 1056–1058. [CrossRef]

11. Gantt, B.; Hoque, S.; Fahey, K.M.; Willis, R.D.; Delgado-Saborit, J.M.; Harrison, R.M.; Zhang, K.M.; Jefferson, D.A.; Kalberer, M.; Bunker, K.L.; et al. Factors affecting the ambient physicochemical properties of cerium-containing particles generated by nanoparticle diesel fuel additive use. *Aerosol Sci. Technol.* **2015**, *49*, 371–380. [[CrossRef](#)]
12. Hussain, S.; Al-Nsour, F.; Rice, A.B.; Marshburn, J.; Yingling, B.; Ji, Z.; Zink, J.I.; Walker, N.J.; Garantziotis, S. Cerium dioxide nanoparticles induce apoptosis and autophagy in human peripheral blood monocytes. *ACS Nano* **2012**, *6*, 5820–5829. [[CrossRef](#)] [[PubMed](#)]
13. Yokel, R.A.; Hussain, S.; Garantziotis, S.; Demokritou, P.; Castranova, V.; Cassee, F.R. The yin: An adverse health perspective of nanoceria: Uptake, distribution, accumulation, and mechanisms of its toxicity. *Environ. Sci. Nano* **2014**, *1*, 406–428. [[CrossRef](#)] [[PubMed](#)]
14. Fu, P.P.; Xia, Q.; Hwang, H.M.; Ray, P.C.; Yu, H. Mechanisms of nanotoxicity: Generation of reactive oxygen species. *J. Food Drug Anal.* **2014**, *22*, 64–75. [[CrossRef](#)]
15. Auffan, M.; Rose, J.; Orsiere, T.; De Meo, M.; Thill, A.; Zeyons, O.; Proux, O.; Masion, A.; Chaurand, P.; Spalla, O.; et al. CeO₂ nanoparticles induce DNA damage towards human dermal fibroblasts in vitro. *Nanotoxicology* **2009**, *3*, 161–171. [[CrossRef](#)]
16. Benameur, L.; Auffan, M.; Cassien, M.; Liu, W.; Culcasi, M.; Rahmouni, H.; Stocker, P.; Tassistro, V.; Bottero, J.Y.; Rose, J.; et al. DNA damage and oxidative stress induced by CeO₂ nanoparticles in human dermal fibroblasts: Evidence of a clastogenic effect as a mechanism of genotoxicity. *Nanotoxicology* **2015**, *9*, 696–705. [[CrossRef](#)]
17. Chen, J.; Patil, S.; Seal, S.; McGinnis, J.F. Rare earth nanoparticles prevent retinal degeneration induced by intracellular peroxides. *Nat. Nanotechnol.* **2006**, *1*, 142–150. [[CrossRef](#)]
18. Zheng, Q.; Fang, Y.; Zeng, L.; Li, X.; Chen, H.; Song, H.; Huang, J.; Shi, S. Cytocompatible cerium oxide-mediated antioxidative stress in inhibiting ocular inflammation-associated corneal neovascularization. *J. Mater. Chem. B* **2019**. [[CrossRef](#)]
19. Patil, S.; Reshetnikov, S.; Haldar, M.K.; Seal, S.; Mallik, S. Surface-derivatized nanoceria with human carbonic anhydrase II inhibitors and fluorophores: A potential drug delivery device. *J. Phys. Chem. C* **2007**, *111*, 8437–8442. [[CrossRef](#)]
20. Hanafy, B.I.; Cave, G.W.V.; Barnett, Y.; Pierscionek, B. Ethylene glycol coated nanoceria protects against oxidative stress in human lens epithelium. *RSC Adv.* **2019**, *9*, 16596–16605. [[CrossRef](#)]
21. Andley, U.P.; Rhim, J.S.; Chylack, L.T.; Fleming, T.P. Propagation and immortalization of human lens epithelial cells in culture. *Investig. Ophthalmol. Vis. Sci.* **1994**, *35*, 3094–3102.
22. Mittler, R. ROS Are Good. *Trends Plant. Sci.* **2017**, *22*, 11–19. [[CrossRef](#)] [[PubMed](#)]
23. Zhang, Q.; Raouf, M.; Chen, Y.; Sumi, Y.; Sursal, T.; Junger, W.; Brohi, K.; Itagaki, K.; Hauser, C.J. Circulating mitochondrial DAMPs cause inflammatory responses to injury. *Nature* **2010**, *464*, 104–107. [[CrossRef](#)] [[PubMed](#)]
24. Nasrazadani, S.; Hassani, S. Modern analytical techniques in failure analysis of aerospace, chemical, and oil and gas industries. In *Handbook of Materials Failure Analysis with Case Studies from the Oil and Gas Industry*; Butterworth-Heinemann: Oxford, UK, 2015; pp. 39–54.
25. Saraste, A.; Pulkki, K. Morphologic and biochemical hallmarks of apoptosis. *Cardiovasc. Res.* **2000**, *45*, 528–537. [[CrossRef](#)]
26. Lovrić, J.; Cho, S.J.; Winnik, F.M.; Maysinger, D. Unmodified cadmium telluride quantum dots induce reactive oxygen species formation leading to multiple organelle damage and cell death. *Chem. Biol.* **2005**, *12*, 1227–1234. [[CrossRef](#)] [[PubMed](#)]
27. Jana, S.K.; Banerjee, P.; Das, S.; Seal, S.; Chaudhury, K. Redox-active nanoceria depolarize mitochondrial membrane of human colon cancer cells. *J. Nanoparticle Res.* **2014**, *16*, 2441. [[CrossRef](#)]
28. Keil, V.C.; Funke, F.; Zeug, A.; Schild, D.; Müller, M. Ratiometric high-resolution imaging of JC-1 fluorescence reveals the subcellular heterogeneity of astrocytic mitochondria. *Pflügers Arch. Eur. J. Physiol.* **2011**, *462*, 693–708. [[CrossRef](#)]
29. Zamaraeva, M.V.; Sabirov, R.Z.; Maeno, E.; Ando-Akatsuka, Y.; Bessonova, S.V.; Okada, Y. Cells die with increased cytosolic ATP during apoptosis: A bioluminescence study with intracellular luciferase. *Cell Death Differ.* **2005**, *12*, 1390–1397. [[CrossRef](#)]
30. Richter, C.; Schweizer, M.; Cossarizza, A.; Franceschi, C. Control of apoptosis by the cellular ATP level. *FEBS Lett.* **1996**, *378*, 107–110. [[CrossRef](#)]
31. Kleiman, N.J.; Spector, A. DNA single strand breaks in human lens epithelial cells from patients with cataract. *Curr. Eye Res.* **1993**, *12*, 423–431. [[CrossRef](#)]

32. Dayem, A.A.; Hossain, M.K.; Lee, S.B.; Kim, K.; Saha, S.K.; Yang, G.M.; Choi, H.Y.; Cho, S.G. The role of reactive oxygen species (ROS) in the biological activities of metallic nanoparticles. *Int. J. Mol. Sci.* **2017**, *18*, 120. [[CrossRef](#)] [[PubMed](#)]
33. Shi, Y. Caspase activation, inhibition, and reactivation: A mechanistic view. *Protein Sci.* **2004**, *13*, 1979–1987. [[CrossRef](#)] [[PubMed](#)]
34. Pagliari, F.; Mandoli, C.; Forte, G.; Magnani, E.; Pagliari, S.; Nardone, G.; Licocchia, S.; Minieri, M.; Di Nardo, P.; Traversa, E. Cerium oxide nanoparticles protect cardiac progenitor cells from oxidative stress. *ACS Nano* **2012**, *6*, 3767–3775. [[CrossRef](#)] [[PubMed](#)]
35. Rai, Y.; Pathak, R.; Kumari, N.; Sah, D.K.; Pandey, S.; Kalra, N.; Soni, R.; Dwarakanath, B.S.; Bhatt, A.N. Mitochondrial biogenesis and metabolic hyperactivation limits the application of MTT assay in the estimation of radiation induced growth inhibition. *Sci. Rep.* **2018**, *8*, 1531. [[CrossRef](#)]
36. Kwon, H.J.; Cha, M.Y.; Kim, D.; Kim, D.K.; Soh, M.; Shin, K.; Hyeon, T.; Mook-Jung, I. Mitochondria-Targeting Ceria Nanoparticles as Antioxidants for Alzheimer's Disease. *ACS Nano* **2016**, *10*, 2860–2870. [[CrossRef](#)]
37. Pinna, A.; Malfatti, L.; Galleri, G.; Manetti, R.; Cossu, S.; Rocchitta, G.; Migheli, R.; Serra, P.A.; Innocenzi, P. Ceria nanoparticles for the treatment of Parkinson-like diseases induced by chronic manganese intoxication. *RSC Adv.* **2015**, *5*, 20432–20439. [[CrossRef](#)]
38. Volpe, C.M.O.; Villar-Delfino, P.H.; Dos Anjos, P.M.F.; Nogueira-Machado, J.A. Cellular death, reactive oxygen species (ROS) and diabetic complications review—Article. *Cell Death Dis.* **2018**, *9*, 119. [[CrossRef](#)]
39. Polreis, A.; Schmidt-Erfurth, U. Diabetic Cataract—Pathogenesis, Epidemiology and Treatment. *J. Ophthalmol.* **2010**, *2010*. [[CrossRef](#)]
40. Heckert, E.G.; Seal, S.; Self, W.T. Fenton-like reaction catalyzed by the rare earth inner transition metal cerium. *Environ. Sci. Technol.* **2008**, *42*, 5014–5019. [[CrossRef](#)]
41. Singh, S.; Kumar, A.; Karakoti, A.; Seal, S.; Self, W.T. Unveiling the mechanism of uptake and sub-cellular distribution of cerium oxide nanoparticles. *Mol. Biosyst.* **2010**, *6*, 1813–1820. [[CrossRef](#)]
42. Asati, A.; Santra, S.; Kaitanis, C.; Perez, J.M. Surface-charge-dependent cell localization and cytotoxicity of cerium oxide nanoparticles. *ACS Nano* **2010**, *4*, 5321–5331. [[CrossRef](#)] [[PubMed](#)]
43. Singh, S.; Ly, A.; Das, S.; Sakthivel, T.S.; Barkam, S.; Seal, S. Cerium oxide nanoparticles at the nano-bio interface: Size-dependent cellular uptake. *Artif. Cells, Nanomed. Biotechnol.* **2018**, *46*, S956–S963. [[CrossRef](#)] [[PubMed](#)]
44. Pierscionek, B.K.; Li, Y.; Schachar, R.A.; Chen, W. The effect of high concentration and exposure duration of nanoceria on human lens epithelial cells. *Nanomed. Nanotechnol. Biol. Med.* **2012**, *8*, 383–390. [[CrossRef](#)] [[PubMed](#)]
45. Pierscionek, B.K.; Keenan, J.; Yasseen, A.; Colhoun, L.M.; Li, Y.B.; Schachar, R.A.; Chen, W. CeO nanoparticles have no detrimental effect on eye lens proteins. *Curr. Anal. Chem.* **2010**, *6*, 172–176. [[CrossRef](#)]
46. Fröhlich, E. The role of surface charge in cellular uptake and cytotoxicity of medical nanoparticles. *Int. J. Nanomedicine* **2012**, *7*, 5577–5591. [[CrossRef](#)]

Sample Availability: Not available.



© 2020 by the authors. Licensee MDPI, Basel, Switzerland. This article is an open access article distributed under the terms and conditions of the Creative Commons Attribution (CC BY) license (<http://creativecommons.org/licenses/by/4.0/>).

Appendix

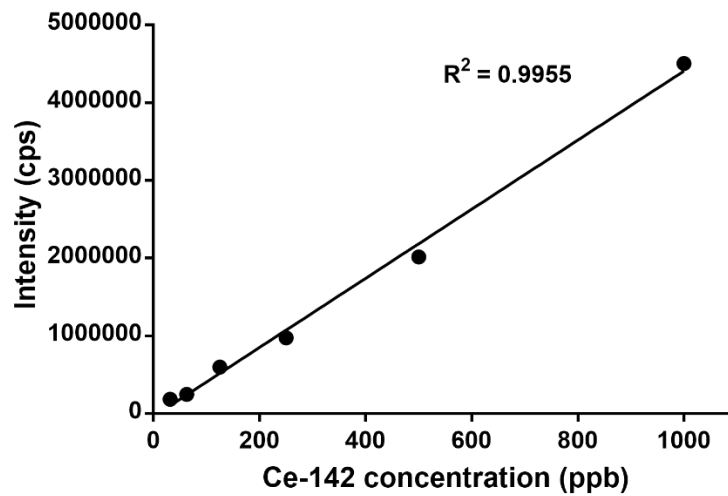
1- Calculation of XRD crystallite size employing the Scherrer equation

$$d_{\text{XRD}} = \frac{0.94\lambda}{\text{FWHM} \cos \theta}$$

where λ is the x-ray radiation wavelength (\AA), θ is the Bragg diffraction angle for (111) plane, and FWHM is full width half maximum (in radians) of the diffraction peak at (111).

$$d_{\text{XRD}} = \frac{0.94 \times 1.5}{0.0427 \cos 28.4} = 34.6 \text{ \AA} = 3.46 \text{ nm}$$

2- ICP calibration curve (cerium)



3- Negative control of HLECs stained with Hoechst 33342 (blue) showing no EGCNPs green fluorescence at ex/em: 488/530 nm

